Quickest Change Detection in Nonlinear Hidden Markov Models Using a Generalized CUSUM Procedure

by

Dongchang Li

A thesis
presented to the University of Waterloo
in fulfillment of the
thesis requirement for the degree of
Doctor of Philosophy
in
Applied Mathematics

Waterloo, Ontario, Canada, 2025

© Dongchang Li 2025

Examining Committee Membership

The following served on the Examining Committee for this thesis. The decision of the Examining Committee is by majority vote.

External Examiner:	Venugopal V. Veeravalli Professor, Department of Electrical and Computer Engineering, Department of Statistics, University of Illinois at Urbana-Champaign
Supervisor:	Navaratnam Sri Namachchivaya Professor, Department of Applied Mathematics
Internal Member:	Matthew Scott Associate Professor, Department of Applied Mathematics
	Chris Bauch Professor, Department of Applied Mathematics
Internal-External Member:	Leilei Zeng Professor, Department of Statistics and Actuarial Science

Author's Declaration

I hereby declare that I am the sole author of this thesis. This is a true copy of the thesis, including any required final revisions, as accepted by my examiners.

I understand that my thesis may be made electronically available to the public.

Abstract

In modern aircraft engine environments, fault diagnosis is important for process monitoring due to the increasing demand for high performance, increased safety, and reliability of dynamic systems. Early detection of process changes, while the system is still operating in a controllable region, can prevent major system breakdowns and catastrophes. For jet engines in operation, it is crucial both to track the state of the system and to determine whether it has entered or is approaching a new dynamic mode in real-time. Hence, the focus of this thesis is to examine and develop the change detection theory and procedures to detect and mitigate dynamic instabilities in modern jet engines.

The Moore-Greitzer partial differential equation is a commonly used mathematical model to capture changes in flow and pressure in axial-flow jet engine compressors. We first focus on a reduced planar system of the Moore-Greitzer compressor model, which describes the coupling of the disturbances with the mean axial flow and the pressure rise coefficient. In this work, we study the QCD problems in the nonlinear hidden Markov models (HMMs), where the observational data is obtained by measuring the pressure rise coefficient. We also explain in detail why the standard QCD scheme, well-established in both Bayesian and minimax settings, does not apply to our problems. As such, the generalized CUSUM procedure, where the post-change distribution depends on the unknown change point, is considered the most relevant change detection scheme. Although this statistic does not satisfy a simple recursion, we impose the standard filtering theory to recursively approximate the associated log-likelihood ratios using particle methods. To reduce computational costs in detection due to non-recursiveness and increasing particle requirements over time, we review the CUSUM-like procedure with an immediate change assumption, which supports a recursive formula.

More specifically, this research centers on instances where the change excites the reduced planar system from a pre-existing steady state to a new equilibrium or periodic oscillations in the post-change regime. The performance of the generalized CUSUMs using particle filters is examined with random simulations in the aforementioned pure surge modes of the Moore–Greitzer model with external forcing. For various forms of the post-change limit cycles with different phases, we observe some similarities and differences between the generalized CUSUMs and a special CUSUM statistic that assumes the change occurs immediately. It has been determined that the magnitude of the observed differences depends on the phase error between the assumed and observed post-change cycle phases, as well as whether the pre-change steady state is within the post-change limit cycle. Introducing signal noise effectively randomizes and mitigates the phase effect of the post-change limit cycle.

In the second component of this research, we address the change detection problems in the full Moore-Greitzer PDE model. In the model, the derivative of the disturbance flow in the axial direction at the compressor inlet is combined with a modified version of the previous ODE system. The dimensionality of the underlying model increases dramatically due to the PDE nature of the system. Instead of surge instability of the engine compressor, the additive change embedded in the ODE system makes the PDE system go through the Hopf bifurcation, resulting in a rotating stall instability for the Moore-Greitzer model. To simulate and identify such instability in the compressor system, we need to obtain time series solutions of a finite-dimensional ($n \ll \infty$) Moore-Greitzer system with an additive change that excites a stall instability. Due to the semigroup property of the PDE model, it is possible to employ the Fourier spectral method to discretize the spatial part of the PDE solution to obtain the time series. Then, we focus on simplifying the finite-dimensional Moore-Greitzer model using proper orthogonal decomposition (POD), which reduces the dimensions but retains enough fidelity to represent the compressor model with fewer basis functions ($N \ll n$). The accuracy of the reduced-order model is validated by reconstructing the Moore-Greitzer PDE system with these N POD modes, which take about 95% energy of the full-order model, under both the usual L^2 inner product space and the H^1 Sobolev space.

For the deterministic Moore-Greitzer model, we model the disturbances on compressor mass flow and pressure, followed by the stability analysis for the Moore-Greitzer PDE system with external deterministic forcing d_Φ and d_Ψ. Then, we propose the generalized CUSUM statistics to detect the dynamics change (i.e., a stall instability), caused by d_Φ and d_Ψ, using POD bases and particle filters. Furthermore, we investigate the reconstructions for the stochastic versions of the Moore-Greitzer model using the stochastic POD modes from *in situ* data, and deterministic POD modes generated from *a priori* data. From the validated reduced-order models, we utilize a particle method to implement the generalized CUSUM procedure to detect the stall bifurcation in the stochastic Moore-Greitzer compressor systems. The relevant simulation results of testing the effectiveness of these generalized CUSUM statistics with *in situ* and *a priori* POD modes are conducted. Some random simulations on stochastic cases based on various types of observations and POD modes are also performed. The simulation results demonstrate the generalized CUSUM statistics are more effective and less sensitive, with respect to different observations and POD modes, compared to the recursive CUSUM-like procedure that assumes an instant change.

Acknowledgements

First of all, I would like to deeply thank my supervisor, Professor Navaratnam Sri Namachchivaya, for the insightful learning experiences I have had under his guidance, as well as for his unwavering support and recognition, both of which hold great significance for me. Professor Navaratnam Sri Namachchivaya is the one who introduced me to the research in the field of stochastic processes, more specifically, the quickest change detection problems. Throughout my Ph.D. study, he always provided the most relevant references for each project of my research and kindly suggested me to take diverse graduate courses in applied mathematics and statistics. He has been patiently giving our research group a series of lectures, on different aspects of random dynamical systems, estimation and filtering theory, which enrich our mathematical understandings and help our research projects. Furthermore, his approach to mentoring students has profoundly influenced my prospective career and personal development.

I wish to extend my deep gratitude to Professor Peter Baxendale, for his invaluable comments and insights, not only in understanding the stochastic analysis of the existing change detection schemes in the literature, but in the study of change detection problems in nonlinear hidden Markov models, specifically within the framework of the Moore-Greitzer model. I am deeply grateful for the opportunity that Professor Navaratnam Sri Namachchivaya has given me to engage in weekly discussions concerning my research work with Peter, thereby gaining insight into his perspective on analyzing mathematical issues within the context of my Ph.D. studies.

I also wish to express my sincere appreciation to the members of my examining committee, Professor Matthew Scott and Professor Chris Bauch, as well as my internal/external examiner, Professor Leilei Zeng, and my external examiner, Professor Venugopal V. Veeravalli, for their generous dedication of time and perspectives in reviewing my thesis. Their invaluable critiques and suggestions will be instrumental in enhancing the quality and depth of this work. I wish to express my heartfelt appreciation to Professor Sivabal Sivaloganathan, who formerly served as a member of my Ph.D. committee. His wisdom, mentorship, and kindness left a lasting impression on my journey.

Furthermore, I am deeply grateful to my family for their consistent support and boundless encouragement, without which this academic journey would not have been possible.

Dedication

This is dedicated to my wife, Jiayu Zhu.

Table of Contents

Examining Committee ii

Author's Declaration iii

Abstract iv

Acknowledgements vi

Dedication vii

List of Figures xii

List of Tables xvi

1 Introduction 1

1.1 Motivation 1

1.2 Outline of the Thesis 7

1.3 Contributions of the Thesis 8

2 Background 10

2.1 Moore-Greitzer Model 10

2.1.1 Model Derivation 11

2.1.2 Stability Analysis 16

2.1.3 Bifurcation Analysis . . . 18
2.2 Basic QCD Problem Formulations . . . 20
2.3 Bayesian Quickest Change Detection . . . 22
2.3.1 Shiryaev's Problem . . . 22
2.3.2 Bayesian Shiryaev Algorithm . . . 23
2.4 Minimax Quickest Change Detection . . . 24
2.4.1 Lorden's Criterion . . . 24
2.4.2 Page's CUSUM Procedure . . . 25
2.4.3 Threshold Computation for CUSUM Statistics in Change Detection 27
2.5 Simulation Results . . . 28
2.6 Lai's Optimal Detection Theory [49] . . . 29
2.6.1 Generalization of Lorden's Asymptotic Theory . . . 29
2.6.2 Uniform (over k) Lower Bound Under Alternative Performance Criterion . . . 33

3 Quickest Change Detection in HMMs 36
3.1 Change Detection in the Standard Model using Page's CUSUM Procedures 37
3.1.1 An Example Under the i.i.d. Setting . . . 38
3.1.2 The Standard Model . . . 38
3.1.3 Non-standard Models . . . 40
3.2 Change Detection in Nonhomogeneous HMM . . . 41
3.2.1 Time Inhomogeneous HMM . . . 42
3.2.2 Recursive Formula for Filtering . . . 43
3.2.3 Likelihoods . . . 44
3.2.4 Change Points for HMM . . . 44
3.3 Change Detection in Nonlinear HMMs using Particle Filters . . . 47
3.3.1 Nonlinear Change Detection: Problem Setup . . . 47
3.3.2 Construction of the Change Detection Statistics using Particle Filters 48

3.3.3 A Comparison of the Generalized CUSUM and the CUSUM-like Procedure with Instant Change . . . 50
3.4 Change Detection in Moore-Greitzer Model of a Compressor . . . 52
3.4.1 Pure Surge and the QCD Problem Setup . . . 52
3.4.2 QCD in a Deterministic Stable Reduced Planar System . . . 54
3.4.3 QCD in a Deterministic Surge Compressor Model . . . 56
3.4.4 QCD in a Stochastic Surge Compressor model . . . 64

4 Reduced Order Modeling of the Deterministic Moore-Greitzer Compressor Systems 68
4.1 Proper Orthogonal Decomposition . . . 70
4.1.1 Continuous-time POD . . . 71
4.1.2 Operators Γ and $\Gamma^*\Gamma$ . . . 71
4.1.3 Optimization Problem Setup . . . 74
4.1.4 Snapshot Version . . . 77
4.1.5 Computational Scheme . . . 83
4.2 Model Reduction of Deterministic Moore-Greitzer Compressors using POD-Galerkin Procedure . . . 84
4.2.1 Moore-Greitzer Model . . . 85
4.2.2 Representation of POD Basis using Fourier Basis . . . 88
4.2.3 Galerkin Projection using POD Modes . . . 91
4.3 Model Reconstruction using POD-Galerkin with L^2 and H^1 Inner Products 95
4.3.1 Computational Scheme for Calculating the POD Modes in the H^1 Sobolev Space . . . 96
4.3.2 Simulation Results of Reconstructing the Moore-Greitzer PDE solutions using L^2-POD-Galerkin and H^1-POD-Galerkin . . . 97

5 QCD for the Stall Instability of the Compressor Models 103
5.1 Stall Detection in Deterministic Moore-Greitzer PDE Systems . . . 104

5.1.1 Deterministic Moore–Greitzer PDE systems with Disturbances on Compressor Flow and Pressure . . . 104
5.1.2 Stability Analysis with Disturbances d_Φ and d_Ψ . . . 106
5.2 Generalized CUSUM Statistics for Stall Detection in Deterministic Moore–Greitzer PDE System using a POD-Galerkin Procedure . . . 110
5.2.1 Stall Detection: Problem Setup . . . 111
5.2.2 Construction of the Stall Detection Statistics using POD Bases and Particle Filters . . . 112
5.3 Reduced Order Modeling of Stochastic Moore-Greitzer PDE Systems using Extended POD-Galerkin Procedure . . . 116
5.3.1 Stochastic Moore-Greitzer PDE Systems . . . 117
5.3.2 Extended POD Galerkin Projection on the Stochastic Moore-Greitzer Model . . . 119
5.3.3 Snapshot Collection and POD Basis Construction . . . 121
5.4 Stall Detection in Stochastic Moore–Greitzer PDE Systems . . . 123

6 Conclusions and Future Work **135**
6.1 QCD Problems in Nonlinear HMMs . . . 135
6.2 Detection of Stall Instability in the Deterministic and Stochastic Moore-Greitzer PDE Systems . . . 137

References **139**

APPENDICES **148**

A Change Detection in Nonhomogeneous HMM **149**
A.1 Proof of Lemma 3.1.1 . . . 149
A.2 Proof of (3.27) . . . 150

B The POD-Galerkin Procedure on the Moore-Greitzer PDE System **151**

C The Fourier-Galerkin Procedure on the Stochastic Moore-Greitzer PDE System **158**

List of Figures

2.1 A diagram of an aircraft gas turbine engine [66]. 11

2.2 **Left**: A stochastic sequence with observations from $f_0 \sim \mathcal{N}(0,1)$ before the change (time slot 500), and with observations from $f_1 \sim \mathcal{N}(0.1,1)$ after the change. **Right**: Evolution of the CUSUM statistic with the threshold $c = 2.0$. 28

3.1 Scheme of calculating $p(Y_n|Y_1^{n-1})$ for a HMM. 45

3.2 **a)** The evolution of the deterministic signals with a change $(d_\Phi, d_\Psi) = (-0.4, 0.05)$ implanted at $\nu = 150$ **(top left)**. **b)** The evolution of the observations (Ψ_n) corrupted by an additive Gaussian noise **(top right)**. **c)** The generalized CUSUM statistics (i.e., T_n) **(bottom left)** and **d)** the CUSUM statistics that assume an instant change (i.e., $\widehat{T}_n$) **(bottom right)** with 10 ensembles of observations using a particle filtering approach with 50 particles. 55

3.3 Signal Ψ of the purge model for $\nu = 142$ is out of phase (**left**) and for $\nu = 114$ is in phase (**right**) with respect to the phase of Ψ for $\nu = 1$. 57

3.4 **a)** The evolution of the deterministic signals with a change $(d_\Phi, d_\Psi) = (-0.5, 0.5)$ implanted at $\nu = 142$ **(top left)**. **b)** The evolution of the observations (Ψ_n) corrupted by an additive Gaussian noise **(top right)**. **c)** The generalized CUSUM statistics (i.e., T_n) **(bottom left)** and **d)** the CUSUM statistics that assume an instant change (i.e., $\widehat{T}_n$) **(bottom right)** with 10 ensembles of observations using a particle filtering approach with 50 particles. 58

3.5 **a)** The evolution of the deterministic signals with a change $(d_\Phi, d_\Psi) = (-0.5, 0.5)$ implanted at $\nu = 114$ **(top left)**. **b)** The evolution of the observations (Ψ_n) corrupted by an additive Gaussian noise **(top right)**. **c)** The generalized CUSUM statistics (i.e., T_n) **(bottom left)** and **d)** the CUSUM statistics that assume an instant change (i.e., $\widehat{T}_n$) **(bottom right)** with 10 ensembles of observations using a particle filtering approach with 50 particles. 59

3.6 **a)** The evolution of the deterministic signals with a change $(d_\Phi, d_\Psi) = (-0.2, 0.2)$ implanted at $\nu = 150$ **(top left)**. **b)** The evolution of the observations (Ψ_n) corrupted by an additive Gaussian noise **(top right)**. **c)** The generalized CUSUM statistics (i.e., T_n) **(bottom left)** and **d)** the CUSUM statistics that assume an instant change (i.e., $\widehat{T}_n$) **(bottom right)** with 10 ensembles of observations using a particle filtering approach with 50 particles. 60

3.7 **a)** The evolution of the deterministic signals with a change $(d_\Phi, d_\Psi) = (-0.2, 0.2)$ implanted at $\nu = 120$ **(top left)**. **b)** The evolution of the observations (Ψ_n) corrupted by an additive Gaussian noise **(top right)**. **c)** The generalized CUSUM statistics (i.e., T_n) **(bottom left)** and **d)** the CUSUM statistics that assume an instant change (i.e., $\widehat{T}_n$) **(bottom right)** with 10 ensembles of observations using a particle filtering approach with 50 particles. 61

3.8 **a)** The evolution of the stochastic signals with a change $(d_\Phi, d_\Psi) = (-0.5, 0.5)$ implanted at $\nu = 142$ **(top left)**. **b)** The evolution of the observations (Ψ_n) corrupted by an additive Gaussian noise **(top right)**. **c)** The generalized CUSUM statistics (i.e., T_n) **(bottom left)** and **d)** the CUSUM statistics that assume an instant change (i.e., $\widehat{T}_n$) **(bottom right)** with 10 ensembles of observations using a particle filtering approach with 50 particles. 66

3.9 **a)** The evolution of the stochastic signals with a change $(d_\Phi, d_\Psi) = (-0.2, 0.2)$ implanted at $\nu = 150$ **(top left)**. **b)** The evolution of the observations (Ψ_n) corrupted by an additive Gaussian noise **(top right)**. **c)** The generalized CUSUM statistics (i.e., T_n) **(bottom left)** and **d)** the CUSUM statistics that assume an instant change (i.e., $\widehat{T}_n$) **(bottom right)** with 10 ensembles of observations using a particle filtering approach with 50 particles. 67

4.1 The evolution of the deterministic ODE, i.e., (Φ, Ψ), with a limit cycle behavior **(left)**, and the evolution of the deterministic PDE over time t towards a steady state at two fixed values of θ **(right)**. 86

4.2 The evolution of the deterministic ODE, i.e., (Φ, Ψ) towards the steady states **(left)**, and the evolution of the deterministic PDE over time t with oscillations at two fixed values of θ **(right)**. 87

4.3 POD modes $U_\alpha(\theta)$ **(left)** and POD coefficients $q_\alpha(t)$ **(right)**. 90

4.4 The POD reconstructions (with a Galerkin procedure) using different numbers of POD modes of the deterministic PDE of $g(t, \theta_2)$ represented by 128 Fourier modes. 99

4.5 The POD reconstructions using 8 POD modes with L^2-Galerkin procedure (**left**) and H^1-Galerkin procedure (**right**) of the deterministic PDE of $g(t, \theta_2)$ represented by 128 Fourier modes. 101

4.6 The POD reconstructions using 4 POD modes with L^2-Galerkin procedure (**left**) and H^1-Galerkin procedure (**right**) of the deterministic PDE of $g(t, \theta_2)$ represented by 128 Fourier modes. 102

4.7 The L^2 errors of the POD reconstructions without (**left**) and with (**right**) the Galerkin projection compared to the real PDE solution of the Moore-Geitzer model using 128 Fourier modes at a fixed value of θ. 102

5.1 The evolution of the deterministic ODE, i.e., (Φ, Ψ) **(left)**, and the evolution of the deterministic PDE over time t with the change happening at $k = 100$ at two fixed values of θ **(right)**. 109

5.2 The evolution of the deterministic ODE, i.e., (Φ, Ψ) **(left)**, and the evolution of the deterministic PDE over time t with the change happens at $k = 200$ at two fixed values of θ **(right)**. 110

5.3 The evolution of the ODE, i.e., (Φ, Ψ) **(left)**, and the evolution of the stochastic PDE over time t with the change happening at $k = 100$ at two fixed values of θ **(right)**. 123

5.4 The POD reconstructions of the stochastic data $g(t, \theta_1)$ and $g(t, \theta_{32})$ using 4 *in situ* POD modes (**left**) and using 4 *a priori* POD modes (**right**). . . . 128

5.5 The POD reconstructions of the stochastic data $g(t, \theta_1)$ and $g(t, \theta_{32})$ using 6 *in situ* POD modes (**left**) and using 6 *a priori* POD modes (**right**). . . . 129

5.6 The first 6 *in situ* POD modes directly generated from the snapshots with additive noise. 130

5.7 The first 6 *a priori* POD modes directly generated from the deterministic snapshots with complex limit cycle behaviors. 131

5.8 The generalized CUSUM statistics (i.e., T_n) and the CUSUM statistics that assume an instant change (i.e., $\widehat{T}_n$) with 6 ensembles of observations using a particle filtering approach with 100 particles, 6 *in situ* and *a priori* POD modes and $V_n \sim \mathcal{N}(0, 0.04)$. 132

5.9 The generalized CUSUM statistics (i.e., T_n) and the CUSUM statistics that assume an instant change (i.e., $\widehat{T}_n$) with 6 ensembles of observations using a particle filtering approach with 100 particles, 6 *in situ* and *a priori* POD modes and $V_n \sim \mathcal{N}(0, 0.09)$. 133

5.10 The generalized CUSUM statistics (i.e., T_n) and the CUSUM statistics that assume an instant change (i.e., $\widehat{T}_n$) with 6 ensembles of observations using a particle filtering approach with 100 particles, 6 *in situ* and *a priori* POD modes and $V_n \sim \mathcal{N}(0, 0.16)$. 134

List of Tables

2.1 Table of average run length (ARL) of CUSUM statistics T_n over 100 trials for different threshold values. 27

3.1 The key parameter values used in all the simulations of the pure surge modes of the compressor system. 54

4.1 Comparisons of the mean squared errors of $\mathcal{E}^2_{L^2}(g, g_{\text{POD}})$, $\mathcal{E}^2_{L^2}(g, g_{\text{pod}})$, and $\mathcal{E}^2_{H^1}(g, g_{\text{pod}})$ for $\epsilon_1 = 0.01$, $\epsilon_2 = 0.004$, $\epsilon_3 = 0.002$ and $\epsilon_4 = 0.001$. 101

Chapter 1

Introduction

1.1 Motivation

Gas turbine engines are critical components in various fields, from aviation to power generation, and the compressors within these engines play a key role in their performance. In a large number of applications of engine compressors, it is crucial both to track the system state and to determine whether or not it has entered or is approaching a new dynamic mode in real-time. As such, this thesis is motivated to study the change detection theory and algorithms to address anomaly detection in engine compressors. One of the most studied compressor models is the Moore-Greitzer model [61], which captures the dynamic behavior of axial flow compressors in jet engines. This model is especially valuable for understanding the phenomena of compressor stall and surge [38, 44], which can severely compromise engine efficiency and safety. Modern engines are designed to operate at their peak performance. As such, any deviation from normal operating conditions must be detected as early as possible to prevent catastrophic failure or efficiency losses. The *quickest change detection* (QCD) [94] problem arises in this context, where the objective is to detect the onset of anomalies, such as surge or rotating stall, quickly and accurately. Compressors in gas turbines are susceptible to instabilities that can lead to system-wide failures. Quick detection of changes in operational regimes, such as approaching stall conditions, allows for immediate intervention, thus preventing mechanical damage or even complete system failure.

The problem of detecting abrupt changes in stochastic systems and time series, often referred to as the QCD problem, has attracted extensive attention over the past decades. This includes diverse applications in science and engineering, such as radio location [81],

quality control engineering [54], and surveillance monitoring [32]. In such a problem, there is usually an unknown change that happens in the statistical properties of the stochastic processes during the period of observation. The observations are obtained sequentially, and as long as their behavior is consistent with the normal or "in-control" state, it is desirable to let the process continue. If the system deviates from the normal state or enters an "out-of-control" state, then it is imperative to detect the change as rapidly as possible and take any necessary action while limiting the risk of false alarms. The objective of the QCD problem is to detect the change-point as soon as possible under a false alarm constraint. As such, the QCD problem is also considered an optimization problem that aims to find the best trade-off between detection delay and false alarms (see, for example, [94]).

The quickest change detection problem for finding a change in a stochastic dynamical system has been investigated for more than sixty years since the seminal work of Page [65] and Shiryaev [80]. In general, there are two classical formulations of the QCD problem, namely *Bayesian formulation* and *Non-Bayesian formulation*, and the difference between these two formulations is essentially based on distinct assumptions on the change-point and optimality criteria for detection delay and false alarms. In the Bayesian formulation, the change point is treated as a random variable with a given prior distribution, and the original work involved with this formulation dates from the 1960s when Shiryaev studied a sequence of independent identically distributed (i.i.d.) observations provided that the change point is assumed as a geometric random variable [80]. The optimal solution to Shiryaev's problem was proposed by Shiryaev in [80, 82]. Since then, a number of generalized versions of the Bayesian formulation, where the observations are non-i.i.d. or the change time is assumed to be a uniform improper distribution, have been investigated with some special applications discussed in [92, 69, 81]. In fact, it is quite challenging to derive an exact optimal solution for the associated Bayesian QCD problem when the observations are non-i.i.d. To that end, the general Bayesian *asymptotic* theory was studied by Tartakovsky and Veeravalli, and the detailed asymptotic results of the generalized Bayesian QCD problem can be found in [92].

Bayesian quickest change detection is powerful because it incorporates prior knowledge of the change point and provides a probabilistic framework for decision-making, making it suitable for dynamic environments. However, this prior knowledge of the process change is usually not available in the case of anomaly detection in engine compressors. This motivates us to study the detection theory and the QCD procedure in non-Bayesian settings, in particular, the *minimax formulation*, where the stopping rule minimizes the worst-case detection delay while ensuring that false alarms rarely occur. In the *minimax formulation*, the change point is modeled as an unknown but deterministic variable. This formulation of the QCD problem has been widely explored in many applications, including but not

limited to sensor networks [8, 63] and climate change detection [73], where no prior knowledge about the change point is available to the decision maker. For this non-Bayesian formulation, there are two well-known criteria proposed by Lorden [54] and Pollak [67]. In [54], Lorden showed that Page's cumulative sum (CUSUM) procedure [65] is asymptotically optimal for Lorden's criterion, which will be discussed and elaborated in Chapter 2. Later, Moustakides [62] and Ritov [75] proved that the CUSUM procedure is indeed exactly optimal for Lorden's formulation. In [67], Pollak considered another performance metric of detection delay and studied the corresponding minimax QCD problem named *Pollak's problem* under the i.i.d. setting. The algorithms based on the Shiryaev-Roberts statistic [91] provide asymptotically optimal solutions as fewer false alarms are accepted for Pollak's problem. In [49], for a non-i.i.d. setting, Lai showed a generalized version of the CUSUM algorithm and extended the minimax asymptotic results for both Lorden's and Pollak's criteria.

In fact, Lorden's criterion ensures robustness by minimizing the worst-case detection delay, making it particularly well-suited for applications such as surge or rotating stall detection in gas turbine compressors, where delays in detecting surge or rotating stall onsets can lead to severe engine failure. Additionally, Lorden's criterion does not assume a specific distribution for the surge or stall onset time, making it more robust to unpredictable surge or stall events. This motivates us to investigate the instability detection of the Moore-Greitzer PDE model under the minimax formulation with Lorden's optimal detection theory. In Lorden's optimal detection theory [54], all random variables, including the observation signals and the associated log-likelihood ratios (LLR), are independent and identically distributed (i.i.d.). Under this i.i.d. setting, the CUSUM rule is defined in terms of partial sums of the LLR, and one is looking for a stopping time at which the statistic exceeds a certain threshold. On the other hand, Lai considered the case in [49] where the observation signal is no longer a sequence of i.i.d. random variables, and showed a generalized version of the CUSUM algorithm is asymptotically optimal, with respect to the worst average detection delay, when the average run length goes to infinity. Indeed, this generalization of the CUSUM, represented as T_n in this thesis, is defined as the maximum of the LLR over all possibilities of the change point k from 1 to the current time n, where the corresponding LLR involves the comparison of the probability distributions for the change occurring at k and without change. A large number of iterative computations are needed to test each possibility of the post-change distribution and then evaluate the relevant LLR for every $n = 1, 2, \cdots$. A computationally easier replacement, denoted as $\widehat{T}_n$ here, is proposed by Fuh in [33], and it compares the scenario that the change occurring immediately with the case that there is no change. More detailed definitions and expressions for T_n and $\widehat{T}_n$ can be found in Chapter 3.

In many real-world applications of QCD, the original signals or states of a system contaminated by some unknown change are usually inaccessible to the detector. However, observations are functions of states that can be obtained and utilized. The application considered in this thesis is an example of such a QCD problem. This motivates us to study the QCD problems in hidden Markov models (HMMs), which typically consist of the underlying Markov process X governed by a stochastic differential equation (SDE) with linear or nonlinear drift, and an observational process Y, which is corrupted by a random process. Consider a discrete-time hidden Markov model where the signal X_n and observations Y_n, $n \geq 0$, satisfy the following stochastic dynamics,

$$\begin{aligned} X_n &= \begin{cases} f(X_{n-1}, \theta_0) + U_n, & n < k, \\ f(X_{n-1}, \theta_1) + U_n, & n \geq k, \end{cases} \\ Y_n &= h(X_n) + V_n, \end{aligned} \tag{1.1}$$

where k represents the change point, and θ_0 and θ_1 indicate that the state process is in the pre-change and post-change regimes, respectively; f and h have the proper dimensions. U_n and V_n are i.i.d. random processes with some known densities. Chen and Willett previously investigated the detection of changes in hidden Markov models (HMMs) in [21] and [22], and sought a CUSUM-like procedure based on the sequential probability ratio test (SPRT) [99] for the non-i.i.d. case and explored detection of HMM transient signals.

A specific QCD application in HMM that draws much of our attention is relevant to health management [97] and anomaly detection [23] in engine compressor systems [38, 61], from which the associated HMMs in (1.1) can be well characterized. Notice that the change is only added in the hidden signals, but can be indirectly reflected in the observational process. The key issue is what happens to the state X_k at the time of the change. To address this issue, Fuh [33] uses the statistic $\widehat{T}_n$, although it appears that he is considering two HMMs with different parameters. Up to time $k-1$ we observe for the first HMM, and from time k onwards we observe from the second HMM. This seems equivalent to considering two engines—one with a bird stuck in it and the other without (see Section 3.4.1). At time k, we switch from observing the engine without the bird to observing the engine with the bird. However, this is not the physical model that we are focused on in this thesis. In [34], Fuh investigated the QCD problem in the dynamic system of HMMs, and the formula he used for the likelihood ratio (i.e., LR_n^k) depends on the state x_{k-1} (corresponding to Fuh's notation), where k represents the change point. Notice that the distribution of the state x_{k-1} must be estimated from the observations up to time $k-1$ using the pre-change parameter values, not the post-change parameter values. This is why the post-change transition densities of the observation at time n given all the past observations for $n \geq k$ depend on the change point k and on n. Thus, the standard model

(see Section 3.1.2) studied in [90, 49, 92] does not apply to the QCD problems in the HMMs related to the engine compressor models. Furthermore, Fuh and Mei provide a somewhat more detailed discussion of the transition in [35]. One scenario describes the state process at the change point k with some given distribution independent of all the pre-change states and observations. The other scenario uses the changed Markov transition probabilities to determine how the signal or state at time k depends on the corresponding signal at $k-1$. In this thesis, we are interested in the second scenario, though the first scenario may be mathematically easier. They observe that for asymptotic results, the precise distribution of X_k should not matter much.

Over the past decades, state estimation of stochastic hidden signals from observational data has attracted much attention in different fields of science and engineering. However, real-world random dynamical systems studied in many QCD applications, such as jet engine anomaly diagnosis, typically involve some nonlinear drifts with a sudden additive change. The QCD problems in the nonlinear HMMs constructed from these underlying signals have not been extensively studied and deeply understood beyond linearizations. One major difficulty results from the lack of robust and accurate likelihood ratio approximation that characterizes the asymptotically optimal detector using the generalized CUSUM procedure. To address this issue, it is natural to recall nonlinear filtering techniques that provide recursive algorithms for approximating the conditional density of the state variables. As one of the most well-established numerical schemes for the nonlinear filter, particle methods [3] are a powerful tool to approximate the prior and posterior distributions of nonlinear stochastic processes. Therefore, we can use it to estimate the log-likelihood ratio given in the generalized CUSUM statistic for the QCD problems in nonlinear HMMs. The asymptotic optimality of the generalized CUSUMs with likelihoods estimated by a particle filtering approach has been studied in [96]. Azimi-Sadjadi and Krishnaprasad proposed a particle filtering approach to change detection for nonlinear systems in [5], and modified the CUSUM detection statistic such that the intensive computational complexity in the particle filter implementation is reduced. However, the recursiveness of the modified statistic given in [5] is based on knowing the probability of change at time n conditioned on no change before n. This probability is not always easily evaluated or specified, especially in the QCD problems in the engine compressor model. So it is still essential to test the effectiveness of the original non-recursive CUSUM algorithm and compare it with the recursive CUSUM statistic that assumes an instant change, to find some insightful compromise for the computational efficiency and theoretical accuracy of the change detection procedures [12].

Note that we assume there is no prior knowledge of the unknown change point k, and the pre- and post-change distributions are completely specified. This thesis focuses on

tests with statistics to detect the change in such HMMs that can be computed iteratively as new data arrives. Such QCD tests are constructed by exploiting the general asymptotic framework introduced in [49], following the procedure for detecting changes in HMMs introduced in [34] and imposing the particle filters detection algorithm investigated in [1, 5, 96].

Although the CUSUM-based change detection technique and its generalization are well-established in statistical theory, applying these methods to the nonlinear dynamics of compressors, as described by the Moore-Greitzer model, introduces new challenges. First of all, the Moore-Greitzer model, although simplified, retains sufficient fidelity to represent real-world engine compressor systems. The semi-group property of the Moore-Greitzer model suggests that the PDE evolution can be efficiently captured in Fourier space using Fourier spectral methods [104, 59]. This allows for theoretical advancements in analyzing the Moore-Greitzer model, particularly in understanding stability, bifurcations, and the long-term behavior of solutions. However, the dimensionality of the Fourier-Galerkin transformed equations remains insufficiently reduced to facilitate the effective implementation of the generalized CUSUM algorithm using particle filters. This motivates us to investigate the reduced order modeling (ROM), based on the projection of state variables on a low-dimensional subspace, which is a promising tool for significantly alleviating computational costs [2, 24]. Bases for this subspace are typically constructed by proper orthogonal decomposition (POD) [84, 20] of a set of high-fidelity solution snapshots. POD was initially introduced in fluid dynamics by Lumley [56] to extract coherent structures from turbulent flows. It provides an optimal basis for representing a given dataset by maximizing the variance captured by each successive mode. The key idea is to decompose a large and complex system into a set of orthonormal modes ranked by their energetic contribution. In Chapter 4, we first expand the functional analytic framework of POD introduced in [26] and apply it to our Moore-Greitzer PDE model. We also rigorously show how to characterize compressor instabilities, in particular, the stall bifurcations, using POD-Galerkin procedures with L^2 and H^1 inner products. Further error analysis and discussion regarding the POD reconstruction of the PDE evolutions are given at the end.

On the other hand, real-world compressor systems are subject to disturbances in mass flow rate and pressure. The nonlinear nature of the Moore-Greitzer model implies that a small number of these disturbances can grow into significant instabilities in the PDE component of the Moore-Greitzer model, causing a stall bifurcation for the compressor systems. This growth of the stall instability becomes much faster when there is a small additive noise given in the PDE part of the Moore-Greitzer model. Consequently, Chapter 5 of this thesis is motivated to first deal with reduced order model design using POD based on the stochastic Moore-Greitzer PDE model with additive noise. This facilitates the

conduct of numerical experiments in the context of generalized CUSUM tests employing particle filters, thereby enabling their direct testing and validation in practical applications for detecting stall instability within the deterministic and stochastic Moore-Greitzer PDE models.

1.2 Outline of the Thesis

The outline of this thesis is as follows. Chapter 1 gives an introduction to this thesis. Chapter 2 introduces the Moore-Greitzer PDE model, the stability and bifurcation analysis of the model, and the mathematical background of the CUSUM procedures applied to the QCD problems.

In Chapter 3, we present how filtering is imposed to approximate the change detection statistics in time inhomogeneous HMMs, and explain why the standard model does not apply to the QCD problems in our HMMs. A particular example of constructing the generalized CUSUM procedure using particle filters is also given in this chapter. From a theoretical perspective, this chapter succinctly discusses the differences and similarities between the generalized CUSUM and the CUSUM-like procedure with instant change. For simulations, we implement these CUSUM rules in the QCD problems with a surge-like onset in the Moore-Greitzer compressor model, and test their performances in different scenarios.

Chapter 4 develops reduced order modeling of the deterministic Moore-Greitzer model using proper orthogonal decomposition. The conceptual framework of the dimension reduction without assuming ergodicity is expanded in this chapter. We explore the representation of POD bases using Fourier bases so that the reduced order equation of ODEs for the Moore-Greitzer PDE model can be derived. The simulations and error analysis for reconstructing the Moore-Greitzer PDE model using POD-Galerkin with L^2 and H^1 inner products are also discussed in this chapter.

In Chapter 5, we examine the effectiveness of the generalized CUSUM statistics using particle filters to detect the stall instability in the reduced-order deterministic Moore-Greitzer model. A stochastic version of the Moore-Greitzer PDE model with additive noise is studied as the disturbances incorporated in the ODE component induce the stall instability of the stochastic PDE component with less delay.

1.3 Contributions of the Thesis

In this section, we summarize the main contributions of this thesis:

One of the main contributions of this thesis is to present a detailed mathematical formulation of change detection in non-homogeneous HMMs. Additionally, this thesis aims to provide an explanation from a filtering theory perspective on why the standard model primarily studied in [36, 90, 49, 92] does not apply to the QCD problems in our nonlinear HMMs (e.g., surge and rotating stall instabilities of engine compressor models excited by external forcing). In [35], Fuh and Mei mentioned that $\widehat{T}_n$ usually works well even though T_n theoretically incorporates the true post-change measures. However, the HMM conditional likelihood-based change detection was studied in [25] and considered to outperform the relevant CUSUM. To the best of our knowledge, detecting the onset of instability in random dynamical systems using T_n and $\widehat{T}_n$ has not been widely studied. To this end, other contributions of this thesis involve two general studies of the QCD problems from a dynamical system perspective:

1. Surge detection:

   (i) From a pre-change steady state to a post-change steady state with a few transients in between:

   - Under the mean field deviation scenario, the expected closeness between the CUSUM procedure that assumes an immediate change and the generalized CUSUM rule that depends on where the change point possibly occurs is tested and verified.
   - We observe that the detection delay caused by the CUSUM statistic assuming instant change depends on whether the post-change transient dynamics go towards the same direction as the post-change steady state.

   (ii) From a pre-change steady state to a post-change stable limit cycle:

   - Both the phase and the range of post-change cycles are raised and considered key factors affecting the performance of $\widehat{T}_n$. Some similarities for the performance of T_n and $\widehat{T}_n$ under the "in phase" cases are observed and analyzed.
   - The sensitivity of $\widehat{T}_n$ in terms of different phases of the post-change limit cycles is experimentally validated. In particular, the spiking oscillations given by $\widehat{T}_n$ in the "out of phase" cases are clarified and compared to the robust performance of the proposed generalized CUSUM procedure T_n.

2. Stall detection:

   (i) We develop reduced order modeling of the deterministic Moore-Greitzer model using proper orthogonal decomposition.

   - This study investigates the depiction of POD bases employing Fourier series, facilitating the derivation of reduced-order equations pertinent to the Moore-Greitzer PDE model using a POD-Galerkin procedure.
   - Expand the conceptual framework of the POD technique without assuming ergodicity.
   - Analyze and compare the error of reconstructing the Moore-Greitzer PDE model using POD-Galerkin with L^2 and H^1 inner products.

   (ii) We examine the effectiveness of the generalized CUSUM statistics using particle filters to detect the stall instability in the reduced-order deterministic Moore-Greitzer model.

   - Reduced order model design using deterministic POD modes for the stochastic Moore-Greitzer PDE model with additive noise.
   - The POD reconstruction of the stochastic Moore-Greitzer PDE model using the stochastic *in situ* POD modes and deterministic *a priori* POD modes yields similar approximation results.
   - The simulation results illustrate that the generalized CUSUM statistics are more effective to detect the stall instability and more robust with respect to various observations and POD modes when compared to the recursive CUSUM-like procedure, which presumes an abrupt change.

Chapter 2

Background

2.1 Moore-Greitzer Model

The Moore-Greitzer compressor model is a widely recognized tool in the study of the performance and stability of centrifugal compressors. [61] introduces the original set of equations modeling airflow through compression systems, laying the groundwork for subsequent studies. This model focuses on understanding the complex dynamics of compressor flow, and the study in [15] establishes the existence of a unique global solution to the Moore-Greitzer PDE model, demonstrating that the system possesses a finite-dimensional global attractor. Xiao and Başar [104] analyze the center manifold of the viscous Moore-Greitzer model, facilitating a reduction of the infinite-dimensional system to a finite-dimensional one for further analysis. The research in [103] offers a quantitative analysis of rotating stall and surge phenomena within the Moore-Greitzer PDE framework, enhancing the understanding of compressor instabilities. The authors in [60] conduct a multi-scale analysis near deterministic stall bifurcation points in the presence of additive noise, providing insights into instability margins under uncertainties.

There are typically two types of instabilities that occur in the flow through the compressor: surge and stall (rotating stall). Both surge and stall in a compression system are self-excited instabilities involving an interaction between the compressor and associated ducts.

- **Surge instability:** Surge is characterized by large amplitude oscillations of annulus-averaged mass flow through the engine and plenum pressure rise. Essentially, one-dimensional surge cycles take one of two forms: (i) in mild surge, the mass flow and

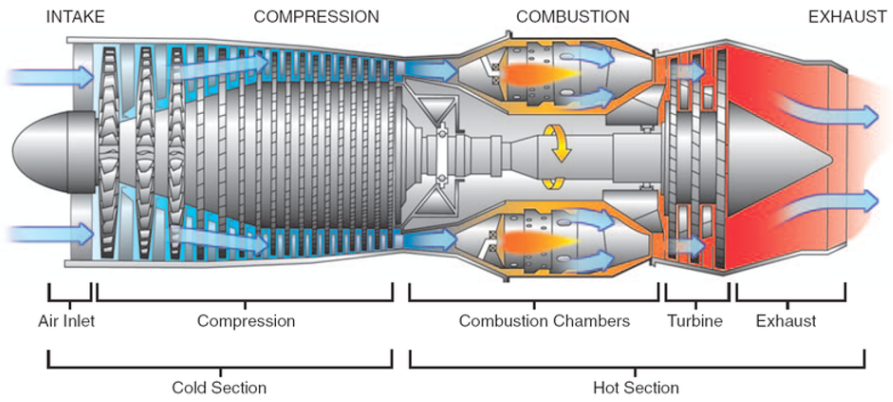


Figure 2.1: A diagram of an aircraft gas turbine engine [66].

plenum pressure fluctuate near the system Helmholtz frequency, but the mass flow never reverses; (ii) in deep surge, the annulus-averaged mass flow does the reverse and the frequency is lower. During part of the cycle, the mean-mass flow may reverse during the instability, thrusting air out from the front of the engine. The frequency in this mode is associated with repeated blowdown and repressurization of the plenum. This puts a large stress on the components of the engine and seriously impairs its performance.

- **Rotating stall instability:** Moore and Greitzer [61] clarified and redefined the problem of rotating stall of axial flow compressors. At low flows, virtually all compressors exhibit zones of stalled flow which propagate tangentially, with blade passages cyclically stalling and recovering. Hence, when stall occurs, there are regions of relatively low airflow that form at isolated locations around the rim of the compressor. In this context, the phenomenon can become sufficiently pronounced to induce a reversal of flow within these isolated regions. Therefore, this places substantial stress on engine components and diminishes overall performance.

2.1.1 Model Derivation

The Moore-Greitzer model presupposes a high hub-to-tip ratio, which is slightly less than, yet nearly equal to one, indicating that the blades are relatively short in relation to the hub radius. Consequently, as the radial variations are insubstantial, the compression system may be effectively modeled as two-dimensional, defined by the axial and angular coordinates. Let θ, η, t represent the circumferential coordinate, axial coordinate, and time,

respectively.

At the inlet, an irrotational flow is assumed, that is, the velocity potential $\varphi(t,\theta,\eta)$ satisfies Laplace's equations. Furthermore, the velocity potential $\varphi(t,\theta,\eta)$ is decomposed as

$$\varphi(t,\theta,\eta) = \Phi(t) + \varphi'(t,\theta,\eta), \tag{2.1}$$

where $\varphi'(t,\theta,\eta)$ is the disturbance velocity from the mean flow at the entrance duct given by

$$\Phi(t) = \frac{1}{2\pi}\int_0^{2\pi} \varphi(t,\theta,0)d\theta.$$

The Moore-Greitzer model of a compressor is comprised of two ordinary differential equations in non-dimensionalized time t for mean axial flow $\Phi(t)$ and pressure rise coefficient $\Psi(t)$

$$\frac{d\Phi(t)}{dt} = \frac{1}{l_c}\left(-\Psi(t) + \frac{1}{2\pi}\int_0^{2\pi} \psi_c(\Phi(t) + \varphi'(t,\theta,\eta)|_{\eta=0})d\theta\right) \tag{2.2}$$

$$\frac{d\Psi(t)}{dt} = \frac{1}{4B^2 l_c}(\Phi(t) - F_T^{-1}(\Psi(t))) \tag{2.3}$$

coupled with a partial differential equation for upstream disturbance velocity $\varphi'(t,\theta,\eta)$ which satisfies Laplace's equation

$$\varphi'_{\theta\theta}(t,\theta,\eta) + \varphi'_{\eta\eta}(t,\theta,\eta) = 0, \quad (\theta,\eta) \in [0,2\pi] \times (-\infty, 0) \tag{2.4}$$

subject to the boundary conditions

$$\lim_{\eta\to-\infty} \varphi'(t,\theta,\eta) = 0 \tag{2.5}$$

and

$$\left[m\varphi'_t + \frac{1}{a}\varphi'_{t\eta} - \psi_c(\Phi + \varphi'_\eta) + \frac{1}{2\pi}\int_0^{2\pi} \psi_c(\Phi + \varphi'_\eta)d\theta + \frac{1}{2a}\varphi'_{\theta\eta} - \frac{\nu}{2a}\varphi'_{\eta\theta\theta}\right]_{\eta=0} = 0 \tag{2.6}$$

where a is the internal compressor lag, m is the duct parameter and ψ_c is the compressor characteristic function

$$\psi_c(\varphi) = \psi_{c0} + H\left(1 + \frac{3}{2}\left(\frac{\varphi}{W} - 1\right) - \frac{1}{2}\left(\frac{\varphi}{W} - 1\right)^3\right), \tag{2.7}$$

where ψ_{c0} is a shut-off value parameter, $H > 0$ is the semiheight parameter, and $W > 0$ is the semiwidth parameter. The inverse of the throttle characteristic function is given by

$$F_T^{-1}(\Psi(t)) = \gamma\sqrt{\Psi(t)}.$$

We assume that the initial conditions $\Phi(t=0)=\Phi_0$, $\Psi(t=0)=\Psi_0$, and $\varphi(t=0,\theta,\eta)=\varphi'_0(\theta,\eta)$ are provided. The disturbance velocity $\varphi'(t,\theta,\eta)$, which is periodic in θ, vanishes as $\eta\to-\infty$, and the Laplace's equation has a solution of the form

$$\varphi'(\theta,t,\eta)=\sum_{n\in\mathbb{Z}\setminus\{0\}}\tilde{\varphi}_n(t)e^{|n|\eta+in\theta}, \tag{2.8}$$

where i represents the imaginary unit of complex numbers. Notice that the constant solution, which is associated with $n=0$ in (2.8), will not satisfy the far field boundary condition, $\varphi'(t,\theta,\eta=\infty)=0$, and cannot be part of the solution of (2.4).

Definition 2.1.1. *Let $\breve{L}^2(0,2\pi)$ be the space of all square integrable 2π-periodic functions with* **zero average***, that is,*

$$\int_0^{2\pi}\varphi(\theta)d\theta=0 \quad \textit{for any } \varphi\in\breve{L}^2(0,2\pi),$$

its Fourier series is

$$\varphi(\theta)=\sum_{n\in Z\setminus\{0\}}\tilde{\varphi}_n e^{in\theta}, \quad \textit{where} \quad \tilde{\varphi}_n=\int_0^{2\pi}\varphi(\theta)e^{-in\theta}d\theta.$$

It follows from (2.8) that

$$\varphi'_\eta(\theta,t,\eta)=\sum_{n\in\mathbb{Z}\setminus\{0\}}|n|\tilde{\varphi}_n(t)e^{|n|\eta+in\theta}.$$

Then, we write the first two terms of (2.6) as follows,

$$\begin{aligned}
&\frac{\partial}{\partial t}\left(m\varphi'+\frac{1}{a}\varphi'_\eta\right)\Big|_{\eta=0}=m\frac{\partial\varphi'}{\partial t}+\frac{1}{a}\frac{\partial\varphi'_\eta}{\partial t}\Big|_{\eta=0}\\
&=m\sum_{n\in\mathbb{Z}\setminus\{0\}}\frac{\partial}{\partial t}\tilde{\varphi}_n(t)e^{|n|\eta+in\theta}+\frac{1}{a}\frac{\partial}{\partial t}\left(\sum_{n\in\mathbb{Z}\setminus\{0\}}|n|\tilde{\varphi}_n(t)e^{|n|\eta+in\theta}\right)_{\eta=0}\\
&=\sum_{n\in\mathbb{Z}\setminus\{0\}}\left(m+\frac{|n|}{a}\right)\frac{\partial\tilde{\varphi}_n(t)}{\partial t}e^{|n|\eta+in\theta}\Big|_{\eta=0}\\
&=\frac{1}{a}\sum_{n\in\mathbb{Z}\setminus\{0\}}\left[\left(1+\frac{ma}{|n|}\right)|n|\frac{\partial\tilde{\varphi}_n(t)}{\partial t}e^{|n|\eta+in\theta}\right]_{\eta=0}.
\end{aligned}$$

As such, the first two terms of the left-hand side of the boundary condition (2.6) simplify to

$$\frac{\partial}{\partial t}\left(m\varphi' + \frac{1}{a}\varphi'_\eta\right)\Big|_{\eta=0} = \frac{1}{a}\sum_{n\in\mathbb{Z}\setminus\{0\}}\left(1+\frac{ma}{|n|}\right)|n|\frac{\partial\tilde{\varphi}_n(t)}{\partial t}e^{in\theta}$$

We define the circumferentially varying velocity of upstream disturbance, i.e., $\frac{\partial\varphi'}{\partial\eta}|_{\eta=0}$ along the axial direction at the inlet, as

$$g(t,\theta) = \varphi'_\eta(t,\theta,\eta)\Big|_{\eta=0} = \sum_{n\in\mathbb{Z}\setminus\{0\}}|n|\tilde{\varphi}_n(t)e^{in\theta}. \tag{2.9}$$

From (2.8) and (2.9), we can rewrite the rest of (2.6) as

$$\frac{1}{a}\sum_{n\in\mathbb{Z}\setminus\{0\}}\left(1+\frac{ma}{|n|}\right)|n|\frac{\partial\tilde{\varphi}_n(t)}{\partial t}e^{in\theta} = \psi_c(\Phi(t)+g(t,\theta)) - \bar{\psi}_c(t) - \frac{1}{2a}g_\theta(t,\theta) + \frac{\nu}{2a}g_{\theta\theta}(t,\theta), \tag{2.10}$$

where

$$\bar{\psi}_c(t) := \bar{\psi}_c(\Phi(t), g(t)) = \frac{1}{2\pi}\int_0^{2\pi}\psi_c(\Phi(t)+g(t,\theta))d\theta. \tag{2.11}$$

Now we need to write the left-hand side of (2.10) in terms of the time derivative of the upstream disturbance velocity $g(t,\theta)$. To this end, we introduce a linear operator $K : \breve{L}^2(0,2\pi) \to \breve{L}^2(0,2\pi)$. More precisely, given a function $\varphi(t,\theta) = \sum_{n\in Z\setminus\{0\}}\tilde{\varphi}_n(t)e^{in\theta}$, define the operator K such that

$$K(\varphi) = K(\sum_{n\in\mathbb{Z}\setminus\{0\}}\tilde{\varphi}_n e^{in\theta}) = \sum_{n\in\mathbb{Z}\setminus\{0\}}\left(1+\frac{ma}{|n|}\right)\tilde{\varphi}_n\, e^{in\theta}, \tag{2.12}$$

and

$$K(e^{in\theta}) = \left(1+\frac{ma}{|n|}\right)e^{in\theta}$$

for $n \neq 0$. Then K can be extended as a positive definite self-adjoint linear operator on $\breve{L}^2(0,2\pi)$. Making use of the inlet velocity

$$g(t,\theta) = \sum_{n\in\mathbb{Z}\setminus\{0\}}|n|\tilde{\varphi}_n(t)e^{in\theta}$$

and acceleration

$$\frac{\partial g(t,\theta)}{\partial t} = \sum_{n\in\mathbb{Z}\setminus\{0\}}|n|\frac{\partial\tilde{\varphi}_n(t)}{\partial t}e^{in\theta},$$

we can express the left-hand side of (2.10) in terms of the operator K as

$$\frac{\partial}{\partial t}\left(m\varphi' + \frac{1}{a}\varphi'_\eta\right)\Big|_{\eta=0} = \frac{1}{a}\sum_{n\in\mathbb{Z}\setminus\{0\}}\left(1+\frac{ma}{|n|}\right)|n|\frac{\partial\tilde{\varphi}_n(t)}{\partial t}e^{in\theta} = \frac{1}{a}K\left(\frac{\partial g}{\partial t}\right). \tag{2.13}$$

Now, we can rewrite (2.10) as

$$\frac{1}{a}K\frac{\partial g}{\partial t}(t,\theta) = \psi_c(\Phi(t)+g(t,\theta)) - \bar{\psi}_c(t) - \frac{1}{2a}g_\theta(t,\theta) + \frac{\nu}{2a}g_{\theta\theta}(t,\theta) \tag{2.14}$$

by also defining $\bar{\psi}_c(t)$ by (2.11). Manipulating the above equations yields the following PDE

$$\frac{\partial g}{\partial t}(t,\theta) = K^{-1}\left(\frac{\nu}{2}\frac{\partial^2 g}{\partial\theta^2} - \frac{1}{2}\frac{\partial g}{\partial\theta}\right) + aK^{-1}(\psi_c(\Phi(t)+g(t,\theta)) - \bar{\psi}_c(\Phi,g)), \tag{2.15}$$

where the inverse K^{-1} is well defined and has an explicit formula on any finite linear combination of functions of the form $e^{in\theta}$. Precisely, for any finite subset $I \in (\mathbb{Z}\setminus\{0\})$ we have

$$K^{-1}\left(\sum_{n\in I}c_n e^{in\theta}\right) = \sum_{n\in I}\left(\frac{|n|}{|n|+ma}\right)c_n e^{in\theta}. \tag{2.16}$$

Remark 2.1.1. *For every time $t\in[0,\infty)$, the solution $g(t,\cdot)$ lies in $\mathcal{H}$ which is an infinite-dimensional Hilbert space, $\mathcal{H} := \breve{L}^2(0,2\pi) = \left\{g\in L^2 : \int_0^{2\pi} g(\theta)d\theta = 0\right\}$ equipped with the inner product $\langle\cdot,\cdot\rangle_{\mathcal{H}}$ as well as the induced norm $\|\cdot\|_{\mathcal{H}}$. Let us also define $L^2([0,\infty),\mathcal{H})$ as a space of functions for $g(t,\theta)$. Note that $L^2([0,\infty),\mathcal{H})$ contains the set of functions $g(t,\theta)$ such that the mapping $t\mapsto g(t,\cdot)$ is an L^2 mapping of $[0,\infty)$ to $\mathcal{H}$.*

Combining (2.15) with the ODE system (i.e., (2.2) and (2.3)) yields the following deterministic viscous Moore-Greitzer model,

$$\frac{\partial}{\partial t}\begin{bmatrix} g \\ \Phi \\ \Psi \end{bmatrix} = \begin{bmatrix} K^{-1}(\frac{\nu}{2}\frac{\partial^2}{\partial\theta^2} - \frac{1}{2}\frac{\partial}{\partial\theta}) & 0 & 0 \\ 0 & 0 & 0 \\ 0 & 0 & 0 \end{bmatrix}\begin{bmatrix} g \\ \Phi \\ \Psi \end{bmatrix} + \begin{bmatrix} aK^{-1}(\psi_c(\Phi+g) - \overline{\psi}_c(\Phi,g)) \\ \frac{1}{l_c}(\overline{\psi}_c(\Phi,g) - \Psi) \\ \frac{1}{4l_cB^2}(\Phi - \gamma\sqrt{\Psi}) \end{bmatrix}, \tag{2.17}$$

where l_c is the effective flow-passage non-dimensional length of the compressor and ducts, and B is the dimensionless Greitzer parameter. Note that we also have some regularity conditions for g and require

$$g(t,0) = g(t,2\pi), \quad g_\theta(t,0) = g_\theta(t,2\pi)$$

and

$$\int_0^{2\pi} g(t,\theta)d\theta = 0.$$

Moreover, the compressor static characteristic is as follows,

$$\psi_c(\Phi) = \psi_{c_0} + H\left[1 + \frac{3}{2}\left(\frac{\Phi}{W} - 1\right) - \frac{1}{2}\left(\frac{\Phi}{W} - 1\right)^3\right]. \tag{2.18}$$

We also define

$$\overline{\psi}_c(\Phi, g) := \frac{1}{2\pi}\int_0^{2\pi} \psi_c(\Phi + g)d\theta. \tag{2.19}$$

In addition,

$$\Psi_V(\Phi) = \frac{1}{\gamma^2}\Phi^2, \tag{2.20}$$

where the throttle coefficient $\gamma > 0$ is proportional to the valve opening.

2.1.2 Stability Analysis

Calculating equilibrium values $x_e = [g_e, \Phi_e, \Psi_e]^T$ yields a trivial solution $g_e = 0$ and leaves us with the following two equations for Φ_e and Ψ_e:

$$\Psi_e = \psi_c(\Phi_e)$$

$$\Phi_e = F_T^{-1}(\Psi_e) = \gamma\sqrt{\Psi_e}$$

We can then write the state x in terms of small perturbations $y = [\delta g, \delta\Phi, \delta\Psi]^T$ about the equilibrium point x_e

$$x = x_e + y.$$

The evolution of the perturbations around the equilibrium is obtained by substituting the above relation into the original dynamic equation and expanding it using Taylor's series about the equilibrium x_e. As such, the nonlinear equations of the perturbations near equilibrium are

$$\frac{\partial}{\partial t}\begin{bmatrix}\delta g\\ \delta\Phi\\ \delta\Psi\end{bmatrix} = \mathcal{A}\begin{bmatrix}\delta g\\ \delta\Phi\\ \delta\Psi\end{bmatrix} + \mathcal{B}\begin{bmatrix}\delta g^2 + \delta g\delta\Phi\\ \delta\Phi^2\\ \delta\Psi^2\end{bmatrix} + \mathcal{C}\begin{bmatrix}-\delta g^3 + 3\delta g^2\delta\Phi + 3\delta g\delta\Phi^2\\ \delta\Phi^3\\ \delta\Psi^3\end{bmatrix}, \tag{2.21}$$

where

$$\mathcal{A} = \begin{bmatrix} K^{-1}(\frac{\nu}{2}\frac{\partial^2}{\partial\theta^2} - \frac{1}{2}\frac{\partial}{\partial\theta} + a\psi_c'(\Phi_e)) & 0 & 0 \\ 0 & \frac{1}{l_c}\psi_c'(\Phi_e) & -\frac{1}{l_c} \\ 0 & \frac{1}{4B^2 l_c} & -\frac{1}{4B^2 l_c}\frac{\gamma}{2\sqrt{\Psi_e}} \end{bmatrix}$$

$$\mathcal{B} = \frac{1}{2}\begin{bmatrix} K^{-1}a\psi_c''(\Phi_e) & 0 & 0 \\ 0 & \frac{1}{l_c}\psi_c''(\Phi_e) & 0 \\ 0 & 0 & \frac{1}{16B^2 l_c}\frac{\gamma}{\sqrt{\Psi_e}^3} \end{bmatrix}$$

and

$$\mathcal{C} = \frac{1}{6}\begin{bmatrix} K^{-1}a\psi_c'''(\Phi_e) & 0 & 0 \\ 0 & \frac{1}{l_c}\psi_c'''(\Phi_e) & 0 \\ 0 & 0 & -\frac{3}{32B^2 l_c}\frac{\gamma}{\sqrt{\Psi_e}^5} \end{bmatrix}.$$

The stability of the system can be analyzed by examining the eigenvalues of $\mathcal{A}$. There are infinite eigenvalues λ_n to be found from the first diagonal entry of $\mathcal{A}$ and the remaining two eigenvalues $\mu_{1,2}$ are to be found from the 2-by-2 bottom right submatrix. Taking $v = [e^{\pm in\theta}, 0, 0]^T$, the eigenvalue equation $\mathcal{A}v = \lambda_n v$ is satisfied for

$$\lambda_n = \left(1 + \frac{ma}{|n|}\right)^{-1}\left(a\psi_c'(\Phi_e) - \frac{\nu}{2}n^2 \pm \frac{1}{2}(i|n|)\right). \tag{2.22}$$

The remaining eigenvalues $\mu_{1,2}$ are found by solving the characteristic equation corresponding to the bottom right submatrix of $\mathcal{A}$:

$$\mu^2 + \left(\frac{1}{l_c}\frac{\gamma}{8B^2\sqrt{\Psi_e}} - \frac{1}{l_c}\psi_c'(\Phi_e)\right)\mu - \frac{1}{4B^2 l_c^2}\left(\frac{\gamma\psi_c'(\Phi_e)}{2\sqrt{\Psi_e}} - 1\right) = 0. \tag{2.23}$$

The eigenvalues are

$$\mu_{1,2} = \frac{1}{2l_c}\left[\left(\psi_c'(\Phi_e) - \frac{\gamma}{8B^2\sqrt{\Psi_e}}\right) \pm \sqrt{\left(\psi_c'(\Phi_e) + \frac{\gamma}{8B^2\sqrt{\Psi_e}}\right)^2 - \frac{1}{B^2}}\right] \tag{2.24}$$

The eigenvectors corresponding to the above eigenvalues are

$$v_{1,2} = \begin{bmatrix} 0 \\ 1 \\ \frac{1}{2}\left[\left(\psi_c'(\Phi_e) + \frac{\gamma}{8B^2\sqrt{\Psi_e}}\right) \mp \sqrt{\left(\psi_c'(\Phi_e) + \frac{\gamma}{8B^2\sqrt{\Psi_e}}\right)^2 - \frac{1}{B^2}}\right] \end{bmatrix} \tag{2.25}$$

2.1.3 Bifurcation Analysis

A bifurcation is characterized by a minor alteration in a system parameter resulting in a qualitative change in its dynamic behavior. This phenomenon is essential in the study of nonlinear dynamical systems, where the stability and structures of equilibrium are subject to change as parameters fluctuate. The Hopf bifurcation represents a pivotal occurrence in such systems where a stable equilibrium point loses stability and gives rise to a periodic orbit (limit cycle) as a system parameter is changed. It describes how oscillations can emerge in a system through a smooth transition. The well-known Hopf Bifurcation Theorem (cf. Theorem 3.4.2 in [41]) is given as follows.

Theorem 2.1.1 (Hopf Bifurcation Theorem [41])**.** *Suppose that the system $\dot{x} = f_\mu(x)$, $x \in \mathbb{R}^n$, $\mu \in \mathbb{R}$ has an equilibrium (x_0, μ_0) at which the following properties are satisfied:*

(H1) $D_x f_{\mu_0}(x_0)$ has a simple pair of pure imaginary eigenvalues and no other eigenvalues with zero real parts.

Then (H1) implies that there is a smooth curve of equilibria $(x(\mu), \mu)$ with $x(\mu_0) = x_0$. The eigenvalues $\lambda(\mu)$, $\bar{\lambda}(\mu)$ of $D_x f_{\mu_0}(x_0)$ which are imaginary at $\mu = \mu_0$ vary smoothly with μ, moreover,

(H2)

$$\frac{d}{d\mu}(Re\lambda(\mu))|_{\mu=\mu_0} \neq 0.$$

If the nonlinear coefficient, denoted as a, of the cubic nonlinear term in the normal form is nonzero, i.e., $a \neq 0$, there is a surface of periodic solutions in the center manifold which has quadratic tangency with the eigenspace of $\lambda(\mu)$, $\bar{\lambda}(\mu)$. If $a < 0$, then these periodic solutions are stable limit cycles, while if $a > 0$, the periodic solutions are repelling.

For the Moore-Greitzer PDE system, the Hopf bifurcation occurs when the real parts of a pair of eigenvalues of $\mathcal{A}$ cross the imaginary axis (satisfying the (H1) condition given above) while the derivative of the real part with respect to its bifurcation parameter γ is non-zero (satisfying the crossing condition shown in (H2)). Note that the real part of the eigenvalues in (2.22) and (2.24) all contain $\psi_c'(\Phi_e)$, where $\Phi_e = \Phi_e(\gamma)$. In this model, there are three types of Hopf bifurcations which can possibly occur, depending on the value of γ:

- **PDE Hopf bifurcation**: The critical bifurcation point for PDE instability is γ_c such that $\mathrm{Re}(\lambda_1) = 0$. It is not feasible to solve for γ_c explicitly, but we know that γ_c is the solution to

$$\Phi_e(\gamma_c)\left(2 - \frac{\Phi_e(\gamma_c)}{W}\right) - \frac{\nu W^2}{3aH} = 0.$$

When $\gamma < \gamma_c$, bifurcation occurs. At this particular value γ_c,

$$\frac{\partial}{\partial\gamma}\mathrm{Re}(\lambda_1)\Big|_{\gamma_c} = \psi_c''(\Phi_e(\gamma_c))\frac{\partial\Phi_e}{\partial\gamma}\bigg|_{\gamma_c} = \left(\frac{3H}{W^2}\sqrt{1 - \frac{\nu W}{3aH}}\right)\frac{\partial\Phi_e}{\partial\gamma}\bigg|_{\gamma_c} \neq 0.$$

- **ODE Hopf bifurcation**: The critical bifurcation point for ODE instability is γ_c such that $\mathrm{Re}(\mu_{1,2}) = 0$. Again, it is not feasible to solve for γ_c explicitly, but we know that γ_c is the solution to

$$\Phi_e(\gamma_c)\left(2 - \frac{\Phi_e(\gamma_c)}{W}\right) - \frac{\gamma_c^2}{4B^2}\frac{W^2}{3H} = 0.$$

When $\gamma < \gamma_c$, bifurcation occurs. At this particular value γ_c,

$$\frac{\partial}{\partial\gamma}\mathrm{Re}(\mu_{1,2})\Big|_{\gamma_c} = \frac{16B^2}{l_c\gamma_c^3}(\psi_c'(\Phi_e(\gamma_c)))^2 - \frac{1}{l_c}\frac{\partial\Phi_e}{\partial\gamma}\bigg|_{\gamma_c}\left(\frac{\psi_c'(\Phi_e(\gamma_c))}{\Phi_e(\gamma_c)} + \psi_c''(\Psi_e(\gamma_c))\right) \neq 0.$$

Combined PDE and ODE bifurcation: It is possible for both PDE and ODE eigenvalues to cross the imaginary axis, which is achieved when γ_c satisfies

$$\psi_c'(\Phi_e(\gamma_c)) = \frac{\gamma_c^2}{8B^2}\frac{1}{\Phi_e(\gamma_c)} = \frac{\nu}{2a}.$$

For this case, there are two crossing conditions related to the rate of change of the real part of the eigenvalues with respect to

$$\frac{3H}{2W^2}\sqrt{1 - \frac{\nu W}{3aH}}\frac{\partial\Phi_e}{\partial\gamma}\bigg|_{\gamma_c} \neq 0,$$

and

$$\frac{16B^2}{l_c\gamma_c^3}\left(\frac{\nu}{2a}\right)^2 - \frac{1}{l_c}\frac{\partial\Phi_e}{\partial\gamma}\bigg|_{\gamma_c}\left(\frac{\gamma_c^2}{8B^2} \pm \frac{3H}{2W^2}\sqrt{1 - \frac{\nu W}{3aH}}\right) \neq 0.$$

More details about the Hopf bifurcation analysis can be found in [104, 103, 59], and we may verify the type of Hopf bifurcation by the sign of the indicator [103]

$$\Delta := \frac{\psi_{c_0} + H\left[1 + \frac{3}{2}\sqrt{1 - \frac{\nu W}{3aH}} - \frac{1}{2}\left(\sqrt{1 - \frac{\nu W}{3aH}}\right)^3\right]}{W\left(1 + \sqrt{1 - \frac{\nu W}{3aH}}\right)} - \frac{a}{4B^2\nu} \tag{2.26}$$

Surge bifurcation happens when $\Delta > 0$, stall bifurcation happens when $\Delta < 0$. When $\Delta = 0$, then the combined PDE and ODE bifurcation occurs.

2.2 Basic QCD Problem Formulations

In this section, we introduce the basic QCD problem in detail with some mathematical preliminaries. Provided that both the pre- and post-change distributions of the observed sequence are known, we will give an overview of two standard formulations of the QCD problem: the Bayesian formulation with *Shiryaev's Problem* and the minimax formulation with *Lorden's Problem*. This will be followed by some simulation results of the cumulative sum (CUSUM) test for a sequence of i.i.d. random variables. Let us start with some notations and definitions that are usually utilized and referred to in QCD problems.

Symbol	Definition
$\mathcal{R}^\infty$	the set of sequences of real numbers
$\mathcal{B}^\infty$	the Borel σ-field in $\mathcal{R}^\infty$
$\mathbb{P}_n$	Probability measure when the change occurs at time n.
$\mathbb{E}_n$	Probability expectation when the change occurs at time n.
$\mathbb{P}_0$	Probability measure when the change does not occur.
$\mathbb{E}_0$	Probability expectation when the change does not occur.
$(x)^+$	$\max\{x, 0\}$
ess sup X	Essential supremum of X, i.e., smallest K such that $\mathbb{P}(X \leq K) = 1$.

Definition 2.2.1 (Stopping time)**.** *A stopping time with respect to the random sequence* $\{Y_n, n = 1, 2, \cdots\}$ *is a random variable* τ *with the property that for each* n*, the event* $\{\tau = n\} \in \sigma\{Y_1, \cdots, Y_n\}$*, where* $\sigma(Y_1, \cdots, Y_n)$ *denotes the sigma-algebra generated by* $(Y_1, \cdots, Y_n)$*.*

Definition 2.2.2 (Average run length)**.** *The average run length (ARL) is the interval between out-of-control events that can be expected. For example,* $\mathbb{E}_0[\tau]$ *represents the average number of runs expected before seeing a false alarm signal when the process is in control.*

Definition 2.2.3 (Ergodic hypothesis)**.** *It is assumed that the average of a process parameter over time and the average over the statistical ensemble are the same. If states (e.g., $Y_1, Y_2, \cdots$) are uniformly distributed in phase space initially, they will remain so at all times.*

Definition 2.2.4 (Markov inequality)**.** *If X is a nonnegative random variable and $a > 0$, then the probability that X is at least a is at most the expectation of X divided by a: $\mathbb{P}(X \geq a) \leq \mathbb{E}(X)/a$.*

We let $\{Y_i\}_{i=1}^{\infty}$ denote a sequence of random variables whose distribution changes at some unknown time k. As such, we have

$$Y_i \sim \begin{cases} f_0, & \text{if } \ i < k, \\ f_1, & \text{if } \ i \geq k, \end{cases} \tag{2.27}$$

where f_0 and f_1 represent the pre- and post-change probability density function (pdf) of Y_i, respectively. Let us consider a probability space $(\mathcal{R}^{\infty}, \mathcal{B}^{\infty}, \mathbb{P}_{\pi})$ where

$$\mathbb{P}_{\pi} = (1 - \pi)\mathbb{P}_0 + \pi\mathbb{P}_1$$

and where $\mathbb{P}_0$ and $\mathbb{P}_1$ are two probability measures on $(\mathcal{R}^{\infty}, \mathcal{B}^{\infty})$ such that, under $\mathbb{P}_j$, $Y_1, Y_2, \cdots$ are i.i.d. with probability density f_j, for $j = 0, 1$. In the basic setup, $\{Y_i\}_{i=1}^{\infty}$ is known as a sequence of independent identically distributed (i.i.d.) random variables, and we assume both pre- and post-change distributions are specified by the observer. As mentioned in the previous chapter, the objective is to construct a detection procedure to identify the change as quickly as possible under the false alarm constraint.

Based on the available information given at each time slot, the observer has to decide whether to stop and claim that the change has happened or continue to take another observation in the next time interval. The stopping time τ is defined as the time step in which the change is declared, and τ represents a random variable with respect to the sigma-algebra $\sigma\{Y_1, \cdots, Y_n\}$ generated by all available observations up to time n. Motivated by the goal of the QCD problem, the quickest detection methodology is designed considering a trade-off between *detection delay* and *false alarms*. No matter which change detection formulation we are interested in, there are typically three outcomes for the QCD problem based on a decision made by the change detector. The first one represents a scenario in which the detector correctly declares that the change has occurred, and then the *detection delay* can be calculated as the difference between the actual change time and the declared time. The second case happens when the change time claimed by the detector is prior to the actual change time, then a *false alarm* will be triggered. The third one is called *missed detection*, and this is the case where the claim that a change has happened has never been made, provided that the change occurs in the system.

2.3 Bayesian Quickest Change Detection

In the context of the Bayesian QCD problem, the change point k is assumed to be a random variable with a known distribution. Moreover, the measure of delay is described by the average detection delay (ADD):

$$\mathrm{ADD}(\tau) = \mathbb{E}[(\tau - k)^+] = \sum_{n=0}^{\infty} \mathbb{P}(n = k)\mathbb{E}_n[(\tau - k)^+]. \tag{2.28}$$

Note that the ADD can be rewritten as follows,

$$\mathbb{E}[(\tau - k)^+] = \mathbb{E}(\tau) - \mathbb{E}[\tau \wedge (k-1)],$$

where $\tau \wedge k = \min\{\tau, k\}$. As such, it is reasonable to consider $\mathbb{E}(\tau) < \infty$ for the Bayesian QCD problem; otherwise, $\mathbb{E}(\tau) = \infty$ implies that the ADD is infinite. In addition, we consider the probability of false alarm (PFA), i.e.,

$$\mathrm{PFA}(\tau) = \mathbb{P}(\tau < k) = \sum_{n=0}^{\infty} \mathbb{P}(n = k)\mathbb{P}_n(\tau < k), \tag{2.29}$$

as the measure of false alarms. Consequently, we can define the following feasible set of stopping times satisfying a constraint α on PFA,

$$\mathcal{T}_\alpha = \{\tau : \mathrm{PFA}(\tau) \leq \alpha\}, \tag{2.30}$$

where $0 \leq \alpha \leq 1$. In this section, we study one of the most well-known Bayesian QCD problems, namely Shiryaev's Problem.

2.3.1 Shiryaev's Problem

Under the Bayesian formulation, Shiryaev's Problem is considered an optimization problem, which is to minimize the ADD subject to an upper limit on PFA. In other words, Shiryaev's problem is defined as follows.

Shiryaev's Problem ([80]): For a given α, find a stopping time $\tau \in \mathcal{T}_\alpha$ such that $\mathrm{ADD}(\tau)$ is minimized.

In [80] and [82], Shiryaev shows that the above problem can be solved exactly if we assume the change point ν is geometrically distributed with the parameter $0 < \rho < 1$, i.e.,

$$\mathbb{P}(k = n) = \rho(1-\rho)^{n-1}\mathbb{I}_{\{n \geq 1\}}, \tag{2.31}$$

where $\mathbb{I}$ represents an indicator function, e.g.,

$$\mathbb{I}_{\{n\geq 1\}} = \begin{cases} 1, & n \geq 1 \\ 0, & n < 1. \end{cases} \tag{2.32}$$

Note that here, we assume there is no probability that the change has occurred prior to the observations, which implies that

$$\mathbb{P}(k = 0) = 0. \tag{2.33}$$

2.3.2 Bayesian Shiryaev Algorithm

To show the optimal solution to Shiryaev's Problem, which is given by the following Theorem 2.3.1 shown below, we first define

$$\pi_n = \mathbb{P}(k \leq n | Y_1, \cdots, Y_n) \tag{2.34}$$

as the probability that the change has happened, given the observations, is up to n. Under the geometric prior of the change point, using Bayes' rule, we can find the sequence $\{\pi_n\}$ evolves via the recursion:

$$\pi_{n+1} = \frac{LR(Y_{n+1})[\pi_n + \rho(1-\pi_n)]}{LR(Y_{n+1})[\pi_n + \rho(1-\pi_n)] + (1-\rho)(1-\pi_n)}, \tag{2.35}$$

where

$$LR(Y_n) = \frac{f_1(Y_n)}{f_0(Y_n)} \tag{2.36}$$

is called the likelihood ratio (recall that f_0 and f_1 denote the pdf in the pre-change and post-change regime, respectively), and $\pi_0 = 0$. Notice that the detailed proof of the optimal solution of Shiryaev's Problem was given in [80, 82]. Let us also illustrate the Shiryaev algorithm (from Theorem 2.3.1) and the following pseudo-code, which will help us simulate the Shiryaev test as a computational scheme to detect the change point in some i.i.d. models.

Theorem 2.3.1. *([82]): If $A_\alpha \in (0,1)$ can be chosen such that*

$$PFA(\tau_c) = \alpha, \tag{2.37}$$

the stopping time

$$\tau_c = \inf\{n \geq 0 : \pi_n \geq A_\alpha\} \tag{2.38}$$

is Bayesian optimal with the geometric prior.

Algorithm 1 Computation of the Shiryaev algorithm

$\pi_0 \leftarrow 0$
$\tilde{\pi}_0 = \rho$
$n \leftarrow 0$
repeat
  $n \leftarrow n + 1$
  {Observe Y_n}
  $\pi_n \leftarrow [\tilde{\pi}_{n-1} f_1(Y_n)]/[\tilde{\pi}_{n-1} f_1(Y_n) + (1 - \tilde{\pi}_{n-1}) f_0(Y_n)]$
  $\tilde{\pi}_n \leftarrow \pi_n + (1 - \pi_n)\rho$
until $\pi_n \geq A_\alpha$
{Stop and declare the change point}

2.4 Minimax Quickest Change Detection

In the context of the minimax formulation of the QCD problem, the change point is regarded as an unknown yet deterministic variable. In the absence of information regarding the change point, it is impractical to articulate the probability of a false alarm, a measure that is utilized in the Bayesian framework. Consequently, it is imperative to consider alternative metrics for detection delay and false alarms, as opposed to the criteria employed in the Bayesian QCD problem.

2.4.1 Lorden's Criterion

Under Lorden's criterion, the measure of delay is described by the worst average detection delay (WADD):

$$\mathrm{WADD}(\tau) = \sup_{n \geq 1} \operatorname{ess\,sup} \mathbb{E}_n[(\tau - n)^+ | X_1, \cdots, X_{n-1}], \tag{2.39}$$

where the essential supremum of some random variable Y gives the smallest y such that $\mathbb{P}(Y \leq y) = 1$. In other words, WADD is understood as the largest expected value of the worst detection delay over all possible change points. For the measure of the probability of a false alarm, the false alarm rate is defined as

$$\mathrm{FAR}(\tau) = \frac{1}{\mathbb{E}_0[\tau]}, \tag{2.40}$$

where $\mathbb{E}_0[\tau]$ is called the average run length (ARL). As mentioned before, ARL $\mathbb{E}_0[\tau]$ is measured under $\mathbb{P}_0$ and represents the mean time between two consecutive false alarms

conditioned on the change never occurring. Now, if we define the following set of stopping times satisfying a constraint α on the FAR,

$$\mathcal{D}_\alpha = \{\tau : \text{FAR}(\tau) \leq \alpha\}, \tag{2.41}$$

then we can define Lorden's Problem in the following way:

Lorden's Problem ([54]): For a given α, find a stopping time $\tau \in \mathcal{D}_\alpha$ such that $\text{WAAD}(\tau)$ is minimized.

2.4.2 Page's CUSUM Procedure

Page's CUSUM algorithm [65] is known as an optimal solution to the minimax QCD problem described in Lorden's formulation, and the associated asymptotic optimality and exact optimality for the CUSUM algorithm was proved in [54] and [62, 75], respectively. Under the i.i.d. setting, we define the log-likelihood ratio, denoted as Z_i for all $i \geq 1$, employed in the CUSUM rule as

$$Z_i = \log \frac{f_1(Y_i)}{f_0(Y_i)}, \quad i \geq 1. \tag{2.42}$$

Moreover, let us first initialize $S_0 = 0$ and define

$$S_n = Z_1 + \cdots + Z_n, \quad n \geq 1, \tag{2.43}$$

then the CUSUM statistic, denoted as T_n, is given by

$$T_n = S_n - \min_{0 \leq k \leq n} S_k, \quad n \geq 1. \tag{2.44}$$

For any given threshold $c > 0$ which is selected such that $\text{ARL}(\tau) = \gamma$ where γ is a positive constant, we define the corresponding CUSUM stopping time [65]

$$\tau_c := \inf\{n \geq 1 : T_n \geq c\}. \tag{2.45}$$

The following Lemma 2.4.1 was proved in [54] under the i.i.d. setting, and we shall show it is also valid in the general non-i.i.d. setting in the next chapter.

Lemma 2.4.1.

$$T_n = (T_{n-1} + Z_n)^+. \tag{2.46}$$

Remark 2.4.1. *The recursion (2.46) indicates that essentially all the computational load in the implementation of the CUSUM statistic is involved with the calculation of Z_n. In the i.i.d. case Z_n depends only on Y_n. In the Markov case Z_n depends on Y_{n-1} and Y_n. In other cases, the formula for Z_n may be much more complicated, possibly depending on the entire set of observations $\{Y_1, Y_2, \cdots, Y_n\}$.*

If we consider S_n as a random walk, then (2.44) basically means we are looking for some big difference in a random walk from the lowest value it has taken up to its current value. Clearly, T_n is nonnegative. So, T_n is almost like a random walk, except it is not allowed to be negative. Since T_n is to seek the largest divergence for the random walk S_n, the alternative description of (2.45) can be derived as follows,

$$\tau_c = \inf \left\{ n \geq 1 : \max_{0 \leq k \leq n} \sum_{i=k+1}^{n} Z_i \geq c \right\}. \tag{2.47}$$

To understand more about why Page's CUSUM procedure works for detecting the change, we first introduce the definition of the Kullback-Leibler (K-L) divergence.

Definition 2.4.1. *([94]) The K-L divergence between two probability density functions f_1 and f_0 is defined as*

$$D(f_1||f_0) = \int f_1(y) \log \frac{f_1(y)}{f_0(y)} dx. \tag{2.48}$$

Note that $D(f_1||f_0) \geq 0$ with equality if and only if $f_1 = f_0$ almost surely. Indeed, we have

$$\mathbb{E}_1(Z_i) = \int \log \left(\frac{f_1(y)}{f_0(y)} \right) f_1(y) dx = I > 0 \tag{2.49}$$

and

$$\mathbb{E}_0(Z_i) = \int \log \left(\frac{f_1(y)}{f_0(y)} \right) f_0(y) dx = -\int \log \left(\frac{f_0(y)}{f_1(y)} \right) f_0(y) dx = -J < 0, \tag{2.50}$$

where I is the Kullback-Liebler information of f_1 relative to f_0, and J is the Kullback-Liebler information of f_0 relative to f_1. Note that (2.49) and (2.50) indicate the motivation for the CUSUM algorithm. Consequently, the objective function in the stopping time of a minimax type of QCD problem can be understood from a more general point of view: we look for some function Z_i which is biased towards negative values before the change and towards positive values after the change. This is true for both the i.i.d. setting and non-i.i.d. setting, and the only difference (shown in the next chapter) is, instead of marginal probability densities given in (2.42), the log-likelihood ratio for the non-i.i.d. setting involves some conditional probability densities.

2.4.3 Threshold Computation for CUSUM Statistics in Change Detection

From [95], we learn that the value of a constant threshold applied in the CUSUM statistic, in practice, is typically chosen such that the average run length (ARL) function remains constant, i.e.,

$$\mathbb{E}_0(\tau_c) = \gamma,$$

for a fixed γ, where $\mathbb{E}_0$ and τ_c denote the expectation under the pre-change distribution and the optimal stopping time (i.e., (2.47)) of the CUSUM algorithm, respectively. As mentioned in [95], we can impose the following steps to compute the threshold:

- Make M simulations of the system under f_0 for a sufficiently long period.
- Fix a c and compute the M alarm times $\tau_c(m)$, $m = 1, \cdots, M$ that are, in fact, false alarms.
- Estimate the mean time of the false alarm by

$$\mathbb{E}_0(\tau_c) \simeq \sum_{m=1}^{M} \frac{\tau_c(m)}{M}.$$

- Repeat the computation of $\tau_c(m)$ for $m = 1, \cdots, M$ while varying the value of c until the desired false alarm rate γ, is obtained.

If we are now interested in the case where the pre-change and post-change distributions are stationary, then the above method is applicable to find appropriate values of thresholds for the CUSUM statistic T_n defined in (2.44). As a test, we fix $\gamma = 100$ for the ARL functions in the CUSUM procedure and let $M = 500$ and $N = 250$. Note that M and N represent the number of false alarm computations and the number of measurements, respectively. Some important simulation results from MATLAB are summarized in the following Table 2.1. From the table, it is straightforward to see that when the threshold $c = 1.18$ the estimated false alarm mean time (i.e., $\mathbb{E}_0(\tau_c)$) is fairly close to the fixed value of $\gamma = 100$. As such, $c = 1.18$ could be an acceptable threshold value for the CUSUM procedure of the QCD problem associated with $\mathbb{E}_0(\tau_c) = 100$.

	$c = 1.70$	$c = 1.50$	$c = 1.20$	$c = 1.15$	$c = 1.18$
$\mathbb{E}_0(\tau_c)$	160.2340	133.690	101.384	94.474	100.680

Table 2.1: Table of average run length (ARL) of CUSUM statistics T_n over 100 trials for different threshold values.

2.5 Simulation Results

Let us now investigate an example of the QCD problem under the i.i.d. setting and try implementing the CUSUM algorithm to detect the change in simulations.

Example 2.5.1. *We consider a sequence of i.i.d. observations* $\{Y_1, Y_2, \cdots, Y_{1000}\}$. *Before the change point (at time slot 500, i.e.,* $k = 500$*), the observations are distributed according to pdf* f_0 *(normal distribution with zero mean and unit variance), and the samples after the change point are distributed according to pdf* f_1 *(normal distribution with 0.1 mean and unit variance). Hence, the change in distribution is introduced by increasing the mean value of the distribution from 0 to 0.1 at time slot 500.*

The following figures are given to demonstrate the basic conceptual elements of the CUSUM algorithm mentioned above. In fact, Figure 2.2 illustrates the evolution of the observations with the change and the CUSUM statistic. In Figure 2.2, we can see that the first time the CUSUM statistic exceeds the threshold value $c = 2.0$ is at time interval 682, thus producing a detection delay of 682 – 500 = 182 time steps.

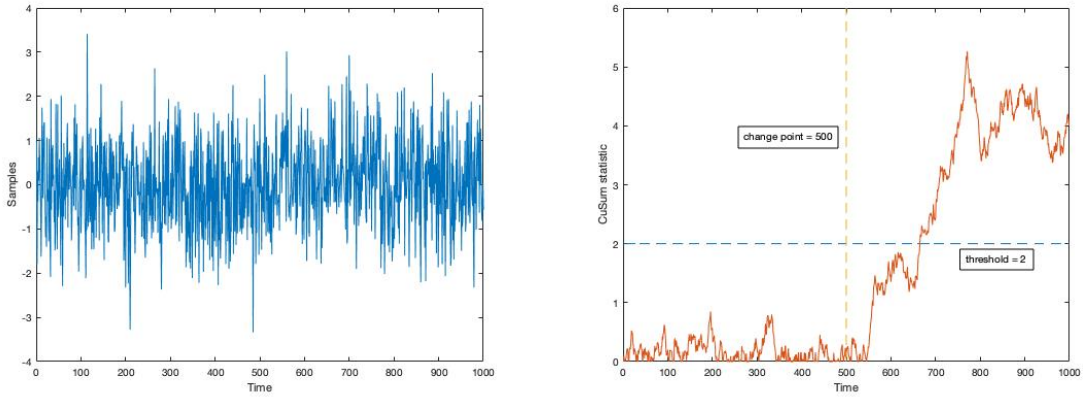


Figure 2.2: **Left**: A stochastic sequence with observations from $f_0 \sim \mathcal{N}(0, 1)$ before the change (time slot 500), and with observations from $f_1 \sim \mathcal{N}(0.1, 1)$ after the change. **Right**: Evolution of the CUSUM statistic with the threshold $c = 2.0$.

Notice that from the evolution of the observations (see the left plot of Figure 2.2), the change cannot be identified visually since the data is fairly noisy. This actually implies the effectiveness of the CUSUM algorithms for detecting the changes in the i.i.d. models for the associated formulations. In addition, you could also notice that, before the change,

the statistics tend to hover around zero; after the change, the statistics start to take off. This is due to the fact that the expectation of the log-likelihood ratio is biased towards negative values before the change and towards positive values after the change.

2.6 Lai's Optimal Detection Theory [49]

2.6.1 Generalization of Lorden's Asymptotic Theory

Suppose that under $\mathbb{P}_0$, the conditional density function of X_n given $X_1, \cdots, X_{n-1}$ is $f_0(X_n|X_1, \cdots, X_{n-1})$ for every $n \geq 1$ and that under $\mathbb{P}_k$, the conditional density function is $f_0(X_n|X_1, \cdots, X_{n-1})$ for $n < k$ and is $f_1(X_n|X_1, \cdots, X_{n-1})$ for $n \geq k$. Let

$$Z_i = \log \frac{f_1(X_i|X_1, \cdots, X_{i-1})}{f_0(X_i|X_1, \cdots, X_{i-1})}. \tag{2.51}$$

To obtain the generalization of the CUSUM procedure that attains the asymptotic lower bound for the detection delay in the non-i.i.d. setting, we first need the following condition on the Z_i:

$$\lim_{n\to\infty} \sup \operatorname{ess\,sup} \mathbb{P}_k \left(\max_{t\leq n} \sum_{i=k}^{k+t} Z_i \geq I(1+\delta)n | X_1, \cdots, X_{k-1} \right) = 0, \quad \forall \delta > 0. \tag{2.52}$$

To understand (2.52) more precisely, let us focus on the inequality, i.e.,

$$\max_{t\leq n} \sum_{i=k}^{k+t} Z_i \geq I(1+\delta)n$$

inside of the probability measure; if we ignore the max, let $t = n$ and divide both sides by n, it becomes

$$\frac{1}{n} \sum_{i=\nu}^{\nu+n} Z_i \geq I(1+\delta).$$

Then, it follows from the *law of large numbers* that the left-hand side of the above inequality is getting close to some expected value as n becomes very large. In particular, I reduces to $I(f_1|f_0) = \mathbb{E}_1[\log(f_1(X_1)/f_2(X_1))]$ when it comes to the i.i.d. setting. Therefore, (2.52) basically implies that Z_i cannot be too large on average (less than or equal to I) under $\mathbb{P}_k$.

Theorem 2.6.1 ([49]). *Suppose that (2.52) holds for some positive constant I. Then as $\gamma \to \infty$*

$$\begin{aligned} \inf\{ WADD(\tau) : \mathbb{E}_0(\tau) \geq \gamma\} &\geq \inf\left\{ \sup_{k\geq 1} \mathbb{E}_k(\tau - k | \tau \geq k) : \mathbb{E}_0(\tau) \geq \gamma \right\} \\ &\geq (I^{-1} + o(1)) \log \gamma, \end{aligned} \tag{2.53}$$

where $WADD(\tau)$ is defined in (2.39).

Notice that in [54], Lorden basically states that if we use the CUSUM algorithm, the worst average detection delay is less than or equal to some expected value (i.e., $\mathrm{WADD}(\tau) \leq \mathbb{E}_1(\tau)$). Lorden also has that general theorem, which says that for any general stopping time τ, we get the statement that looks like (2.53). The hard work in proving Theorem 3 in [54] is that, whatever stopping time we take, we cannot do anything better than the equality shown in (2.53). So, the crucial part in Lorden's Theorem 3 [54] is nothing to do with CUSUM but is the statement about the very general stopping time. Similarly, the above Lai's Theorem 2.6.1 has nothing to do with CUSUM, and it is just the general statement about the stopping time τ.

Proof. If $\mathbb{E}_0(\tau) \geq \gamma$, then for some $k \geq 1$, it is straightforward to see

$$\mathbb{P}_0(\tau \geq k) > 0. \tag{2.54}$$

Let $m < \gamma$ be a (fixed) positive integer, then there exists a $k \geq 1$ such that

$$\mathbb{P}_0(\tau < k + m | \tau \geq k) \leq m/\gamma. \tag{2.55}$$

We prove (2.55) by contradiction. If (2.55) is not true, we then have $\mathbb{P}_0(\tau \geq k + m | \tau \geq k) < 1 - m/\gamma$ for all $k \geq 1$ with $\mathbb{P}_0(\tau \geq k) > 0$, which implies

$$\begin{aligned} \mathbb{E}_0(\tau) &= \sum_{l=1}^{\infty} \mathbb{P}_0(\tau \geq l) \\ &= \sum_{i=1}^{m} \sum_{j=0}^{\infty} \mathbb{P}_0(\tau \geq mj + i). \end{aligned} \tag{2.56}$$

Since

$$\begin{aligned} \frac{\mathbb{P}_0(\tau \geq mj + i)}{\mathbb{P}_0(\tau \geq i)} &= \frac{\mathbb{P}_0(\tau \geq mj + i)}{\mathbb{P}_0(\tau \geq m(j-1) + i)} \cdot \frac{\mathbb{P}_0(\tau \geq m(j-1) + i)}{\mathbb{P}_0(\tau \geq m(j-2) + i)} \cdots \frac{\mathbb{P}_0(\tau \geq m + i)}{\mathbb{P}_0(\tau \geq i)} \\ &= \mathbb{P}_0(\tau \geq mj + i | \tau \geq m(j-1) + i) \cdots \mathbb{P}_0(\tau \geq m + i | \tau \geq i) \\ &< (1 - m/\gamma)^j, \end{aligned} \tag{2.57}$$

we have

$$\begin{aligned}\mathbb{E}_0(\tau) &< \sum_{i=1}^{m}\sum_{j=0}^{\infty}(1-m/\gamma)^j\mathbb{P}_0(\tau \geq i) \\ &\leq \sum_{i=1}^{m}\sum_{j=0}^{\infty}(1-m/\gamma)^j \\ &= m \cdot \frac{\gamma}{m} \\ &= \gamma\end{aligned} \tag{2.58}$$

which is a contradiction. Hence, (2.55) is proved. □

Now, let us define m as follows,

$$m = \sup\{n \in N^* : n \leq (\log\gamma)^2\},$$

where N^* represents the collection of all positive integers. Suppose $\mathbb{E}_0(\tau) \geq \gamma$, then we can choose k (which depends on γ) such that (2.54) and (2.55) are satisfied. We first show that as $\gamma \to \infty$

$$\mathbb{P}_k\{C_\delta|\tau \geq k\} \to 0, \tag{2.59}$$

where

$$C_\delta = \left\{0 \leq \tau - k < (1-\delta)I^{-1}\log\gamma, \sum_{i=k}^{\tau} Z_i < (1-\delta^2)\log\gamma\right\} \tag{2.60}$$

for the chosen k and every $0 < \delta < 1$. Let $\mathcal{F}_n$ be the σ-field generated by $X_1, \cdots, X_n$ and let $\mathbb{P}_{n,k}$ be the restriction of $\mathbb{P}_k$ to $\mathcal{F}_n$. Then

$$\begin{aligned}\frac{d\mathbb{P}_{n,k}}{d\mathbb{P}_{0,n}} &= \frac{f^{(k)}(X_1,\cdots,X_n)}{f_0(X_1,\cdots,X_n)} \\ &= \prod_{i=2}^{n}\frac{f^{(k)}(X_i|X_1,\cdots,X_{i-1})}{f_0(X_i|X_1,\cdots,X_{i-1})} \\ &= \prod_{i=2}^{k-1}\frac{f_0(X_i|X_1,\cdots,X_{i-1})}{f_0(X_i|X_1,\cdots,X_{i-1})}\prod_{i=k}^{n}\frac{f_1(X_i|X_1,\cdots,X_{i-1})}{f_0(X_i|X_1,\cdots,X_{i-1})} \\ &= \exp\left(\sum_{i=k}^{n} Z_i\right), \quad \text{for} \quad n \geq k.\end{aligned} \tag{2.61}$$

Since $\tau \geq k$ as defined in C_δ, we can replace n with τ in the last line of (2.61) so that

$$\begin{aligned}\mathbb{P}_k(C_\delta) &= \int_{C_\delta} \exp\left(\sum_{i=k}^{\tau} Z_i\right) d\mathbb{P}_0 \\ &\leq \exp\{(1-\delta^2)\log\gamma\}\mathbb{P}_0(C_\delta).\end{aligned} \tag{2.62}$$

Because

$$\{\tau \geq k\} \in \mathcal{F}_{k-1} \Rightarrow \mathbb{P}_k\{\tau \geq k\} = \mathbb{P}_0\{\tau \geq k\}, \tag{2.63}$$

then

$$\frac{\mathbb{P}_k(C_\delta)}{\mathbb{P}_k\{\tau \geq k\}} \leq \exp\{(1-\delta^2)\log\gamma\}\frac{\mathbb{P}_0(C_\delta)}{\mathbb{P}_0\{\tau \geq k\}}, \tag{2.64}$$

which implies that

$$\mathbb{P}_k\{C_\delta|\tau \geq k\} \leq \exp\{(1-\delta^2)\log\gamma\}\mathbb{P}_0\{\tau - k < (1-\delta)I^{-1}\log\gamma|\tau \geq k\}. \tag{2.65}$$

For all large γ (such that $(1-\delta)I^{-1} < \log\gamma$), it follows from (2.55) that the inequality (2.65) becomes

$$\begin{aligned}\mathbb{P}_k\{C_\delta|\tau \geq k\} &\leq \gamma^{1-\delta^2}\mathbb{P}_0\{\tau < k+m|\tau \geq k\} \\ &\leq \gamma^{1-\delta^2} m/\gamma \\ &\leq \gamma^{1-\delta^2}(\log\gamma)^2/\gamma \\ &= \frac{(\log\gamma)^2}{\gamma^{\delta^2}}.\end{aligned} \tag{2.66}$$

Notice that

$$\lim_{\gamma\to\infty} \frac{(\log\gamma)^2}{\gamma^{\delta^2}} = 0. \tag{2.67}$$

As such, (2.59) follows. Since $\{\tau \geq k\} \in \mathcal{F}_{k-1}$, we also have

$$\begin{aligned}&\mathbb{P}_k\left\{0 \leq \tau - k < (1-\delta)I^{-1}\log\gamma, \sum_{i=k}^{\tau} Z_i \geq (1-\delta^2)\log\gamma|\tau \geq k\right\} \\ &\leq \operatorname{ess\,sup}\mathbb{P}_k\left(\max_{t\leq(1-\delta)I^{-1}\log\gamma}\sum_{i=k}^{k+t} Z_i \geq I(1+\delta)(1-\delta)I^{-1}\log\gamma|X_1,\cdots,X_{k-1}\right) \\ &\leq \sup\operatorname{ess\,sup}\mathbb{P}_k\left(\max_{t\leq(1-\delta)I^{-1}\log\gamma}\sum_{i=k}^{k+t} Z_i \geq I(1+\delta)(1-\delta)I^{-1}\log\gamma|X_1,\cdots,X_{k-1}\right) \\ &\to 0\end{aligned} \tag{2.68}$$

as $\gamma \to \infty$. Now, the sum of (2.59) and (2.68) is given by

$$\mathbb{P}_k\{0 \le \tau - k < (1-\delta)I^{-1}\log\gamma | \tau \ge k\} \to 0 \tag{2.69}$$

so that

$$\mathbb{P}_k\{\tau - k \ge (1-\delta)I^{-1}\log\gamma | \tau \ge k\} \to 1. \tag{2.70}$$

From Markov inequality, we then have

$$\mathbb{E}_k\{\tau - k | \tau \ge k\} \ge (1 - \delta + o(1))I^{-1}\log\gamma \tag{2.71}$$

as $\gamma \to \infty$. Note that the lower bound in (2.71) is valid for some unspecified k (which is relevant to the ARL constraint via (2.54) and (2.55)). As such, we have to take the supremum of $\mathbb{E}_k\{\tau - k | \tau \ge k\}$ for all $k \ge 1$ and find the following inequality,

$$\sup_{k\ge 1} \mathbb{E}_k\{\tau - k | \tau \ge k\} \ge (I^{-1} + o(1))\log\gamma. \tag{2.72}$$

Since $\{\tau \ge k\} \in \mathcal{F}_{k-1}$, we have

$$\operatorname{ess\,sup} \mathbb{E}_k\{(\tau - k + 1)^+ | X_1, \cdots, X_{k-1}\} \ge \mathbb{E}_k\{\tau - k | \tau \ge k\}. \tag{2.73}$$

Hence, (2.53) follows from (2.72).

2.6.2 Uniform (over k) Lower Bound Under Alternative Performance Criterion

As mentioned before, the asymptotic lower bound for $\mathbb{E}_k\{\tau - k | \tau \ge k\}$ derived in Theorem 2.6.1 is given only at the k that maximizes the expected delay. To find the asymptotic lower bound for $\mathbb{E}^{(k)}\{\tau - k | \tau \ge k\}$ at any given k, let us first change the ARL constraint into the condition that $\mathbb{P}_0(\tau < k + m | \tau \ge k) \le m/\gamma$, where $\liminf_{\gamma\to\infty}(m/\log\gamma) > I^{-1}$ but $\log m = o(\log\gamma)$. Then, we would like to show that the inequality in (2.71) holds for any given $k \ge 1$ under this new probability condition. Note that the conditional probability, i.e.,

$$\mathbb{P}_0(\tau < k + m | \tau \ge k) = \mathbb{P}_0(k \le \tau < k + m)/\mathbb{P}_0(\tau \ge k),$$

is nearly singular when the denominator is very small. So, let us ignore the denominator and establish a simpler probability constraint, i.e., $\mathbb{P}_0(k \le \tau < k + m) \le \alpha$. We shall require this constraint to hold for all $k \ge 1$ and some m_α that depends only on α, i.e.,

$$\sup_{k\ge 1} \mathbb{P}_0(k \le \tau < k + m_\alpha) \le \alpha, \tag{2.74}$$

where

$$\liminf_{\alpha\to 0}(m_\alpha/|\log\alpha|) > I^{-1} \text{ but } \log m_\alpha = o(\log\alpha) \text{ as } \alpha\to 0. \tag{2.75}$$

Since we are interested in a less pessimistic measure of delay — conditional average detection delay, (i.e., $\mathbb{E}^{(k)}\{\tau-k|\tau\geq k\}$) and the denominator has been ignored, the assumption in (5) can be relaxed as follows,

$$\lim_{n\to\infty}\sup_{k\geq 1}\mathbb{P}^{(k)}\left(\max_{t\leq n}\sum_{i=k}^{k+t}Z_i\geq I(1+\delta)n\right)=0,\quad \forall\delta>0. \tag{2.76}$$

Theorem 2.6.2 ([49]). *Suppose that* (2.74), (2.75) *and* (2.76) *hold for some positive constant* I. *Then as* $\alpha\to 0$

$$\mathbb{E}^{(k)}(\tau-k)^+\geq\{\mathbb{P}_0(\tau\geq k)/I+o(1)\}|\log\alpha| \tag{2.77}$$

uniformly in $k\geq 1$.

Proof. For any $\delta>0$, we define C_δ by (13) with $\log\gamma$ replaced by $\log\alpha^{-1}$, i.e.,

$$C_\delta=\left\{0\leq\tau-k<(1-\delta)I^{-1}\log\alpha^{-1},\sum_{i=k}^{\tau}Z_i<(1-\delta^2)\log\alpha^{-1}\right\}. \tag{2.78}$$

Then, using the same change of measure argument as in (2.61), (2.62) and (2.65) yields

$$\mathbb{P}^{(k)}\{C_\delta\}\leq\exp\{(1-\delta^2)\log\alpha^{-1}\}\mathbb{P}_0\{0\leq\tau-k<(1-\delta)I^{-1}\log\alpha^{-1}\}. \tag{2.79}$$

Since $m_\alpha>(1-\delta)I^{-1}\log\alpha^{-1}$ for all small α, we have

$$\begin{aligned}\mathbb{P}^{(k)}\{C_\delta\}&\leq\exp\{(1-\delta^2)\log\alpha^{-1}\}\alpha\\&=\alpha^{-(1-\delta^2)+1}\end{aligned} \tag{2.80}$$

for all sufficiently small α, which implies that

$$\mathbb{P}^{(k)}\{C_\delta\}\to 0 \text{ as } \alpha\to 0, \tag{2.81}$$

for all $k\geq 1$. Moreover, it follows from the assumption as shown in (2.76) that

$$\begin{aligned}&\mathbb{P}^{(k)}\left\{0\leq\tau-k<(1-\delta)I^{-1}\log\alpha^{-1},\sum_{i=k}^{\tau}Z_i\geq(1-\delta^2)\log\alpha^{-1}\right\}\\&\leq\sup_{k\geq 1}\mathbb{P}^{(k)}\left(\max_{t\leq(1-\delta)I^{-1}\log\alpha^{-1}}\sum_{i=k}^{k+t}Z_i\geq I(1+\delta)(1-\delta)I^{-1}\log\alpha^{-1}\right)\\&\to 0\end{aligned} \tag{2.82}$$

as $\alpha \to 0$. Consequently, combining (2.81) and (2.82) gives

$$\mathbb{P}^{(k)}\{0 \le \tau - k < (1-\delta)I^{-1}\log\alpha^{-1}\} \to 0 \text{ as } \alpha \to 0, \tag{2.83}$$

for all $k \ge 1$. Since

$$\mathbb{P}^{(k)}\{\tau - k \ge 0\} - \mathbb{P}^{(k)}\{\tau - k \ge (1-\delta)I^{-1}\log\alpha^{-1}\} \to 0 \text{ as } \alpha \to 0, \tag{2.84}$$

it follows from Markov inequality that

$$\begin{aligned} E^{(k)}(\tau - k)^+ &\ge (1-\delta)I^{-1}|\log\alpha|\mathbb{P}^{(k)}\{\tau - k \ge (1-\delta)I^{-1}\log\alpha^{-1}\} \\ &= (1-\delta)I^{-1}|\log\alpha|[\mathbb{P}^{(k)}\{\tau \ge k\} + o(1)]. \end{aligned} \tag{2.85}$$

Using (2.63) yields (2.77), and the proof of Theorem 2.6.2 is complete. □

Chapter 3

Quickest Change Detection in HMMs

In many real-world applications of QCD, the original signals or states of a system contaminated by some unknown change are usually inaccessible to the detector. However, observations are functions of the states that can be obtained and utilized. The application considered in this chapter is an example of such a QCD problem. This motivates us to study the QCD problems in hidden Markov models (HMMs), which typically consist of the underlying Markov process X governed by a stochastic differential equation (SDE) with linear or nonlinear drift, and an observational process Y, which is corrupted by a random process. Consider a discrete-time hidden Markov model where the signal X_n and observations Y_n, $n \geq 0$, satisfy the following stochastic dynamics,

$$\begin{aligned} X_n &= \begin{cases} f(X_{n-1}, \theta_0) + U_n, & n < k \\ f(X_{n-1}, \theta_1) + U_n, & n \geq k, \end{cases} \\ Y_n &= h(X_n) + V_n, \end{aligned} \tag{3.1}$$

where k represents the change point, and θ_0 and θ_1 indicate that the state process is in the pre-change and post-change regimes, respectively; f and h have the proper dimensions. U_n and V_n are i.i.d. random processes with some known densities. Chen and Willett previously investigated the detection of changes in hidden Markov models (HMMs) in [21] and [22], and sought a CUSUM-like procedure based on the sequential probability ratio test (SPRT) [99] for the non-i.i.d. case and explored detection of HMM transient signals. This chapter aims to present a detailed mathematical formulation of change detection in nonhomogeneous HMMs.

In [34], Fuh investigated the QCD problem in the dynamic system of HMMs, and the formula he used for the likelihood ratio (i.e., LR_n^k) depends on the state x_{k-1} (corresponding

to Fuh's notation), where k represents the change point. Notice the distribution of the state x_{k-1} must be estimated from the observations up to the time $k-1$ using the pre-change parameter values, not the post-change parameter values. This is why the post-change transition densities of the observation at time n given all the past observations for $n \geq k$ depend on the change point k as well as n. Thus the standard model (see Section 3.1.2) studied in [90, 49, 92] does not apply to the QCD problems in the HMMs related to the engine compressor models. Additionally, Fuh and Mei give a somewhat more detailed discussion of the transition in [35]. One scenario describes the state process at change point k with some given distribution independent of all the pre-change states and observations. The other scenario uses the changed Markov transition probabilities to determine how the signal or state at time k depends on the corresponding signal at $k-1$. In this chapter, we are interested in the second scenario, from which we provide an explanation on why the standard model studied primarily in [36, 90, 49, 92] does not apply to the QCD problems in our nonlinear HMMs related to the Moore-Greitzer compressor models.

3.1 Change Detection in the Standard Model using Page's CUSUM Procedures

Given a sequence of observations $\{Y_1, Y_2, \cdots\} = \mathbb{Y}$, we assume that, for each $k \geq 1$, a probability measure $\mathbb{P}_k$ on $\mathbb{Y}$ corresponds to change at time k (so that Y_{k-1} is the last unchanged observation); and $\mathbb{P}_0$ represents a probability measure on $\{Y_1, Y_2, \cdots\}$ corresponding to no change. For the simplicity of notations, we write $(Y_1, \cdots, Y_n) = Y_1^n$. For $k \geq 0$, let $p_k(\cdot)$ and $p_k(\cdot|\cdot)$ denote joint densities and conditional densities with respect to the measure $\mathbb{P}_k$. Before the change happens, we assume $p_k(Y_1^n) = p_0(Y_1^n)$ for any $n < k$. For any $k, n \geq 1$, we consider the log-likelihood ratio of $\mathbb{P}_k$ relative to $\mathbb{P}_0$ given the observations up to time n:

$$LLR_n^k := \log \frac{p_k(Y_1^n)}{p_0(Y_1^n)}. \tag{3.2}$$

Since $p_k(Y_1^n) = p_0(Y_1^n)$ when $n < k$, $LLR_n^k = 0$ for any $n < k$. Then we define

$$T_n = \max_{k \geq 1} LLR_n^k = \max_{1 \leq k \leq n+1} LLR_n^k. \tag{3.3}$$

We propose to use the stopping times of the form

$$\tau = \inf\{n \geq 1 : T_n \geq c\} \tag{3.4}$$

for appropriate threshold values c. We shall see that T_n reduces to Page's CUSUM statistic in the i.i.d. setting.

3.1.1 An Example Under the i.i.d. Setting

Suppose that under $\mathbb{P}_k$ the Y_n are independent and that Y_n has density $f_0(y)$ for $n < k$ and density $f_1(y)$ for $n \geq k$. Then

$$p_0(Y_1^n) = \prod_{i=1}^{n} f_0(Y_i)$$

and

$$p_k(Y_1^n) = \begin{cases} \prod_{i=1}^{n} f_0(Y_i), & n < k \\ \prod_{i=1}^{k-1} f_0(Y_i) \times \prod_{i=k}^{n} f_1(Y_i), & n \geq k. \end{cases}$$

Then

$$LLR_n^k = \begin{cases} 0, & n < k \\ \sum_{i=k}^{n} Z_i = S_n - S_{k-1}, & n \geq k, \end{cases}$$

where

$$Z_i = \log \frac{f_1(Y_i)}{f_0(Y_i)}, \tag{3.5}$$

and $S_0 = 0$, and

$$S_n = \sum_{i=1}^{n} Z_i, \quad n \geq 1.$$

Therefore,

$$\begin{aligned} T_n &= \max_{1 \leq k \leq n+1} LLR_n^k \\ &= \max_{1 \leq k \leq n+1} (S_n - S_{k-1}) \\ &= \max_{0 \leq k \leq n} (S_n - S_k), \end{aligned} \tag{3.6}$$

which is Page's CUSUM statistic. It satisfies the recursive formula

$$T_n = (T_{n-1} + Z_n)^+. \tag{3.7}$$

3.1.2 The Standard Model

In [49], Lai generalized Lorden's asymptotic detection theory beyond the i.i.d. assumption and focused on two sequences of conditional probability densities $f_{0,i}(Y_i|Y_1^{i-1})$ and $f_{1,i}(Y_i|Y_1^{i-1})$. With the convention that $f_{j,1}(Y_1|Y_0) = f_{j,1}(Y_1)$, $j \in \{0, 1\}$,

$$p_0(Y_1^n) = \prod_{i=1}^{n} f_{0,i}(Y_i|Y_1^{i-1}). \tag{3.8}$$

Moreover, we have

$$p_k(Y_1^n) = \prod_{i=1}^{n} f_{0,i}(Y_i|Y_1^{i-1}), \quad n < k,$$

and

$$p_k(Y_1^n) = \prod_{i=1}^{k-1} f_{0,i}(Y_i|Y_1^{i-1}) \times \prod_{i=k}^{n} f_{1,i}(Y_i|Y_1^{i-1}),$$

for all $n \geq k$. Equivalently, the conditional densities $p_k(Y_i|Y_1^{i-1})$ are given by

$$p_k(Y_i|Y_1^{i-1}) = f_{0,i}(Y_i|Y_1^{i-1}), \quad i < k, \tag{3.9}$$

and

$$p_k(Y_i|Y_1^{i-1}) = f_{1,i}(Y_i|Y_1^{i-1}), \quad i \geq k. \tag{3.10}$$

It is worth noting that this model is used in [90, 49, 92], and the main assumption about this standard model is that the post-change conditional density $p_k(Y_i|Y_1^{i-1})$ does not depend on the change point k for $i \geq k$. Now, we may see how the pre- and post-change conditional probability density functions come into the log-likelihood ratio LLR_n^k. We extend the definition (3.5) and write

$$Z_i = \log \frac{f_{1,i}(Y_i|Y_1^{i-1})}{f_{0,i}(Y_i|Y_1^{i-1})}, \quad i \geq 1. \tag{3.11}$$

Define $S_0 = 0$, as before,

$$S_n = \sum_{i=1}^{n} Z_i, \quad n \geq 1. \tag{3.12}$$

Using (3.9) and (3.10) gives

$$LLR_n^k = \begin{cases} 0, & n < k \\ \sum_{i=k}^{n} Z_i = S_n - S_{k-1}, & n \geq k. \end{cases} \tag{3.13}$$

Therefore, we have

$$T_n = \max_{1 \leq k \leq n} (Z_k + \cdots + Z_n). \tag{3.14}$$

Notice that T_n is almost the same as what we have in (3.6), and the only difference is the log-likelihood ratio given in T_n is related to the conditional probability density functions. Similarly, it satisfies the simple recursion

$$T_n = (T_{n-1} + Z_n)^+. \tag{3.15}$$

3.1.3 Non-standard Models

In the subsequent section, we will obtain the formula

$$p_k(Y_1^n) = \prod_{i=1}^{k-1} f_{0,i}(Y_i|Y_1^{i-1}) \times \prod_{i=k}^{n} f_{1,i}^{(k)}(Y_i|Y_1^{i-1}), \tag{3.16}$$

where now $f_{1,i}^{(k)}(Y_i|Y_1^{i-1})$ depends non-trivially on k for $i \geq k$. Therefore, the standard model does not apply. The conditional log-likelihood ratio

$$Z_i^{(k)} = \log \frac{f_{1,i}^{(k)}(Y_i|Y_1^{i-1})}{f_{0,i}(Y_i|Y_1^{i-1})} \tag{3.17}$$

also depends non-trivially on k for $i \geq k$. In this more general setting, (3.14) is replaced by

$$T_n = \max_{1 \leq k \leq n} (Z_k^{(k)} + \cdots + Z_n^{(k)}), \tag{3.18}$$

which does not satisfy a simple recursion anymore. Because of the increased computational load associated with T_n, Fuh [33] proposes a CUSUM statistic as follows,

$$\widehat{T}_n = \max_{1 \leq k \leq n} (Z_k^{(1)} + \cdots + Z_n^{(1)}), \tag{3.19}$$

which satisfies the simple recursion, i.e.,

$$\widehat{T}_n = (\widehat{T}_{n-1} + Z_n^{(1)})^+. \tag{3.20}$$

The effect of using $\widehat{T}_n$ is that we are always comparing the scenario that the change occurs immediately with the case that there is no change. This avoids the issue of behavior at the change point. We note that for the standard model, $T_n = \widehat{T}_n$, and the following lemma gives a transparent proof.

Lemma 3.1.1. *$T_n = \widehat{T}_n$ if*

$$p_k(Y_k^n|Y_1^{k-1}) = p_1(Y_k^n|Y_1^{k-1})$$

for all $n \geq k \geq 1$.

Proof. For $n \geq k \geq 1$ we have

$$\begin{aligned} p_k(X_1^n) &= p_k(X_k^n|X_1^{k-1})p_k(X_1^{k-1}) \\ &= p_k(X_k^n|X_1^{k-1})p_0(X_1^{k-1}) \end{aligned}$$

and

$$p_0(X_1^n) = p_0(X_k^n|X_1^{k-1})p_0(X_1^{k-1}).$$

Therefore

$$LLR_n^k = \log \frac{p_k(X_1^n)}{p_0(X_1^n)} = \log \frac{p_k(X_k^n|X_1^{k-1})}{p_0(X_k^n|X_1^{k-1})}.$$

Moreover, we have

$$\begin{aligned} LLR_n^1 - LLR_{k-1}^1 &= \log \left(\frac{p_1(X_1^n)}{p_0(X_1^n)} \Big/ \frac{p_1(X_1^{k-1})}{p_0(X_1^{k-1})} \right) \\ &= \log \frac{p_1(X_k^n|X_1^{k-1})}{p_0(X_k^n|X_1^{k-1})}. \end{aligned}$$

Now, we see if $p_k(X_k^n|X_1^{k-1}) = p_1(X_k^n|X_1^{k-1})$ for all $1 \leq k \leq n$, then

$$LLR_n^k = LLR_n^1 - LLR_{k-1}^1$$

for all $1 \leq k \leq n$. Hence

$$\begin{aligned} T_n &= \max_{1 \leq k \leq n+1} LLR_n^k = \max_{1 \leq k \leq n+1} (LLR_n^1 - LLR_{k-1}^1) \\ &= \max_{1 \leq k \leq n} (LLR_n^1 - LLR_k^1) = \widehat{T}_n. \end{aligned}$$

□

3.2 Change Detection in Nonhomogeneous HMM

Over the past decades, state estimation of stochastic hidden signals from observational data has attracted much attention in different fields of science and engineering. However, real-world random dynamical systems studied in many QCD applications, such as jet engine anomaly diagnosis, typically involve some nonlinear drifts with a sudden additive change. The QCD problems in the nonlinear HMMs constructed from these underlying signals have

not been extensively studied and deeply understood beyond linearizations. One major difficulty results from the lack of robust and accurate likelihood ratio approximation that characterizes the asymptotically optimal detector using the generalized CUSUM procedure. To address this issue, it is natural to recall nonlinear filtering techniques that provide recursive algorithms for approximating the conditional density of the state variables. In this section, we start with the general case of an HMM with a change point, which can be considered as a particular example of a non-homogeneous HMM.

3.2.1 Time Inhomogeneous HMM

Suppose that $\{(X_n, Y_n) : n \geq 0\}$ is an HMM. Thus the signal $\{X_n : n \geq 0\}$ is a $\mathbb{R}^d$ valued Markov chain with transition probability densities $g_n(x, \cdot)$, so that

$$\mathbb{P}(X_n \in A | X_{n-1}) = \int_A g_n(X_{n-1}, u)du, \quad n \geq 1,$$

and initial distribution $g_0(\cdot)$, so that

$$\mathbb{P}(X_0 \in A) = \int_A g_0(u)du.$$

The observations $\{Y_n : n \geq 0\}$ (let us assume for simplicity they are real-valued) have likelihood functions $f_n(y|x)$, so that

$$\mathbb{P}(Y_n \in B | X_0^\infty, Y_0^{n-1}) = \int_B f_n(y|X_n)dy, \quad n \geq 0.$$

The joint density of $(X_0, X_1, \ldots, X_n, Y_0, Y_1, \ldots, Y_n) = (X_0^n, Y_0^n)$ is given by

$$F(x_0^n, y_0^n) = g_0(x_0)f_0(y_0|x_0)\prod_{k=1}^{n}\Big(g_k(x_{k-1}, x_k)f_k(y_k|x_k)\Big), \tag{3.21}$$

and then the joint density of the observable sequence $(Y_0, Y_1, \ldots, Y_n) = Y_0^n$ is

$$\int \cdots \int F(x_0^n, y_0^n)dx_n \cdots dx_0. \tag{3.22}$$

We will use $p(\cdot)$ and $p(\cdot|\cdot)$ as a general symbol for joint density and conditional density. Thus (3.21) and (3.22) may be rewritten as

$$p(X_0^n, Y_0^n) = g_0(X_0)f_0(Y_0|X_0)\prod_{k=1}^{n}\Big(g_k(X_{k-1}, X_k)f_k(Y_k|X_k)\Big). \tag{3.23}$$

and

$$p(Y_0^n) = \int \cdots \int \left(g_0(x_0) f_0(Y_0|x_0) \prod_{k=1}^{n} \Big(g_k(x_{k-1}, x_k) f_k(Y_k|x_k) \Big) \right) dx_n \cdots dx_0. \tag{3.24}$$

3.2.2 Recursive Formula for Filtering

Here we are concerned with the conditional density $p(X_n|Y_0^n)$ of X_n given the observations $Y_0, Y_1, \cdots, Y_n$. The recursive nature of (3.23) yields the following standard recursive formula for $p(X_n|Y_0^n)$, see for example [6].

Lemma 3.2.1.

$$p(X_n, Y_0^n) = \int g_n(X_{n-1}, X_n) f_n(Y_n|X_n) p(X_{n-1}, Y_0^{n-1}) dX_{n-1}. \tag{3.25}$$

Proof. We have

$$p(X_n, Y_0^n) = \int p(X_{n-1}, X_n, Y_0^n) dX_{n-1}.$$

Now $p(X_{n-1}, X_n, Y_0^n) = p(X_{n-1}, X_n, Y_0^{n-1}, Y_n)$ and the Markov property at time $n-1$ gives

$$p(X_{n-1}, X_n, Y_0^{n-1}, Y_n) = p(X_{n-1}, Y_0^{n-1}) p(X_n, Y_n|X_{n-1}, Y_{n-1})$$

Also

$$p(X_n, Y_n|X_{n-1}, Y_{n-1}) = g_n(X_{n-1}, X_n) f_n(Y_n|X_n).$$

Therefore

$$\begin{aligned} p(X_n, Y_0^n) &= \int p(X_{n-1}, X_n, Y_0^n) dX_{n-1} \\ &= \int p(X_{n-1}, Y_0^{n-1}) g_n(X_{n-1}, X_n) f_n(Y_n|X_n) dX_{n-1} \end{aligned}$$

and the proof is done. □

Proposition 3.2.1.

$$p(X_n|Y_0^n) = \frac{\int g_n(X_{n-1}, X_n) f_n(Y_n|X_n) p(X_{n-1}|Y_0^{n-1}) dX_{n-1}}{\int \int g_n(X_{n-1}, X_n) f_n(Y_n|X_n) p(X_{n-1}|Y_0^{n-1}) dX_{n-1} dX_n}. \tag{3.26}$$

In the Gaussian setting, this is the Kalman filter. To update from time $n-1$ to time n we need

- the time n transition density $p(X_n|X_{n-1}) = g_n(X_{n-1}, X_n)$, and
- the time n likelihood function $f_n(Y_n|X_n)$.

3.2.3 Likelihoods

Here we consider the likelihood $p(Y_n|Y_0^{n-1})$ of observation Y_n given the previous observations $Y_0, Y_1, \cdots, Y_{n-1}$. From the joint $p(X_n, Y_0^n)$ given in the numerator of (3.26), we write

$$p(Y_n|Y_0^{n-1}) = \iint g_n(X_{n-1}, X_n) f_n(Y_n|X_n) \\ p(X_{n-1}|Y_0^{n-1}) dX_{n-1} dX_n. \tag{3.27}$$

This result is proven in Appendix A.2, and more relevant details can be found in [1]. The formula (3.27) for $p(Y_n|Y_0^{n-1})$ uses

- the conditional density $p(X_{n-1}|Y_0^{n-1})$ calculated recursively using (3.26) up to time $n-1$,
- the time n transition density $p(X_n|X_{n-1}) = g_n(X_{n-1}, X_n)$, and
- the time n likelihood function $f_n(y|x)$.

The diagram presented in Figure 3.1 provides a concise summary of the recursive computation of likelihoods utilizing standard filtering techniques.

3.2.4 Change Points for HMM

Suppose now the HMM changes from a given time-homogeneous HMM at some unknown time k to a different time-homogeneous HMM. Let $g(x, x')$ and $f(y|x)$ be the transition density and likelihood function for the pre-change HMM, and let $\widetilde{g}(x, x')$ and $\widetilde{f}(y|x)$ be the transition density and likelihood function for the post-change HMM. Thus

$$g_n(x, x') = \begin{cases} g(x, x') & \text{if } n < k \\ \widetilde{g}(x, x') & \text{if } n \geq k \end{cases}$$

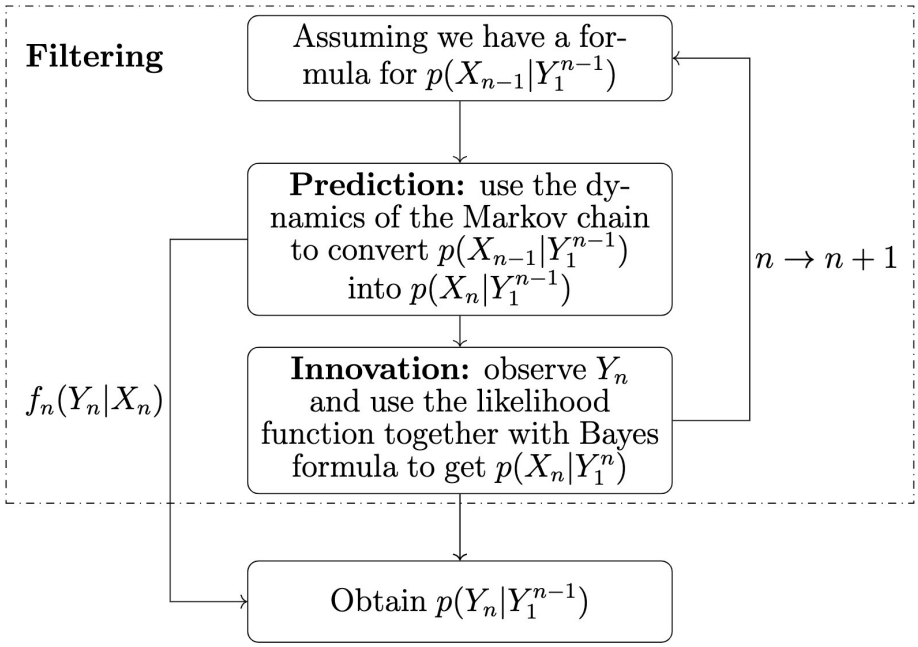


Figure 3.1: Scheme of calculating $p(Y_n|Y_1^{n-1})$ for a HMM.

and

$$f_n(y|x) = \begin{cases} f(y|x) & \text{if } n < k \\ \widetilde{f}(y|x) & \text{if } n \geq k. \end{cases}$$

In order to use the recursive formula (3.26) for $p(X_n|Y_1^n)$ in terms of $p(X_{n-1}|Y_1^{n-1})$ it is necessary to know whether to use $g(x, x')$ and $f(y|x)$, or else use $\widetilde{g}(x, x')$ and $\widetilde{f}(y|x)$. That is, it is necessary to know whether $n < k$ or $n \geq k$.

Since the formula (3.26) is recursive, to get the accurate values for $p(X_n|Y_1^n)$ and $p(Y_n|Y_1^{n-1})$ at time n it is necessary to get the correct values for $p(X_j|Y_1^j)$ for all $j = 1, 2, \ldots, n$. Let us denote the joint density of $(Y_0, Y_1, \cdots, Y_n)$ under $\mathbb{P}_0$ and $\mathbb{P}_k$ as $p_0(Y_0^n)$ and $p_k(Y_0^n)$, respectively. Note that $\mathbb{P}_0$ and $\mathbb{P}_k$ are defined at the beginning of Section 3.1. For $n < k$, the change has not happened by time n, and we have $p_k(Y_0^n) = p_0(Y_0^n)$. But for $k \leq n$, we have to incorporate the effect of the change into the formula for $p_k(Y_0^n)$. That is, the value of the joint density

$$p_k(Y_0, Y_1, \ldots, Y_n) = p_k(Y_0) \prod_{j=1}^{n} p_k(Y_j|Y_1^{j-1})$$

will be different in each of the cases $k = 1$, $k = 2$, ..., $k = n$, and $k > n$. This differs from the standard model, allowing only the two possibilities corresponding to $k \leq n$ and $k > n$. For $n \geq k$, the likelihood ratio for p_k versus p_0 is

$$LR_n^k := \frac{p_k(Y_0^n)}{p_0(Y_0^n)} = \frac{\prod_{i=1}^{k-1} p_0(Y_i|Y_1^{i-1}) \times \prod_{i=k}^{n} p_k(Y_i|Y_1^{i-1})}{\prod_{i=1}^{n} p_0(Y_i|Y_1^{i-1})} = \frac{\prod_{i=k}^{n} p_k(Y_i|Y_1^{i-1})}{\prod_{i=k}^{n} p_0(Y_i|Y_1^{i-1})} = \prod_{i=k}^{n} \Lambda_i^{(k)}, \tag{3.28}$$

where

$$\Lambda_i^{(k)} = \frac{p_k(Y_i|Y_1^{i-1})}{p_0(Y_i|Y_1^{i-1})}. \tag{3.29}$$

At the change point k, it follows from (3.27) that we have

$$\begin{aligned} \Lambda_k^{(k)} = \frac{p_k(Y_k|Y_1^{k-1})}{p_0(Y_k|Y_1^{k-1})} &= \frac{\iint \widetilde{g}(X_{k-1}, X_k)\widetilde{f}(Y_k|X_k)p_k(X_{k-1}|Y_0^{k-1})dX_{k-1}dX_k}{\iint g(X_{k-1}, X_k)f(Y_k|X_k)p_0(X_{k-1}|Y_0^{k-1})dX_{k-1}dX_k} \\ &= \frac{\iint \widetilde{g}(X_{k-1}, X_k)\widetilde{f}(Y_k|X_k)p_0(X_{k-1}|Y_0^{k-1})dX_{k-1}dX_k}{\iint g(X_{k-1}, X_k)f(Y_k|X_k)p_0(X_{k-1}|Y_0^{k-1})dX_{k-1}dX_k}. \end{aligned} \tag{3.30}$$

Notice that we have imposed $p_k(X_{k-1}|Y_0^{k-1}) = p_0(X_{k-1}|Y_0^{k-1})$ in (3.30). Therefore, both $p_0(Y_k|Y_1^{k-1})$ and $p_k(Y_k|Y_1^{k-1})$ are calculated based on the same posterior density (i.e., $p_0(X_{k-1}|Y_0^{k-1})$) at time $k-1$. However, in the standard model, $p_k(Y_k|Y_1^{k-1})$ is calculated by $p_1(X_{k-1}|Y_0^{k-1})$. This also explains why the likelihood ratio in (3.28) should depend on knowledge of k.

It follows from (3.9) that for any $n < k$, the conditional density of Y_n given Y_1^{n-1} is $f_{0,n}(Y_n|Y_1^{n-1})$ when the pre-change process is considered. However, the post-change distribution in the context of our hidden Markov model inherently depends on the time of the change. As such, the application of the standard model is rendered inapplicable in this scenario, leading to the invalidity of equation (3.10). So after the change occurs, the conditional density of Y_n given Y_1^{n-1} is now given as $f_{1,n}^{(k)}(Y_n|Y_1^{n-1})$ where $n \geq k$, and the superscript (k) in the conditional density indicates the post-change distribution depends on the change point k. Then, the log-likelihood ratio at time step n is given by

$$Z_n^{(k)} = \log\left(\frac{f_{1,n}^{(k)}(Y_n|Y_1^{n-1})}{f_{0,n}(Y_n|Y_1^{n-1})}\right), \tag{3.31}$$

and the associated generalized CUSUM statistic is given by (3.18).

Tartakovsky *et al.* [90, 87] have also mentioned the possibility that the post-change conditional density may depend on the change point k. In particular, Fuh [34] investigated

the QCD problem in HMMs with a similar model for the change, where the likelihood ratio depends on the discrete-time signal X_{k-1} (according to our notations). The X_{k-1} distribution must be estimated from the observations Y_1^{k-1} using the pre-change parameter values, not the post-change parameter values. This is why the post-change transition densities $f_{1,i}^{(k)}(Y_i|Y_1^{i-1})$ for $i \geq k$ depend on the change point k as well as i.

3.3 Change Detection in Nonlinear HMMs using Particle Filters

Although real-world dynamical systems are mostly in continuous time, for example, in aircraft and spacecraft dynamical models, observational data are usually collected at some intervals of time, which yields a sequence of discrete-time observations. When a change occurs at some unknown time in such HMMs with continuous time signal and discrete time observations, we shall study how the generalized CUSUM procedure works for detecting the change in this case. As one of the most well-established numerical schemes for the nonlinear filter, the particle methods [3] are a powerful tool to approximate the prior and posterior distributions of nonlinear stochastic processes. Therefore, we can use it to estimate the log-likelihood ratio given in the generalized CUSUM statistic for QCD problems in nonlinear HMMs. The asymptotic optimality of the generalized CUSUMs with likelihoods estimated using a particle filtering approach has been studied in [96]. Azimi-Sadjadi and Krishnaprasad proposed a particle filtering approach to change detection for non-linear systems in [5], and modified the CUSUM detection statistic so that the intensive computational complexity in the implementation of the particle filter is reduced. However, the recursiveness of the modified statistic given in [5] is based on knowing the probability of change at time n conditioned on no change before n. This probability is not always easily evaluated or specified, especially in QCD problems in the engine compressor model. So, it is still essential to test the effectiveness of the original non-recursive CUSUM algorithm and compare it with the recursive CUSUM statistic that assumes an instant change, to find some insightful compromise for the computational efficiency and theoretical accuracy of the change detection procedures.

3.3.1 Nonlinear Change Detection: Problem Setup

Suppose we have a continuous time signal $\{X(t) : t \geq 0\}$ for some observations at discrete times, $\gamma, 2\gamma, \cdots$, where γ denotes the unit time interval. For instance, the signal $X(t)$ is

governed by the following stochastic differential equation,

$$dX(t) = \begin{cases} f(X(t), \theta_0)dt + \sigma dW(t), & t < \kappa \\ f(X(t), \theta_1)dt + \sigma dW(t), & t \geq \kappa, \end{cases} \tag{3.32}$$

where the change happens at an unknown time $\kappa = (k-1)\gamma$, and k refers to the change point in the discrete-time model (see (3.1)). As before, θ_0 and θ_1 indicate that the state process is in the pre-change regime and post-change regime, respectively; $\{W(t) : 0 \leq t \leq T\}$ is a Wiener process, and $f(X(t), \theta_0)$ and $f(X(t), \theta_1)$ have some proper dimensions. The observation at time n is of the form

$$Y_n = h(X(n\gamma)) + V_n, \tag{3.33}$$

where V_n is i.i.d. with known density. Most commonly, $V_n \sim \mathcal{N}(0, \tau^2)$, for $n = 1, \cdots, N$, which is independent of $W(t)$. We can distinguish continuous and discrete time versions of X using $X(t)$ for continuous-time and $X_n = X(n\gamma)$ for the value at the time of the n^{th} observation. The evolution of the state process from time n to time $n+1$ determines the transition probability density $p(X_{n+1}|X_n)$ for the Markov chain $\{X_n : n \geq 0\}$. The system

$$\begin{aligned} &\mathbb{P}(X_{n+1} \in A|X_n) = \int_A p(x|X_n)dx \\ &Y_n = h(X_n) + V_n \end{aligned} \tag{3.34}$$

is now a discrete-time system, analogous to (3.32) and (3.33); A represents a subset of the state space for the signal.

3.3.2 Construction of the Change Detection Statistics using Particle Filters

It follows from (3.27) that

$$\begin{aligned} p(Y_n|Y_1^{n-1}) = \int \int & p(Y_n|X_n)p(X_n|X_{n-1}) \\ & p(X_{n-1}|Y_1^{n-1})dX_{n-1}dX_n. \end{aligned} \tag{3.35}$$

The explicit form of the likelihood function $p(Y_n|X_n)$ in relation to $Y_n - h(X_n)$ can be ascertained due to the known density of the observational noise V_n. If the state process with the dynamics given in (3.32) is linear, we have an explicit formula for the conditional

density $p(X_n|X_{n-1})$ since we know the relevant distribution is Gaussian. In the case of nonlinear dynamics, the estimation of the state-space models can be solved by the following procedure: Suppose that at time $n-1$ we approximate the conditional density $p(X_{n-1}|Y_1^{n-1})$ by a collection of M particles with masses $q_{n-1}^{(i)}$ and positions $X_{n-1}^{(i)}$ with total mass $\sum_{i=1}^{M} q_{n-1}^{(i)} = 1$. Then, the particles at time $n-1$ are propagated forward independently using the Euler-Maruyama scheme [42] for the stochastic differential equation (3.32) on the interval $(n-1)\gamma \leq t \leq n\gamma$, giving new positions $X_n^{(i)}$ for $i = 1, 2, \cdots, M$. Notice that the Euler-Maruyama scheme is general enough to handle both additive and multiplicative noise, so the calculations of $p(Y_n|Y_{n-1})$ using particle filters can be applied to the generalized CUSUM statistics even if the signal noise is multiplicative. After the state transition process, the prediction $p(X_n|Y_1^{n-1})$ at time n can be approximated by the updated particles with the associated weights, i.e.,

$$p(X_n|Y_1^{n-1}) \approx \sum_{i=1}^{M} q_{n-1}^{(i)} \delta(X_n - X_n^{(i)}), \tag{3.36}$$

where $\delta(\cdot)$ is the Dirac delta function. Substituting the above approximation into (3.35) yields $p(Y_n|Y_1^{n-1})$ as

$$\begin{aligned} &\int p(Y_n|X_n) \sum_{i=1}^{M} q_{n-1}^{(i)} \delta(X_n - X_n^{(i)}) dX_n \\ =&\sum_{i=1}^{M} \int p(Y_n|X_n) q_{n-1}^{(i)} \delta(X_n - X_n^{(i)}) dX_n \\ =&\sum_{i=1}^{M} q_{n-1}^{(i)} p(Y_n|X_n^{(i)}). \end{aligned} \tag{3.37}$$

Given the density of the observational noise V_n, the likelihood function $p(Y_n|X_n^{(i)})$ can be calculated explicitly. Now, let us consider the "changed" nonlinear HMM and use p_{θ_0} and p_{θ_1} to distinguish the particle approximations of the conditional probabilities under the pre-change distribution from the post-change distribution. Therefore, the log-likelihood ratio becomes

$$\begin{aligned} Z_n^{(k)} &= \log \left(\frac{f_{1,n}^{(k)}(Y_n|Y_1^{n-1})}{f_{0,n}(Y_n|Y_1^{n-1})} \right) \\ &\approx \log \left(\frac{\sum_{i=1}^{M} q_{1,n-1}^{k,i} p_{\theta_1}\left(Y_n|X_n^{k,i}\right)}{\sum_{i=1}^{M} q_{0,n-1}^{(i)} p_{\theta_0}\left(Y_n|X_n^{(i)}\right)} \right). \end{aligned} \tag{3.38}$$

Notice that the change point k is unknown, and $Z_n^{(k)}$ is an $n \times n$ lower triangular matrix because $f_{1,n}^{(k)}(Y_n|Y_1^{n-1}) = f_{0,n}(Y_n|Y_1^{n-1})$ for all $n < k$. For any $n \geq k$, $X_n^{k,i}$ represents the position of the particle i at time n conditioned on the change that occurs at time k. The generalized CUSUM statistic we consider in this thesis is given by

$$\begin{aligned} T_n &= \max_{1\leq k\leq n} (Z_k^{(k)} + \cdots + Z_n^{(k)}) \\ &= \max_{1\leq k\leq n} \sum_{i=k}^{n} \log \frac{f_{1,i}^{(k)}(Y_i|Y_1^{i-1})}{f_{0,i}(Y_i|Y_1^{i-1})}, \end{aligned} \tag{3.39}$$

where $f_0(\cdot|\cdot)$ and $f_1^{(k)}(\cdot|\cdot)$ represent the conditional probability density function of the pre-change distribution and post-change distribution, respectively. The associated probability measure defined on the sequence of observations corresponding to change at time k and no change is $\mathbb{P}_k$ and $\mathbb{P}_0$. Notice that T_n is theoretically given by (3.39), but for computations we need to replace the first expression in (3.38) with the second expression in (3.38). The utilization of the particle method is applied in this section to approximate the log-likelihood ratios and T_n to identify a change in the hidden Markov model with nonlinear dynamics. The asymptotic optimality of the generalized CUSUM rule using particle filters has been proved in [96].

3.3.3 A Comparison of the Generalized CUSUM and the CUSUM-like Procedure with Instant Change

In [35], Fuh and Mei mentioned that $\widehat{T}_n$ usually works well, even though T_n theoretically incorporates the true post-change measures. However, the HMM conditional likelihood-based change detection was studied in [25] and considered to outperform the relevant CUSUM. A specific QCD application in HMM that draws much of our attention is relevant to the health management [97] and anomaly detection [23] in the engine compressor systems [38, 61], from which the associated HMMs in (3.1) can be well characterized. Notice that the change is only added in the hidden signals but can be indirectly reflected in the observational process. The key issue is what happens to the state X_k at the time of the change. To address this issue, Fuh [33] uses the statistic $\widehat{T}_n$, although it appears that he is considering two HMMs with different parameters. Up to time $k-1$ we observe for the first HMM, and from time k onwards we observe from the second HMM. This seems equivalent to considering two engines—one with a bird stuck in it and the other without. At time k, we switch from observing the engine without the bird to observing the engine with the bird. However, this is not the physical model that we are focused on. While the generalized

CUSUM procedure is theoretically optimal in the asymptotic sense [33] to address the QCD problems in nonlinear HMMs, the computational burden of evaluating (3.39) using particle filters could be more evident as the total number of observations increases. However, one may realize that it is easy to describe $\mathbb{P}_0$ (no change) and $\mathbb{P}_1$ (immediate change), but there is some ambiguity in how to describe $\mathbb{P}_k$ for general k. The issue is what happens to the state Y_k at the time of the change. Fuh [33] mitigates this issue by using the statistic $\widehat{T}_n$ described below,

$$\widehat{T}_n = \max_{1\leq k\leq n} (Z_k^{(1)} + \cdots + Z_n^{(1)}), \tag{3.40}$$

where for any $n \geq 1$, the LLR $Z_n^{(1)}$ is expressed and approximated as follows,

$$\begin{aligned} Z_n^{(1)} &= \log\left(\frac{f_{1,n}^{(1)}(Y_n|Y_1^{n-1})}{f_{0,n}(Y_n|Y_1^{n-1})}\right) \\ &\approx \log\left(\frac{\sum_{i=1}^{M} q_{1,n-1}^{1,i} p_{\theta_1}\left(Y_n|X_n^{1,i}\right)}{\sum_{i=1}^{M} q_{0,n-1}^{(i)} p_{\theta_0}\left(Y_n|X_n^{(i)}\right)}\right). \end{aligned} \tag{3.41}$$

Notice that we can ignore all the superscripts (1) in (3.41) as this reduces to the standard model. Hence, the QCD scheme using $\widehat{T}_n$ can be defined with respect to the following stopping time,

$$\tau_c = \inf\{n \geq 1 : \widehat{T}_n \geq c\}, \tag{3.42}$$

for some threshold $c > 0$. Compared with (3.38), much fewer particles are needed to implement $Z_n^{(1)}$ in practice. With the recursiveness mentioned in (3.20), the computational complexity of simulating $\widehat{T}_n$ via particle methods can be dramatically reduced. But it is expected that $\widehat{T}_n$ could be theoretically less accurate than T_n especially in the HMM case, since it does not account for what happens to the observation Y_k at the change point. To compare T_n with $\widehat{T}_n$ from (3.39) and (3.40), it is indeed essential to check the differences and similarities between the distributions of $Z_n^{(k)}$ and $Z_n^{(1)}$ for some n and for all $1 \leq k \leq n$. Although T_n does not own any recursive form, the compromise of being computationally efficient for $\widehat{T}_n$ regards its detection performance in terms of detecting the change under a certain false alarm constraint with more delay. This comparison will be discussed in more detail in the next sections of this chapter, which includes more analysis and simulations.

3.4 Change Detection in Moore-Greitzer Model of a Compressor

Although the issues about jet engine anomaly detection [23] and health management [97] have been investigated over many years, QCD algorithms have been barely applied to jet engines with streaming data. Jet engines are built with four modules in a row: intake fan, air compressor, combustor, and turbine. There are approximately 100 sensors incorporated in the engine that measure different performance parameters, such as the pressure and temperature of the engine gas path, as well as the vibration levels of the rotating components. The data collected by these sensors is essential in providing an accurate assessment of the engine's performance and ensuring optimal functionality.

Undoubtedly, fault diagnosis or anomaly detection of engine performance plays an important role in promoting the safety and reliability of aircraft engines. When the engine system undergoes a change, e.g., an anomaly in the operating or maintenance parameters, it is urgent to detect the change as soon as possible and limit the false alarm risks to take some emergency action. As a result, it is natural to believe that the change detection with the generalized CUSUM scheme proposed here could be a vital procedure for detecting abrupt changes in some modules of jet engines, such as the engine compressor systems. In this section, we focus on a specific system of jet engine compressor models that capture the so-called pure surge instability of the Moore-Greitzer model [61], and employ the QCD method introduced in this chapter to detect a change in the system.

3.4.1 Pure Surge and the QCD Problem Setup

Let us now focus on studying a special case of the Moore-Greitzer ODE system — pure surge modes via a reduced, planar model with a close coupled valve [44, 37]. The governing equations for the mass flow rate (denoted as Φ) and the inlet pressure (denoted as Ψ) are given by

$$\begin{aligned} \Phi' &= \frac{1}{l_c}(\Psi_C(\Phi) - \Psi_V(\Phi) - \Psi), \\ \Psi' &= \frac{1}{4B^2 l_c}(\Phi - \gamma_T\sqrt{\Psi}), \end{aligned} \tag{3.43}$$

where $'$ represents the time derivative, l_c is the effective flow-passage non-dimensional length of the compressor and ducts, B is the dimensionless Greitzer parameter, γ_T is the

throttle gain. Moreover, the turbomachine static characteristic is as follows,

$$\Psi_C(\Phi) = \Psi_{C0} + H\left(1 + \frac{3}{2}\tilde{\Phi} - \frac{1}{2}\tilde{\Phi}^3\right), \tag{3.44}$$

where

$$\tilde{\Phi} = \frac{\Phi - \Phi_0}{W} - 1,$$

H and W are constant parameters, and Ψ_{C0} and Φ_0 denote the initial turbomachine pressure and initial mass flow rate, respectively. $\Psi_V(\Phi) = \frac{1}{\gamma^2}\Phi^2$ where the throttle coefficient $\gamma > 0$ is proportional to the valve opening. To obtain the fixed points of the system (3.43), it is essential to investigate the roots of the cubic polynomial equation

$$\begin{aligned} &\Psi_C(\Phi_e) - \Psi_V(\Phi_e) - \frac{1}{\gamma_T^2}\Phi_e^2 = 0, \\ &\Psi_e = \Psi_C(\Phi_e) - \Psi_V(\Phi_e). \end{aligned} \tag{3.45}$$

Using the standard technique to solve the above polynomial, we find there is only one real root and a pair of imaginary roots. More details with regard to the stability and bifurcation analysis of the pure surge model for the Moore-Greitzer compressor can be found in [44].

At some unknown time, the dynamic equation has been changed from (3.43) to

$$\begin{aligned} \Phi' &= \frac{1}{l_c}(\Psi_C(\Phi) - \Psi_V(\Phi) - \Psi + d_\Psi), \\ \Psi' &= \frac{1}{4B^2 l_c}(\Phi - \gamma_T\sqrt{\Psi} - d_\Phi), \end{aligned} \tag{3.46}$$

by adding two-dimensional constant "anomalies" $(d_\Psi, -d_\Phi)$. This particular form of mass flow and pressure disturbances is studied in [37] for the purpose of stall/surge control, where the constant negative mass flow disturbance pushes the equilibrium over the surge line. As mentioned in the previous Section 3.3.2, we employ the Euler-Maruyama discretization scheme to simulate the continuous-time signal $\Phi(t)$ and $\Psi(t)$. Let us define X_n as a two-dimensional discrete-time vector that contains both components of the pure surge model at time n, i.e., $X_n = (\Phi_n, \Psi_n)$. We also define the following discrete-time observations denoted as Y_n with the Gaussian noise V_n,

$$Y_n = H_n X_n + V_n, \tag{3.47}$$

where H_n is a real matrix of dimension $M \times 2$, $M \in \{1, 2\}$; and $V_n \sim \mathcal{N}(0, v_n)$, a vector of dimension M. Hence we consider $\{(X_n, Y_n) : n \geq 1\}$ as a nonlinear hidden Markov model.

3.4.2 QCD in a Deterministic Stable Reduced Planar System

As a practical application of change detection in nonlinear state space systems, let us first study a QCD problem in the pure surge engine compressor model, where a two-dimensional nonlinear differential equation governs the dynamics of the signal. It is postulated that the observation is limited to solely the second component, i.e., the pressure of the engine compressor, leading to incomplete accessible data. More arguments about what would happen if we observed the first component of the compressor system are given at the end of this subsection. In simulations, we let $V_n \sim \mathcal{N}(0, 0.1)$, $\gamma_T = 0.66$, and the size of the change is given as $(d_\Phi, d_\Psi) = (-0.4, 0.05)$.

Table 3.1: The key parameter values used in all the simulations of the pure surge modes of the compressor system.

l_c	total aerodynamic length of compressor and ducts	8.0
H	semi-height of cubic axisymmetric characteristic	0.18
W	semi-width of cubic characteristic	0.25
B	dimensionless Greitzer parameter	0.5
γ	throttle gain	1.9
Ψ_{C_0}	shut-off value of compressor characteristic	0.3006

Notice that we are considering the pure surge signals without the noise, and we first plot (see Figure 3.2) the deterministic dynamics of the mass flow rate and the pressure, i.e., $\{(\Phi_n, \Psi_n) : 0 \leq n \leq 300\}$, with a change $(d_\Phi, d_\Psi) = (-0.4, 0.05)$ implanted at $\nu = 150$. The state noise effect on the performance of the aforementioned CUSUM statistics will be briefly discussed and summarized in Section 3.4.4. In the HMM, the continuous-time signal X_t is governed by a differential equation with cubic nonlinear drift given in Ψ_C:

$$\begin{pmatrix} d\Phi(t) \\ d\Psi(t) \end{pmatrix} = \begin{pmatrix} \frac{1}{l_c}(\Psi_C(\Phi) - \Psi_V(\Phi) - \Psi) \\ \frac{1}{4B^2 l_c}(\Phi - \gamma_T\sqrt{\Psi}) \end{pmatrix} dt. \tag{3.48}$$

At some unknown time, the dynamic equation has been changed from (3.48) to

$$\begin{pmatrix} d\Phi(t) \\ d\Psi(t) \end{pmatrix} = \begin{pmatrix} \frac{1}{l_c}(\Psi_C(\Phi) - \Psi_V(\Phi) - \Psi + d_\Psi) \\ \frac{1}{4B^2 l_c}(\Phi - \gamma_T\sqrt{\Psi} - d_\Phi) \end{pmatrix} dt \tag{3.49}$$

by adding two-dimensional constant forcing $(d_\Psi, -d_\Phi)$. More specifically, we let $H_n = (0, 1)$ such that the discrete-time measurements denoted as Y_n (see (3.47)) with the Gaussian noise V_n are given by

$$Y_n = \Psi_n + V_n. \tag{3.50}$$

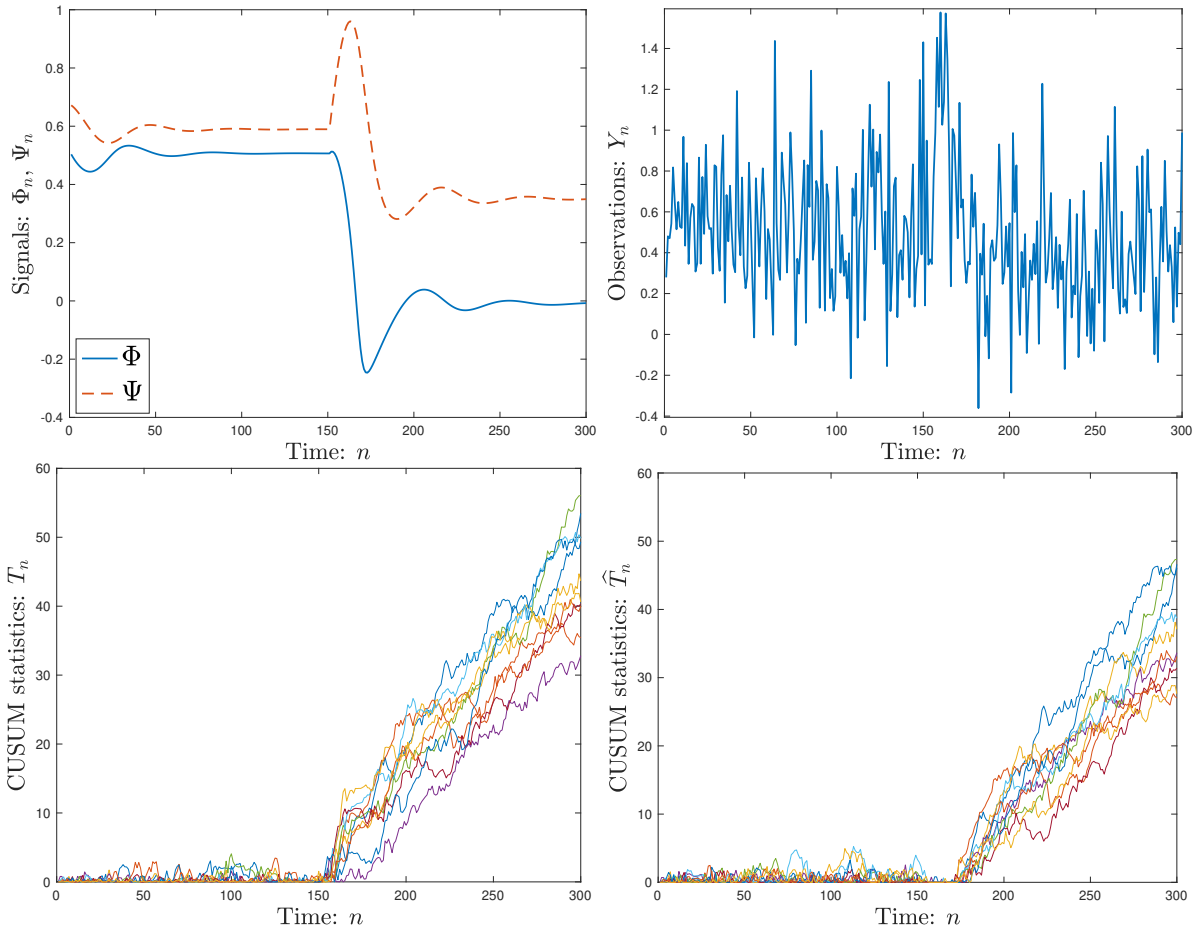


Figure 3.2: **a)** The evolution of the deterministic signals with a change $(d_\Phi, d_\Psi) = (-0.4, 0.05)$ implanted at $\nu = 150$ **(top left)**. **b)** The evolution of the observations (Ψ_n) corrupted by an additive Gaussian noise **(top right)**. **c)** The generalized CUSUM statistics (i.e., T_n) **(bottom left)** and **d)** the CUSUM statistics that assume an instant change (i.e., $\widehat{T}_n$) **(bottom right)** with 10 ensembles of observations using a particle filtering approach with 50 particles.

Once again, the change has been only added to the (hidden) signals but can be reflected in observations. Under the pre-change regime, it follows from Figure 3.2 **a)** that the two components of the signal stay around the pre-change steady state, i.e., $(\Phi_e^{\text{pre}}, \Psi_e^{\text{pre}}) = (0.5067, 0.5893)$. After the change happens, Φ (blue) and Ψ (red) first propagate with some transients and then reach the post-change fixed point, i.e., $(\Phi_e^{\text{post}}, \Psi_e^{\text{post}}) = (-0.0090, 0.3509)$. Even though it is somewhat easy to spot the change by looking at the pre- and post-change evolutions of Φ and Ψ, when some fair amount of noise contaminates the observations, it follows from the subplot **b)** of Figure 3.2 that it is challenging to identify where the change occurs visually. Fortunately, we could impose the generalized CUSUM algorithm (for non-independent and non-stationary data) where the log-likelihood ratio is approximated by the particle filtering approach to detect the change with some appropriate threshold given a specific false alarm constraint.

In Figure 3.2 **c)**, we plot ten samples of the generalized CUSUM statistics (that is, T_n), whose effectiveness is given as it hovers around 0 before about 150 time instants (which is the real changepoint) and starts to increase after that. $\widehat{T}_n$ in **d)** shows a similar trend, but the crucial difference between T_n and $\widehat{T}_n$, as shown in Figure 3.2, is $\widehat{T}_n$ causes a "flatness" along zeros from $n = 150$ to the time instant roughly $n = 175$ when Ψ (which is the second component we are observing) is still evolving in transient dynamics. This is because $\widehat{T}_n$ assumes the post-change transient behavior happens instantaneously at $n = 1$, whereas T_n processes the change in dynamics as it happens. More interestingly, if the transient dynamics move in the right direction after the change occurs towards the post-change steady state, we could see more closeness of T_n and $\widehat{T}_n$. Specifically, if we observe the engine model's first component, this "flatness" is expected to disappear.

Note that in this section, the post-change distribution is still formed by a fixed point even if it takes a little while to get there from the pre-change equilibrium, but the dynamics for pre-change and post-change systems are not dramatically shifted. The immediate effect of this is that $p_k(Y_n|Y_1^{n-1})$ and $p_1(Y_n|Y_1^{n-1})$ will not be too different as long as the transient part between the pre-change and the post-change regimes does not last too long.

3.4.3 QCD in a Deterministic Surge Compressor Model

Typically, two types of instabilities can occur in the flow through the compressor, namely surge and stall (rotating stall). In particular, surge instability is characterized by large amplitude oscillations of annulus averaged mean mass flow through the engine and plenum pressure rise. During part of the surge cycle, the mean mass flow may become reversed during the instability, thrusting air out from the front of the engine, which puts a large

stress on the components of the engine and seriously impairs its performance. This indeed motivates us to study the QCD problem in pure surge modes where the post-change limit cycle, i.e., the surge behavior, is excited from an external forcing (d_Φ, d_Ψ) given in the signal dynamics at some unknown but deterministic change point ν.

In what follows, we shall see some experimental results with the same HMM introduced in (3.48)–(3.50) but with different sizes of the change (i.e., (d_Φ, d_Ψ)). Since the "phase" of the post-change limit cycle (i.e., the post-change signals) depends on where the change occurs, this brings each possibility of the superscript (k), $1 \leq k \leq n$, into the calculation of the log-likelihood ratio (i.e., $Z_n^{(k)}$). While $Z_n^{(1)}$ is recursive and computationally efficient, it is only involved with the calculation corresponding to the post-change limit cycle whose phase is assumed at $k = 1$. Compared with the previous subsection, the post-change dynamics of the original signals are drastically changed, and more interesting differences and similarities between T_n and $\widehat{T}_n$ for detecting the relevant change will be discussed in the following subsections.

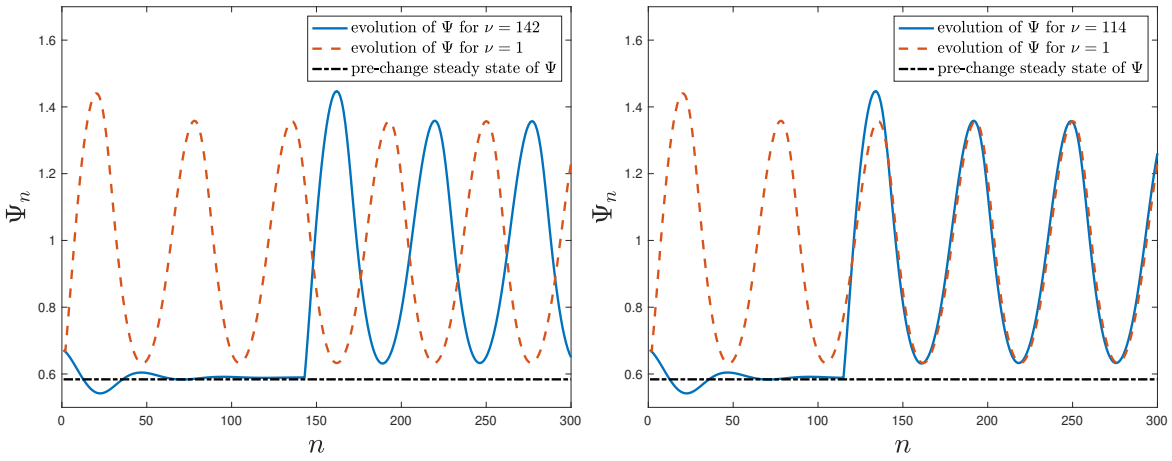


Figure 3.3: Signal Ψ of the purge model for $\nu = 142$ is out of phase (**left**) and for $\nu = 114$ is in phase (**right**) with respect to the phase of Ψ for $\nu = 1$.

The pre-change equilibrium is outside of the post-change limit cycle

Let us discuss a few cases when the pre-change steady state is outside the post-change limit cycle. These examples are varied based on different change points ν, for which the phase tested by T_n is somewhat similar or distinct from the phase assumed by $\widehat{T}_n$. Note that

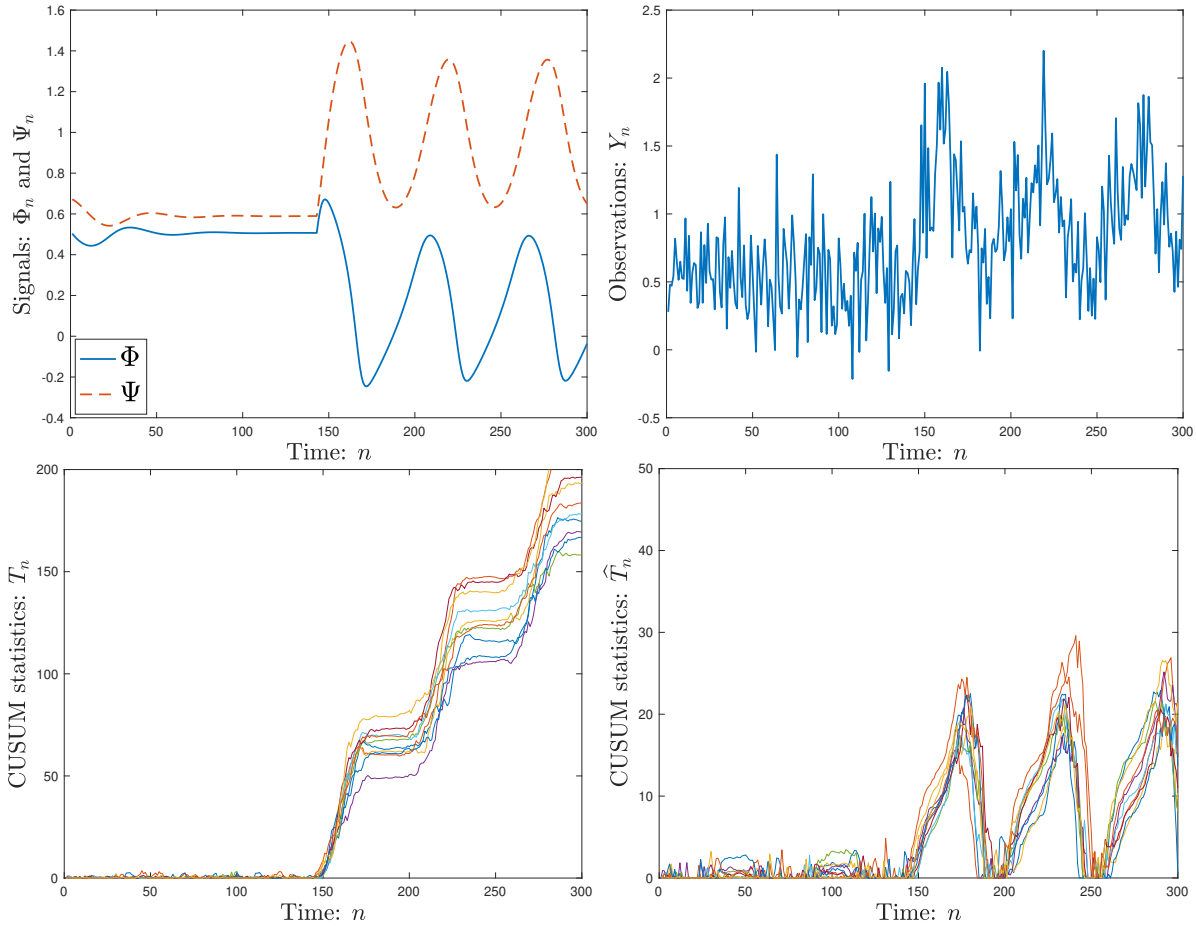


Figure 3.4: **a)** The evolution of the deterministic signals with a change $(d_\Phi, d_\Psi) = (-0.5, 0.5)$ implanted at $\nu = 142$ **(top left)**. **b)** The evolution of the observations (Ψ_n) corrupted by an additive Gaussian noise **(top right)**. **c)** The generalized CUSUM statistics (i.e., T_n) **(bottom left)** and **d)** the CUSUM statistics that assume an instant change (i.e., $\widehat{T}_n$) **(bottom right)** with 10 ensembles of observations using a particle filtering approach with 50 particles.

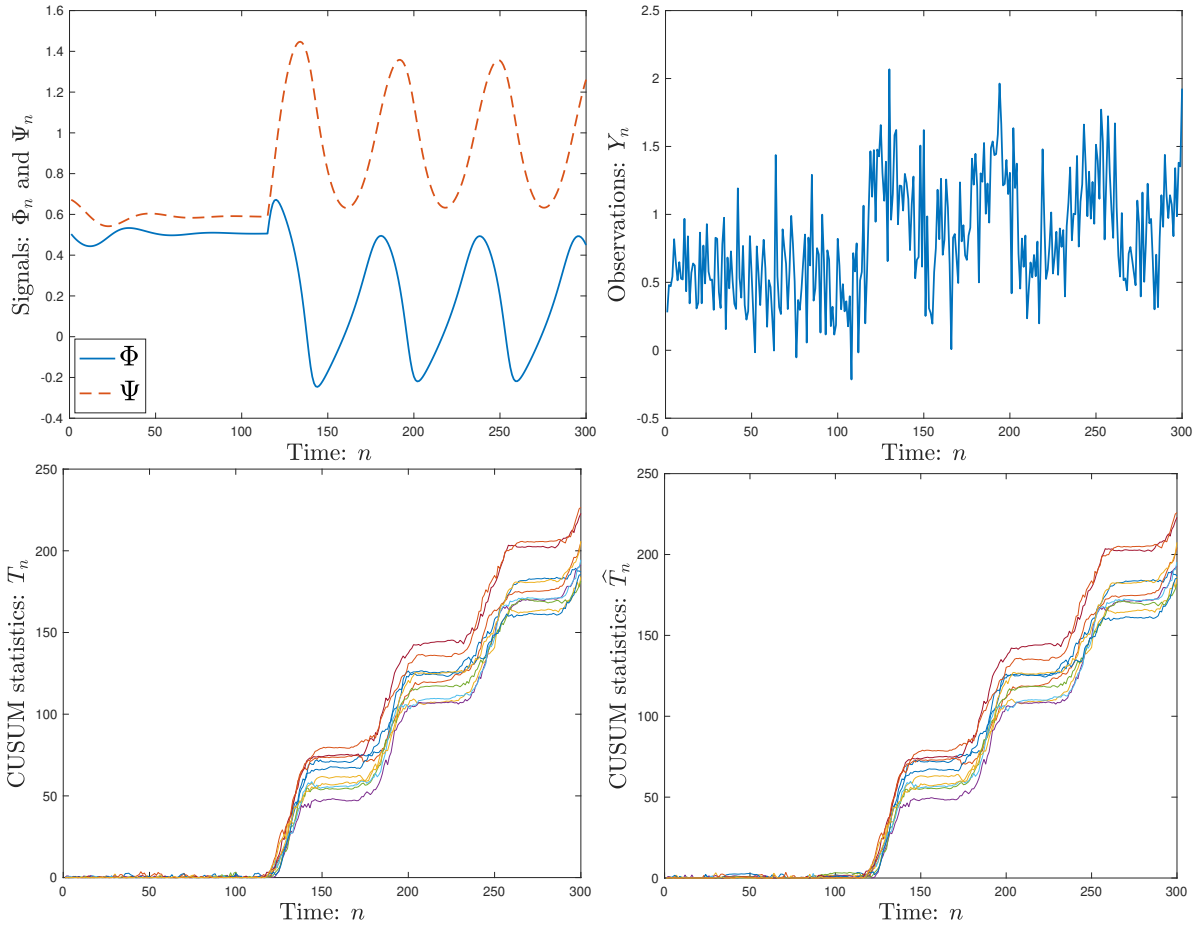


Figure 3.5: **a)** The evolution of the deterministic signals with a change $(d_\Phi, d_\Psi) = (-0.5, 0.5)$ implanted at $\nu = 114$ **(top left)**. **b)** The evolution of the observations (Ψ_n) corrupted by an additive Gaussian noise **(top right)**. **c)** The generalized CUSUM statistics (i.e., T_n) **(bottom left)** and **d)** the CUSUM statistics that assume an instant change (i.e., $\widehat{T}_n$) **(bottom right)** with 10 ensembles of observations using a particle filtering approach with 50 particles.

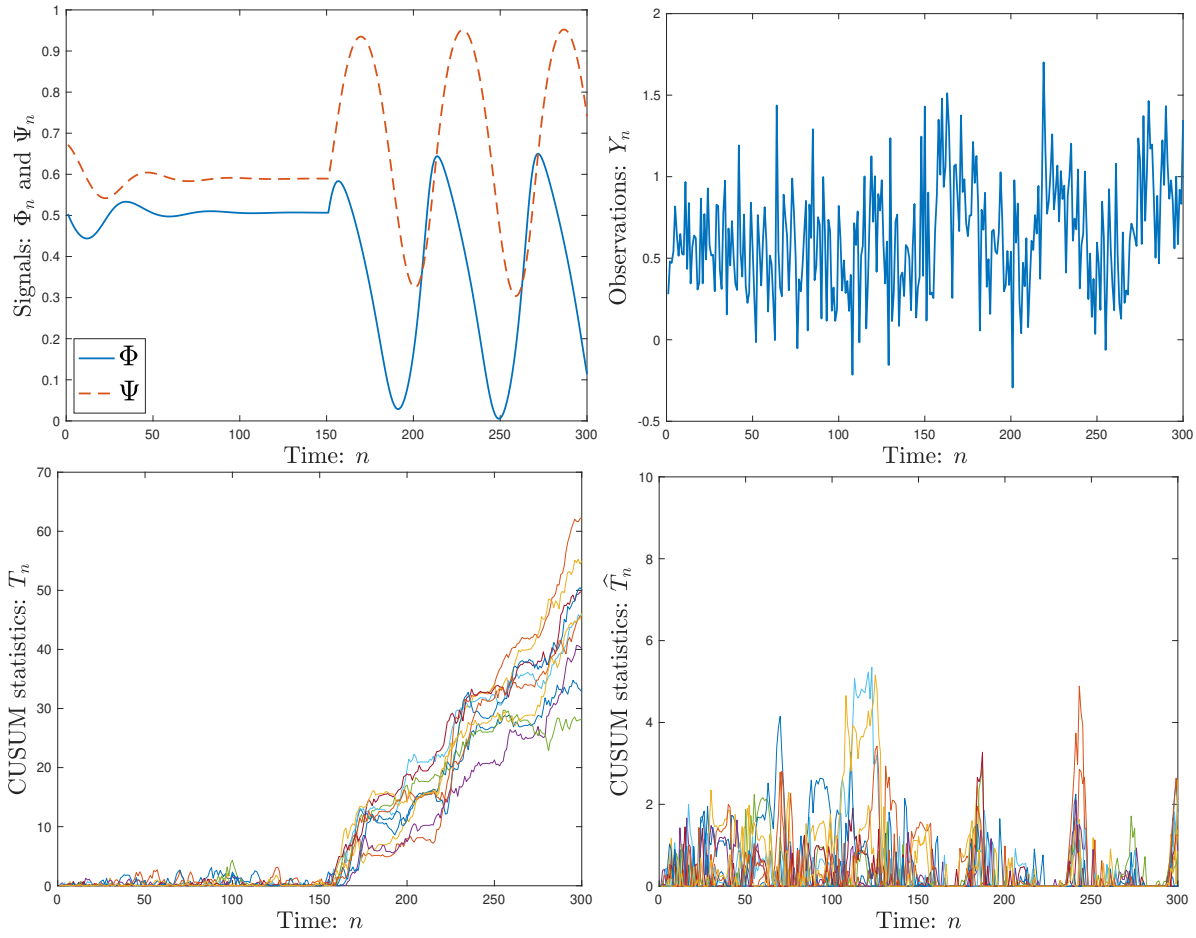


Figure 3.6: **a)** The evolution of the deterministic signals with a change $(d_\Phi, d_\Psi) = (-0.2, 0.2)$ implanted at $\nu = 150$ **(top left)**. **b)** The evolution of the observations (Ψ_n) corrupted by an additive Gaussian noise **(top right)**. **c)** The generalized CUSUM statistics (i.e., T_n) **(bottom left)** and **d)** the CUSUM statistics that assume an instant change (i.e., $\widehat{T}_n$) **(bottom right)** with 10 ensembles of observations using a particle filtering approach with 50 particles.

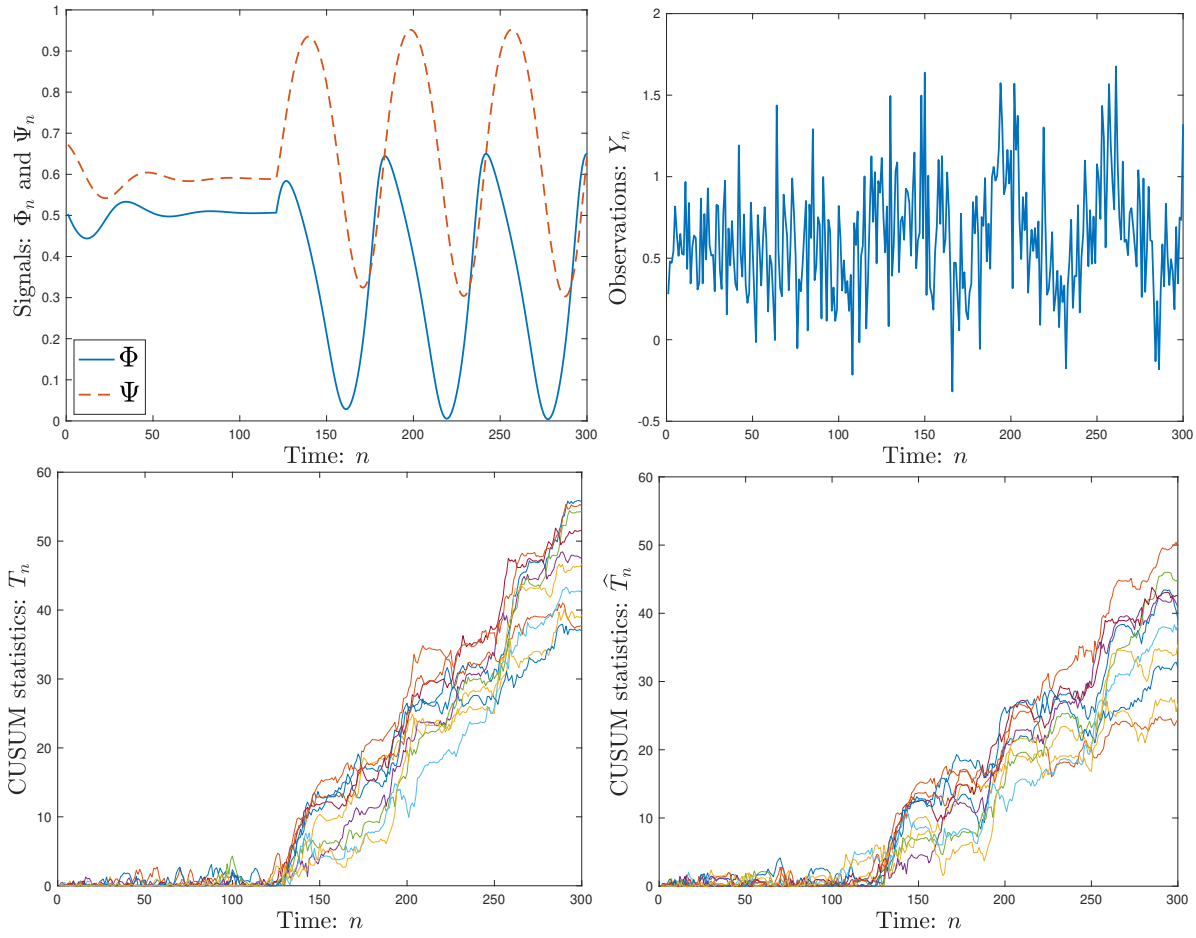


Figure 3.7: **a)** The evolution of the deterministic signals with a change $(d_\Phi, d_\Psi) = (-0.2, 0.2)$ implanted at $\nu = 120$ **(top left)**. **b)** The evolution of the observations (Ψ_n) corrupted by an additive Gaussian noise **(top right)**. **c)** The generalized CUSUM statistics (i.e., T_n) **(bottom left)** and **d)** the CUSUM statistics that assume an instant change (i.e., $\widehat{T}_n$) **(bottom right)** with 10 ensembles of observations using a particle filtering approach with 50 particles.

"outside" refers to the fixed height of pre-change Ψ; the component we observe is outside the height interval of post-change Ψ. We shall see T_n and $\widehat{T}_n$ show quite a lot of distinct comparisons in both "in phase" and "out of phase" cases. Notice that "in phase" indicates the change point ν is equal to integer multiples of the period of the post-change limit cycle, i.e., $\nu = NT_{\text{cycle}}$, where N denotes a positive integer, and T_{cycle} represents the period of the limit cycle. Oppositely, we can define the "out of phase" case as $\nu = (N + 1/2)T_{\text{cycle}}$. Figure 3.3 illustrates those two situations where the signal evolution of Ψ with instant change (i.e., $k = 1$) is "out of phase" and "in phase" when it is compared with the real change scenario (i.e., $k = \nu$). We will later explain and conclude why the "phase" of the limit cycle matters in terms of distinguishing T_n and $\widehat{T}_n$ in more details. But the essential argument here is that the transient change of phase as we move into the limit cycle for instant change ($k = 1$) is different from the real change of phase when it comes to $k = \nu$. As a more concrete example, we specify $(d_\Phi, d_\Psi) = (-0.5, 0.5)$ for this subsection, and all the other parameters are the same as before and given in Table 3.1.

1): Out of phase when $\nu = 142$: Indeed, the subplot **a)** in Figure 3.4 illustrates how the deterministic (but hidden) signals evolve with time. There exists a change occurring at around 142 time units since the dynamics have been drastically changed, i.e., from a stable fixed point to a stable limit cycle (with the period $T_{\text{cycle}} = 57$). Figure 3.4 **b)** gives a noisy observational process. In Figure 3.4 **c)**, we plot 10 samples of the generalized CUSUM statistics using particle filters, from which we see T_n hovers around zero before roughly time step 142 and starts to increase dramatically afterward. This presents the power of T_n using particle filters for the relevant QCD problem in such HMMs. In comparison, $\widehat{T}_n$ yields some "spiking oscillations" after time 142, which reflects degraded performance for change detection using $\widehat{T}_n$ though its recursive property can save a lot of computations in practice. On the other hand, one may realize that there is some "flatness" on the T_n in the regions where $\widehat{T}_n$ is decreasing to zero. This happened because the phase of the post-change cycle depends on where the change occurs. The CUSUM statistic that assumes the change happens immediately can be misleading due to the error for the phase it assumes and the real phase coming from the observations. This motivates us to further investigate how the phase of the post-change limit cycle affects the behaviors of the CUSUM statistics, i.e., T_n and $\widehat{T}_n$.

When analyzing signal phase changes, it is imperative to consider the discrepancy between the phase with an instantaneous change (i.e., $\nu = 1$) and the phase at the actual moment of change (i.e., $\nu = 142$). The natural questions are how big the difference between these two phases is and how much this phase difference would affect the calculations of the log-likelihood ratios ($Z_n^{(k)}$ and $Z_n^{(1)}$) as well as the CUSUM statistics (T_n and $\widehat{T}_n$). According to the previous Section 3.3.3, $\widehat{T}_n$ performs the calculations assuming the change

happens at time 1, whereas T_n is searching for the best possible change point scenario, up to the current time step n, which corresponds to the real phase of the post-change limit cycle. From this perspective, it is not difficult to understand why T_n should be much more effective than $\widehat{T}_n$ in this QCD problem where the change makes the system dynamics shift from a fixed point to a limit cycle. Recall that there is no model noise in the signals, so as time goes on, the randomness of the initial distribution of a reference point for Ψ (since only Ψ is observed) dies away as filtering proceeds. Consequently, in the pre-change regime, one will be more and more sure that the relevant point is approaching the exact orbit, which is the pre-change steady state. Similar logic applies to the post-change distributions. By examining the relative heights of the signal (Ψ) assuming change occurs at $\nu = 1$ and the real observations in which $\nu = 142$, to the pre-change fixed value Ψ_e, it is clear why T_n and $\widehat{T}_n$ behave as given in Figure 3.4.

2) In phase when $\nu = 114$: In this case, $k = 2T_{\text{cycle}} = 114$, the post-change cycle for $\nu = 1$ has the same phase as the post-change cycle for $k = 114$, so we shall see some intriguing similarities between T_n and $\widehat{T}_n$.

It follows from Figure 3.5 that both T_n and $\widehat{T}_n$ are valid in terms of detecting the change with some acceptable delays given an appropriate threshold. Moreover, Figure 3.5 **c)** and **d)** also illustrate very similar behavior and trend for T_n and $\widehat{T}_n$, which we believe is because of the in-phase effect that $\widehat{T}_n$ assumes in this case. This indeed makes the conditional probability density $p_k(Y_n|Y_1^{n-1})$ close to the relevant pdf of $p_1(Y_n|Y_1^{n-1})$, which essentially explains why T_n and $\widehat{T}_n$ given in Figure 3.5 look very similar to each other.

The pre-change equilibrium is inside of the post-change limit cycle

In this subsection, we let $(d_\Phi, d_\Psi) = (-0.2, 0.2)$ so that the post-change limit cycle contains the pre-change fixed point inside. Similarly, we would like to examine the "in phase" and "out of phase" cases in this particular scenario. As we simulate the original signals on both pre-change and post-change regimes, we find out that the period of the post-change limit cycle, in this case, is $T_{\text{cycle}} = 60$. Again, we aim to figure out why the performance of $\widehat{T}_n$ is degraded when Ψ_e is outside of the cycle and even crushed when Ψ_e is inside of the cycle.

1) Out of phase when $\nu = 150$: In Figure 3.6, the pre-change steady state of Φ and Ψ is inside of the post-change cycle. But it is extremely difficult to determine where the change occurs by simply looking at the observations (i.e., Figure 3.6 **b)**). Since the pre-change steady state is inside of the post-change limit cycle now, besides the out-of-phase effect after the change occurs, the event that gives contradictory information to $\widehat{T}_n$ as Ψ_n and Y_n run opposite sides of Ψ_e happens more frequently, especially immediately after the real

change-point. This makes $\widehat{T}_n$ extremely confused, and the relevant simulation results are given below in Figure 3.6 **d)**. Notice that the vertical scale of Figures 3.6 **c)** and **d)** is quite different, because in this case $\widehat{T}_n$ can hardly gain any Kullbeck-Leibler divergence from the pre-change and post-change distributions, so the vertical scale of the Figure 3.6 **d)** almost coincides with the vertical scale of the Figure 3.6 **c)** for which the process is in the pre-change regime (i.e., from $n = 1$ to around $n = 150$).

2) In phase when $\nu = 120$: In the case of "in phase" with the fixed point inside the limit cycle, one could check the simulation results given in Figure 3.7, especially the samples of T_n and $\widehat{T}_n$ in Figures 3.7 **c)** and **d)**. Although the T_n and $\widehat{T}_n$ are significantly different in the "out of phase" case (see Fig. 3.6), it is impressive to see they are both somewhat applicable to detect the change (i.e., the surge cycle) in the pure surge modes of the fan or compressor system of the engine model when the post-change cycles are "in phase".

3.4.4 QCD in a Stochastic Surge Compressor model

Let us now consider the pure surge signals governed by the following nonlinear stochastic differential equation:

$$\begin{pmatrix} d\Phi(t) \\ d\Psi(t) \end{pmatrix} = \begin{pmatrix} \frac{1}{l_c}(\Psi_C(\Phi) - \Psi_V(\Phi) - \Psi) \\ \frac{1}{4B^2 l_c}(\Phi - \gamma_T\sqrt{\Psi}) \end{pmatrix} dt + \sigma \begin{pmatrix} dW_1(t) \\ dW_2(t) \end{pmatrix}, \tag{3.51}$$

where $W_1(t)$ and $W_2(t)$ are independent standard Wiener processes. At some unknown time, the dynamic equation has been changed from (3.51) to

$$\begin{pmatrix} d\Phi(t) \\ d\Psi(t) \end{pmatrix} = \begin{pmatrix} \frac{1}{l_c}(\Psi_C(\Phi) - \Psi_V(\Phi) - \Psi + d_\Psi) \\ \frac{1}{4B^2 l_c}(\Phi - \gamma_T\sqrt{\Psi} - d_\Phi) \end{pmatrix} dt + \sigma \begin{pmatrix} dW_1(t) \\ dW_2(t) \end{pmatrix}. \tag{3.52}$$

by adding the external forcing $(d_\Psi, -d_\Phi)$. Similarly, we observe the pressure rise coefficients of the surge model such that the discrete-time measurements denoted as Y_n with the Gaussian noise V_n are given by

$$Y_n = \Psi_n + V_n. \tag{3.53}$$

Without considering the signal noise, the only randomness of the particle filtering in the calculations of the prior density (i.e., the prediction step) is from the initialization of the particles. As a result, the estimation or approximation of the conditional densities, $p_k(Y_n|Y_1^{n-1})$, is primarily affected by the phases of the post-change cycles corresponding to different values of $k = 0, 1, \cdots, n$. The difference between T_n and $\widehat{T}_n$ can be evidently identified as we discussed in the previous section. It follows from Figures 3.8 and 3.9 that

adding small-intensity Gaussian noise on the signal, e.g., $\sigma^2 = 0.0002$, can randomize the phase effect on approximating post-change distributions using particle filters for distinct change-point assumptions. These assumptions are involved with comparing $p_k(Y_n|Y_1^{n-1})$, $k = 2, \cdots, n$, with $p_1(Y_n|Y_1^{n-1})$. For the simulation results in Figures 3.8 and 3.9, the following parameter values are used

$$(\Phi_0, \Psi_0) = (0.51, 0.66),\ v_n \sim \mathcal{N}(0, 0.1),\ H = 0.18,\ l_c = 8.0,$$

$$\Psi_{C_0} = 0.3006,\ B = 0.5,\ W = 0.25,\ \gamma = 1.9,\ \gamma_T = 0.66,\ \sigma^2 = 0.0002.$$

For the simulations in Figure 3.8, $(d_\Phi, d_\Psi) = (-0.5, 0.5)$ and $\nu = 142$. This corresponds to the "out of phase" case where the pre-change equilibrium is outside of the post-change limit cycle. In Figure 3.9, $(d_\Phi, d_\Psi) = (-0.2, 0.2)$ and $\nu = 150$ are used, and this corresponds to the "out of phase" case where the pre-change equilibrium is inside of the post-change limit cycle. In both cases, we do not see a clear difference between T_n and $\widehat{T}_n$. If we only compare T_n (or only $\widehat{T}_n$) in Figures 3.8 and 3.9, we may see it is more difficult to effectively detect the change when the pre-change equilibrium is inside of the post-change limit cycle.

The phenomenon shown with respect to the deterministic signal cases can be effectively mitigated by introducing a certain degree of signal noise. This technique serves to randomize the phase effect of the post-change limit cycle, thereby reducing its impact.

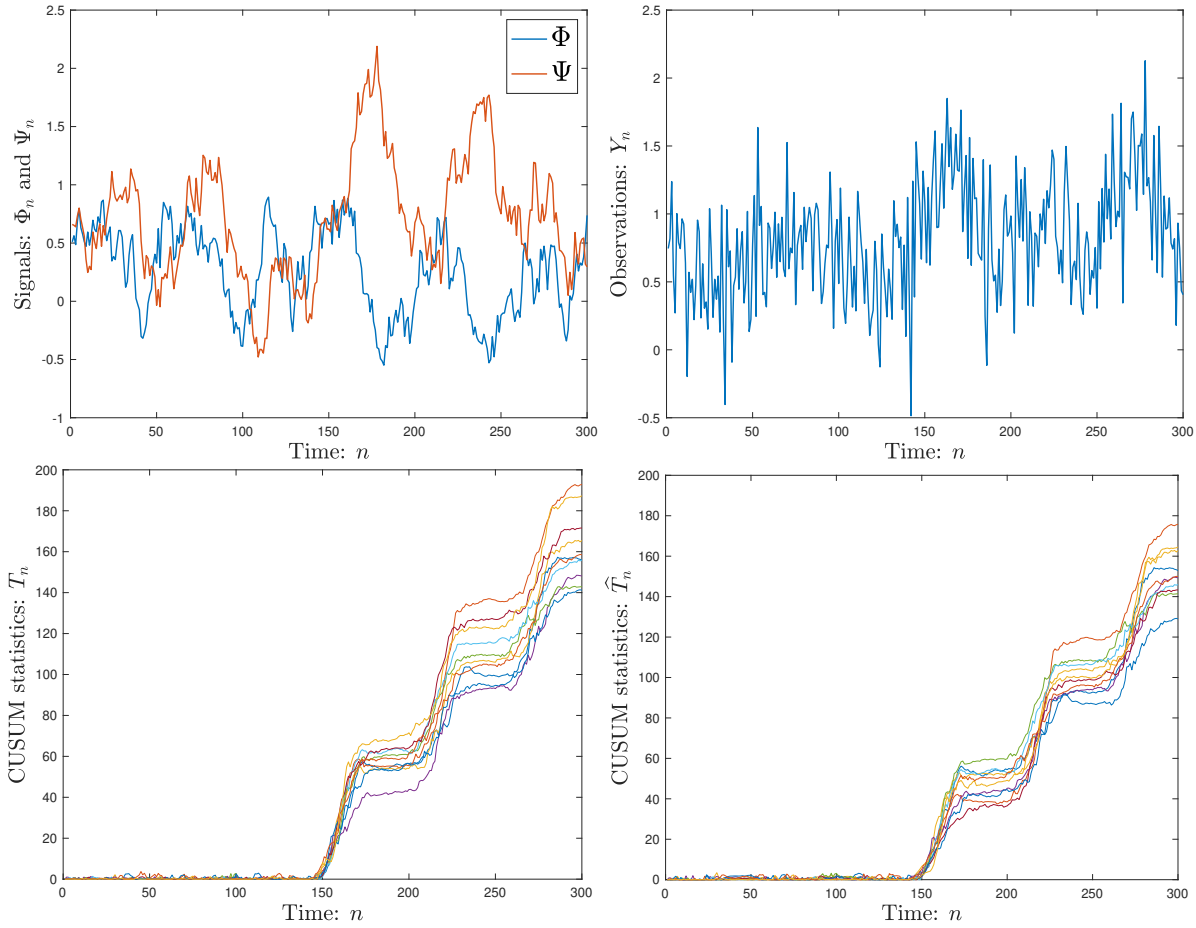


Figure 3.8: **a)** The evolution of the stochastic signals with a change $(d_\Phi, d_\Psi) = (-0.5, 0.5)$ implanted at $\nu = 142$ **(top left)**. **b)** The evolution of the observations (Ψ_n) corrupted by an additive Gaussian noise **(top right)**. **c)** The generalized CUSUM statistics (i.e., T_n) **(bottom left)** and **d)** the CUSUM statistics that assume an instant change (i.e., $\widehat{T}_n$) **(bottom right)** with 10 ensembles of observations using a particle filtering approach with 50 particles.

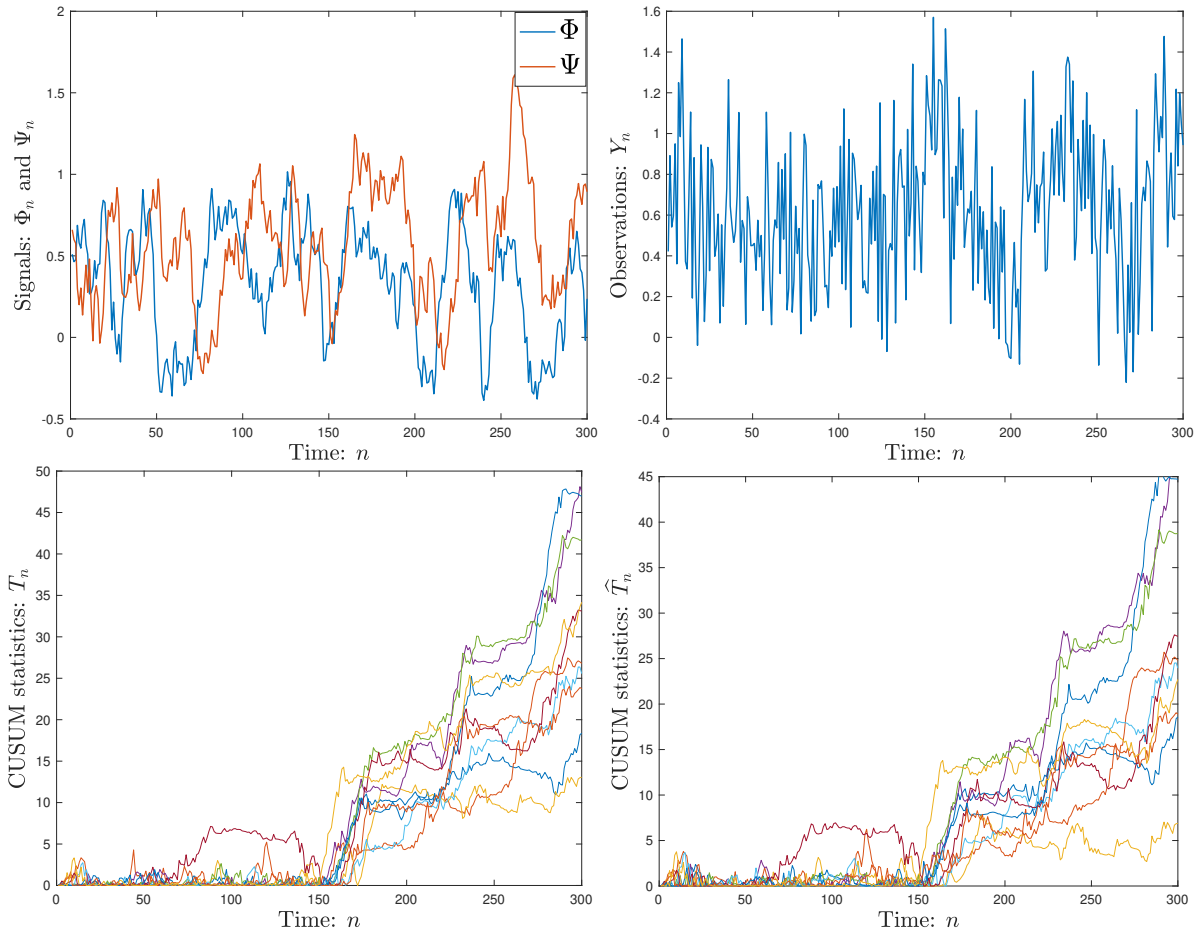


Figure 3.9: **a)** The evolution of the stochastic signals with a change $(d_\Phi, d_\Psi) = (-0.2, 0.2)$ implanted at $\nu = 150$ **(top left)**. **b)** The evolution of the observations (Ψ_n) corrupted by an additive Gaussian noise **(top right)**. **c)** The generalized CUSUM statistics (i.e., T_n) **(bottom left)** and **d)** the CUSUM statistics that assume an instant change (i.e., $\widehat{T}_n$) **(bottom right)** with 10 ensembles of observations using a particle filtering approach with 50 particles.

Chapter 4

Reduced Order Modeling of the Deterministic Moore-Greitzer Compressor Systems

Reduced order modeling (ROM), based on a projection of state variables in a low-dimensional subspace, is a promising tool to significantly alleviate computational costs [2, 24]. The bases for this subspace are typically constructed by proper orthogonal decomposition (POD) [84, 20] of a set of high-fidelity solution snapshots. Although many approaches have already been developed for the reduction of linear computational models [74, 39], we will explore strategies to efficiently reduce nonlinear computational models. More specifically, model reduction of large-scale complex systems, such as electric power systems and climate systems, with uncertainties or external disturbances, can effectively capture the essential dynamics while minimizing computational complexity. This chapter contains a concise overview of how this can be approached, with an application of the deterministic Moore-Greitzer model. The stochastic elements and external disturbances will be added and analyzed further along with the Moore-Greitzer PDE system in the next chapter.

In the analysis of functional data of random processes that are assumed sampled from a stochastic process $X \in L^2[0,T]$, i.e., the Hilbert space of square-integrable functions on $[0,T]$ with the usual inner product $\langle \varphi, \psi \rangle := \int_0^T \varphi(s)\psi(s)ds$ for any two functions $\varphi, \psi \in L^2[0,T]$. The Karhunen-Loéve expansion of X, under certain technical conditions, is assumed to exist such that

$$X(t) = \mu_X(t) + \sum_{j=1}^{\infty} \xi_j \varphi_j(t),$$

where the mean function $\mu_{_X}(t) = \mathbb{E}[X(t)]$ and the basis functions $\varphi_j(t)$ are the orthonormal eigenfunctions of the covariance *kernel* $\Gamma_{_X}(s,t) = \mathrm{Cov}\big[X(s), X(t)\big]$. The eigenvalues corresponding to $\varphi_j(t) \in L^2[0,T]$ satisfy

$$\int_0^T \Gamma_{_X}(s,t)\varphi_j(s)ds = \lambda_j\varphi_j(t) \quad \text{and} \qquad \Gamma_{_X}(s,t) = \sum_{j=1}^{\infty} \lambda_j\varphi_j(t)\varphi_j(s).$$

The random coefficients ξ_j are given by the projection of $X(t) - \mu_{_X}(t)$ in the direction of the j^{th} eigenfunction φ_j, that is,

$$\xi_j := \big\langle X(t) - \mu_{_X}(t), \varphi_j \big\rangle.$$

Furthermore, $\big\{\xi_j\big\}$ are an uncorrelated sequence of random variables with zero mean and variance λ_j and since the process $X \in L^2[0,T]$, we have $\sum_{j=1}^{\infty} \lambda_j < \infty$. The extension of this method to incorporate spatial velocity correlations was a crucial development introduced to the field of fluid dynamics by Lumley [57]. It is assumed that fluid flows are turbulent and time-stationary; ensemble averaging was employed to derive spatial velocity correlations under these assumptions. The orthonormal eigenfunctions derived from these velocity correlations were subsequently utilized as a logical and quantitative framework for identifying coherent structures.

Although solutions are technically defined over the interval $[0,T]$, they are typically observed only at discrete points within this range. Sirovich [84] introduced the POD method of snapshots to improve the efficiency of identifying the $n \ll \infty$ basis functions by collecting data at various time intervals. This approach is particularly useful for analyzing fluid dynamics and identifying dominant structures. The key condition is that the snapshots must be linearly independent or alternatively result from ergodic dynamical systems. For a function $w(t,x)$, the POD aims to express it as:

$$w(t,x) \approx \sum_{\alpha=1}^{n} a_\alpha(t)\psi_\alpha(x)$$

Here, $\psi_\alpha(x)$ are the spatial basis functions, or modes, which are orthogonal in the spatial domain, and $a_\alpha(t)$ are temporal coefficients that capture the temporal evolution of the function. The number of modes retained, n, is selected to achieve a desired approximation accuracy.

One unresolved issue is how to effectively represent a given functional data set using a limited number of basis functions without assuming ergodicity. The current literature offers scant answers, with the notable exception of Djouadi and Sahyoun [26], who thoroughly

examine the theoretical aspects of dimension reduction techniques within a functional analytic framework. This conceptual framework is expanded in this chapter [11]. The techniques introduced in their work address the challenge posed by the linear independence of snapshots. Additionally, we explore the theoretical fundamentals of these techniques to determine an optimal set of basis functions for the Moore-Greitzer PDE system. These findings offer an efficient method for constructing basis functions to be used for PDE-based model reduction.

Along with POD, Galerkin approximations are used to build weak solutions of the PDEs by constructing solutions of certain finite-dimensional (n) approximations to the PDEs. Many ROM techniques in fluid mechanics arise from the POD-Galerkin projection approach [4, 17]. Suppose we are given the PDE in the following form

$$\frac{\partial w}{\partial t}(t,x) = \mathcal{A}w(x,t) + \mathcal{N}(w,\cdots,w^{\tilde{h}})(t,x), \tag{4.1}$$

where $\tilde{h}$ represents the exponent of the maximum nonlinearity. As an example of quadratic nonlinear PDE, i.e., $\tilde{h} = 2$, the Galerkin projection reduces the PDE model to a set of reduced-order equations, i.e., ODEs, by projecting the governing equations onto a subspace spanned by the reduced basis functions, resulting in the following form:

$$\dot{a}_\gamma(t) = \sum_{\alpha=1}^{n} a_\alpha(t)\langle \mathcal{A}\psi_\alpha, \psi_\gamma\rangle + \sum_{\alpha,\beta=1}^{n} a_\alpha(t)a_\beta(t)\langle \mathcal{N}(\psi_\alpha,\psi_\beta),\psi_\gamma\rangle,$$

where $\gamma = 1,\cdots,n$.

4.1 Proper Orthogonal Decomposition

As mentioned, POD was initially introduced in fluid dynamics by Lumley [56] to extract coherent structures from turbulent flows. It provides an optimal basis to represent a given dataset by maximizing the variance captured by each successive mode. The core idea is to decompose a large, complex system into a set of orthogonal modes, ranked by their energetic contribution. The mathematical foundation of POD involves eigenvalue decomposition of the covariance matrix of the dataset.

In this section, the theoretical properties of the POD techniques within a functional analytic framework are established. That framework was originally introduced by Djouadi and Sahyoun [26] and later extended by Baxendale [11]. We present below the results in [11], which provide an efficient approach for constructing basis functions to be used in model reduction.

4.1.1 Continuous-time POD

In this section, we first assume that $t \in [0, T]$ and define the following function spaces:

Definition 4.1.1 (Functions $f(t)$ of time)**.** *We have $f : [0, T] \to \mathbb{R}$ with the $L^2([0, T])$ inner product $\langle f, g\rangle_T = \int_0^T f(t)g(t)dt$ and norm $\|f\|_T = \langle f, f\rangle_T^{1/2}$.*

Definition 4.1.2 ($\mathbb{R}^d$ valued functions $\phi(x)$ of space)**.** *We introduce a real Hilbert space H of functions $\phi : \Omega \to \mathbb{R}^d$ with some inner product $\langle \phi, \psi\rangle_H$ and norm $\|\phi\|_H = \langle \phi, \phi\rangle_H^{1/2}$.*

Definition 4.1.3 (Functions $u(t, x)$ of time and space)**.** *We have $u : [0, t] \times \Omega \to \mathbb{R}^d$ with inner product $\langle u, v\rangle_2 = \int_0^T \langle u(t, \cdot), v(t, \cdot)\rangle_H dt$ and norm $\|u\|_2 = \langle u, u\rangle_2^{1/2}$. Let us denote this space of functions $u(t, x)$ as $L^2([0, T], H)$. Notice that this space is defined in [26] but with different notation $L_2([0, T]) \times H$.*

Consider an instance where we have a function $g(t, x)$, serving as a solution to a particular partial differential equation (PDE). We are assuming that $g(t, x)$ is observed over continuous time and belongs to $L^2([0, T]) \times H$. Therefore, for each fixed t, the function mapping x to $g(t, x)$ takes its values in an infinite-dimensional space H. Our objective is to identify a finite-dimensional space of functions, labeled as J, so that $g(t, \cdot)$ remains approximated by elements within J. To achieve this, we seek J and a trajectory $p(t) \in J$ such that $g(t, \cdot)$ approximates $p(t)$ across the interval $t \in [0, T]$. Specifically, for a given integer n, we aim to find a finite collection of functions $\{U_\alpha(x) : 1 \le \alpha \le n\}$ in H and associated functions $\{b_\alpha(t) : 1 \le \alpha \le n\}$ in $L^2([0, T])$, ensuring that $g(t, \cdot)$ approximates the path defined by $p(t) = \sum_{\alpha=1}^n b_\alpha(t)U_\alpha$. To quantify "approximation", we must choose an appropriate norm, typically dependent on the PDE and the function space where these PDE solutions are valid. The space H is selected such that the PDE solutions reside in H, guaranteeing continuous dependence on initial conditions with respect to the H norm. Given that $g \in L^2([0, T]) \times H$ for a suitable H, closeness is sensibly measured with the norm $\|\cdot\|_2$ in this space. Therefore, our goal is to minimize the L^2-errors between the original function $g(t, x)$ and the POD approximation, i.e., $\sum_{\alpha=1}^n b_\alpha(t)U_\alpha(x)$. This approach allows us to translate the dynamics of $t \mapsto g(t, x)$—governed by the infinite-dimensional PDE—to a finite-dimensional dynamics of $t \mapsto (b_1(t), b_2(t), \cdots, b_n(t))$, which is governed by an ordinary differential equation (ODE).

4.1.2 Operators Γ and $\Gamma^*\Gamma$

Given a function $g(t, x) : [0, T] \times \Omega \to \mathbb{R}^d$, consider the operator $\Gamma : H \to L^2([0, T])$ defined by

$$(\Gamma\phi)(t) = \langle \phi, g(t, \cdot)\rangle_H, \quad \phi \in H. \tag{4.2}$$

For $\phi \in H$ and $f \in L^2([0,T])$, we have the relation

$$\begin{aligned}\langle \Gamma\phi, f\rangle_T &= \int_0^T (\Gamma\phi)(t) f(t) dt \\ &= \int_0^T \langle \phi, g(t,\cdot)\rangle_H f(t) dt \\ &= \left\langle \phi, \int_0^T g(t,\cdot) f(t) dt \right\rangle_H \\ &= \langle \phi, \Gamma^* g\rangle_H,\end{aligned}$$

where $\Gamma^* : L^2([0,T]) \to H$ is defined by

$$(\Gamma^* f)(x) = \int_0^T g(t,x) f(t) dt, \quad f \in L^2([0,T]).$$

For $\phi, \psi \in H$, we have

$$\begin{aligned}\langle \phi, \Gamma^*\Gamma\psi\rangle_H &= \langle \Gamma\phi, \Gamma\psi\rangle_T \\ &= \int_0^T (\Gamma\phi)(t)(\Gamma\psi)(t) dt \\ &= \int_0^T \langle \phi, g(t,\cdot)\rangle_H \langle \psi, g(t,\cdot)\rangle_H dt,\end{aligned} \tag{4.3}$$

and so

$$\Gamma^*\Gamma\psi = \int_0^T \langle \psi, g(t,\cdot)\rangle_H g(t,\cdot) dt. \tag{4.4}$$

Lemma 4.1.1. *Let $\{\phi_i, i \geq 1\}$ be any complete orthonormal basis for H. Then*

$$\sum_{i\geq 1} \langle \phi_i, \Gamma^*\Gamma\phi_i\rangle_H = \|g\|_2^2 < \infty. \tag{4.5}$$

Proof. Using (4.3) we have

$$\begin{aligned}\sum_{i\geq 1}\langle \phi_i, \Gamma^*\Gamma\phi_i\rangle_H &= \sum_{i\geq 1}\langle \Gamma\phi_i, \Gamma\phi_i\rangle_T \\ &= \int_0^T \sum_{i\geq 1}((\Gamma\phi_i)(t))^2 dt \\ &= \int_0^T \sum_{i\geq 1}\langle \phi_i, g(t,\cdot)\rangle_H^2 dt \\ &= \int_0^T \sum_{i\geq 1}\|g(t,\cdot)\|_H^2 dt \\ &= \|g\|_2^2.\end{aligned}$$

□

Notice that the operator $\Gamma^*\Gamma$ maps the Hilbert space H into itself. This operator is symmetric, non-negative, and, according to Lemma 4.1.1, it is a trace-class operator. Consequently, there exists a complete orthonormal basis $\{\nu_i : i \geq 1\}$ of eigenfunctions in H with corresponding eigenvalues $\lambda_1^2 \geq \lambda_2^2 \geq \cdots \geq 0$, satisfying the eigenvalue problem:

$$(\Gamma^*\Gamma)\nu_i(x) = \lambda_i^2\nu_i, \quad i \geq 1.$$

Furthermore,

$$(\Gamma^*\Gamma)\phi(x) = \sum_{i\geq 1}\lambda_i^2\langle \phi, \nu_i\rangle_H \nu_i(x), \quad \phi \in H.$$

Additionally, the eigenvalues λ_i^2 satisfy the summation:

$$\sum_{i\geq 1}\lambda_i^2 = \sum_{i\geq 1}\langle \nu_i, \Gamma^*\Gamma\nu_i\rangle_H = \|g\|_2^2 < \infty. \tag{4.6}$$

It is important to note a difference in notation from [26]: our eigenvalues λ_i^2 are associated directly with $(\Gamma^*\Gamma)$, whereas [26] defines eigenvalues relative to the operator $(\Gamma^*\Gamma)^{1/2}$. This analysis addresses the properties of the eigenvalues and eigenvectors but does not focus on explicit methods of computing them in a continuous-time context.

4.1.3 Optimization Problem Setup

Fix a dimension $n \geq 1$, and denote by $\mathcal{S}_n$ the set of all functions of the form

$$F(t,x) \;=\; \sum_{\alpha=1}^{n} b_\alpha(t)\, U_\alpha(x), \tag{4.7}$$

where each $b_\alpha(t)$ lies in $L^2([0,T])$ and each $U_\alpha(x)$ belongs to the Hilbert space H. Define

$$\mu_n \;=\; \inf_{F\,\in\,\mathcal{S}_n} \big\|\, g(t,x) \;-\; F(t,x)\big\|_2,$$

and consider the following two problems:

Problem 4.1.1. *For $n \geq 1$, determine the value of μ_n and describe the function $F(t,x)$ that attains this infimum.*

Problem 4.1.2. *For $n \geq 1$, define*

$$\widehat{\mu}_n \;=\; \sup\big\{\textstyle\sum_{i\geq 1} \langle \Gamma^*\Gamma\, U_\alpha,\, U_\alpha\rangle_H \;:\; \{U_1,\ldots,U_n\} \text{ is an orthonormal set in } H\big\},$$

and find the value of $\widehat{\mu}_n$ as well as the optimal orthonormal family $\{U_1,\ldots,U_n\}$.

Recall that $\Gamma^*\Gamma$ is the operator $H \to H$ introduced in (4.4). The first result below reduces the task of solving Problem 4.1.1 to the task of solving Problem 4.1.2. It is closely based on the essential idea in Theorem 1 of [26].

Theorem 4.1.1. *Suppose the supremum in the definition of $\widehat{\mu}_n$ in Problem 4.1.2 is attained by an orthonormal set $\{\widehat{U}_1,\ldots,\widehat{U}_n\} \subset H$. Then*

$$\mu_n^2 \;=\; \|g\|_2^2 \;-\; \widehat{\mu}_n,$$

and this infimum in Problem 4.1.1 is realized by

$$F(t,x) \;=\; \sum_{a=1}^{n} \big(\Gamma\widehat{U}_\alpha\big)(t)\; \widehat{U}_\alpha(x).$$

Proof. First of all, the Gram-Schmidt orthogonalization process yields a complete orthonormal system $\{\phi_i : i \geq 1\}$ such that $\psi_\alpha \in \text{span}\{\phi_1, \cdots, \phi_n\}$ for all $\alpha = 1, \cdots, n$. Thus, after

some elementary rearranging, we may assume F is of the form $\sum_{\alpha=1}^{n} \widehat{b}_\alpha(t)\phi_\alpha(x)$ where the set $\{\phi_1, \cdots, \phi_n\}$ gives the first n terms of a complete orthonormal system $\{\phi_i : i \geq\}$. Then

$$\begin{aligned}\|g(t,x) - F(t,x)\|_2^2 &= \left\| g(t,x) - \sum_{\alpha=1}^{n} \widehat{b}_\alpha(t)\phi_\alpha(x) \right\|_2^2 \\ &= \int_0^T \left\| g(t,\cdot) - \sum_{\alpha=1}^{n} \widehat{b}_\alpha(t)\phi_\alpha(x) \right\|_H^2 dt \\ &= \int_0^T \sum_{i\geq 1} \left\langle g(t,\cdot) - \sum_{\alpha=1}^{n} \widehat{b}_\alpha(t)\phi_\alpha(x) \right\rangle_H^2 dt\end{aligned}$$

Notice that the third equality follows from Lemma 4.1.1. Interchanging the summation and the integral in the last line of the above equation and utilizing (4.2) gives

$$\begin{aligned}\|g(t,x) - F(t,x)\|_2^2 &= \sum_{i\geq 1} \int_0^T \left((\Gamma\phi_i)(t) - \sum_{\alpha=1}^{n} \widehat{b}_\alpha(t)\langle \phi_i, \phi_\alpha\rangle_H \right)^2 dt \\ &= \sum_{i\geq 1}^{n} \int_0^T \left((\Gamma\phi_i)(t) - \widehat{b}_i(t) \right)^2 dt + \sum_{i\geq n+1} \int_0^T \left((\Gamma\phi_i)(t) \right)^2 dt \\ &= \sum_{i\geq 1}^{n} \int_0^T \left((\Gamma\phi_i)(t) - \widehat{b}_i(t) \right)^2 dt + \|g\|_2^2 - \sum_{i=1}^{n} \langle \Gamma^*\Gamma\phi_i, \phi_i\rangle^2,\end{aligned}$$

where the last equality uses (4.3) and (4.5). The first term can be minimized by choosing $\widehat{b}_i(t) = (\Gamma\phi_i)(t)$ and the third term can be minimized by using the solution of Problem 4.1.2. Thus $\mu_n^2 = \|g\|_2^2 - \widehat{\mu}_n$ and the optimizing function is given by $\phi(x)_\alpha = \widehat{U}_\alpha(x)$ and then $\widehat{b}_\alpha = (\Gamma\widehat{U}_\alpha)(t)$. □

Theorem 4.1.2. *In Problem 4.1.2, the supremum $\widehat{\mu}_n = \sum_{\alpha=1}^{n} \lambda_\alpha^2$, where $\{\lambda_j\}_{j\geq 1}$ are the eigenvalues of $\Gamma^*\Gamma$ in nonincreasing order. Moreover, this maximum is attained by an orthonormal set $\{\nu_1, \ldots, \nu_n\} \subset H$, where each ν_j is an eigenfunction of $\Gamma^*\Gamma$ with eigenvalue λ_j^2.*

Proof. For $\phi \in H$ we have $\phi = \sum_{j\geq 1} \langle \phi, \nu_j\rangle_H \nu_j$, so that $\Gamma^*\Gamma\phi = \sum_{j\geq 1} \lambda_j^2 \langle \phi, \nu_j\rangle_H \nu_j$. Then

$$\sum_{\alpha=1}^{n} \langle \Gamma^*\Gamma\phi_\alpha, \phi_\alpha\rangle = \sum_{\alpha=1}^{n} \sum_{j\geq 1} \lambda_j^2 \langle \phi_\alpha, \nu_j\rangle^2.$$

Taking $\phi_\alpha = \nu_\alpha$ for $1 \le \alpha \le n$ gives

$$\sum_{\alpha=1}^{n} \langle \Gamma^*\Gamma\nu_\alpha, \nu_\alpha\rangle = \sum_{\alpha=1}^{n}\sum_{j\ge 1} \lambda_j^2 \langle \nu_\alpha, \nu_j\rangle^2 = \sum_{\alpha=1}^{n} \lambda_\alpha^2.$$

This show that $\widehat{\mu}_n = \sum_{\alpha=1}^{n} \lambda_\alpha^2$.

Now suppose $\{\phi_1, \cdots, \phi_n\}$ is an orthonormal set. We have

$$\sum_{\alpha=1}^{n} \langle \Gamma^*\Gamma\phi_\alpha, \phi_\alpha\rangle = \sum_{\alpha=1}^{n}\sum_{j\ge 1} \lambda_j^2 \langle \phi_\alpha, \nu_j\rangle^2 = \sum_{j\ge 1} \lambda_j^2\gamma_j, \tag{4.8}$$

where $\gamma_j = \sum_{\alpha=1}^{n} \langle \phi_\alpha, \nu_j\rangle^2$. Clearly $\gamma_j \ge 0$ for all $j = 1, 2, \cdots$. Also $\gamma_j \le \|\phi_j\|^2 = 1$ and

$$\sum_{j\ge 1} \gamma_j = \sum_{\alpha=1}^{n} \left(\sum_{j\ge 1} \langle \phi_\alpha, \nu_j\rangle^2 \right) = \sum_{\alpha=1}^{n} \|\phi_\alpha\|^2 = n. \tag{4.9}$$

If $\gamma_j = 1$ for $1 \le j \le n$ and $\gamma_j = 0$ for $j > n$, then (4.8) becomes

$$\sum_{\alpha=1}^{n} \langle \Gamma^*\Gamma\phi_\alpha, \phi_\alpha\rangle = \sum_{j=1}^{n} \lambda_j^2.$$

Otherwise $\sum_{k=1}^{n} \gamma_k < n$ and we may define

$$\alpha_j = \frac{1-\gamma_j}{n - \sum_{k=1}^{n} \gamma_k}, \quad 1 \le j \le n.$$

Clearly, $\alpha_j \ge 0$ and $\sum_{j=1}^{n} \alpha_j = 1$. For $j > n$ we have

$$\lambda_j^2 \le \lambda_n^2 \le \alpha_n\lambda_n^2 \le \sum_{k=1}^{n} \alpha_k\lambda_k^2.$$

Using this inequality in (4.8) gives

$$\sum_{\alpha=1}^{n} \langle \Gamma^*\Gamma\phi_\alpha, \phi_\alpha\rangle \le \sum_{j=1}^{n} \lambda_j^2\gamma_j + \sum_{j>n} \gamma_j \left(\sum_{k=1}^{n} \alpha_k\lambda_k^2 \right). \tag{4.10}$$

Notice that we can rewrite the right-hand side of the inequality in (4.10) as

$$\sum_{j=1}^{n} \lambda_j^2 \gamma_j + \sum_{j>n} \gamma_j \left(\sum_{k=1}^{n} \alpha_k \lambda_k^2 \right) = \sum_{j=1}^{n} \lambda_j^2 \gamma_j + \sum_{k>n} \gamma_k \left(\sum_{j=1}^{n} \alpha_j \lambda_j^2 \right)$$

by the change of indices (i.e., $j \leftrightarrow k$) in the second term. As such, (4.10) gives

$$\sum_{\alpha=1}^{n} \langle \Gamma^* \Gamma \phi_\alpha, \phi_\alpha \rangle \leq \sum_{j=1}^{n} \lambda_j^2 \left(\gamma_j + \alpha_j \sum_{k>n} \gamma_k \right)$$

It then follows from (4.9) that

$$\sum_{\alpha=1}^{n} \langle \Gamma^* \Gamma \phi_\alpha, \phi_\alpha \rangle \leq \sum_{j=1}^{n} \lambda_j^2 \left(\gamma_j + \alpha_j \left(n - \sum_{k=1}^{n} \gamma_k \right) \right) = \sum_{j=1}^{n} \lambda_j^2.$$

This proves $\widehat{\mu}_n \leq \sum_{j=1}^{n} \lambda_j^2$, and the proof is complete. □

Corollary 4.1.1. *Combining Theorem 4.1.1 and Theorem 4.1.2 yields, for $n \geq 1$,*

$$\inf_{F \in \mathcal{S}_n} \left\| g(t,x) \; - \; F(t,x) \right\|_2^2 \; = \; \sum_{i>n} \lambda_i^2,$$

with a minimizer given by

$$F(x,t) = \sum_{i=1}^{n} \big(\Gamma \, \nu_i \big)(t) \, \nu_i(x).$$

In other words, the best n-dimensional approximation of $g(t,x)$ in L^2-norm is determined by the first n eigenfunctions of $\Gamma^\top \Gamma$, and the corresponding error is the tail sum $\sum_{i>n} \lambda_i$.

4.1.4 Snapshot Version

Rather than having the function $g(t,x)$ defined for every $t \in [0,T]$, suppose we only have its values at a finite set of times $\{t_1, t_2, \ldots, t_M\}$. Label these "snapshot" functions as

$$g_i(x) \; = \; g\big(t_i, x\big), \quad i = 1, \ldots, M.$$

We regard $g = \{g_1, \ldots, g_M\}$ as our data set. Our goal is to approximate g (in a L^2 sense) using a subspace of dimension n, spanned by $\{U_1, \ldots, U_n\} \subset H$, just as in the continuous case.

Replacing Integrals with Finite Sums. Originally, for a function $f\colon [0,T] \to \mathbb{R}$, we had

$$\int_0^T f(t)\,dt \quad \text{and} \quad \langle f, h\rangle_T \;=\; \int_0^T f(t)\,h(t)\,dt,$$

within an $L^2([0,T])$ space. In the "snapshot" setting, we switch to an M-dimensional vector

$$f \;=\; [\,f_1,\, f_2,\, \ldots,\, f_M]^\top,$$

and

$$\int_0^T f(t)\,dt \;\longmapsto\; \frac{1}{M}\sum_{i=1}^{M} f(t_i), \quad \langle f, h\rangle_T \;\longmapsto\; \frac{1}{M}\sum_{i=1}^{M} f_i\,h_i.$$

Hence, the corresponding norm for a set of snapshots $g = \{\, g_i\colon i = 1, \ldots, M\}$ with $g_i \in H$ becomes

$$\|g\|_2 = \left(\frac{1}{M}\sum_{i=1}^{M} \|g_i\|_H^2\right)^{1/2}.$$

Approximating the Snapshots. We want to represent each $g_i(x)$ in terms of an n-dimensional subspace $\operatorname{span}\{U_1, \ldots, U_n\} \subset H$. Equivalently, find real coefficients $\{b_i^{(\alpha)}\}_{\alpha=1}^n$ for each snapshot at time t_i so that

$$g_i(x) \;\approx\; \sum_{\alpha=1}^{n} b_i^{(\alpha)}\,U_\alpha(x).$$

Hence, we seek to minimize

$$\left\| g_i(x) - \sum_{\alpha=1}^{n} b_i^\alpha U_{(\alpha)}(x) \right\|_2 = \left(\frac{1}{M}\sum_{i=1}^{M} \left\| g_i(x) - \sum_{\alpha=1}^{n} b_i^\alpha U_{(\alpha)}(x) \right\|_H^2 \right)^{1/2}.$$

Defining the Operators Γ and $\Gamma^*\Gamma$. In this snapshot version, operators Γ and $\Gamma^*\Gamma$ are defined as follows. Given snapshots $g = \{g_i : 1 \le i \le M\}$, the operator $\Gamma : H \mapsto \mathbb{R}^M$ is defined by

$$(\Gamma\phi)_i = \langle \phi, g_i\rangle_H, \quad 1 \le i \le M. \tag{4.11}$$

If $\phi \in H$ and $h \in \mathbb{R}^M$ then

$$\begin{aligned}\langle \Gamma\phi, h\rangle_T &= \frac{1}{M}\sum_{i=1}^{M}(\Gamma\phi)_i h_i \\ &= \frac{1}{M}\sum_{i=1}^{M}\langle \phi, g_i\rangle_H h_i \\ &= \left\langle \phi, \frac{1}{M}\sum_{i=1}^{M} h_i g_i \right\rangle_H \\ &= \langle \phi, \Gamma^* h\rangle_H,\end{aligned}$$

where $\Gamma^* : \mathbb{R}^M \mapsto H$ is given by

$$(\Gamma^* h)(x) = \frac{1}{M}\sum_{i=1}^{M} h_i g_i(x), \quad x \in \Omega.$$

For $\phi, \psi \in H$ we get

$$\begin{aligned}\langle \phi, \Gamma\Gamma^*\psi\rangle_H &= \langle \Gamma\phi, \Gamma\psi\rangle_T \\ &= \frac{1}{M}\sum_{i=1}^{M}(\Gamma\phi)_i(\Gamma\psi)_i \\ &= \frac{1}{M}\sum_{i=1}^{M}\langle \phi, g_i\rangle_H\langle \psi, g_i\rangle_H dt\end{aligned} \tag{4.12}$$

and so

$$\Gamma^*\Gamma\psi = \frac{1}{M}\sum_{i=1}^{M}\langle \psi, g_i\rangle_H g_i. \tag{4.13}$$

Lemma 4.1.2. *Let $\{\phi_i : i \geq 1\}$ be any complete orthonormal basis for H. Then*

$$\sum_{i\geq 1}\langle \phi_i, \Gamma^*\Gamma\phi_i\rangle_H = \sum_{i\geq 1}\|\Gamma\phi_i\|_T^2 = \|g\|_2^2 < \infty \tag{4.14}$$

Proof. Using (4.12) we have

$$\begin{aligned}\sum_{i\geq 1}\langle \phi_i, \Gamma^*\Gamma\phi_i\rangle_H &= \sum_{i\geq 1}\left(\frac{1}{M}\sum_{j=1}^{M}\langle \phi_i, g_i\rangle_H^2\right)\\ &= \frac{1}{M}\sum_{j=1}^{M}\left(\sum_{i\geq 1}\langle \phi_i, g_i\rangle_H^2\right)\\ &= \frac{1}{M}\sum_{j=1}^{M}\|g_i\|_H^2\\ &= \|g\|_2^2.\end{aligned}$$

□

The important difference for the version with snapshots is that now there is a computational method for finding the eigenfunctions and eigenvalues. Since $\Gamma^*\Gamma$ sends H to the finite-dimensional space $\text{span}\{g_1, g_2, \cdots, g_M\}$, then every eigenfunction of $\Gamma^*\Gamma$ with a non-zero eigenvalue must be of the form $\sum_{i=1}^{M}\gamma_i g_i$ for some vector $\gamma = (\gamma_i, \cdots, \gamma_M)$. Let C be the $M \times M$ matrix given by

$$C_{ij} = \frac{1}{M}\langle g_i, g_j\rangle_H, \quad 1 \leq i, j \leq M. \tag{4.15}$$

The non-negative eigenvalues coincide with those of $\Gamma^*\Gamma$, and one obtains the usual "method of snapshots": diagonalize C to find its top n eigenvalues, then use them to pick an n-dimensional approximation. This yields a practical way to compute the largest eigenfunctions of $\Gamma^*\Gamma$ by only dealing with an $M \times M$ matrix instead of directly working in H. Consequently, it reproduces the same POD approach as in the continuous case, but in a discretized snapshot form.

Proposition 4.1.1. *(i) If $\gamma = (\gamma_i, \cdots, \gamma_M)$ is an eigenvector of C with eigenvalue $\lambda \neq 0$ then $\phi = \sum_{i=1}^{M}\gamma_i g_i$ is an eigenfunciton of $\Gamma^*\Gamma$ with eigenvalue λ.*

(ii) If $\phi \in H$ is an eigenfunction of $\Gamma^*\Gamma$ with eigenvalue $\lambda \neq 0$ then there exists an eigenvector $\gamma = (\gamma_i, \cdots, \gamma_M)$ of C with eigenvalue λ such that $\phi = \sum_{i=1}^{M}\gamma_i g_i$.

Proof. (i) If $\gamma = (\gamma_i, \cdots, \gamma_M)$ we have

$$\begin{aligned}
(\Gamma^*\Gamma)\left(\sum_{i=1}^M \gamma_i g_i\right) &= \sum_{i=1}^M \gamma_i (\Gamma^*\Gamma g_i) \\
&= \sum_{i=1}^M \gamma_i \frac{1}{M} \sum_{i=1}^M \langle g_i, g_j\rangle_H g_j \\
&= \frac{1}{M} \sum_{j=1}^M \left(\sum_{i=1}^M \gamma_i \langle g_i, g_j\rangle_H\right) g_j \qquad (4.16) \\
&= \frac{1}{M} \sum_{i=1}^M \left(\sum_{j=1}^M \gamma_j \langle g_j, g_i\rangle_H\right) g_i \\
&= \sum_{i=1}^M \left(\sum_{j=1}^M \gamma_j C_{ij}\right) g_i
\end{aligned}$$

It follows immediately that $\phi = \sum_{i=1}^M \gamma_i g_i$ satisfies $(\Gamma^*\Gamma)\phi = \lambda\phi$. Also

$$\|\phi\|_H^2 = \sum_{i,j=1}^M \gamma_i \gamma_j \langle g_i, g_j\rangle_H = M \sum_{i,j=1}^M \gamma_i C_{ij} \gamma_j = M\lambda \sum_{j=1}^M \gamma_j^2 \neq 0,$$

so that$\phi \neq 0$. Therefore ϕ is an eigenfunction of $\Gamma^*\Gamma$ with eigenvalue λ.

(ii) Let $\mathcal{M} = \{\gamma \in \mathbb{R}^M : \sum_{i=1}^M \gamma_i g_i = 0\}$ and note that the subspace $\mathcal{M}$ is trivial if and only if the $\{g_1, \cdots, g_M\}$ are linearly independent. Moreover

- $\gamma \in \mathcal{M}$ implies $(\gamma C)_j = \frac{1}{M}\langle \sum_{i=1}^M \gamma_i g_i, g_j\rangle_H = 0$ for all j so that $\gamma C = 0$.
- $\gamma C = 0$ implies $\| \sum_{i=1}^M \gamma_i g_i\|_H^2 = \sum_{i=1}^M \gamma_i g_i \langle g_i, g_j\rangle_H = M \sum_{i=1}^M \gamma_i g_i = 0$ so that $\gamma \in \mathcal{M}$.

Therefore $\mathcal{M}$ is the null space for the matrix C. Now suppose ϕ is an eigenfunction of $\Gamma^*\Gamma$ with eigenvalue $\lambda \neq 0$ and write$\phi = \sum_{i=1}^M \gamma_i g_i$. The calculation (4.16) shows that $\gamma C - \lambda\gamma \in \mathcal{M}$. Since $\lambda \neq 0$ we may write $\gamma C - \lambda\gamma = \lambda\widehat{\gamma}$ for some $\widehat{\gamma} \in \mathcal{M}$. Since $\widehat{\gamma} C = 0$ we have $(\gamma + \widehat{\gamma})C = \lambda(\gamma + \widehat{\gamma})$. Also, since the eigenfunction $\phi = \sum_i \gamma_i g_i = \sum_i (\gamma_i + \widehat{\gamma}_i) g_i$ is assumed to be non-zero, then $\gamma + \widehat{\gamma} \neq 0$. Therefore λ is an eigenvalue of C with left eigenvector $\gamma + \widehat{\gamma}$.

□

Therefore, we determine all the non-zero eigenvalues of $\Gamma^*\Gamma$ and their associated eigenfunctions by identifying all the non-zero eigenvalues of C and their related left eigenvectors. More details of this snapshot method, including the following remarks, can be found in [11].

Remark 4.1.1. *For any operator, eigenvectors of the operator with eigenvalue 0 are vectors in the null space of the operator. For the matrix C acting on $\mathbb{R}^M$, the null space is $\mathcal{M}$, which has some dimension $d \geq 0$, say. Then C has $M - d$ positive eigenvalues (not necessarily distinct, so counted with multiplicities). The range of $\Gamma^*\Gamma$ acting on H is span$\{g_1, \cdots, g_M\} \equiv H_0$, say, and this has dimension $M - d$. The null space of $\Gamma^*\Gamma$ will be the orthogonal complement of H_0 in H.*

Remark 4.1.2. *The discretization in time, passing from continuous observations $0 \leq t \leq T$ to snapshots at times $\{t_i : 1 \leq i \leq m\}$, makes an important divergence here, especially in the calculation of eigenvalues and eigenfunctions for $\Gamma^*\Gamma$. We need the snapshots g_i and the inner products $\langle g_i, g_j \rangle_H$. Typically the functions g_i will be described using some sort of spatial discretization, and then details of those descriptions will be used to obtain the (approximate) values of the inner products $\langle g_i, g_j \rangle_H$. The details of the spatial discretization are not important here.*

Given the snapshots $\{g_i : 1 \leq i \leq M\}$ consider

$$\mu_n = \inf \left\| g_i(x) - \sum_{\alpha=1}^{n} b_i^{(\alpha)} U_\alpha(x) \right\|_2 = \inf \left(\frac{1}{M} \sum_{i=1}^{M} \left\| g_i - \sum_{\alpha=1}^{n} b_i^{(\alpha)} U_\alpha(x) \right\|_H^2 \right)^{1/2}$$

where the infimum is over functions of the form $F_i(x) = \sum_{\alpha=1}^{n} b_i^{(\alpha)} U_\alpha(x)$ for functions $U_1(x), \cdots, U_n(x)$ and vectors $b^{(1)}, \cdots, b^{(n)}$. Recall the mapping $\Gamma^*\Gamma$ from H to H given by

$$\Gamma^*\Gamma\phi = \frac{1}{M} \sum_{i=1}^{M} \langle \phi, g_i \rangle_H g_i.$$

It is symmetric and non-negative definite and finite rank, so it has a finite number of positive eigenvalues $\lambda_1 \geq \lambda_2 \geq \cdots \geq 0$ with corresponding orthonormal eigenvectors $\nu_1, \nu_2, \cdots$. Corresponding to Corollary **??**, we have

Corollary 4.1.2. *Given snapshots $\{g_i(x) : 1 \leq i \leq M\}$, for $n \geq 1$*

$$\mu_n^2 = \sum_{i>n} \lambda_i,$$

attained with $F_i(x) = \sum_{\alpha=1}^{n} (\Gamma\nu_\alpha)_i \nu_\alpha(x)$.

4.1.5 Computational Scheme

Given a set of snapshots, we have a way of calculating the approximation $\sum_{\alpha=1}^{n}(\Gamma\nu_\alpha)_i\nu_\alpha(x)$. Recall the $M \times M$ matrix C:

$$C_{ij} = \frac{1}{M}\langle g_i, g_j\rangle_H, \quad 1 \le i, j \le M.$$

Suppose C has positive eigenvalues $\lambda_1 \ge \lambda_2 \ge \cdots > 0$ with corresponding eigenvectors $\gamma^{(1)}, \gamma^{(2)}, \cdots$. Each eigenvector $\gamma^\alpha = (\gamma_1^{(\alpha)}, \cdots, \gamma_M^{(\alpha)}) \in \mathbb{R}^M$. Since C is symmetric, the eigenvectors $\gamma^{(\alpha)}$ may be assumed to be orthogonal in $\mathbb{R}^M$. (Orthogonality happens automatically for distinct eigenvalues, and within any eigenspace of dimension greater than one the eigenvectors can be chosen to be orthogonal.) Suppose each $\gamma^{(\alpha)}$ is scaled to be of length 1 in $\mathbb{R}^M$, that is $\sum_{i=1}^{M}(\gamma_i^{(\alpha)})^2 = 1$. The operator $\Gamma^*\Gamma$ has the same positive eigenvalues as C with eigenvectors with the eigenvalues $\sum_{i=1}^{M}\gamma_i^{(\alpha)}g_i$. Define

$$\nu_\alpha = \frac{1}{\sqrt{M\lambda_\alpha}}\sum_{i=1}^{M}\gamma_i^{(\alpha)}g_i.$$

We have

$$\begin{aligned}
\langle\nu_\alpha, \nu_\beta\rangle_H &= \frac{1}{M\sqrt{\lambda_\alpha\lambda_\beta}}\sum_{i,j=1}^{M}\gamma_i^{(\alpha)}\gamma_j^{(\beta)}\langle g_i, g_j\rangle_H \\
&= \frac{1}{\sqrt{\lambda_\alpha\lambda_\beta}}\sum_{i,j=1}^{M}\gamma_i^{(\alpha)}C_{ij}\gamma_j^{(\beta)} \\
&= \frac{1}{\sqrt{\lambda_\alpha\lambda_\beta}}\sum_{i=1}^{M}\lambda_\beta\gamma_i^{(\alpha)}\gamma_j^{(\beta)} \\
&= \begin{cases} 0 & \text{if } \alpha \ne \beta \\ 1 & \text{if } \alpha = \beta. \end{cases}
\end{aligned}$$

Therefore the ν_α form an orthonormal system of eigenvectors of $\Gamma^*\Gamma$. Also

$$\begin{aligned}(\Gamma\nu_\alpha)_i &= \langle \nu_\alpha, g_i\rangle_H \\ &= \frac{1}{\sqrt{M\lambda_\alpha}}\sum_{j=1}^{M}\gamma_j^{(\alpha)}\langle g_j, g_i\rangle_H \\ &= \frac{\sqrt{M}}{\sqrt{\lambda_\alpha}}\sum_{j=1}^{M}\gamma_j^{(\alpha)}C_{ij} \\ &= \frac{\sqrt{M}}{\sqrt{\lambda_\alpha}}(\gamma^{(\alpha)}C)_i \\ &= \frac{\sqrt{M}}{\sqrt{\lambda_\alpha}}\lambda_\alpha\gamma_i^{(\alpha)} \\ &= \sqrt{M\lambda_\alpha}\gamma_i^{(\alpha)}\end{aligned}$$

Corollary 4.1.3. *Given snapshots* $\{g_i(x) : 1 \le i \le M\}$, *for* $n \ge 1$

$$\mu_n^2 = \sum_{i>n}\lambda_i,$$

attained with

$$F_i(x) = \sum_{\alpha=1}^{n}\sqrt{M\lambda_\alpha}\gamma_i^{(\alpha)}\left(\frac{1}{\sqrt{M\lambda_\alpha}}\sum_{j=1}^{M}\gamma_j^{(\alpha)}g_j\right) = \sum_{j=1}^{M}\left(\sum_{\alpha=1}^{n}\gamma_i^{(\alpha)}\gamma_j^{(\alpha)}\right)g_j.$$

So, given the snapshots, we need to be able to compute the matrix

$$C_{ij} = \frac{1}{M}\langle g_i, g_j\rangle_H$$

using the inner product on the function space C. *After we have* C, *then all the rest is just finding eigenvalues and eigenvectors and using the Euclidean norm in* $\mathbb{R}^M$.

4.2 Model Reduction of Deterministic Moore-Greitzer Compressors using POD-Galerkin Procedure

The deterministic Moore-Greitzer model is a simplified mathematical framework that describes the dynamics of compressor stalls and surges in jet engines. It is an essential tool

for understanding the nonlinear and complex behaviors of axial flow compressors. In this section, we focus on the model reduction of the deterministic Moore-Greitzer model using POD techniques.

4.2.1 Moore-Greitzer Model

The Moore-Greitzer model of a compressor, discussed in detail in Section 2.1.1, consists of two ordinary differential equations in non-dimensionalized time t for mean axial flow $\Phi(t)$ and pressure rise coefficient $\Psi(t)$, coupled with a partial differential equation for the circumferentially varying velocity of upstream disturbance, denoted as $g(t,\theta)$. Mathematically, the Moore-Greitzer PDE model is given as

$$\frac{\partial}{\partial t}\begin{bmatrix} g \\ \Phi \\ \Psi \end{bmatrix} = \begin{bmatrix} K^{-1}(\frac{\nu}{2}\frac{\partial^2}{\partial\theta^2} - \frac{1}{2}\frac{\partial}{\partial\theta}) & 0 & 0 \\ 0 & 0 & 0 \\ 0 & 0 & 0 \end{bmatrix}\begin{bmatrix} g \\ \Phi \\ \Psi \end{bmatrix} + \begin{bmatrix} aK^{-1}(\psi_c(\Phi+g) - \overline{\psi}_c(\Phi,g)) \\ \frac{1}{l_c}(\overline{\psi}_c(\Phi,g) - \Psi) \\ \frac{1}{4l_cB^2}(\Phi - \gamma\sqrt{\Psi}) \end{bmatrix}, \tag{4.17}$$

where l_c is the effective flow-passage non-dimensional length of the compressor and ducts, and B is the dimensionless Greitzer parameter. $K : \breve{L}^2(0,2\pi) \to \breve{L}^2(0,2\pi)$ is a linear operator that has the property:

$$K(e^{i\tilde{n}\theta}) = \left(1 + \frac{ma}{|\tilde{n}|}\right)e^{i\tilde{n}\theta}$$

for $\tilde{n} \neq 0$. Then K can be extended as a positive definite, self-adjoint linear operator on $\breve{L}^2(0,2\pi)$. Moreover, the inverse K^{-1} is well-defined and has an explicit formula on any finite linear combination of functions of the form $e^{i\tilde{n}\theta}$, where $\breve{L}^2(0,2\pi)$ is defined in Definition 2.1.1. More precisely, for any finite subset $I \in (\mathbb{Z}\setminus\{0\})$ we have

$$K^{-1}\left(\sum_{\tilde{n}\in I} c_{\tilde{n}}e^{i\tilde{n}\theta}\right) = \sum_{\tilde{n}\in I}\left(\frac{|\tilde{n}|}{|\tilde{n}|+ma}\right)c_{\tilde{n}}e^{i\tilde{n}\theta}. \tag{4.18}$$

For every time $t \in [0,\infty)$, the solution $g(t,\cdot)$ lies in $\mathcal{H}$ which is an infinite-dimensional Hilbert space, $\mathcal{H} := \breve{L}^2(0,2\pi) = \left\{g \in L^2 : \int_0^{2\pi} g(\theta)d\theta = 0\right\}$ equipped with the inner product $\langle\cdot,\cdot\rangle_{\mathcal{H}}$ as well as the induced norm $\|\cdot\|_{\mathcal{H}}$. Let us also define $L^2([0,\infty),\mathcal{H})$ as a space of functions for $g(t,\theta)$. Note that $L^2([0,\infty),\mathcal{H})$ contains the set of functions $g(t,\theta)$ such that the mapping $t \mapsto g(t,\cdot)$ is an L^2 mapping of $[0,\infty)$ to $\mathcal{H}$. Also, we have some regularity conditions for g and require

$$g(t,0) = g(t,2\pi), \quad g_\theta(t,0) = g_\theta(t,2\pi)$$

and

$$\int_0^{2\pi} g(t,\theta)d\theta = 0.$$

Moreover, the compressor static characteristic is as follows,

$$\psi_c(\Phi) = \psi_{c_0} + H\left[1 + \frac{3}{2}\left(\frac{\Phi}{W} - 1\right) - \frac{1}{2}\left(\frac{\Phi}{W} - 1\right)^3\right]. \tag{4.19}$$

We also define

$$\overline{\psi}_c(\Phi, g) := \frac{1}{2\pi}\int_0^{2\pi} \psi_c(\Phi + g)d\theta. \tag{4.20}$$

In addition,

$$\Psi_V(\Phi) = \frac{1}{\gamma^2}\Phi^2, \tag{4.21}$$

where the throttle coefficient $\gamma > 0$ is proportional to the valve opening.

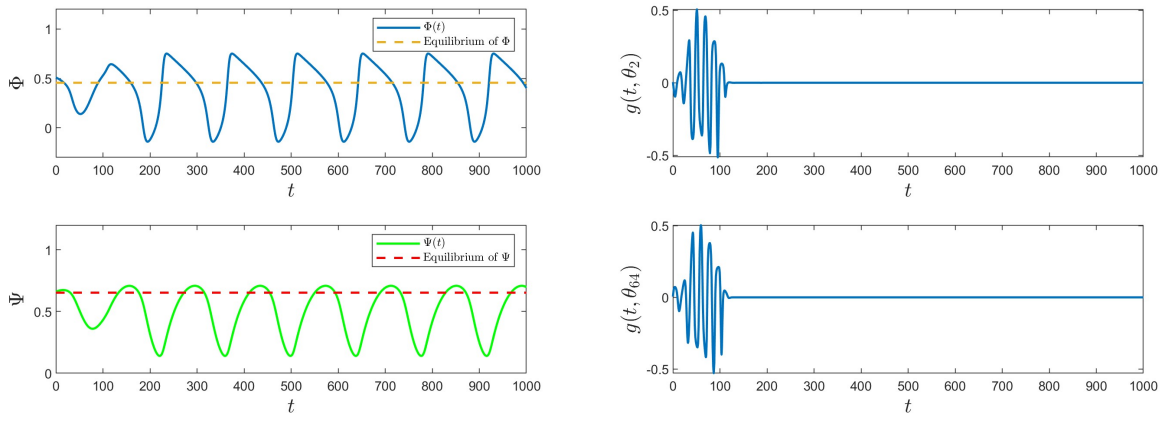


Figure 4.1: The evolution of the deterministic ODE, i.e., (Φ, Ψ), with a limit cycle behavior **(left)**, and the evolution of the deterministic PDE over time t towards a steady state at two fixed values of θ **(right)**.

The sources of instability are twofold: (stall) the upstream nonuniform disturbance generates a locally higher angle of attack, and propagates along the blade row without

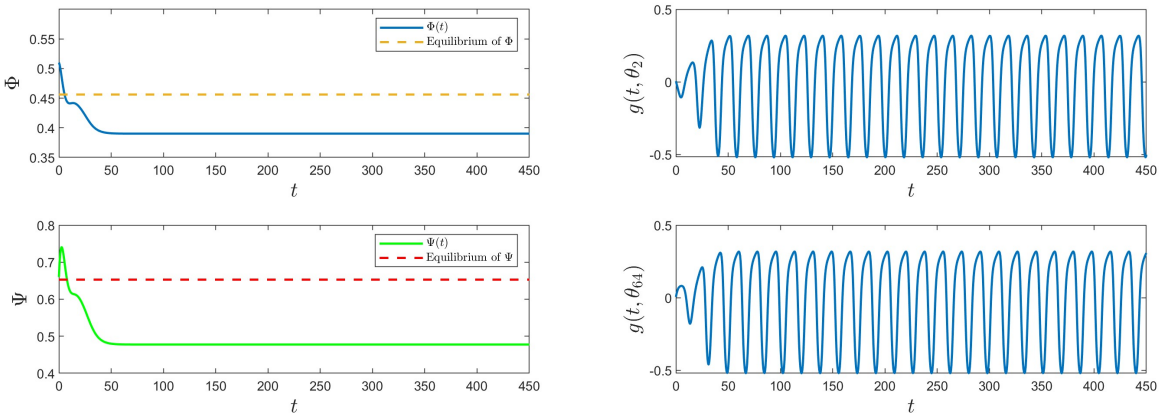


Figure 4.2: The evolution of the deterministic ODE, i.e., (Φ, Ψ) towards the steady states **(left)**, and the evolution of the deterministic PDE over time t with oscillations at two fixed values of θ **(right)**.

mitigation; (surge) the average mean flow and pressure rise oscillate constantly and formulate standing waves. Figure 4.1 and Figure 4.2 illustrate the examples of the surge and stall instabilities in the Moore-Greitzer model with the following configuration parameters

$$l_c = 8,\ H = 0.18,\ W = 0.25,\ m = 1.75,\ \nu = 0.1,\ a = 1/3.5,\ \psi_{c_0} = 1.67H.$$

The surge configuration in Figure 4.1 is achieved with parameter values $B = 2$ and $\gamma = 0.6$. In this case, $g(t, \theta)$ governed by the PDE part of the Moore-Greitzer model is stable, but $\Phi(t)$ and $\Psi(t)$ go through a Hopf bifurcation, causing a limit cycle behavior for the ODE part of the model. It also follows from the right subplot of Figure 4.1 that the instability of the ODEs transiently affects the PDEs, resulting in a momentary surge in the otherwise stable solutions. The stall configuration in Figure 4.2 is simulated with parameter values $B = 0.95$ and $\gamma = 0.5645$. The eigenvalues of the PDE become positive in this configuration, which indicates that $g(t, \theta)$ goes through a Hopf bifurcation. The right subplot of Figure 4.2 depicts the oscillations of the PDE part evolving with time t at two fixed values of θ. Interestingly, it is worth mentioning that a standing wave in the PDE is changing the steady state of $\Phi(t)$ and $\Psi(t)$, and this deviation from its original equilibrium can be identified from the left subplot of Figure 4.2. In the following subsections, we will focus on the reduced-order modeling of the Moore-Greitzer PDE system using the POD technique applied to the stall instability case where $g(t, \theta)$ generates a standing wave.

4.2.2 Representation of POD Basis using Fourier Basis

In this subsection, we introduce how the POD basis for the reduced-order model is related to the Fourier basis functions, which are used to describe the full-order snapshots. For each temporal instance $t \in [0, \infty)$, the solution $g(t, \cdot)$ exists within $\mathcal{H}$, a Hilbert space of functions, defined as follows,

$$\mathcal{H} := \Big\{ g \in L^2 : \int_0^{2\pi} g(\theta) d\theta = 0 \Big\}.$$

Let us also define $L^2([0, \infty), \mathcal{H})$ as a space of functions for $g(t, \theta)$. Note that $L^2([0, \infty), \mathcal{H})$ contains the set of functions $g(t, \theta)$ such that the mapping $t \mapsto g(t, \cdot)$ is an L^2 mapping of $[0, \infty)$ to $\mathcal{H}$. For fixed $N > 0$, we let $I_N = \{-N, -N+1, \cdots, -2, -1\} \cup \{1, 2, \cdots, N-1, N\}$. We look for an approximate solution using the Fourier spectral method with $g(t, \theta)$ of the form

$$g(t, \theta) = \sum_{\tilde{n} \in I_N} g_{\tilde{n}}(t) e^{i\tilde{n}\theta}$$

valid over some interval of time. Take snapshots of this solution at equally spaced times $t_1 < t_2 < \cdots < t_M$. Thus gives us full-order snapshots

$$g(t_k, \theta) = \sum_{\tilde{n} \in I_N} g_{\tilde{n}}(t_k) e^{i\tilde{n}\theta}, \quad 1 \le k \le M.$$

Define the $M \times M$ matrix C:

$$C_{j,k} = \frac{1}{M} \langle g(t_j, \cdot), g(t_k, \cdot) \rangle_{\mathcal{H}}, \quad 1 \le j, k \le M,$$

where $\mathcal{H}$ is defined as before. Note here that each snapshot $g(t_k, \theta)$ is real-valued, and so $\overline{g_{\tilde{n}}(t)} = g_{-\tilde{n}}(t)$. If we wish to take advantage of the orthogonality of the Fourier modes $e^{i\tilde{n}\theta}$, we need to consider the complexification $\mathcal{H}^{\mathbb{C}}$ of $\mathcal{H}$ with its corresponding inner product. Then, we can write

$$\begin{aligned}
C_{i,k} &= \frac{1}{M} \langle g(t_j, \cdot), g(t_k, \cdot) \rangle_{\mathcal{H}^{\mathbb{C}}} \\
&= \frac{1}{M} \sum_{\tilde{m}, \tilde{n} \in I_N} \int_0^{2\pi} g_{\tilde{m}}(t_j) e^{i\tilde{m}\theta} \overline{g_{\tilde{n}}(t_k) e^{i\tilde{n}\theta}} d\theta \\
&= \frac{1}{M} \sum_{\tilde{m}, \tilde{n} \in I_N} g_{\tilde{m}}(t_j) \overline{g_{\tilde{n}}(t_k)} \int_0^{2\pi} e^{i(\tilde{m}-\tilde{n})\theta} d\theta \\
&= \frac{2\pi}{M} \sum_{\tilde{n} \in I_N} g_{\tilde{n}}(t_j) \overline{g_{\tilde{n}}(t_k)}.
\end{aligned}$$

Notice that $g_{\tilde{n}}(t_j)\overline{g_{\tilde{n}}(t_k)} + g_{-\tilde{n}}(t_j)\overline{g_{-\tilde{n}}(t_k)} = 2Re(g_{\tilde{n}}(t_j)\overline{g_{\tilde{n}}(t_k)})$ so that $C_{jk} \in \mathbb{R}$.

Suppose C has positive eigenvalues $\lambda_1 \geq \lambda_2 \geq \cdots > 0$ with corresponding eigenvectors $\gamma^{(1)}, \gamma^{(2)}, \cdots$. Each eigenvector $\gamma^{(\alpha)} = (\gamma_1^{(\alpha)}, \cdots, \gamma_M^{(\alpha)}) \in \mathbb{R}^M$. Since C is symmetric the eigenvectors $\gamma^{(\alpha)}$ may be assumed to be orthogonal in $\mathbb{R}^M$. Suppose each $\gamma^{(\alpha)}$ is scaled to be of length 1 in $\mathbb{R}^M$, that is $\sum_{i=1}^M (\gamma_i^{(\alpha)})^2 = 1$. Define

$$U_\alpha(\theta) = \frac{1}{\sqrt{M\lambda_\alpha}} \sum_{k=1}^M \gamma_k^{(\alpha)} g(t_k, \theta).$$

Then the POD modes are the orthonormal functions $U_1(\theta), U_2(\theta), U_3(\theta), \cdots$. Since each snapshot is a linear combination of Fourier modes, and each POD mode is a linear combination of snapshots, then each POD mode is a linear combination of Fourier modes. More precisely

$$\begin{aligned} U_\alpha(\theta) &= \frac{1}{\sqrt{M\lambda_\alpha}} \sum_{k=1}^M \gamma_k^{(\alpha)} g(t_k, \theta) \\ &= \frac{1}{\sqrt{M\lambda_\alpha}} \sum_{k=1}^M \gamma_k^{(\alpha)} \left(\sum_{\tilde{n} \in I_N} g_{\tilde{n}}(t_k) e^{i\tilde{n}\theta} \right) \\ &= \sum_{\tilde{n} \in I_N} \left(\frac{1}{\sqrt{M\lambda_\alpha}} \sum_{k=1}^M \gamma_k^{(\alpha)} g_{\tilde{n}}(t_k) \right) e^{i\tilde{n}\theta} \\ &= \sum_{\tilde{n} \in I_N} c_{\alpha,\tilde{n}} e^{i\tilde{n}\theta}, \end{aligned} \tag{4.22}$$

say, where

$$c_{\alpha,\tilde{n}} = \frac{1}{\sqrt{M\lambda_\alpha}} \sum_{k=1}^M \gamma_k^{(\alpha)} g_{\tilde{n}}(t_k).$$

The relation between the POD and Fourier basis functions is subtly non-trivial if one would like to figure out the reduced-order dynamic equations for the Moore-Greitzer PDE system, because the operator K^{-1} given in the Moore-Greitzer PDE model is only effective as shown in (4.18) when it comes to the Fourier basis. Therefore, when we apply a Galerkin projection for the Moore-Greitzer PDE using POD modes, it is imperative to obtain the representation of POD modes using Fourier basis functions to apply a correct form of K^{-1} for the reduced-order ODEs. This procedure will be shown in more detail in the next subsection. More specifically,

$$K^{-1}U_\alpha(\theta) = \sum_{\tilde{n} \in I_N} c_{\alpha,\tilde{n}} K^{-1}(e^{i\tilde{n}\theta}) = \sum_{\tilde{n} \in I_N} c_{\alpha,\tilde{n}} \left(\frac{|\tilde{n}|}{|\tilde{n}| + ma} \right) e^{i\tilde{n}\theta},$$

and

$$K^{-1}(U_\alpha(\theta)U_\beta(\theta)) = \sum_{\tilde{k},\tilde{n}\in I_N} c_{\alpha,\tilde{k}}c_{\beta,\tilde{n}}K^{-1}(e^{i(\tilde{k}+\tilde{n})\theta})$$
$$= \sum_{\tilde{k},\tilde{n}\in I_N} c_{\alpha,\tilde{k}}c_{\beta,\tilde{n}}\left(\frac{|\tilde{k}+\tilde{n}|}{|\tilde{k}+\tilde{n}|+ma}\right)e^{i(\tilde{k}+\tilde{n})\theta}.$$

However, if one is interested in the POD approximation without Galerkin projection, the reconstruction of $g(t,\theta)$ using n POD modes can be performed as follows,

$$g_{\text{POD}}(t,\theta) \approx \sum_{\alpha=1}^{n} q_\alpha(t)U_\alpha(\theta), \tag{4.23}$$

where the POD coefficients $q_\alpha(t)$ can be calculated by projecting the full-order snapshots onto the space spanned by the POD modes. Figure 4.3 illustrates an example of six modes of POD approximation with the corresponding POD time coefficients. Notice that the full order PDE model given in (4.17) is simulated using 128 Fourier spectrum in the case of stall bifurcation where $g(t,\theta)$ is oscillating. We observe that the six POD modes are linearly dependent on the set of Fourier bases, which verifies the relation given in (4.22). Moreover, it follows from the subplot of $q_1(t),\cdots,q_6(t)$ that the primary dynamics of the oscillations of $g(t,\theta)$ can be effectively captured using the 6 POD modes of reconstruction.

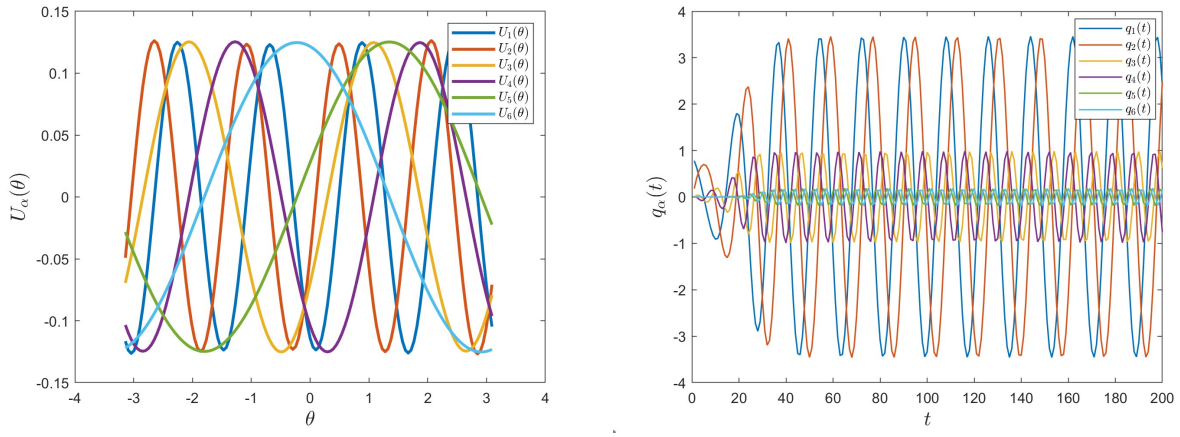


Figure 4.3: POD modes $U_\alpha(\theta)$ **(left)** and POD coefficients $q_\alpha(t)$ **(right)**.

4.2.3 Galerkin Projection using POD Modes

In this subsection, we apply POD techniques given in Section 4.1 to the Moore-Greitzer model introduced in Section 4.2.1. To reduce the dimensionality of the data $(g(\theta,t), \Phi(t), \Psi(t))$, we first find a set of optimal POD bases $\{U_1, \cdots, U_M\}$ by applying a snapshots method (discussed in Section 4.2.1) on $g(t,\theta)$. Then, we use a subset of the POD bases, say the first n modes of the POD expansion, to represent the PDE solution $g(t,\theta)$, denoted as

$$g_{\text{pod}}(t,\theta) = \sum_{\alpha=1}^{n} b_\alpha(t) U_\alpha(\theta), \tag{4.24}$$

where the mapping $t \longmapsto (b_1(t), \cdots, b_n(t)) \in \mathbb{R}^n$ satisfies an n-dimensional ODE. Specifically, this set of ODEs is generated by a so-called POD-Galerkin procedure, where one can project the Moore-Greitzer PDE (4.17) onto these POD modes using Galerkin projection to find an n-dimensional ODE so that the weak solution $g_{\text{pod}}(t,\theta)$ stays close to the real solution $g(t,\theta)$. Combined with $\Phi(t)$ and $\Psi(t)$, we have

$$\begin{bmatrix} g_{\text{pod}}(t,\theta) \\ \Phi(t) \\ \Psi(t) \end{bmatrix} = \begin{bmatrix} \sum_{\alpha=1}^{n} b_\alpha(t) U_\alpha(\theta) \\ \Phi(t) \\ \Psi(t) \end{bmatrix}.$$

Substituting it into the PDE gives us

$$\begin{bmatrix} \sum_{\alpha=1}^{n} \dot{b}_\alpha(t) U_\alpha(\theta) \\ \dot{\Phi}(t) \\ \dot{\Psi}(t) \end{bmatrix} = \begin{bmatrix} G_0(b(t), U(\theta), \Phi(t)) \\ G_1(b(t), \Phi(t), \Psi(t)) \\ G_2(b(t), \Phi(t), \Psi(t)) \end{bmatrix},$$

where the right-hand side depends explicitly on the modes $U(\theta) = (U_1(\theta), \cdots, U_n(\theta))$ and the vector $b(t) = (b_1(t), \cdots, b_n(t))$ and $\Phi(t)$ and $\Psi(t)$. Note that the top entry on each side is an element in the Hilbert space $\mathcal{H}$, and it is notably *not* dependent on $\Psi(t)$ even if $\Phi(t)$ is coupled with $\Psi(t)$. Taking the inner product of the top entry on each side with U_β gives

$$\begin{bmatrix} \dot{b}_\beta(t) \\ \dot{\Phi}(t) \\ \dot{\Psi}(t) \end{bmatrix} = \begin{bmatrix} \langle G_0(b(t), U(\theta), \Phi(t)), U_\beta \rangle_{\mathcal{H}} \\ G_1(b(t), \Phi(t), \Psi(t)) \\ G_2(b(t), \Phi(t), \Psi(t)) \end{bmatrix}, \tag{4.25}$$

which gives an $(n+2)$-dimensional system ODE, where

$$\begin{aligned} G_0(b(t), U(\theta), \Phi(t)) = &\sum_{\alpha=1}^{n} K^{-1} b_\alpha(t) \left(\frac{\nu}{2} U_\alpha''(\theta) - \frac{1}{2} U_\alpha'(\theta) \right) \\ &+ aK^{-1} \left[\psi_c\Big(\Phi + \sum_{\alpha=1}^{n} b_\alpha(t) U_\alpha(\theta)\Big) - \overline{\psi}_c\Big(\Phi, \sum_{\alpha=1}^{n} b_\alpha(t) U_\alpha(\theta)\Big) \right]. \end{aligned} \tag{4.26}$$

Let us now write the right-hand sides of (4.25) more explicitly, particularly the top equation, which depends on those POD bases. To do this, we need to rewrite the PDE and take the POD-Fourier expansion as introduced in Section 4.2.2. From the relation between the POD and Fourier modes (4.22), the POD expansions applied to $g(t,\theta)$ can be rewritten as follows

$$\begin{aligned} g_{\text{pod}}(t,\theta) &= \sum_{\alpha=1}^{n} b_\alpha(t) \sum_{j\in I_N} c_{\alpha,j} e^{ij\theta} \\ &= \sum_{j\in I_N} \left(\sum_{\alpha}^{n} c_{\alpha,j} b_\alpha(t) \right) e^{ij\theta}. \end{aligned} \tag{4.27}$$

Remark 4.2.1. *We shall make the choice of using (4.24) or (4.27) depending on the nature of the governing equation of the dynamic model. Since K^{-1} only acts on Fourier modes in the Moore-Greitzer model, we may make use of the POD-Fourier expansion to incorporate the correct form of K^{-1} in the derivation of the reduced-order equation when we apply the POD-Galerkin procedure on the PDE part of the Moore-Greitzer model.*

Indeed, we have

$$\begin{aligned} \frac{\partial g}{\partial t}(t,\theta) &= \sum_{\alpha=1}^{n} \dot{b}_\alpha(t) U_\alpha(\theta), \\ \frac{\partial g}{\partial \theta}(t,\theta) &= \sum_{\alpha=1}^{n} b_\alpha(t) U'_\alpha(\theta) = \sum_{j\in I_N} ij \Big(\sum_{\alpha=1}^{n} c_{\alpha,j} b_\alpha(t) \Big) e^{ij\theta}, \\ \frac{\partial^2 g}{\partial \theta^2}(t,\theta) &= \sum_{\alpha=1}^{n} b_\alpha(t) U''_\alpha(\theta) = -\sum_{j\in I_N} j^2 \Big(\sum_{\alpha=1}^{n} c_{\alpha,j} b_\alpha(t) \Big) e^{ij\theta}. \end{aligned} \tag{4.28}$$

Using the fact that $K^{-1}(\sum_{j\in I_N} \tilde{\phi}_j e^{ij\theta}) = \sum_{n\in I_N} \left(\frac{|j|}{|j|+ma} \right) \tilde{\phi}_n e^{ij\theta}$, we apply K^{-1} to $g(t,\theta)$:

$$K^{-1} g(t,\theta) = K^{-1} \Big(\sum_{j\in I_N} \Big(\sum_{\alpha=1}^{n} c_{\alpha,j} b_\alpha(t) \Big) e^{ij\theta} \Big) = \sum_{j\in I_N} \left(\frac{|j|}{|j|+ma} \right) \Big(\sum_{\alpha=1}^{n} c_{\alpha,j} b_\alpha(t) \Big) e^{ij\theta}. \tag{4.29}$$

Similarly, applying K^{-1} to the spatial derivatives gives

$$\begin{aligned} K^{-1}\frac{\partial g}{\partial \theta}(t,\theta) &= K^{-1}\Big(\sum_{j\in I_N} ij\Big(\sum_{\alpha=1}^{n} c_{\alpha,j}b_\alpha(t)\Big)e^{ij\theta}\Big) \\ &= \sum_{j\in I_N}\left(\frac{|j|}{|j|+ma}\right) ij\Big(\sum_{\alpha=1}^{n} c_{\alpha,j}b_\alpha(t)\Big)e^{ij\theta}, \\ K^{-1}\frac{\partial^2 g}{\partial \theta^2}(t,\theta) &= -K^{-1}\Big(\sum_{j\in I_N} j^2\Big(\sum_{\alpha=1}^{n} c_{\alpha,j}b_\alpha(t)\Big)e^{ij\theta}\Big) \\ &= -\sum_{j\in I_N}\left(\frac{|j|}{|j|+ma}\right) j^2\Big(\sum_{\alpha=1}^{n} c_{\alpha,j}b_\alpha(t)\Big)e^{ij\theta}. \end{aligned} \tag{4.30}$$

The next step is to appropriately evaluate the Galerkin projections on the linear terms given at the top of (4.26) and nonlinearities at the bottom of (4.26) using the POD expansion given in (4.24), along with the orthogonality property of the POD modes. A detailed POD-Galerkin procedure applied to the Moore-Greitzer PDE system of $g(t,\theta)$ is given in Appendix B. The complete β^{th} equation associated with the PDE for $g(t,\theta)$ approximated by the POD mode expansions with the Galerkin procedure is given by

$$\begin{aligned} \dot{b}_\beta(t) &= \sum_{\alpha=1}^{n}\Big(\sum_{j\in I_N}\left(\frac{|j|}{|j|+ma}\right)\Big(-\frac{\nu}{2}j^2 - ij\frac{1}{2}\Big)c_{\alpha,j}\overline{c_{\beta,j}}\Big)b_\alpha(t) \\ &\quad + \frac{3Ha}{W^2}\Phi(t)\Big(1-\frac{\Phi(t)}{2W}\Big)\sum_{\alpha=1}^{n}\Big(\sum_{j\in I_N}\left(\frac{|j|}{|j|+ma}\right)c_{\alpha,j}\overline{c_{\beta,j}}\Big)b_\alpha(t) \\ &\quad + \Big(\frac{3Ha}{2W^2} - \frac{3Ha}{2W^3}\Phi(t)\Big)\sum_{\alpha_1,\alpha_2=1}^{n}\left(\sum_{\substack{j,k\in I_N \\ (j+k\neq 0)}}\left(\frac{|j+k|}{|j+k|+ma}\right)c_{\alpha_1,j}c_{\alpha_2,k}\overline{c_{\beta,j+k}}\right)b_{\alpha_1}(t)b_{\alpha_2}(t) \\ &\quad - \frac{Ha}{2W^3}\sum_{\alpha_1,\alpha_2,\alpha_3=1}^{n}\left(\sum_{\substack{j,k,l\in I_N \\ (j+k+l\neq 0)}}\left(\frac{|j+k+l|}{|j+k+l|+ma}\right)c_{\alpha_1,j}c_{\alpha_2,k}c_{\alpha_3,l}\overline{c_{\beta,j+k+l}}\right)b_{\alpha_1}(t)b_{\alpha_2}(t)b_{\alpha_3}(t), \end{aligned} \tag{4.31}$$

which are coupled to the ODEs given by

$$\begin{aligned}\dot{\Phi}(t) &= \frac{1}{l_c}\Big(\bar{\psi}_c(\Phi(t),\hat{b}(t)) - \Psi(t)\Big)\\ \dot{\Psi}(t) &= \frac{1}{4B^2 l_c}\Big(\Phi(t) - \gamma\sqrt{\Psi(t)}\Big)\end{aligned} \tag{4.32}$$

Notice that $\hat{b}(t) := ((b_1(t),\cdots,b_n(t))$, implying that $\bar{\psi}_c(\Phi(t),\hat{b}(t))$ depends on Φ as well as the decomposed time coefficients $b_1(t),\cdots,b_n(t)$ coming from $g(t,\theta)$ by averaging θ over $[0,2\pi]$. Using (4.19) yields

$$\bar{\psi}_c(t) = \psi_c(\Phi(t)) - \frac{3H}{2W^2}\left(\frac{\Phi(t)}{W} - 1\right)\frac{1}{2\pi}\int_0^{2\pi} g^2(t,\theta)d\theta - \frac{H}{2W^3}\int_0^{2\pi} g^3(t,\theta)d\theta,$$

where we can express

$$\begin{aligned} g^2(t,\theta) &= \sum_{\alpha_1=1}^{n} b_{\alpha_1}(t)U_{\alpha_1}(\theta)\sum_{\alpha_2=1}^{n} b_{\alpha_2}(t)U_{\alpha_2}(\theta)\\ &= \sum_{\alpha_1=1}^{n} b_{\alpha_1}(t)\sum_{j\in I_N} c_{\alpha_1,j}e^{ij\theta}\sum_{\alpha_2=1}^{n} b_{\alpha_2}(t)\sum_{k\in I_N} c_{\alpha_2,k}e^{ik\theta}\\ &= \sum_{\alpha_1,\alpha_2=1}^{n}\sum_{j,k\in I_N} c_{\alpha_1,j}c_{\alpha_2,k}e^{i(j+k)\theta}b_{\alpha_2}(t)b_{\alpha_1}(t),\\ g^3(t,\theta) &= \sum_{\alpha_1,\alpha_2,\alpha_3=1}^{n}\sum_{j,k,l\in I_N} c_{\alpha_1,j}c_{\alpha_2,k}c_{\alpha_3,l}e^{i(j+k+l)\theta}b_{\alpha_2}(t)b_{\alpha_1}(t)b_{\alpha_3}(t). \end{aligned}$$

As such, we can write $\bar{\psi}_c$ as follows,

$$\begin{aligned}\bar{\psi}_c(\Phi(t),\hat{b}(t)) = \psi_c(\Phi(t)) &- \frac{3H}{2W^2}\left(\frac{\Phi(t)}{W} - 1\right)\sum_{\alpha_1,\alpha_2=1}^{n}\sum_{\substack{j,k\in Z\setminus\{0\}\\(j+k=0)}} c_{\alpha_1,j}c_{\alpha_2,k}b_{\alpha_2}(t)b_{\alpha_1}(t)\\ &- \frac{H}{2W^3}\sum_{\alpha_1,\alpha_2,\alpha_3=1}^{n}\sum_{\substack{j,k,l\in Z\setminus\{0\}\\(j+k+l=0)}} c_{\alpha_1,j}c_{\alpha_2,k}c_{\alpha_3,l}b_{\alpha_2}(t)b_{\alpha_1}(t)b_{\alpha_3}(t).\end{aligned} \tag{4.33}$$

4.3 Model Reconstruction using POD-Galerkin with L^2 and H^1 Inner Products

In this section, we aim to show the precision of the proposed POD-Galerkin method in reconstructing the PDE solutions of the Moore-Greitzer model through simulation results. The previous Theorems 4.1.1 and 4.1.2, and Corollary **??** characterize the POD modes as the best orthonormal bases correlated to the snapshots. It is noteworthy that the Hilbert space, denoted as H throughout Section 4.1, is typically defined using the L^2 norm in the spatial domain. Nevertheless, these POD findings can be generalized to Sobolev spaces utilizing functional analytic techniques [26]. In many physical scenarios, the smoothness of the reduced-order representation is essential. While the L^2 norm is a natural fit for various POD applications, the H^1 norm proves advantageous when derivative information is critical and when maintaining smoothness is necessary. Employing the H^1 norm guarantees that the resulting POD modes are not only close in an integral sense (as indicated by L^2) but also preserve smoothness by minimizing abrupt changes. This aspect is especially relevant in PDE-based models, where solutions are anticipated to exhibit specific regularity properties which align with the characteristics of the Moore-Greitzer PDE system. The contention here is that this methodology could enhance convergence, stability, and physical fidelity in reduced-order models, rendering it an attractive alternative in many situations [51, 64, 46].

For every time $t \in [0, T]$, the Moore-Greitzer PDE solution $g(t, \cdot)$ lies in $\mathcal{H}$ that is a Hilbert space of functions $\phi : \Omega \to \mathbb{R}$ with some inner product $\langle \phi, \psi \rangle_{\mathcal{H}}$ and norm $\|\phi\|_{\mathcal{H}} = \langle \phi, \phi \rangle_{\mathcal{H}}^{1/2}$. To generalize the proper orthogonal decomposition in the H^1 Sobolev space, let us first define $L^2(\Omega)$ as the space of measurable and square integral functions $\phi : \Omega \to \mathbb{R}$, i.e.,

$$\|\phi\|^2_{L^2(\Omega)} = \int_\Omega |\phi(\theta)|^2 d\theta < \infty. \tag{4.34}$$

Similarly, we define $H^1(\Omega)$ as the Hilbert space of continuously differentiable functions $\phi : \Omega \to \mathbb{R}^d$ under the norm

$$\|\phi\|^2_{H^1(\Omega)} = \int_\Omega (|\phi(\theta)|^2 + \|\nabla\phi(\theta)\|^2 d\theta < \infty, \tag{4.35}$$

where $\|\cdot\|$ represents the Euclidean norm in $\mathbb{R}^n$. The inner product for $\phi, \psi \in H^1(\Omega)$ is given as follows,

$$\langle \phi, \psi \rangle_{H^1(\Omega)} = \int_\Omega (\phi(\theta)\psi(\theta) + \nabla\phi(\theta) \cdot \nabla\psi(\theta)) d\theta. \tag{4.36}$$

4.3.1 Computational Scheme for Calculating the POD Modes in the H^1 Sobolev Space

Given the snapshots $\{g_i : 1 \leq i \leq M\}$, we now would like to seek the POD modes $U_1(\theta), \cdots, U_n(\theta)$ such that it minimizes

$$\mu_n = \inf \left\| g_i(\theta) - \sum_{\alpha=1}^{n} b_i^{(\alpha)} U_\alpha(\theta) \right\|_2 = \inf \left(\frac{1}{M} \sum_{i=1}^{M} \left\| g_i(\theta) - \sum_{\alpha=1}^{n} b_i^{(\alpha)} U_\alpha(\theta) \right\|_{H^1(\Omega)}^2 \right)^{1/2}$$

$$= \inf \left(\frac{1}{M} \sum_{i=1}^{M} \left(\left\| g_i(\theta) - \sum_{\alpha=1}^{n} b_i^{(\alpha)} U_\alpha(\theta) \right\|_{L^2(\Omega)}^2 + \epsilon \left\| \nabla g_i(\theta) - \sum_{\alpha=1}^{n} b_i^{(\alpha)} \nabla U_\alpha(\theta) \right\|_{L^2(\Omega)}^2 \right) \right)^{1/2},$$

subject to

$$\sum_{\alpha=1}^{n} |\langle U_\alpha, U_\alpha \rangle_{H^1}|^2 = 1,$$

where the infimum is over functions of the form $F_i(x) = \sum_{\alpha=1}^{n} b_i^{(\alpha)} U_\alpha(x)$ for functions $U_1(x), \cdots, U_n(x)$ and vectors $b^{(1)}, \cdots, b^{(n)}$. Notice that ϵ is a coefficient to be chosen from dimensional analysis [47], and we can also guess the value of ϵ. The optimality of the above minimization problem was proved in Theorem 1 in [26]. It follows from the results introduced in Section 4.1 and [47] that the computational scheme of finding the POD basis functions can be summarized as follows:

$$U_\alpha = \frac{1}{\sqrt{M\lambda_\alpha}} \sum_{i=1}^{M} \gamma_i^{(\alpha)} g_i,$$

where λ_α and γ^α represent the eigenvalues and eigenvectors of the $M \times M$ correlation matrix C defined in the H^1 sense:

$$C_{ij} = \frac{1}{M} \langle g_i, g_j \rangle_{H^1} = \frac{1}{M} \langle g_i, g_j \rangle_{L^2} + \epsilon \frac{1}{M} \langle \nabla g_i, \nabla g_j \rangle_{L^2}, \quad 1 \leq i, j \leq M.$$

Each eigenvector $\gamma^\alpha = (\gamma_1^{(\alpha)}, \cdots, \gamma_M^{(\alpha)}) \in \mathbb{R}^M$. Since C is symmetric, the eigenvectors $\gamma^{(\alpha)}$ may be assumed to be orthogonal in $\mathbb{R}^M$. Suppose each $\gamma^{(\alpha)}$ is scaled to be of length 1 in $\mathbb{R}^M$, that is $\sum_{i=1}^{M} (\gamma_i^{(\alpha)})^2 = 1$. As such, the POD modes are orthonormal in the H^1 inner

product space:

$$\begin{aligned}
\langle U_\alpha, U_\beta \rangle_{H^1} &= \frac{1}{M\sqrt{\lambda_\alpha \lambda_\beta}} \sum_{i,j=1}^{M} \gamma_i^{(\alpha)} \gamma_j^{(\beta)} \langle g_i, g_j \rangle_{H^1} \\
&= \frac{1}{\sqrt{\lambda_\alpha \lambda_\beta}} \sum_{i,j=1}^{M} \gamma_i^{(\alpha)} C_{ij} \gamma_j^{(\beta)} \\
&= \frac{1}{\sqrt{\lambda_\alpha \lambda_\beta}} \sum_{i=1}^{M} \lambda_\beta \gamma_i^{(\alpha)} \gamma_j^{(\beta)} \\
&= \begin{cases} 0 & \text{if } \alpha \neq \beta \\ 1 & \text{if } \alpha = \beta. \end{cases}
\end{aligned}$$

4.3.2 Simulation Results of Reconstructing the Moore-Greitzer PDE solutions using L^2-POD-Galerkin and H^1-POD-Galerkin

In this subsection, we will investigate how the L^2 and H^1 Galerkin projections affect the POD reconstruction for the Moore-Greitzer model. We would like to examine the order of the POD-Galerkin approximation and estimate its L^2 and H^1 errors compared to the full-order model $g(t,\theta) \in L^2([0,T],\mathcal{H})$ where $\mathcal{H}$ is an infinite-dimensional Hilbert space, $\mathcal{H} := \breve{L}^2(0,2\pi) = \left\{ g \in L^2 : \int_0^{2\pi} g(\theta) d\theta = 0 \right\}$. When the set $\{U_\alpha\}_{\alpha=1}^n$ is orthonormal in the usual L^2 space, the mean square error between the full-order model of $g(t,\theta)$ and the L^2-POD-Galerkin reconstruction, denoted by $\mathcal{E}^2_{L^2}(g(t,\theta), g^{L^2}_{\text{pod}}(t,\theta))$, is given as

$$\begin{aligned}
\mathcal{E}^2_{L^2}(g(t,\theta), g^{L^2}_{\text{pod}}(t,\theta)) &= \left\| g(t,\theta) - \sum_{\alpha=1}^{n} b_\alpha(t) U_{(\alpha)}(\theta) \right\|^2_{L^2([0,T],\mathcal{H}(L^2))} \\
&= \int_0^T \left\| g(t,\theta) - \sum_{\alpha=1}^{n} b_\alpha(t) U_{(\alpha)}(\theta) \right\|^2_{\mathcal{H}(L^2)} dt,
\end{aligned} \tag{4.37}$$

where $\mathcal{H}(L^2)$ denotes the Hilbert space of measurable and square-integrable functions satisfying the regularity property, i.e., zero-mean regularity condition. Notice that $b_\alpha(t)$ is the temporal coefficient corresponding to the α-th POD mode, i.e., $U_\alpha(\theta)$ calculated in the standard L^2 computational scheme, evaluated at time t.

When the set $\{\tilde{U}_\alpha\}_{\alpha=1}^n$ is orthonormal in the H^1 Sobolev space, the squared H^1 error between the full-order model of $g(t,\theta)$ and the H^1-POD-Galerkin reconstruction, denoted by $\mathcal{E}^2_{H^1}(g(t,\theta), g^{H^1}_{\text{pod}}(t,\theta))$, is given as

$$\begin{aligned}\mathcal{E}^2_{H^1}(g(t,\theta), g^{H^1}_{\text{pod}}(t,\theta)) &= \left\| g(t,\theta) - \sum_{\alpha=1}^{n} \tilde{b}_\alpha(t)\tilde{U}_{(\alpha)}(\theta) \right\|^2_{L^2([0,T],\mathcal{H}(H^1))} \\ &= \int_0^T \left\| g(t,\theta) - \sum_{\alpha=1}^{n} \tilde{b}_\alpha(t)\tilde{U}_{(\alpha)}(\theta) \right\|^2_{\mathcal{H}(H^1)} dt,\end{aligned} \tag{4.38}$$

where $\mathcal{H}(H^1)$ represents the Hilbert space of continuously differentiable functions under the H^1 norm, i.e., for any $f \in \mathcal{H}(H^1)$,

$$\|f\|^2_{\mathcal{H}(H^1)} = \langle f, f\rangle_{L^2} + \epsilon\langle \nabla f, \nabla f\rangle_{L^2},$$

where f satisfies the same regularity condition as given in the L^2 case, and ϵ quantifies the extent to which additional emphasis is placed on the derivative information.

In the snapshots version, instead of $g(t,\theta)$ for all $t \in [0,T]$, we have snapshots $g(t_i,\theta)$ for times t_i for $1 \le i \le M$. Let us write $g_i(x) = g(t_i, x)$. Now, with a set of snapshots, the associated mean-square error is defined as follows,

$$\mathcal{E}^2_{L^2}(g_i(\theta), g^{L^2}_{\text{pod}}(t,\theta)) = \frac{1}{M}\sum_{i=1}^{M} \left\| g_i(\theta) - \sum_{\alpha=1}^{n} b_i^\alpha U_{(\alpha)}(\theta) \right\|^2_{\mathcal{H}(L^2)}, \tag{4.39}$$

$$\mathcal{E}^2_{H^1}(g_i(\theta), g^{H^1}_{\text{pod}}(t,\theta)) = \frac{1}{M}\sum_{i=1}^{M} \left\| g_i(\theta) - \sum_{\alpha=1}^{n} \tilde{b}_i^\alpha \tilde{U}_{(\alpha)}(\theta) \right\|^2_{\mathcal{H}(H^1)}. \tag{4.40}$$

As a reference, we also compute the mean-square error between the full-order model of $g(t,\theta)$ and the POD reconstruction without the Galerkin procedure:

$$\mathcal{E}^2_{L^2}(g_i(\theta), g^{L^2}_{\text{POD}}(t,\theta)) = \frac{1}{M}\sum_{i=1}^{M} \left\| g_i(\theta) - \sum_{\alpha=1}^{n} q_i^\alpha U_{(\alpha)}(\theta) \right\|^2_{\mathcal{H}(L^2)}. \tag{4.41}$$

Note that $q_i^\alpha := q_\alpha(t)$ is calculated by projecting the snapshots onto the POD modes directly without any Galerkin procedure, so the numerics for $\mathcal{E}^2_{L^2}(g_i(\theta), g^{L^2}_{\text{POD}}(t,\theta))$ should theoretically be much smaller than $\mathcal{E}^2_{L^2}(g_i(\theta), g^{L^2}_{\text{pod}}(t,\theta))$ and $\mathcal{E}^2_{H^1}(g_i(\theta), g^{H^1}_{\text{pod}}(t,\theta))$. As expected, $\mathcal{E}^2_{L^2}(g_i(\theta), g^{L^2}_{\text{POD}}(t,\theta))$ is decreasing as n increases. This phenomenon is indeed

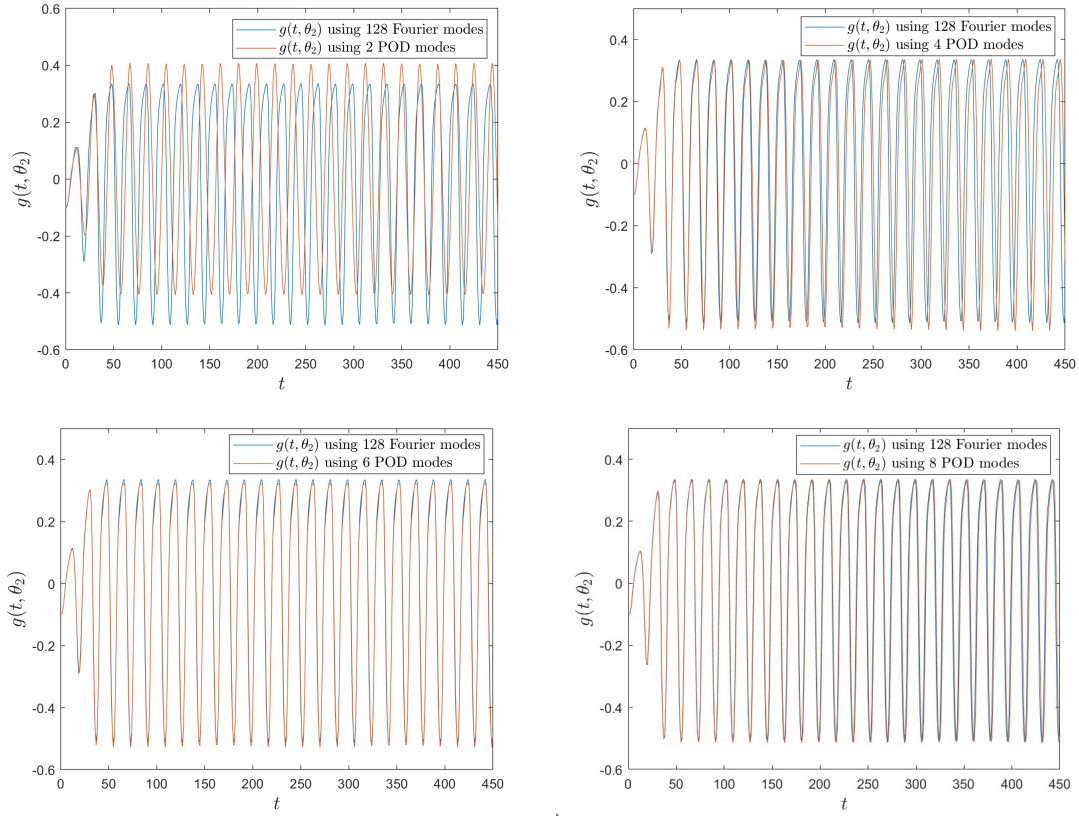


Figure 4.4: The POD reconstructions (with a Galerkin procedure) using different numbers of POD modes of the deterministic PDE of $g(t,\theta_2)$ represented by 128 Fourier modes.

depicted in Figure 4.7 and reflected in Table 4.1. However, a limitation in reconstructing $g_{\text{POD}}^{L^2}(t,\theta)$ is that the entire POD procedure does not yield a reduced-order equation.

Figure 4.4 illustrates L^2-POD reconstructions of the Moore-Greitzer PDE at a fixed value of θ, i.e., $g(t,\theta)$, using 2, 4, 6, and 8 POD modes. Note that the original snapshots of $g(t,\theta)$ are yielded by 128 Fourier modes over the spatial domain using a Fourier spectral method. The parameters of generating this stall instability of $g(t,\theta)$ for all $t \in [0, 450]$ and $\theta \in [0, 2\pi]$ are given as follows,

$$l_c = 8,\ H = 0.18,\ W = 0.25,\ m = 1.75,\ \nu = 0.1,\ a = 1/3.5,\ \psi_{c_0} = 1.67H,$$

and the values of the bifurcation parameters $B = 0.95$ and $\gamma = 0.5645$. The initial conditions of $g(t,\theta)$, Φ and Ψ are chosen as

$$g(0,\theta) = 0.1\cos(\theta),\ \Phi_0 = 0.51,\ \Psi_0 = 0.66.$$

At first glance, it is evident that the accuracy of the reconstructions is enhanced as the number of POD modes is elevated from 2 to 6. Nonetheless, a noticeably greater discrepancy is observed between $g(t,\theta_2)$ and $g_{\text{pod}}^{L^2}(t,\theta_2)$ under the condition of $n = 8$, as opposed to the scenario with $n = 6$. If we are considering the L^2 errors over the whole domain of θ, it follows from Table 4.1 or the right subplot of Figure 4.7 that $\mathcal{E}_{L^2}^2(g, g_{\text{pod}})$ also increases as n goes from 6 to 8. This suggests that the L^2 POD-Galerkin reconstruction does not consistently demonstrate robustness across different numbers of POD modes. Therefore, we are interested in how the reconstruction is influenced when the derivative information regarding θ is incorporated into the POD-Galerkin framework. This drives us to conduct further experiments to reconstruct $g(t,\theta)$ using the H^1 POD-Galerkin method with various estimates for ϵ in the H^1 Sobolev norm.

Table 4.1 illustrates that with $\epsilon_2 = 0.004$ and $n = 8$, $\mathcal{E}_{H^1}^2(g, g_{\text{pod}}) = 6.738 \times 10^{-4}$ is significantly lower than $\mathcal{E}_{L^2}^2(g, g_{\text{pod}}) = 3.270 \times 10^{-2}$. This improvement achieved through the H^1 POD-Galerkin method is further highlighted in Figure 4.5, where the right subplot displays a considerably better alignment between $g(t,\theta_2)$ and its H^1 POD reconstruction compared to the left subplot. Additionally, the information provided in the last four rows of Table 4.1 indicates that the effectiveness of the H^1 POD-Galerkin reconstruction is influenced by the ϵ values employed for projecting the Moore-Greitzer PDE system. Specifically, a decrease in ϵ leads to a more pronounced enhancement in the reconstruction of PDE solutions with higher modes. This suggests that the H^1 POD-Galerkin and L^2 POD-Galerkin methods exhibit similar performance in approximating PDE solutions via reduced-order equations with higher modes. However, the performance of the H^1 POD-Galerkin method can be substantially improved relative to the L^2 POD reconstruction when

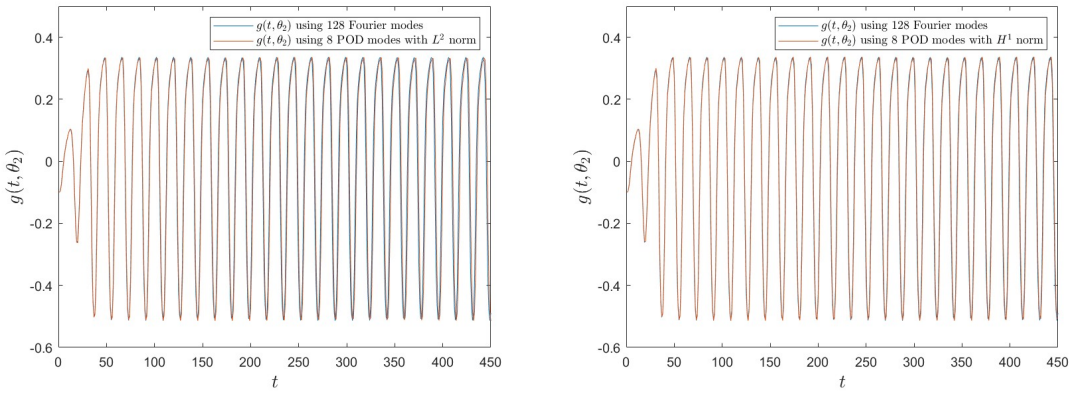


Figure 4.5: The POD reconstructions using 8 POD modes with L^2-Galerkin procedure (**left**) and H^1-Galerkin procedure (**right**) of the deterministic PDE of $g(t,\theta_2)$ represented by 128 Fourier modes.

the number of modes is restricted. Notably, with $n = 4$, the H^1 POD-Galerkin method shows significant enhancement resulting in an H^1 error of 0.0106 when $\epsilon = 0.046$. This comparison is depicted in Figure 4.6, where the improvement is distinctly more evident than in Figure 4.5 for $n = 8$, which aligns with expectations.

POD modes	$n=2$	$n=4$	$n=6$	$n=8$	$n=10$	$n=12$
$\mathcal{E}^2_{L^2}(g, g_{\text{POD}})$	4.760e-2	2.463e-3	8.485e-4	1.604e-4	1.764e-5	6.920e-6
$\mathcal{E}^2_{L^2}(g, g_{\text{pod}})$	1.000	3.330e-1	7.40e-3	3.270e-2	4.900e-3	3.700e-3
$\mathcal{E}^2_{H^1}(g, g_{\text{pod}}, \epsilon_1)$	1.123	1.517e-1	1.065e-1	5.030e-2	1.009e-1	1.089e-1
$\mathcal{E}^2_{H^1}(g, g_{\text{pod}}, \epsilon_2)$	1.029	2.473e-1	1.520e-2	6.738e-4	1.510e-2	1.830e-2
$\mathcal{E}^2_{H^1}(g, g_{\text{pod}}, \epsilon_3)$	1.009	2.872e-1	2.900e-3	6.700e-3	1.600e-3	2.500e-3
$\mathcal{E}^2_{H^1}(g, g_{\text{pod}}, \epsilon_4)$	1.002	3.087e-1	2.800e-3	1.670e-2	6.528e-4	4.520e-4

Table 4.1: Comparisons of the mean squared errors of $\mathcal{E}^2_{L^2}(g, g_{\text{POD}})$, $\mathcal{E}^2_{L^2}(g, g_{\text{pod}})$, and $\mathcal{E}^2_{H^1}(g, g_{\text{pod}})$ for $\epsilon_1 = 0.01$, $\epsilon_2 = 0.004$, $\epsilon_3 = 0.002$ and $\epsilon_4 = 0.001$.

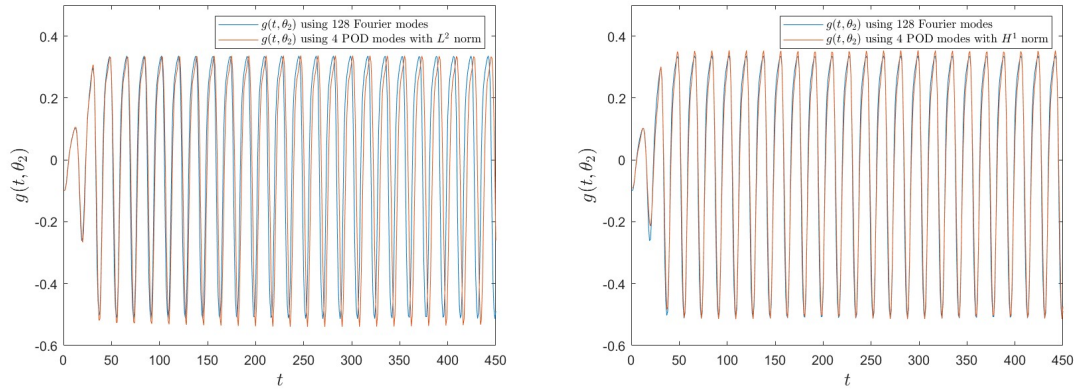


Figure 4.6: The POD reconstructions using 4 POD modes with L^2-Galerkin procedure (**left**) and H^1-Galerkin procedure (**right**) of the deterministic PDE of $g(t, \theta_2)$ represented by 128 Fourier modes.

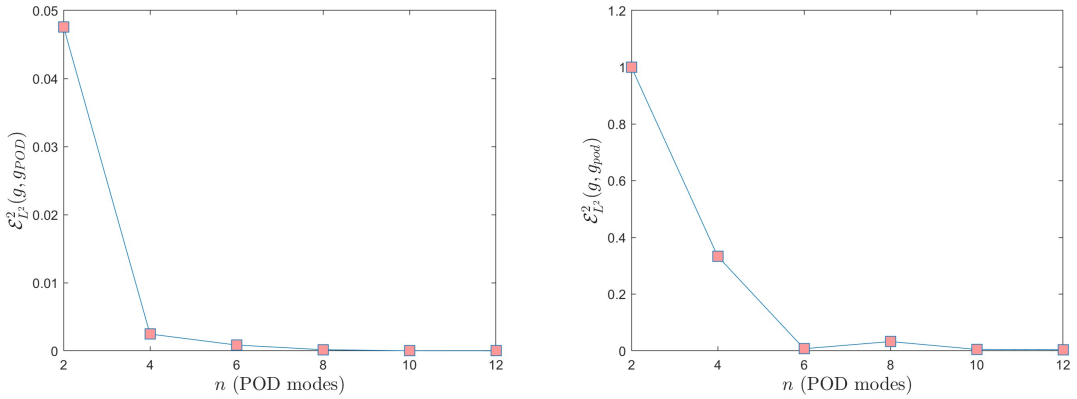


Figure 4.7: The L^2 errors of the POD reconstructions without (**left**) and with (**right**) the Galerkin projection compared to the real PDE solution of the Moore-Geitzer model using 128 Fourier modes at a fixed value of θ.

Chapter 5

QCD for the Stall Instability of the Compressor Models

The detection and management of surge and stall instabilities in compressor systems have been subjects of extensive study over the past several decades. The review in [102] consolidates major contributions in the field of stall detection, presenting the latest methods and algorithms for identifying stall precursors. It offers a comprehensive overview of the advancements in modeling and detection techniques. [55] explores the use of nonlinear feature extraction algorithms, including phase reconstruction of time-series signals and approximate entropy evaluation, to identify small disturbances preceding stall events. The approach demonstrates the potential for early warning systems that can detect subtle flow irregularities indicative of impending stall. Xu et al. [107] present a finite-time backstepping-based adaptive control approach to manage surge and stall instabilities in compressor systems. The method aims to achieve rapid stabilization, enhancing the robustness and reliability of compressor operations. The study in [59] develops low-dimensional approximations using a multiscale analysis approach near the deterministic stall bifurcation point in the presence of additive noise. Subsequently, the authors in [59] examine how additive noise affects Hopf bifurcations in the Moore-Greitzer PDE model, which is essential for understanding flow and pressure variations in axial-flow jet engine compressors. This research develops low-dimensional approximations near deterministic stall bifurcation points, revealing that the reduced models manifest multiplicative noise.

However, there is a paucity of literature addressing the detection of instabilities in compressor systems via QCD techniques, indicating that numerous theoretical and practical gaps remain to be explored regarding this matter. In Chapter 3, we investigated the

effectiveness of the generalized CUSUM statistics with particle filters to detect the surge instability of the ODE part of the Moore-Greitzer model. Even if incorporating the PDE part of the model yields a much higher-dimensional system, the POD-Galerkin procedure introduced in Chapter 4 provides a reasonable reduced-order model so that the QCD method of the generalized CUSUM using particle filtering can be appropriately implemented. Essentially, this chapter deals with the QCD problems in the HMMs where the signals go through a stall bifurcation occurring in the PDE part of the Moore-Greitzer model due to external forcing added to the ODE part of the system, and the observations are linearly dependent on the signals corrupted by a random process. The generalized CUSUM statistics via particle filtering approach and the reduced-order modeling technique by POD are combined to solve the associated QCD problems.

5.1 Stall Detection in Deterministic Moore-Greitzer PDE Systems

In this section, we study Moore-Greitzer PDE systems with disturbances, aiming to improve our understanding of dynamic instabilities, particularly in compressor systems with some external forcing, yet without any randomness. By incorporating the disturbances observed in mass flow and pressure, one can enhance the prediction and control of phenomena such as surge and rotating stall, thereby improving system stability and designing more efficient control strategies for further applications.

5.1.1 Deterministic Moore–Greitzer PDE systems with Disturbances on Compressor Flow and Pressure

Disturbances in a compressor system can significantly affect both the mass flow and pressure characteristics, potentially leading to instability and reduced efficiency. These disturbances can originate from various sources, including external fluctuations, operational changes, or system component degradation. To model the effects of disturbances on mass flow and pressure in a compressor system, recall the PDE-based framework of the Moore-Greitzer model (see (4.17)) and define $\xi_1(\theta, t)$ and $\xi_2(\theta, t)$ as disturbance terms representing external deterministic forcing, e.g., a bird impact. As such, the "changed" or "disturbed"

Moore-Greitzer model is given as follows,

$$\frac{\partial}{\partial t}\begin{bmatrix} g \\ \Phi \\ \Psi \end{bmatrix} = \begin{bmatrix} K^{-1}(\frac{\nu}{2}\frac{\partial^2}{\partial\theta^2} - \frac{1}{2}\frac{\partial}{\partial\theta}) & 0 & 0 \\ 0 & 0 & 0 \\ 0 & 0 & 0 \end{bmatrix}\begin{bmatrix} g \\ \Phi \\ \Psi \end{bmatrix} + \begin{bmatrix} aK^{-1}(\psi_c(\Phi+g) - \overline{\psi}_c(\Phi,g)) \\ \frac{1}{l_c}(\overline{\psi}_c(\Phi,g) - \Psi) \\ \frac{1}{4l_cB^2}(\Phi - \gamma\sqrt{\Psi}) \end{bmatrix} + \begin{bmatrix} 0 \\ \xi_1(\theta,t) \\ \xi_2(\theta,t) \end{bmatrix}.$$

More precisely, the external deterministic forcing can be given as,

$$\begin{bmatrix} 0 \\ \xi_1(\theta,t) \\ \xi_2(\theta,t) \end{bmatrix} = d\mathbb{I}_{\{t\geq k\}}, \quad \text{where} \quad \mathbb{I}_{\{t\geq k\}} = \begin{cases} 0, & t < k \\ 1, & t \geq k, \end{cases} \tag{5.1}$$

and d is the "anomaly" vector given as follows,

$$d = \begin{bmatrix} 0 \\ d_\Psi \\ -d_\Phi \end{bmatrix}. \tag{5.2}$$

Note that the form of the above vector d is carried from (3.46) in Section 3.4.1. More details about these constant "offsets" in mass flow and pressure rise can be found in [37].

While the presence of disturbances in the compressor system is given in the ODE part (i.e., $\Phi(t)$ and $\Psi(t)$) of the Moore-Greitzer model, the effect of these disturbance terms can be reflected in the stabilities of both the ODE and PDE (for $g(t,\theta)$) parts of the system, causing surge and stall bifurcations (see Section 2.1.3). Note that the disturbances can be deterministic (e.g., external forcing functions) or stochastic (e.g., random noise effects). In this subsection, we will only focus on the deterministic case of the Moore-Greitzer model, and investigate the case where the external deterministic forcing triggers the stall instability. To simplify the stability analysis, we rescale the external deterministic forcing and rewrite the PDE as follows,

$$\frac{\partial}{\partial t}\begin{bmatrix} g \\ \Phi \\ \Psi \end{bmatrix} = \begin{bmatrix} K^{-1}(\frac{\nu}{2}\frac{\partial^2}{\partial\theta^2} - \frac{1}{2}\frac{\partial}{\partial\theta}) & 0 & 0 \\ 0 & 0 & 0 \\ 0 & 0 & 0 \end{bmatrix}\begin{bmatrix} g \\ \Phi \\ \Psi \end{bmatrix} + \begin{bmatrix} aK^{-1}(\psi_c(\Phi+g) - \overline{\psi}_c(\Phi,g)) \\ \frac{1}{l_c}(\overline{\psi}_c(\Phi,g) - \Psi) \\ \frac{1}{4l_cB^2}(\Phi - \gamma\sqrt{\Psi}) \end{bmatrix} + \begin{bmatrix} 0 \\ \frac{1}{l_c}d_\Psi \\ -\frac{1}{4B^2l_c}d_\Phi \end{bmatrix}.$$

In the change detection context, we may consider the above PDE as the post-change dynamic equations for the Moore-Greitzer compressor systems. The constants d_Φ and d_Ψ represent the size of the "change" or disturbances given on the flow rate and pressure of the compressor systems. The corresponding vector version or the abstract form (under the post-change regime) is

$$\frac{\partial x}{\partial t} = Ax + f(x) + d, \tag{5.3}$$

where $x = [g, \Phi, \Psi]^T$,

$$A = \begin{bmatrix} K^{-1}(\frac{\nu}{2}\frac{\partial^2}{\partial\theta^2} - \frac{1}{2}\frac{\partial}{\partial\theta}) & 0 & 0 \\ 0 & 0 & 0 \\ 0 & 0 & 0 \end{bmatrix}, \tag{5.4}$$

and

$$f(x) = \begin{bmatrix} aK^{-1}(\psi_c(\Phi + g) - \overline{\psi}_c(\Phi, g)) \\ \frac{1}{l_c}(\overline{\psi}_c(\Phi, g) - \Psi) \\ \frac{1}{4l_cB^2}(\Phi - \gamma\sqrt{\Psi}) \end{bmatrix}. \tag{5.5}$$

Although the change is only added on the $\Phi(t)$ and $\Psi(t)$ components, the strong coupling among $g(t, \theta)$, $\Phi(t)$ and $\Psi(t)$ implies that both the PDE part (i.e., $g(t, \theta)$) and the ODE part (i.e., (Φ, Ψ)) can go through a Hopf bifurcation and yield limit cycle behaviors, depending on different "sizes" of the anomaly d, around the new (post-change) equilibrium for (Φ, Ψ).

5.1.2 Stability Analysis with Disturbances d_Φ and d_Ψ

With the disturbances given in the model, calculating equilibrium values, denoted as $x_e^{(d)} = [g_e^{(d)}, \Phi_e^{(d)}, \Psi_e^{(d)}]^T$, yields a trivial solution $g_e^{(d)} = 0$ and leaves us with the following two equations for $\Phi_e^{(d)}$ and $\Psi_e^{(d)}$:

$$\Psi_e^{(d)} = \psi_c(\Phi_e^{(d)}) + d_\Psi,$$

$$\Phi_e^{(d)} = \gamma\sqrt{\Psi_e^{(d)}} + d_\Phi.$$

Notice that the notations here with superscripts (d) are given to distinguish the notations given in Section 2.1.2 (i.e., the stability analysis without these disturbances d_Φ and d_Ψ). $\Phi_e^{(d)}$ can be solved by finding the root of the following polynomial in $\Phi_e^{(d)}$:

$$-\frac{H}{2W^3}(\Phi_e^{(d)})^3 + \frac{3H}{2W^2}(\Phi_e^{(d)})^2 - \left(\frac{\Phi_e^{(d)} - d_\Phi}{\gamma}\right)^2 + \Psi_{c_0} + d_\Psi = 0 \tag{5.6}$$

and the solution is given as

$$\begin{aligned} \Phi_e^{(d)} = &\sqrt[3]{X_d - Y_d^3 + Z_d + \sqrt{(X_d - Y_d^3 + Z_d)^2 + [2Z_d/Y_d/3 - Y_d^2]^3}} \\ &+ \sqrt[3]{X_d - Y_d^3 + Z_d - \sqrt{(X_d - Y_d^3 + Z_d)^2 + (2Z_d/Y_d/3 - Y_d^2)^3}} - Y_d, \end{aligned} \tag{5.7}$$

where

$$X_d = \frac{W^3(\Psi_{c_0} - \frac{d_\Phi^2}{\gamma^2} + d_\Psi)}{H} = \frac{\gamma^2 W^3(\Psi_{c_0} + d_\Psi) - W^3 d_\Phi^2}{\gamma^2 H}, \tag{5.8}$$

$$Y_d = \frac{2W^3}{3H}\left(\frac{1}{\gamma^2} - \frac{3H}{2W^2}\right), \tag{5.9}$$

$$Z_d = \frac{4W^6}{3H^2}\left(-\frac{1}{\gamma^2} + \frac{3H}{2W^2}\right)\frac{d_\Phi}{\gamma^2}. \tag{5.10}$$

Note that W, H, Ψ_{c_0} and γ are known parameters for which the PDE system is running in a normal regime without any instabilities. However, it follows from the above equations that the equilibrium of the Moore-Greitzer model is shifted once the disturbances d_Φ and d_Ψ enter the system. To study how d_Φ and d_Ψ affect the stabilities of the Moore-Greitzer PDE system, we examine the localized disturbed model introduced below.

We first write the state x in terms of small perturbations $y = [\delta g, \delta\Phi, \delta\Psi]^T$ about the equilibrium point $x_e^{(d)}$

$$x = x_e^{(d)} + y.$$

Similarly, we find the evolution of the perturbations around equilibrium by substituting the above relation into the original dynamic equation and expanding it using Taylor's series about the equilibrium $x_e^{(d)}$. Then, the nonlinear equations of the perturbations near equilibrium are

$$\frac{\partial}{\partial t}\begin{bmatrix}\delta g\\ \delta\Phi\\ \delta\Psi\end{bmatrix} = \mathcal{A}_d\begin{bmatrix}\delta g\\ \delta\Phi\\ \delta\Psi\end{bmatrix} + \mathcal{B}_d\begin{bmatrix}\delta g^2 + \delta g\delta\Phi\\ \delta\Phi^2\\ \delta\Psi^2\end{bmatrix} + \mathcal{C}_d\begin{bmatrix}-\delta g^3 + 3\delta g^2\delta\Phi + 3\delta g\delta\Phi^2\\ \delta\Phi^3\\ \delta\Psi^3\end{bmatrix}, \tag{5.11}$$

where

$$\mathcal{A}_d = \begin{bmatrix} K^{-1}(\frac{\nu}{2}\frac{\partial^2}{\partial\theta^2} - \frac{1}{2}\frac{\partial}{\partial\theta} + a\psi_c'(\Phi_e^{(d)})) & 0 & 0\\ 0 & \frac{1}{l_c}\psi_c'(\Phi_e^{(d)}) & -\frac{1}{l_c}\\ 0 & \frac{1}{4B^2 l_c} & -\frac{1}{4B^2 l_c}\frac{\gamma}{2\sqrt{\Psi_e^{(d)}}}\end{bmatrix}$$

$$\mathcal{B}_d = \frac{1}{2}\begin{bmatrix} K^{-1}a\psi_c''(\Phi_e^{(d)}) & 0 & 0\\ 0 & \frac{1}{l_c}\psi_c''(\Phi_e^{(d)}) & 0\\ 0 & 0 & \frac{1}{16B^2 l_c}\frac{\gamma}{\sqrt{\Psi_e^{(d)^3}}}\end{bmatrix}$$

and

$$\mathcal{C}_d = \frac{1}{6}\begin{bmatrix} K^{-1}a\psi_c'''(\Phi_e^{(d)}) & 0 & 0\\ 0 & \frac{1}{l_c}\psi_c'''(\Phi_e^{(d)}) & 0\\ 0 & 0 & -\frac{3}{32B^2 l_c}\frac{\gamma}{\sqrt{\Psi_e^{(d)^5}}}\end{bmatrix}.$$

To analyze the stability of the system, we examine the eigenvalues of $\mathcal{A}_d$. There are infinite eigenvalues $\lambda_n^{(d)}$ to be found from the first diagonal entry of $\mathcal{A}_d$ and the remaining two eigenvalues $\mu_{1,2}^{(d)}$ are to be found from the 2-by-2 bottom right submatrix. Taking $v = [e^{in\theta}, 0, 0]^T$, the eigenvalue equation $\mathcal{A}_d v = \lambda_n^{(d)} v$ is satisfied for

$$\lambda_n = \left(1 + \frac{ma}{|n|}\right)^{-1} \left(a\psi_c'(\Phi_e^{(d)}) - \frac{\nu}{2}n^2 - \frac{1}{2}(in)\right), \tag{5.12}$$

where

$$\psi_c'(\Phi_e^{(d)}) = \frac{3H}{2W^2}\left(2\Phi_e^{(d)} - \frac{(\Phi_e^{(d)})^2}{W}\right).$$

The remaining eigenvalues $\mu_{1,2}^{(d)}$ are found by solving the characteristic equation corresponding to the bottom right submatrix of $\mathcal{A}_d$:

$$(\mu^{(d)})^2 + \left(\frac{1}{l_c}\frac{\gamma}{8B^2\sqrt{\Psi_e^{(d)}}} - \frac{1}{l_c}\psi_c'(\Phi_e^{(d)})\right)\mu^{(d)} - \frac{1}{4B^2 l_c^2}\left(\frac{\gamma\psi_c'(\Phi_e^{(d)})}{2\sqrt{\Psi_e^{(d)}}} - 1\right) = 0, \tag{5.13}$$

and

$$\mu_{1,2}^{(d)} = \frac{1}{2l_c}\left[\left(\psi_c'(\Phi_e^{(d)}) - \frac{\gamma}{8B^2\sqrt{\Psi_e^{(d)}}}\right) \pm \sqrt{\left(\psi_c'(\Phi_e^{(d)}) + \frac{\gamma}{8B^2\sqrt{\Psi_e^{(d)}}}\right) - \frac{1}{B^2}}\right]. \tag{5.14}$$

The eigenvectors corresponding to the above eigenvalues are

$$v_{1,2}^{(d)} = \begin{bmatrix} 0 \\ 1 \\ \frac{1}{2}\left[\left(\psi_c'(\Phi_e^{(d)}) + \frac{\gamma}{8B^2\sqrt{\Psi_e^{(d)}}}\right) \mp \sqrt{\left(\psi_c'(\Phi_e^{(d)}) + \frac{\gamma}{8B^2\sqrt{\Psi_e^{(d)}}}\right)^2 - \frac{1}{B^2}}\right] \end{bmatrix} \tag{5.15}$$

Consequently, it becomes evident that disturbances in mass flow and pressure induce shifts in the equilibrium of the entire PDE system, which, in turn, influence the eigenvalues of both the ODE and PDE components. This interaction results in corresponding alterations to the stability of the system. Figure 5.1 and Figure 5.2 illustrate two examples in which the disturbances (changes) excite the stall instability of the Moore-Greitzer PDE system. In both examples, the following parameters are used for simulations.

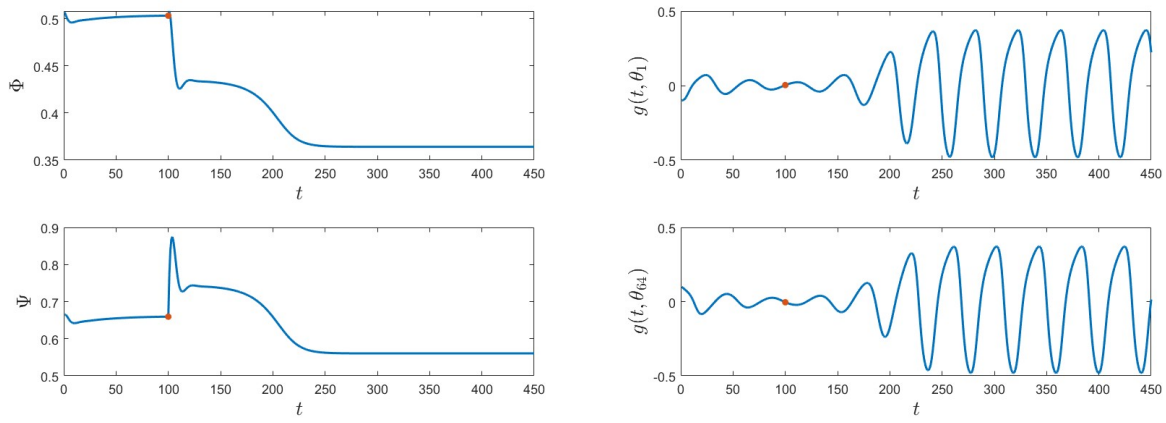


Figure 5.1: The evolution of the deterministic ODE, i.e., (Φ, Ψ) **(left)**, and the evolution of the deterministic PDE over time t with the change happening at $k = 100$ at two fixed values of θ **(right)**.

$$l_c = 8,\ H = 0.18,\ W = 0.25,\ m = 8.75,\ \nu = 0.1,$$

$$a = 1/3.5,\ \psi_{c_0} = 1.67H,\ B = 0.15,\ \gamma = 0.62,$$

$$d_\Phi = -0.1,\ d_\Psi = 0.1.$$

The initial conditions of the system are given as follows,

$$\Phi(0) = 0.51, \quad \Psi(0) = 0.66, \quad g(0, \theta) = 0.1\cos(\theta).$$

The difference between these two examples is that the anomaly vector d, which depends on d_Φ and d_Ψ, is implanted at distinct time steps (marked as red circles in the plots of Figure 5.1 and Figure 5.2). Let k denote the real change time. Specifically, the "change-point" is at time $k = 100$ for Figure 5.1, and the other one is at $k = 200$ for Figure 5.2. From both figures, we notice that the system is stable (for both ODE and PDE components) prior to disturbances entering the system, and $\Phi(t)$, $\Psi(t)$, $g(t, \theta)$ are leading towards their steady states (i.e., $\Phi_e^{(d)}$, $\Psi_e^{(d)}$ and $g_e^{(d)} = 0$). However, once the change enters the ODE system (i.e., $\Phi(t)$ and $\Psi(t)$), right after very short-time transients, the equilibrium of $(\Phi_e^{(d)}, \Psi_e^{(d)})$ has been almost immediately shifted, whereas the PDE component $g(t, \theta)$ is still hovering around the pre-change equilibrium $g_e = 0$. This is due to the fact that the pre-change states of $g(t, \theta)$ are approximately zeros, making it challenging to "displace" them from the stable

region and induce limit cycle behaviors. Furthermore, the initiation of stall instability is delayed when disturbances are introduced at a later stage in the system operation. This is because the PDE system is getting closer to $g_e = 0$ as it evolves under "normal" or pre-change operational conditions, and a relevant comparison can be observed from Figure 5.1 and Figure 5.2. More interestingly, upon the occurrence of the stall bifurcation, the

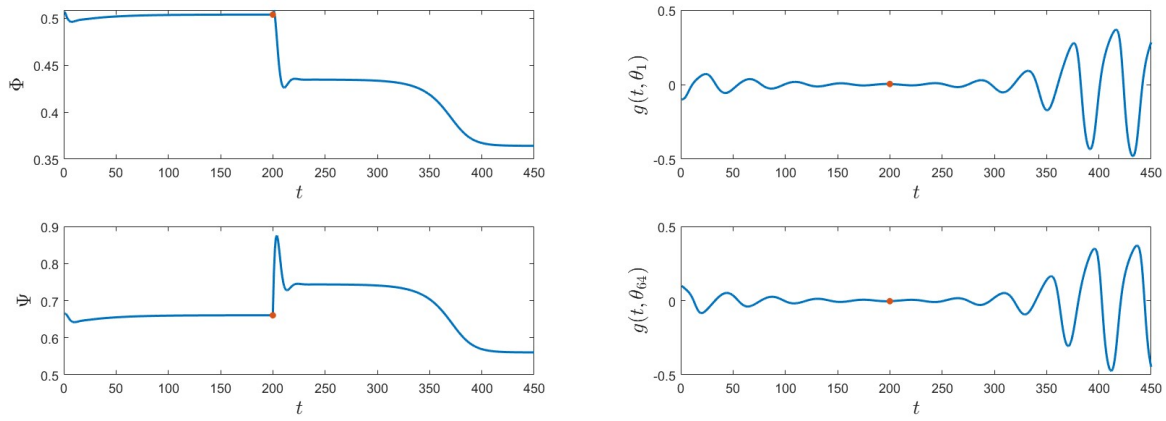


Figure 5.2: The evolution of the deterministic ODE, i.e., (Φ, Ψ) **(left)**, and the evolution of the deterministic PDE over time t with the change happens at $k = 200$ at two fixed values of θ **(right)**.

oscillation of the PDE component as noted in $g(t, \theta)$ leads to a subsequent alteration in the equilibrium of the ODE, as referenced in $(\Phi_e^{(d)}, \Psi_e^{(d)})$. This alteration is attributed to the significant impact on the mean-field characteristic function $\overline{\psi}_c(\Phi, g)$, which undergoes substantial change as $g(t, \theta)$ transitions from a fixed point to limit cycles, consequently modifying the nonlinear dynamics of the ODE component.

5.2 Generalized CUSUM Statistics for Stall Detection in Deterministic Moore–Greitzer PDE System using a POD-Galerkin Procedure

In the previous section, we see how stall instability is induced when disturbances (d_Φ, d_Ψ) are incorporated into the Moore-Greitzer model. A natural question arises about how

to detect and mitigate these changes early so that the engine stays within its optimal parameters. Due to the nonlinear dynamics and high-dimensional nature of the Moore-Greitzer PDE system, the model presents a challenging environment for change detection. Similar to the pure surge cases discussed in Chapter 3, the change detection model remains HMM-based, where the signals are governed by a comprehensive PDE system, and the observations are linearly dependent on the PDE solution $g(t)$ at a specific point of θ, corrupted by a random process (i.e., sensor noise). The complication arises from the fact that the changes presented in the hidden Moore-Greitzer PDE signals cannot be visually identified from the observations. However, given that the CUSUM-based detection rules have demonstrated effectiveness in detecting small shifts across various applications, it stands to reason that implementing them could be beneficial for monitoring compressor systems for early signs of stall instability. In this section, we address these challenges with the aid of the POD dimension reduction technique (introduced in Chapter 4) and the generalized CUSUM statistics using a particle filtering approach (presented in Chapter 3).

5.2.1 Stall Detection: Problem Setup

Suppose $x(t,\theta) = [g(t,\theta), \Phi(t), \Psi(t)]^T$, for all $t \in [0,\infty)$ and $\theta \in (0, 2\pi)$, the Moore-Greitzer signal $x(t,\theta)$ is governed by the following PDE,

$$\frac{\partial x(t,\theta)}{\partial t} = Ax(t,\theta) + f(x(t,\theta)) + d\mathbb{I}_{\{t\geq k\}}, \tag{5.16}$$

where A, $f(x)$ and d is defined in (5.4), (5.5) and (5.2), respectively. The semi-group property of the PDE solution $x(t,\theta)$ allows for decomposing $x(t,\theta)$ into its Fourier modes (i.e., spatial domain) using the Fourier spectral method. This also ensures that the time evolution of the solution can be efficiently computed. Let us now take observations at discrete times, $\gamma, 2\gamma, \cdots$, where γ denotes the unit time interval. As such, the observation at time n and at some point of θ is of the form

$$Y_n = h(x(n\gamma,\theta)) + V_n, \tag{5.17}$$

where V_n is i.i.d. with known density. Most commonly, $V_n \sim \mathcal{N}(0,\tau^2)$, for $n = 1, \cdots, N$. We can distinguish continuous-time and discrete-time versions of x using $x(t,\theta)$ for continuous-time and $x_n = x(n\gamma,\theta)$ for the signal value at the n^{th} unit of time at θ. The evolution of the state process from time n to time $n+1$ determines the transition probability density $p(\mathbf{x}_{n+1}|\mathbf{x}_n)$ for the Markov chain $\{\mathbf{x}_n : n \geq 0\}$. The system

$$\begin{aligned} &\mathbb{P}(\mathbf{x}_{n+1} \in \mathbf{A}|\mathbf{x}_n) = \int_{\mathbf{A}} p(z|\mathbf{x}_n)dz, \\ &Y_n = h(\mathbf{x}_n) + V_n, \end{aligned} \tag{5.18}$$

is now a discrete-time system, analogous to (5.16) and (5.17), where

$$\mathbf{x}_n = \begin{bmatrix} x_{n,1} \\ \vdots \\ x_{n,N'} \\ \Phi_n \\ \Psi_n \end{bmatrix}, \tag{5.19}$$

and $\mathbf{A}$ represents a subset of the state space for the PDE signal. Note that Φ_n and Ψ_n are the discrete-time versions of $\Phi(n\gamma)$ and $\Psi(n\gamma)$, respectively; $x_{n,1}, \cdots, x_{n,N'}$ is the discretized solution of $g(n\gamma, \theta)$ using the fast Fourier transform where N' represents total number of Fourier modes.

5.2.2 Construction of the Stall Detection Statistics using POD Bases and Particle Filters

Although we have shown the effectiveness of T_n in a two-dimensional system (i.e., pure surge case) in Chapter 3, the scalability of our method in high dimensions is not clear. It has been shown that the particle methods are still applicable in high-dimensional systems [3]. However, the effectiveness of the generalized CUSUM statistics T_n and $\widehat{T}_n$ and their comparisons in higher-dimensional systems (with and without stochastic inputs) are still open problems. As such, we would like to examine the performance of the generalized CUSUM statistics T_n and $\widehat{T}_n$ in the stall detection of the Moore-Greitzer PDE system. Notice that the filtering procedures closely resemble those examined in Chapter 3, with the primary distinction being the significantly increased dimensionality of the signal system, i.e., $\mathbf{x}_n$. Recall that the calculations of the log-likelihood ratio in T_n and $\widehat{T}_n$ involve the following conditional density function:

$$p(Y_n|Y_1^{n-1}) = \int\int p(Y_n|\mathbf{x}_n)p(\mathbf{x}_n|\mathbf{x}_{n-1})p(\mathbf{x}_{n-1}|Y_1^{n-1})d\mathbf{x}_{n-1}d\mathbf{x}_n, \tag{5.20}$$

where $\mathbf{x}_n$ and Y_n are defined as before. The explicit form of the likelihood function $p(Y_n|\mathbf{x}_n)$ in relation to $Y_n - h(\mathbf{x}_n)$ can be determined due to the known density of observational noise V_n. In the case of nonlinear dynamics, the estimation of the state-space models can be numerically solved by evaluating the dynamic rule, $p(\mathbf{x}_n|\mathbf{x}_{n-1})$, with particle filters. However, the high-dimensional nature of $\mathbf{x}_n$ makes the computations of $p(\mathbf{x}_n|\mathbf{x}_{n-1})$ very expensive. Fortunately, the POD reconstruction of the Moore-Greitzer PDE system, introduced and

validated in Chapter 4, provides us with a reasonable method of approximating $p(\mathbf{x}_n|\mathbf{x}_{n-1})$ by $p(\mathbf{x}'_n|\mathbf{x}'_{n-1})$, where

$$\mathbf{x}'_n = \begin{bmatrix} x'_{n,1} \\ \vdots \\ x'_{n,M'} \\ \Phi_n \\ \Psi_n \end{bmatrix}, \tag{5.21}$$

where M' represents the total number of POD modes. For any $m' = 1, \cdots, M'$,

$$x'_{n,m'} := x'_{m'}(t_n, \theta) = \sum_{\alpha=1}^{M'} b_\alpha(t_n) U_\alpha^{m'}(\theta), \tag{5.22}$$

where $b(t_n)$ and $U_\alpha^{m'}(\theta)$ denote the discrete-time POD coefficients and the α^{th} discrete-spatial POD modes. Practically, we know $M' \ll N'$. Notice that for the Moore-Greitzer model, the reduced-order dynamic equation of $b_\alpha(t)$ was derived in Chapter 4, see (4.31) and (4.32). Consequently, instead of (5.20), we calculate the conditional density of $p(Y_n|Y_1^{n-1})$ using the following approximation,

$$p(Y_n|Y_1^{n-1}) \approx \int\int p(Y_n|\mathbf{x}'_n) p(\mathbf{x}'_n|\mathbf{x}'_{n-1}) p(\mathbf{x}'_{n-1}|Y_1^{n-1}) d\mathbf{x}'_{n-1} d\mathbf{x}'_n, \tag{5.23}$$

where the transition probability density $p(\mathbf{x}'_n|\mathbf{x}'_{n-1})$ can be more efficiently evaluated using the particles that are evolving with the reduced-order dynamic equation derived by POD-Galerkin procedure. As such, the rest of the calculations of T_n proceed as follows.

Suppose that at time $n-1$ we approximate the conditional density $p(\mathbf{x}'_{n-1}|Y_1^{n-1})$ by a collection of M particles with masses $q_{n-1}^{(i)}$ and positions $\mathbf{x}_{n-1}^{\prime(i)}$ with total mass $\sum_{i=1}^{M} q_{n-1}^{(i)} = 1$. For each particle, we project $\mathbf{x}_{n-1}^{\prime(i)}$ onto the POD modes and obtain the positions of $b_\alpha^{(i)}(t_{n-1})$, for all $\alpha = 1, \cdots, M'$. Then, on the interval $(n-1)\gamma \le t \le n\gamma$, the particles at time $n-1$ are propagated forward independently using the dynamic rule:

$$\begin{bmatrix} \dot{b}_\alpha(t) \\ \dot{\Phi}(t) \\ \dot{\Psi}(t) \end{bmatrix} = \begin{bmatrix} \langle G_0(b(t), U(\theta), \Phi(t)), U_\alpha \rangle_{\mathcal{H}} \\ G_1(b(t), \Phi(t), \Psi(t)) \\ G_2(b(t), \Phi(t), \Psi(t)) \end{bmatrix}, \tag{5.24}$$

where the explicit formula of the above equation is given in (4.31) and (4.32), giving new positions $b_\alpha^{(i)}(t_n)$, for $\alpha = 1, \cdots, M'$ and $i = 1, \cdots, M$. Calculating the linear combinations of $b_\alpha^{(i)}(t_n)$ with the POD modes $U_\alpha^{m'}(\theta)$ yields the new positions $\mathbf{x}_n^{\prime(i)}$ for $i = 1, 2, \cdots, M$.

During the state transition process, the effectiveness of the above calculations significantly depends on the POD modes, i.e., $U_\alpha(\theta)$, $\alpha = 1, \cdots, M'$. Intuitively, we can follow the computational scheme introduced in Section 4.1.5, and more specifically (4.22), to evaluate the relevant POD modes. Even if this requires the availability of the signal data, the prior information of the values of the disturbances, i.e., d_Φ and d_Ψ, makes the POD modes relevant in terms of reconstructing this deterministic Moore-Greitzer model. Consequently, the transformation of the transition probability density, i.e.,

$$p(\mathbf{x}_n|\mathbf{x}_{n-1}) \to p(\mathbf{x}'_n|\mathbf{x}'_{n-1})$$

can be performed accurately in the reduced-order dynamic rule in the stall detection context. After the state transition process, the prediction $p(\mathbf{x}'_n|Y_1^{n-1})$ at time n can be approximated by the updated particles with the associated weights, i.e.,

$$p(\mathbf{x}'_n|Y_1^{n-1}) \approx \sum_{i=1}^{M} q_{n-1}^{(i)} \delta(\mathbf{x}'_n - \mathbf{x}_n'^{(i)}), \tag{5.25}$$

where $\delta(\cdot)$ is the Dirac delta function. Substituting the above approximation into (5.23) yields $p(Y_n|Y_1^{n-1})$ as

$$\begin{aligned} &\int p(Y_n|\mathbf{x}'_n) \sum_{i=1}^{M} q_{n-1}^{(i)} \delta(\mathbf{x}'_n - \mathbf{x}_n'^{(i)}) d\mathbf{x}'_n \\ =&\sum_{i=1}^{M} \int p(Y_n|\mathbf{x}'_n) q_{n-1}^{(i)} \delta(\mathbf{x}'_n - \mathbf{x}_n'^{(i)}) d\mathbf{x}'_n \\ =&\sum_{i=1}^{M} q_{n-1}^{(i)} p(Y_n|\mathbf{x}_n'^{(i)}). \end{aligned} \tag{5.26}$$

Given the density of the observational noise V_n, the likelihood function $p(Y_n|\mathbf{x}_n^{(i)})$ can be calculated explicitly. As such, the log-likelihood ratio becomes

$$\begin{aligned} Z_n^{(k)} &= \log \left(\frac{f_{1,n}^{(k)}(Y_n|Y_1^{n-1})}{f_{0,n}(Y_n|Y_1^{n-1})} \right) \\ &\approx \log \left(\frac{\sum_{i=1}^{M} q_{1,n-1}^{k,i} p_{\theta_1}\left(Y_n|\mathbf{x}_n'^{k,i}\right)}{\sum_{i=1}^{M} q_{0,n-1}^{(i)} p_{\theta_0}\left(Y_n|\mathbf{x}_n'^{(i)}\right)} \right). \end{aligned} \tag{5.27}$$

Notice that the change point k is unknown, and $Z_n^{(k)}$ is an $n \times n$ lower triangular matrix because $f_{1,n}^{(k)}(Y_n|Y_1^{n-1}) = f_{0,n}(Y_n|Y_1^{n-1})$ for all $n < k$. For any $n \geq k$, $\mathbf{x}_n'^{k,i}$ represents the

position of the particle i at time n conditioned on the change that occurs at time k. This particle is indeed evolving the reduced-order dynamic equation obtained from the POD-Galerkin procedure.The generalized CUSUM statistic we consider in this thesis is given by

$$\begin{aligned} T_n &= \max_{1\leq k\leq n}(Z_k^{(k)}+\cdots+Z_n^{(k)}) \\ &= \max_{1\leq k\leq n}\sum_{i=k}^{n}\log\frac{f_{1,i}^{(k)}(Y_i|Y_1^{i-1})}{f_{0,i}(Y_i|Y_1^{i-1})}, \end{aligned} \tag{5.28}$$

where $f_0(\cdot|\cdot)$ and $f_1^{(k)}(\cdot|\cdot)$ represent the conditional probability density function of the pre-change distribution and post-change distribution, respectively. The associated probability measure defined on the sequence of observations corresponding to change at time k and no change is $\mathbb{P}_k$ and $\mathbb{P}_0$. Notice that T_n is theoretically given by (5.28), but for computations we need to replace the first expression in (5.27) with the second expression in (5.27). To lessen computations, Fuh [33] proposes the statistic $\widehat{T}_n$ given below,

$$\widehat{T}_n = \max_{1\leq k\leq n}(Z_k^{(1)}+\cdots+Z_n^{(1)}), \tag{5.29}$$

where for any $n\geq 1$, the LLR $Z_n^{(1)}$ is expressed and approximated as follows,

$$\begin{aligned} Z_n^{(1)} &= \log\left(\frac{f_{1,n}^{(1)}(Y_n|Y_1^{n-1})}{f_{0,n}(Y_n|Y_1^{n-1})}\right) \\ &\approx \log\left(\frac{\sum_{i=1}^{M}q_{1,n-1}^{1,i}p_{\theta_1}\left(Y_n|\mathbf{x}_n'^{1,i}\right)}{\sum_{i=1}^{M}q_{0,n-1}^{(i)}p_{\theta_0}\left(Y_n|\mathbf{x}_n'^{(i)}\right)}\right), \end{aligned} \tag{5.30}$$

where $\mathbf{x}_n'^{1,i}$ denotes the position of the particle i at time n conditioned on the change happening immediately. The dynamic rule of processing the transition probability $p_{\theta_1}(\mathbf{x}_n'^{1,i}|\mathbf{x}_{n-1}'^{1,i})$ is the same POD reduced-order equations used in $p_{\theta_1}(\mathbf{x}_n'^{k,i}|\mathbf{x}_{n-1}'^{k,i})$. Hence, the QCD scheme using $\widehat{T}_n$ can be defined with respect to the following stopping time,

$$\tau_c = \inf\{n\geq 1:\widehat{T}_n\geq c\}, \tag{5.31}$$

for some threshold $c>0$. Even if the above stopping rule is computationally more efficient than the algorithm involving T_n, the results in Chapter 3 indicate that $\widehat{T}_n$ could suffer from the that the post-change regime, after the stall bifurcation occurs, produces the limit cycle behavior for $g(t,\theta)$. As such, it is important to investigate the performance of T_n and $\widehat{T}_n$ in the stall detection context in the deterministic Moore-Greitzer model.

5.3 Reduced Order Modeling of Stochastic Moore-Greitzer PDE Systems using Extended POD-Galerkin Procedure

The Moore-Greitzer PDE model is a well-established framework for analyzing instabilities in axial-flow compressors, particularly rotating stall and surge phenomena in jet engines. However, real-world compressors operate in highly uncertain environments, where factors such as turbulent fluctuations and manufacturing imperfections introduce significant variability. The stochastic extension of this model addresses these uncertainties, making it more realistic and applicable to practical problems. The other motivation for studying the stochastic Moore-Greitzer PDE model is rooted in the need for predictive modeling of compressor instabilities. To rigorously model the stochastic input for the Moore-Greitzer PDE system, we shall introduce the following definitions.

Definition 5.3.1 (Q-Wiener Processes [72])**.** *Given a probability space $(\Omega, \mathcal{F}, \mathbb{P})$, let H be a separable Hilbert space with a complete orthonormal system $\{e_k\}$, and let Q be a trace class nonnegative operator on H. An H-valued stochastic process $\{W_t\}_{t\geq 0}$ is called a Q-Wiener process if*

(i) $W(0) = 0$,

(ii) W *has continuous trajectories,*

(iii) W *has independent increments,*

(iv) $\mathcal{L}(W_t - W_s) = \mathcal{N}(0, (t-s)Q), \quad t \geq s \geq 0$, *where* $\mathcal{L}(W(t))$ *is a Gaussian measure with mean vector 0.*

Definition 5.3.2 (Generalized Q-Wiener Processes [72])**.** *Let H be the same space as in Definition 5.3.1, let W be a Wiener process with covariance operator Q. Let H_1 be a Hilbert space such that $Q^{1/2}H$ is embedded into H_1 with a Hilbert-Schmidt embedding and Q is a trace class operator when extended to H_1. Then W is an H_1-valued Q-Wiener process, we also call W a generalized Q-Wiener process based on H. In particular, when $Q = I$, W is an H_1-valued cylindrical Wiener process (or a generalized cylindrical Wiener process based on H).*

5.3.1 Stochastic Moore-Greitzer PDE Systems

The stochastic Moore-Greitzer PDE model enhances the traditional Moore-Greitzer framework by incorporating random perturbations, thereby providing a more realistic representation of compressor dynamics under operational uncertainties. The authors in [16] derive a modified version of the viscous Moore-Greitzer equation directly from the Navier-Stokes equations using stochastic homogenization techniques. According to Meng et al. [59], the stochastic version of the Moore-Greitzer model with an additive noise can be constructed by adding a $\mathcal{H}$-valued Q-Wiener process such that we can rewrite the PDE,

$$\frac{1}{a}K\frac{\partial g}{\partial t}(t,\theta) = \psi_c(\Phi(t)+g(t,\theta)) - \bar{\psi}_c(t) - \frac{1}{2a}g_\theta(t,\theta) + \frac{\nu}{2a}g_{\theta\theta}(t,\theta) + \sigma\dot{W}_{\mathcal{H}}(t), \tag{5.32}$$

where $\mathcal{H}$ is a separable infinite-dimensional Hilbert space, $\mathcal{H} := \breve{L}^2(0,2\pi) = \left\{g \in L^2 : \int_0^{2\pi} g(\theta)d\theta = 0\right\}$, and σ represents the intensity of the additive disturbance. From a physical point of view, (5.32) models the presence of turbulent airflow entering the axial velocity at the compressor entrance. More specifically, $W_{\mathcal{H}}(t)$ is defined as follows,

$$W_{\mathcal{H}}(t) = \sum_{\tilde{k}\in\mathbb{Z}^+}\sqrt{q_{\tilde{k}}}(\mathbb{B}_{\tilde{k}}(t) + i\mathbb{B}_{-\tilde{k}}(t))e^{i\tilde{k}\theta} + \sum_{\tilde{k}\in\mathbb{Z}^-}\sqrt{q_k}(\mathbb{B}_{-\tilde{k}}(t) - i\mathbb{B}_{\tilde{k}}(t))e^{i\tilde{k}\theta}, \tag{5.33}$$

where $q_{\tilde{k}} = |\tilde{k}|^{-(4\alpha_1+1)-\nu_1}$ for any fixed $\nu_1 > 0$, $\mathbb{B}_{\tilde{k}}(t)$ are i.i.d. Brownian motions, and i represents the imaginary unit of complex numbers. As noted in [59], when $\alpha_1 \geq 0$, $q_{\tilde{k}}$ decays as $\tilde{k}$ increases, then Q is a trace class operator, and $W_{\mathcal{H}}(t)$ is a $\mathcal{H}$-valued Q-Wiener process that is white in time and colored in space. Notice that K defined in (2.12) is a positive definite, self-adjoint linear operator on $\mathcal{H}$. Since the operator K is invertible, from (5.32), the governing equation for $g(t,\theta)$ is given by

$$\frac{\partial g}{\partial t}(t,\theta) = K^{-1}\left(\frac{\nu}{2}\frac{\partial^2 g}{\partial\theta^2}(t,\theta) - \frac{1}{2}\frac{\partial g}{\partial\theta}(t,\theta)\right) + aK^{-1}\big(\psi_c(\Phi(t)+g(t,\theta)) - \bar{\psi}_c(t)\big) + aK^{-1}\sigma\dot{W}_{\mathcal{H}}(t). \tag{5.34}$$

As such, a full stochastic Moore-Greitzer model with additive noise is given as

$$\begin{aligned}\frac{\partial}{\partial t}\begin{bmatrix} g(t,\theta) \\ \Phi(t) \\ \Psi(t)\end{bmatrix} &= \begin{bmatrix} K^{-1}\left(\frac{\nu}{2}\frac{\partial^2}{\partial\theta^2} - \frac{1}{2}\frac{\partial}{\partial\theta}\right) & 0 & 0 \\ 0 & 0 & 0 \\ 0 & 0 & 0\end{bmatrix}\begin{bmatrix} g(t,\theta) \\ \Phi(t) \\ \Psi(t)\end{bmatrix} \\ &\quad + \begin{bmatrix} aK^{-1}\Big(\psi_c(\Phi(t)+g(t,\theta)) - \bar{\psi}_c(t)\Big) \\ \frac{1}{l_c}(\bar{\psi}_c(\Phi(t),g(t,\theta)) - \Psi(t)) \\ \frac{1}{4B^2 l_c}(\Phi(t) - \gamma\sqrt{\Psi(t)})\end{bmatrix} + \begin{bmatrix} aK^{-1}\sigma\dot{W}_{\mathcal{H}}(t) \\ 0 \\ 0\end{bmatrix}\end{aligned} \tag{5.35}$$

where $W_{\mathcal{H}}(t)$ is given in (5.33).

Recall the expression of the mean-zero, periodic inlet velocity

$$g(t,\theta) = \sum_{\tilde{k}\in\mathbb{Z}\setminus\{0\}} \widetilde{g}_{\tilde{k}}(t) e^{i\tilde{k}\theta}. \tag{5.36}$$

The Fourier-Galerkin procedure, that is, projecting (5.35) onto the β-th Fourier basis $e^{i\beta\theta}$ gives

$$\begin{aligned}
\dot{\widetilde{g}}_\beta(t) = {} & \left(\frac{|\beta|}{|\beta|+ma}\right)\Big(-\frac{\nu}{2}\beta^2 - i\beta\frac{1}{2}\Big)\widetilde{g}_\beta(t) + \left(\frac{|\beta|}{|\beta|+ma}\right)\frac{3Ha}{W}\Big(\frac{\Phi(t)}{W} - \frac{1}{2}\frac{\Phi^2(t)}{W^2}\Big)\widetilde{g}_\beta(t) \\
& + \left(\frac{|\beta|}{|\beta|+ma}\right)\frac{3Ha}{2W^2}\Big(1-\frac{\Phi(t)}{W}\Big)\sum_{\substack{j\in\mathbb{Z}\setminus\{0\}\\(\beta\neq j)}} \widetilde{g}_j(t)\,\widetilde{g}_{\beta-j}(t) \\
& - \frac{Ha}{2W^3}\left(\frac{|\beta|}{|\beta|+ma}\right)\sum_{\substack{j,\tilde{k}\in\mathbb{Z}\setminus\{0\}\\(\beta\neq j+k)}} \widetilde{g}_j(t)\,\widetilde{g}_{\tilde{k}}(t)\,\widetilde{g}_{\beta-j-\tilde{k}}(t) \\
& + \begin{cases} aK^{-1}\sigma\sqrt{q_\beta}(\dot{\mathbb{B}}_\beta(t) + i\dot{\mathbb{B}}_{-\beta}(t)), & \text{for} \quad \beta>0 \\ aK^{-1}\sigma\sqrt{q_\beta}(\dot{\mathbb{B}}_{-\beta}(t) - i\dot{\mathbb{B}}_{\beta}(t)), & \text{for} \quad \beta<0, \end{cases}
\end{aligned} \tag{5.37}$$

which are coupled to the ODEs given by

$$\begin{aligned}
\dot{\Phi}(t) &= \frac{1}{l_c}\Big(\psi_c\big(\Phi(t)\big) + \frac{3H}{2W^2}\left(1-\frac{\Phi(t)}{W}\right)\sum_{\substack{j,\tilde{k}\in\mathbb{Z}\setminus\{0\}\\(j+\tilde{k}=0)}} \widetilde{g}_j(t)\,\widetilde{g}_{\tilde{k}}(t) - \frac{H}{2W^3}\sum_{\substack{j,\tilde{k},l\in\mathbb{Z}\setminus\{0\}\\(j+\tilde{k}+l=0)}} \widetilde{g}_j(t)\,\widetilde{g}_{\tilde{k}}(t)\,\widetilde{g}_l(t) - \Psi(t)\Big) \\
\dot{\Psi}(t) &= \frac{1}{4B^2 l_c}\Big(\Phi(t) - \gamma\sqrt{\Psi(t)}\Big).
\end{aligned} \tag{5.38}$$

The details of deriving the above (5.37) and (5.38) are given in Appendix C. While stochastic forcing can introduce instabilities, Fourier spectral techniques with Galerkin truncations can be used to control high-frequency errors and stabilize the solution. The definition of $W_{\mathcal{H}}(t)$ given in (5.33) indicates the amplitudes of the turbulent airflow die down for high frequencies. Therefore, the Fourier spectral method remains effective for the stochastic Moore-Greitzer model as it provides spectral accuracy, characterizes nonlinear interactions well, and can be adapted to stochastic perturbations without significant loss of accuracy.

5.3.2 Extended POD Galerkin Projection on the Stochastic Moore-Greitzer Model

Essentially, (5.37) and (5.38) suggest using a finite-dimensional stochastic differential equation (SDE) to approximate the infinite-dimensional stochastic partial differential equation (SPDE), i.e., (5.35). However, this system of SDEs remains high-dimensional, which could limit the estimation and prediction in the Moore-Greitzer state-space model, e.g., the nonlinear filtering implementation in the SDE (5.37) coupled with (5.38). This motivates us to study the POD technique to extract dominant flow structures from the Moore-Greitzer PDE system with a small stochastic input, i.e., σ is small in (5.32). Notice that a low-intensity noise given in the PDE of $g(t,\theta)$ is necessary since we would like to make sure the stability of $g(t,\theta)$ is still under control in the pre-change regime (i.e., without mass flow and pressure disturbances). Under the post-change regime, the stall bifurcation appears, and the natural question is whether or not the POD technique preserves the essential dynamics of $g(t,\theta)$ while reducing the dimension of the stochastic Moore-Greitzer system.

In Chapter 3, we have shown how to apply the POD Galerkin procedure to the deterministic Moore-Greitzer PDE system and have derived the reduced-order dynamic equation without considering the stochastic input. So the remaining task is to find the POD Galerkin projection on the noise term (i.e., $aK^{-1}\sigma\dot{W}_{\mathcal{H}}(t)$). Instead of (5.36), we now write the PDE solution of $g(t,\theta)$ as follows

$$g(t,\theta) \approx \sum_{\alpha=1}^{M'} b_\alpha(t) U_\alpha(\theta),$$

where M' represents the total number of POD modes, usually chosen based on an energy-distributed approach that ensures the selected POD modes retain the most dynamically significant structures while minimizing computational cost. Taking the inner product of $aK^{-1}\sigma\dot{W}_{\mathcal{H}}(t)$ with the β-th POD basis $U_\beta(\theta)$ yields

$$\begin{aligned}
&\Big\langle aK^{-1}\sigma\Big(\sum_{\tilde{k}\in\mathbb{Z}^+}\sqrt{q_{\tilde{k}}}(\dot{\mathbb{B}}_{\tilde{k}}(t)+i\dot{\mathbb{B}}_{-\tilde{k}}(t))e^{ik\theta}+\sum_{\tilde{k}\in\mathbb{Z}^-}\sqrt{q_{\tilde{k}}}(\dot{\mathbb{B}}_{-\tilde{k}}(t)-i\dot{\mathbb{B}}_{\tilde{k}}(t))e^{i\tilde{k}\theta}\Big), U_\beta(\theta)\Big\rangle \\
=&\Big\langle a\sigma\Big(\sum_{\tilde{k}\in\mathbb{Z}^+}\sqrt{q_{\tilde{k}}}(\dot{\mathbb{B}}_k(t)+i\dot{\mathbb{B}}_{-\tilde{k}}(t))\frac{|\tilde{k}|}{|\tilde{k}|+ma}e^{i\tilde{k}\theta} \\
&+\sum_{\tilde{k}\in\mathbb{Z}^-}\sqrt{q_{\tilde{k}}}(\dot{\mathbb{B}}_{-\tilde{k}}(t)-i\dot{\mathbb{B}}_{\tilde{k}}(t))e^{i\tilde{k}\theta}\frac{|\tilde{k}|}{|\tilde{k}|+ma}\Big), \sum_{j\in\mathbb{Z}\setminus\{0\}}c_{\beta,j}e^{ij\theta}\Big\rangle.
\end{aligned} \tag{5.39}$$

Note that the right-hand side of the above equation uses the transformation between the Fourier basis and the POD mode (see Section 4.2.2). Expanding the inner product makes the right-hand side of the above equation as follows,

$$a\sigma\Big(\sum_{\tilde{k}\in\mathbb{Z}^+}\sqrt{q_{\tilde{k}}}(\dot{\mathbb{B}}_{\tilde{k}}(t)+i\dot{\mathbb{B}}_{-\tilde{k}}(t))\frac{|\tilde{k}|}{|\tilde{k}|+ma}+\sum_{\tilde{k}\in\mathbb{Z}^-}\sqrt{q_{\tilde{k}}}(\dot{\mathbb{B}}_{-k}(t)-i\dot{\mathbb{B}}_{\tilde{k}}(t))\frac{|\tilde{k}|}{|\tilde{k}|+ma}\Big)\widetilde{\mathcal{F}}, \quad (5.40)$$

where

$$\widetilde{\mathcal{F}}=\frac{1}{2\pi}\int_0^{2\pi}e^{i\tilde{k}\theta}\sum_{j\in\mathbb{Z}\setminus\{0\}}\overline{c_{\beta,j}e^{ij\theta}}d\theta.$$

Lastly, we impose the orthogonality of the Fourier bases and write

$$\begin{aligned}&\Big\langle aK^{-1}\sigma\Big(\sum_{\tilde{k}\in\mathbb{Z}^+}\sqrt{q_{\tilde{k}}}(\dot{\mathbb{B}}_{\tilde{k}}(t)+i\dot{\mathbb{B}}_{-\tilde{k}}(t))e^{i\tilde{k}\theta}+\sum_{\tilde{k}\in\mathbb{Z}^-}\sqrt{q_{\tilde{k}}}(\dot{\mathbb{B}}_{-\tilde{k}}(t)-i\dot{\mathbb{B}}_{\tilde{k}}(t))e^{i\tilde{k}\theta}\Big),U_\beta(\theta)\Big\rangle\\ =&a\sigma\Big(\sum_{\tilde{k}\in\mathbb{Z}^+}\sqrt{q_{\tilde{k}}}\frac{|\tilde{k}|}{|\tilde{k}|+ma}(\dot{\mathbb{B}}_{\tilde{k}}(t)+i\dot{\mathbb{B}}_{-\tilde{k}}(t))\overline{c_{\beta,\tilde{k}}}+\sum_{\tilde{k}\in\mathbb{Z}^-}\sqrt{q_{\tilde{k}}}\frac{|\tilde{k}|}{|\tilde{k}|+ma}(\dot{\mathbb{B}}_{-\tilde{k}}(t)-i\dot{\mathbb{B}}_{\tilde{k}}(t))\overline{c_{\beta,\tilde{k}}}\Big)\end{aligned} \quad (5.41)$$

Combined with the reduced-order dynamic equation, derived by the POD-Galerkin procedure applied to the deterministic Moore-Greitzer model, i.e., (4.31) and (4.32), we write

the following stochastic version of the POD reduced-order equation:

$$
\begin{aligned}
\dot{b}_\beta(t) = &\sum_{\alpha=1}^{n}\Big(\sum_{j\in\mathbb{Z}\setminus\{0\}}\left(\frac{|j|}{|j|+ma}\right)\Big(-\frac{\nu}{2}j^2 - ij\frac{1}{2}\Big)c_{\alpha,j}\overline{c_{\beta,j}}\Big)b_\alpha(t)\\
&+\frac{3Ha}{W^2}\Phi(t)\Big(1-\frac{\Phi(t)}{2W}\Big)\sum_{\alpha=1}^{n}\Big(\sum_{j\in\mathbb{Z}\setminus\{0\}}\left(\frac{|j|}{|j|+ma}\right)c_{\alpha,j}\overline{c_{\beta,j}}\Big)b_\alpha(t)\\
&+\Big(\frac{3Ha}{2W^2}-\frac{3Ha}{2W^3}\Phi(t)\Big)\sum_{\alpha_1,\alpha_2=1}^{n}\left(\sum_{\substack{j,\tilde{k}\in\mathbb{Z}\setminus\{0\}\\(j+k\neq 0)}}\left(\frac{|j+\tilde{k}|}{|j+\tilde{k}|+ma}\right)c_{\alpha_1,j}c_{\alpha_2,\tilde{k}}\overline{c_{\beta,j+\tilde{k}}}\right)b_{\alpha_1}(t)b_{\alpha_2}(t)\\
&-\frac{Ha}{2W^3}\sum_{\alpha_1,\alpha_2,\alpha_3=1}^{n}\left(\sum_{\substack{j,\tilde{k},l\in\mathbb{Z}\setminus\{0\}\\(j+\tilde{k}+l\neq 0)}}\left(\frac{|j+\tilde{k}+l|}{|j+\tilde{k}+l|+ma}\right)c_{\alpha_1,j}c_{\alpha_2,\tilde{k}}c_{\alpha_3,l}\overline{c_{\beta,j+\tilde{k}+l}}\right)b_{\alpha_1}(t)b_{\alpha_2}(t)b_{\alpha_3}(t)\\
&+a\sigma\Big(\sum_{\tilde{k}\in\mathbb{Z}^+}\sqrt{q_{\tilde{k}}}\frac{|\tilde{k}|}{|\tilde{k}|+ma}(\dot{\mathbb{B}}_{\tilde{k}}(t)+i\dot{\mathbb{B}}_{-\tilde{k}}(t))\overline{c_{\beta,\tilde{k}}}+\sum_{\tilde{k}\in\mathbb{Z}^-}\sqrt{q_{\tilde{k}}}\frac{|\tilde{k}|}{|\tilde{k}|+ma}(\dot{\mathbb{B}}_{-\tilde{k}}(t)-i\dot{\mathbb{B}}_{\tilde{k}}(t))\overline{c_{\beta,\tilde{k}}}\Big),
\end{aligned}
\tag{5.42}
$$

which is coupled to the ODEs given by

$$
\begin{aligned}
\dot{\Phi}(t) &= \frac{1}{l_c}\Big(\bar{\psi}_c(\Phi(t),\hat{b}(t))-\Psi(t)\Big)\\
\dot{\Psi}(t) &= \frac{1}{4B^2 l_c}\Big(\Phi(t)-\gamma\sqrt{\Psi(t)}\Big)
\end{aligned}
\tag{5.43}
$$

where $\bar{\psi}_c(\Phi(t),\hat{b}(t))$ is expressed the same as (4.33).

5.3.3 Snapshot Collection and POD Basis Construction

To test the effectiveness of reconstructing the stochastic Moore-Greitzer model using POD modes, an issue arises as to how one can construct the POD modes such that the coherent structures of the stochastic system with small turbulence intensities are well-characterized. Intuitively, the POD modes can be generated from either deterministic or stochastic data, depending on how we construct the snapshots as well as the relevant correlation matrix. However, to the best of our knowledge, the optimality of applying the classical POD approach (introduced in Chapter 4 with the standard computational scheme) with stochastic data is still not well understood. On the other hand, generating the POD modes from the stochastic Moore-Greitzer data *in situ* could be a little "overkill" because this requires

solving the full stochastic PDE before performing POD while the intensity of the noise given in our Moore-Greitzer model is moderately low. Since there is prior knowledge on the values of the external forcing (d_Φ and d_Ψ), it seems to us that constructing the POD modes using data obtained from deterministic simulations of the Moore-Greitzer model is a more practical approach. We name the POD modes obtained from the stochastic data and the associated deterministic data as *in situ* and *a priori* POD modes, respectively. For the sake of comparison, we shall test the performance of the generalized CUSUM statistics to detect the stall instability using both *in situ* and *a priori* POD modes in the corresponding reduced order models.

As an example of simulating snapshot data, we let $\alpha = 0$, $\nu = 1$, then

$$q_{\tilde{k}} = \tilde{k}^{-1.1}$$

so that

$$W_{\mathcal{H}}(t) = \sum_{\tilde{k}\in\mathbb{Z}^+} |\tilde{k}|^{-1}(\mathbb{B}_{\tilde{k}}(t) + i\mathbb{B}_{-\tilde{k}}(t))e^{i\tilde{k}\theta} + \sum_{\tilde{k}\in\mathbb{Z}^-} |\tilde{k}|^{-1}(\mathbb{B}_{-\tilde{k}}(t) - i\mathbb{B}_{\tilde{k}}(t))e^{i\tilde{k}\theta}. \tag{5.44}$$

To illustrate the numerical solutions of (5.37) and (5.38) in this example, where $W_{\mathcal{H}}(t)$ is given by (5.44), the following values of the parameters are imposed:

$$l_c = 8,\ H = 0.18,\ W = 0.25,\ m = 8.75,\ \nu = 0.1,$$

$$a = 1/3.5,\ \psi_{c_0} = 1.67H,\ B = 0.15,\ \gamma = 0.62,$$

$$d_\Phi = -0.1,\ d_\Psi = 0.1.$$

Note that the disturbances, i.e., d_Φ and d_Ψ, are added at time $k = 100$, and the initial conditions of the system are given as follows,

$$\Phi(0) = 0.51, \quad \Psi(0) = 0.66, \quad g(0,\theta) = 0.1\sin(\theta).$$

The objective is to investigate the reconstruction of the stochastic Moore-Greitzer signal using deterministic *a priori* and stochastic *in situ* POD modes to evaluate the effectiveness of the reconstruction methodology. As illustrated by Figure 5.3, the introduction of deterministic external forces in the mass flow and pressure induces the stochastic system to undergo transient phases within the period $100 \le t \le 230$. Subsequently, the PDE component, subject to small additive noise, undergoes a Hopf bifurcation, resulting in limit cycle behavior. In contrast, the ODE component associated with Φ and Ψ is shifted to a new steady state.

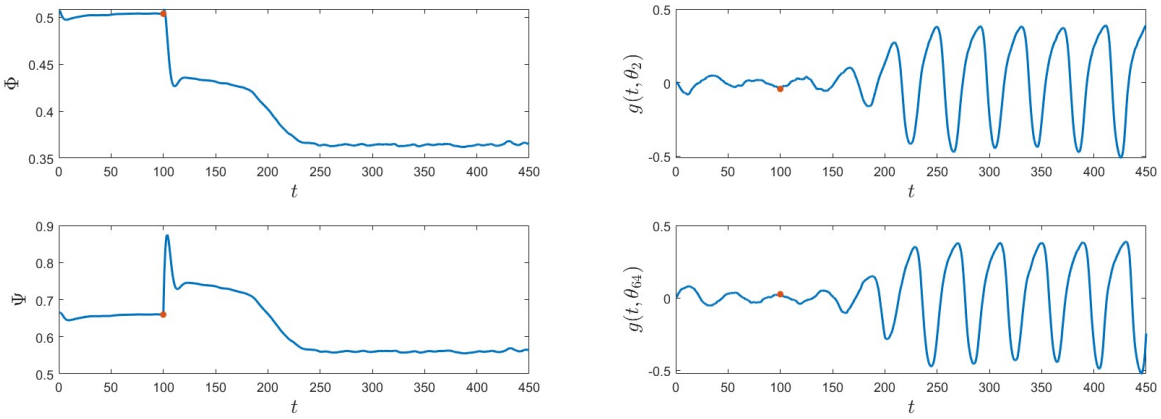


Figure 5.3: The evolution of the ODE, i.e., (Φ, Ψ) **(left)**, and the evolution of the stochastic PDE over time t with the change happening at $k = 100$ at two fixed values of θ **(right)**.

From Figure 5.4, it can be observed that reconstructing the stochastic Moore-Greitzer PDE data with both *in situ* and *a priori* POD modes yields comparable outcomes when θ is positioned at distinct points, such as θ_1 and θ_{32}, utilizing a total of 4 POD modes. It is indeed acknowledged that there is an observable phase discrepancy between the original limit cycles of g and the reconstructed signals. This discrepancy diminishes as the number of POD modes increases from 4 to 6, as depicted in Figure 5.5. This is logical since, theoretically, POD reconstruction is expected to improve with an increased number of POD modes. The relevant *in situ* and *a priori* POD modes are shown in Figures 5.6 and 5.7, respectively. Overall, this critical finding and discussion can eventually benefit the stall detection in that a better reconstruction of the transient dynamics after the change occurs potentially yields less detection delay.

5.4 Stall Detection in Stochastic Moore–Greitzer PDE Systems

In Section 5.2, we investigated the performance of the generalized CUSUM statistics, T_n and $\widehat{T}_n$, using particle filters in the reduced-order deterministic Moore-Greitzer models, obtained from the POD Galerkin procedures with both *in situ* and *a priori* POD bases. In the context of the stochastic Moore-Greitzer model, which incorporates small additive

noise, the findings presented in Section 5.3 indicate that, despite tolerable discrepancies, the use of *a priori* POD modes is more effective for the reconstruction of transient phases occurring subsequent to a change and preceding the emergence of the next steady dynamical phase (i.e., stable limit cycles). As such, our goal in this section is to employ the theoretical formulation given in 5.2, and experimentally implement T_n and $\widehat{T}_n$ to detect the induced stall instability in the stochastic Moore-Greitzer systems with additive noise. More specifically, the signal, i.e., $x(t,\theta) = [g(t,\theta), \Phi(t), \Psi(t)]^T$, is governed by the following stochastic partial differential equations (SPDE),

$$\frac{\partial x(t,\theta)}{\partial t} = Ax(t,\theta) + f(x(t,\theta)) + d\mathbb{I}_{\{t\geq k\}} + \xi(t,\theta), \tag{5.45}$$

where

$$d = \begin{bmatrix} 0 \\ \frac{1}{l_c} d_\Psi \\ -\frac{1}{4B^2 l_c} d_\Phi \end{bmatrix}, \quad \xi(t,\theta) = \begin{bmatrix} aK^{-1}\sigma \dot{W}_{\mathcal{H}}(t) \\ 0 \\ 0 \end{bmatrix},$$

A and f are given in (5.4) and (5.5). Similarly, the discrete-time observations are taken in a way such that the accessible data is only partially observed by the decision maker. In this section, we observe g at a place of θ_1 so that (5.17) becomes

$$Y_n^{(1)} = g(n\widetilde{\gamma}, \theta_1) + V_n. \tag{5.46}$$

Note that $\widetilde{\gamma}$ represents the unit time interval, i.e., $t_n = n\widetilde{\gamma}$. For the ease of notations, we write $Y_n^{(1)}$ as Y_n for the rest of this section. As such, rewriting the above equation gives

$$Y_n = g(t_n, \theta_1) + V_n, \tag{5.47}$$

where V_n is i.i.d. with known density. Most commonly, $V_n \sim \mathcal{N}(0, \tau^2)$, for $n = 1, \cdots, N$.

With the aid of the *a priori* POD modes, generated from *a priori* data containing complex limit cycle behaviors without any disturbances (d and $\xi(t,\theta)$), a stochastic differential equation (SDE) with fewer dimensions, which is analogous to (5.45) but in terms of the POD time coefficients $b_\alpha(t)$, can be derived. Notice that this *a priori* data is obtained by varying the bifurcation parameter γ given in the Moore-Greitzer PDE systems. Define $b(t) = [b_1(t), \cdots, b_{M'}(t)]^T$, we write an abstract form of the reduced-order equation as follows,

$$\frac{db(t)}{dt} = \widetilde{A}b(t) + \widetilde{f}(b(t), \Phi(t)) + a\sigma\widetilde{\xi}_1(t), \tag{5.48}$$

where more specific forms of $\widetilde{A}$ and $\widetilde{f}(b(t), \Phi(t))$ can be identified from (5.42), and

$$\widetilde{\xi}_1(t) = \begin{bmatrix} \sum_{\tilde{k}\in\mathbb{Z}^+} \mathcal{K}(\tilde{k})(\dot{\mathbb{B}}_{\tilde{k}}(t) + i\dot{\mathbb{B}}_{-\tilde{k}}(t))\overline{c_{1,\tilde{k}}} + \sum_{\tilde{k}\in\mathbb{Z}^-} \mathcal{K}(\tilde{k})(\dot{\mathbb{B}}_{-\tilde{k}}(t) - i\dot{\mathbb{B}}_{\tilde{k}}(t))\overline{c_{1,\tilde{k}}} \\ \vdots \\ \vdots \\ \sum_{\tilde{k}\in\mathbb{Z}^+} \mathcal{K}(\tilde{k})(\dot{\mathbb{B}}_{\tilde{k}}(t) + i\dot{\mathbb{B}}_{-\tilde{k}}(t))\overline{c_{M',\tilde{k}}} + \sum_{\tilde{k}\in\mathbb{Z}^-} \mathcal{K}(\tilde{k})(\dot{\mathbb{B}}_{-\tilde{k}}(t) - i\dot{\mathbb{B}}_{\tilde{k}}(t))\overline{c_{M',\tilde{k}}} \end{bmatrix},$$

$$\mathcal{K}(\tilde{k}) = \sqrt{q_{\tilde{k}}}\frac{|\tilde{k}|}{|\tilde{k}| + ma}.$$

The derivation of $\widetilde{\xi}_1(t)$ comes from the projection of the stochastic input onto the POD modes, and some details including q_k can be checked in Section 5.3. Throughout this section, the original SPDE is numerically solved by 128 Fourier modes, i.e., $\tilde{k} = \pm 1, \cdots, \pm 64$, and $q_{\tilde{k}} = \tilde{k}^{-2}$.

Define $\tilde{x} = [b(t), \Phi(t), \Psi(t)]^T$. Making (5.48) coupled with the ODE component of the Moore-Greitzer model, i.e., (5.43), and adding the disturbances d, yields

$$\frac{d\tilde{x}(t)}{dt} = \widetilde{\mathcal{A}}\tilde{x}(t) + \widetilde{F}(\tilde{x}(t)) + d\mathbb{I}_{\{t\geq k\}} + a\sigma\widetilde{\xi}(t), \tag{5.49}$$

where $\widetilde{\mathcal{A}}$ and $\widetilde{F}$ can be obtained from (4.31) and (4.32), and

$$\widetilde{\xi}(t,\theta) = \begin{bmatrix} \widetilde{\xi}_1(t) \\ 0 \\ 0 \end{bmatrix}.$$

Note that once $b(t)$ is obtained, we calculate x', which is defined as follows,

$$x'(t,\theta) = \begin{bmatrix} \sum_{\alpha=1}^{M'} b_\alpha(t)U_\alpha(\theta) \\ \Phi(t) \\ \Psi(t) \end{bmatrix},$$

by incorporating the *a priori* POD modes. It is worth mentioning that the notation x' has nothing to do with the derivatives or any kind, and the purpose here is to make it consistent with the notations used in Section 5.2. Corresponding to what we discussed in Section 5.2, the particle filtering calculations of $Z_n^{(k)}$ and $Z_n^{(1)}$ are involved with the following transition probabilities approximation,

$$p(x_n(\theta)|x_{n-1}(\theta)) \approx p(x'_n(\theta)|x'_{n-1}(\theta)), \tag{5.50}$$

where $x_n(\theta)$ and $x'_n(\theta)$ are discrete-time versions of $x(t,\theta)$ and $x'(t,\theta)$, respectively. The key insight to be drawn from this discussion is that $x_n(\theta)$ originates from the infinite-dimensional SPDE, yet employing a finite-dimensional SDE for $x'_n(\theta)$, as derived through a POD-Galerkin procedure, enhances the practicality and efficiency of the particle filtering implementation relative to the Fourier spectral method, while preserving the essential dynamics of the stochastic Moore-Greitzer model. The rest of the calculations for T_n and $\widehat{T}_n$ follow the discussion given in Section 5.2.

The relevant simulations results are given in Figures 5.8, 5.9 and 5.10, where the following values of the parameters are employed

$$l_c = 8,\ H = 0.18,\ W = 0.25,\ m = 8.75,\ \nu = 0.1,$$

$$a = 1/3.5,\ \psi_{c_0} = 1.67H,\ B = 0.15,\ \gamma = 0.62,$$

$$\sigma = 2,\ d_{\Phi} = -0.1,\ d_{\Psi} = 0.1.$$

Note that the disturbances, i.e., d_{Φ} and d_{Ψ}, are added at time $t = 100$, and the initial conditions of the system are given as follows,

$$\Phi(0) = 0.51, \quad \Psi(0) = 0.66, \quad g(0,\theta) = 0.1\sin(\theta).$$

In Figure 5.8, we plot the generalized CUSUM statistics (i.e., T_n) and the CUSUM statistics that assume an instant change (i.e., $\widehat{T}_n$) with 6 ensembles (different random seeds) of observations using a particle filtering approach with 100 particles and $V_n \sim \mathcal{N}(0, 0.04)$. Note that the Monte Carlo simulations have been performed in terms of the computations of T_n and $\widehat{T}_n$. In each setting of the observational noise $V_n \sim \mathcal{N}(0,\tau^2)$, 6 random picks of 100 sets of CUSUMs are selected and given in Figures 5.8, 5.9 and 5.10. It follows from these 6 subplots in Figure 5.8 that both T_n and $\widehat{T}_n$ stay flat around zero until, roughly speaking, $n = 180$. But T_n starts to increase up to some value about 100 (see the scale of the vertical axis for each subplot), whereas $\widehat{T}_n$ shows some "non-robust" behaviors in each subplot. In some cases, we can clearly see $\widehat{T}_n$ generates much more delay compared to T_n and creates some "up-and-down" behaviors as well. Overall, $\widehat{T}_n$ is much more sensitive to different random seeds of the observational noise and distinct types of POD modes, i.e., *in situ* and *a priori* POD modes, compared to T_n. For both types of POD modes, it follows from Figures 5.8, 5.9 and 5.10 that the Kullback–Leibler information number (defined in 2.4.1) given in T_n is relatively larger than the divergence between the pre-change and post-change distributions given in $\widehat{T}_n$. More experiments, regarding distinct intensities of the sensor noise V_n, showing the effectiveness of T_n compared to $\widehat{T}_n$. As τ^2 (i.e., the variance of V_n) increases, the change of the dynamics in the stochastic Moore-Greitzer model (i.e.,

from a steady state to a limit cycle) induced by the disturbances in the mass flow and pressure rise is more "blurred" in the observations. This makes the stall detection an even more difficult task, especially with the particle filtering approach, so the vertical axis scale of the CUSUMs has been decreased from around 150 in Figure 5.8 to even 30 in Figure 5.10. Intuitively, this issue of improving the performance of T_n and $\widehat{T}_n$ under the high variance observations can be addressed by increasing the number of particles. Nevertheless, there is always a trade-off between a more effective and accurate detection in theory and a more efficient detection in computations. It is also worthwhile mentioning that, among Figures 5.8, 5.9 and 5.10, the time steps where T_n and $\widehat{T}_n$ start to increase is around 100 time steps delayed by the real change point, which is $k = 100$. This is due to the fact that the PDE solution $g(t, \theta)$ enters a transient phase, during about $100 \leq n \leq 200$, before it gives a stable limit cycle, and these transient dynamics cause the delays reflected in the generalized CUSUMs.

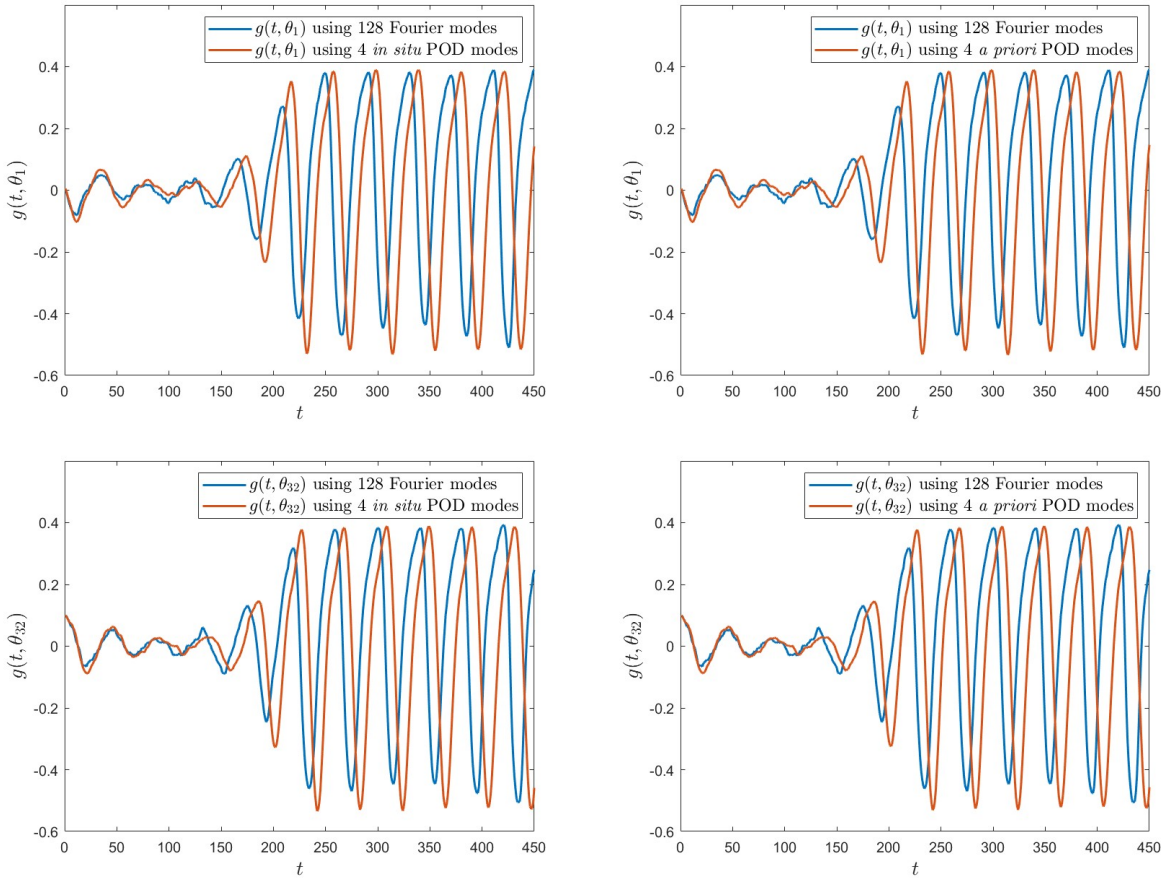


Figure 5.4: The POD reconstructions of the stochastic data $g(t,\theta_1)$ and $g(t,\theta_{32})$ using 4 *in situ* POD modes (**left**) and using 4 *a priori* POD modes (**right**).

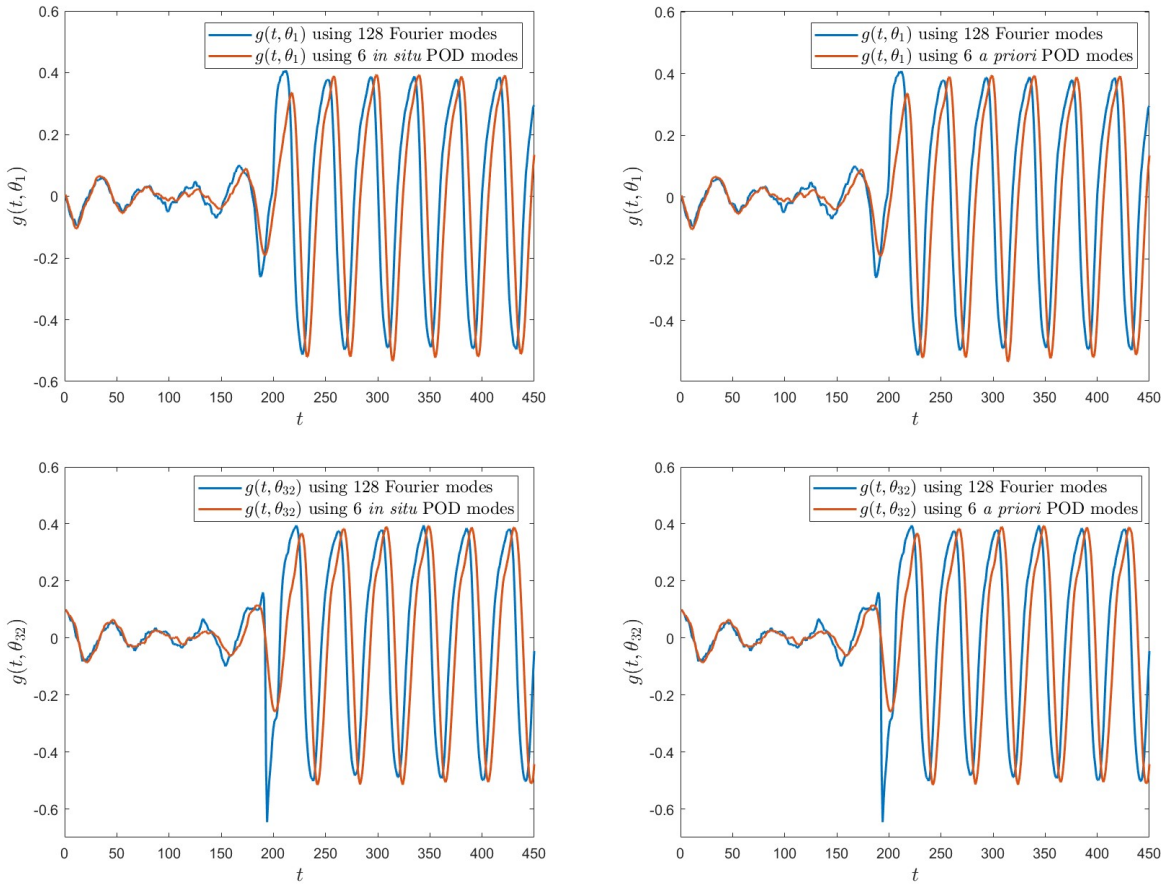


Figure 5.5: The POD reconstructions of the stochastic data $g(t,\theta_1)$ and $g(t,\theta_{32})$ using 6 *in situ* POD modes (**left**) and using 6 *a priori* POD modes (**right**).

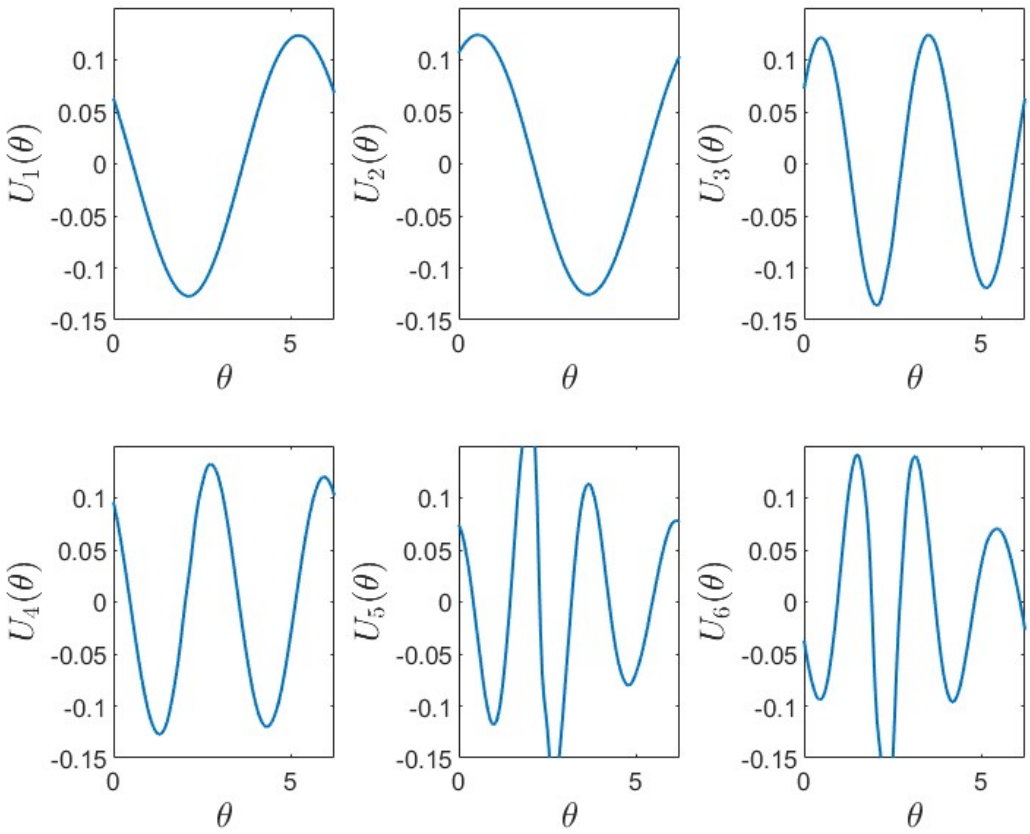


Figure 5.6: The first 6 *in situ* POD modes directly generated from the snapshots with additive noise.

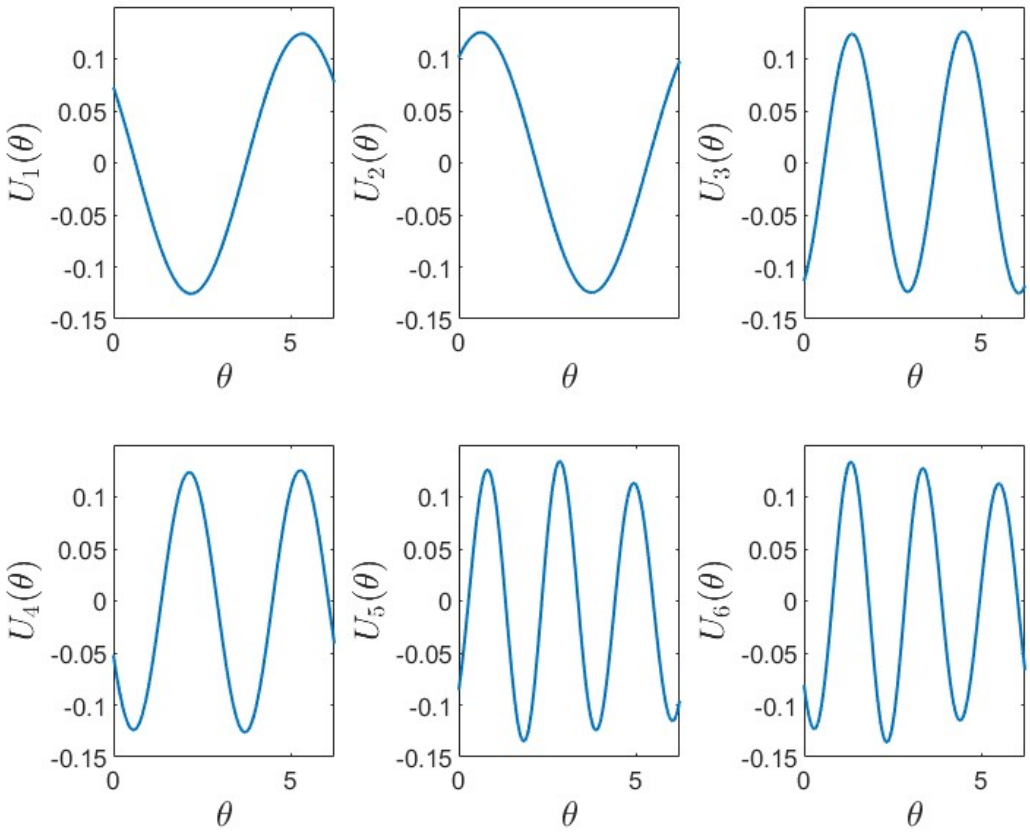


Figure 5.7: The first 6 *a priori* POD modes directly generated from the deterministic snapshots with complex limit cycle behaviors.

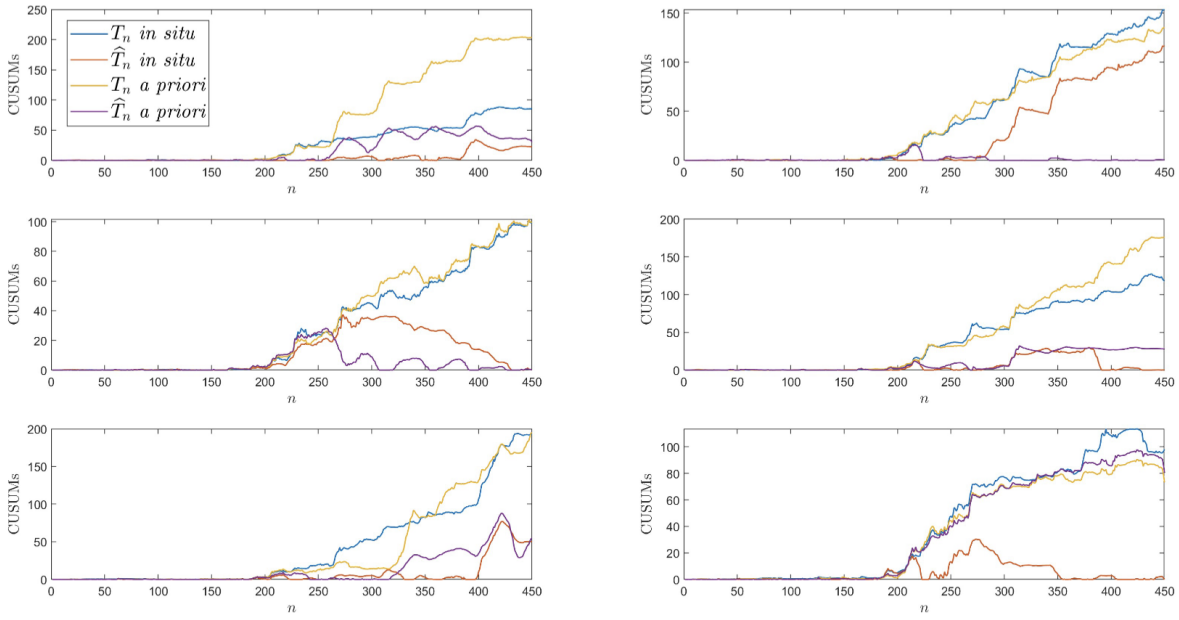


Figure 5.8: The generalized CUSUM statistics (i.e., T_n) and the CUSUM statistics that assume an instant change (i.e., $\widehat{T}_n$) with 6 ensembles of observations using a particle filtering approach with 100 particles, 6 *in situ* and *a priori* POD modes and $V_n \sim \mathcal{N}(0, 0.04)$.

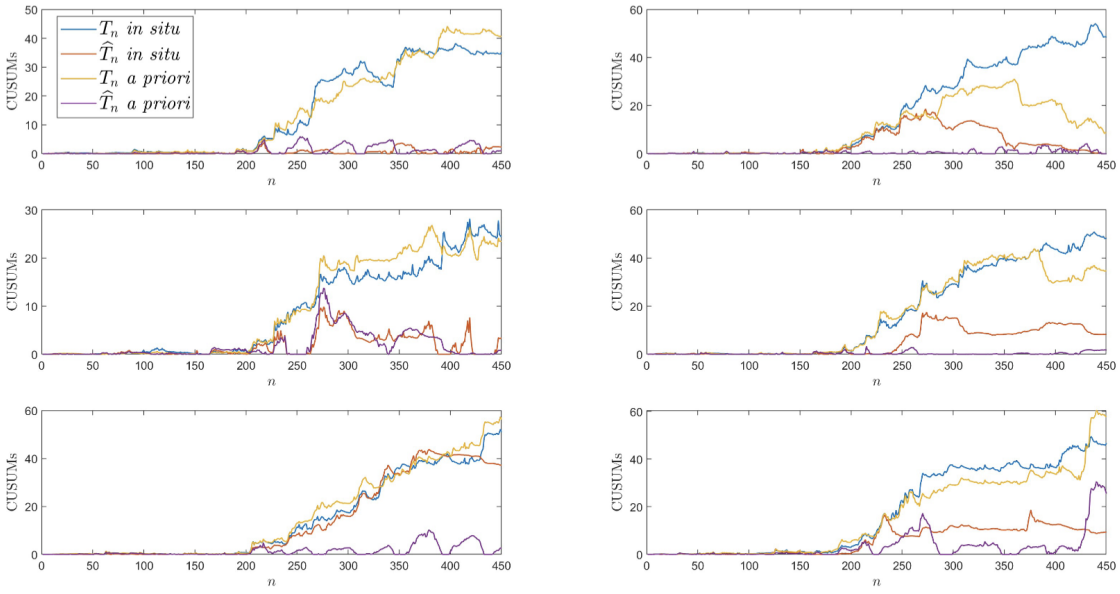


Figure 5.9: The generalized CUSUM statistics (i.e., T_n) and the CUSUM statistics that assume an instant change (i.e., $\widehat{T}_n$) with 6 ensembles of observations using a particle filtering approach with 100 particles, 6 *in situ* and *a priori* POD modes and $V_n \sim \mathcal{N}(0, 0.09)$.

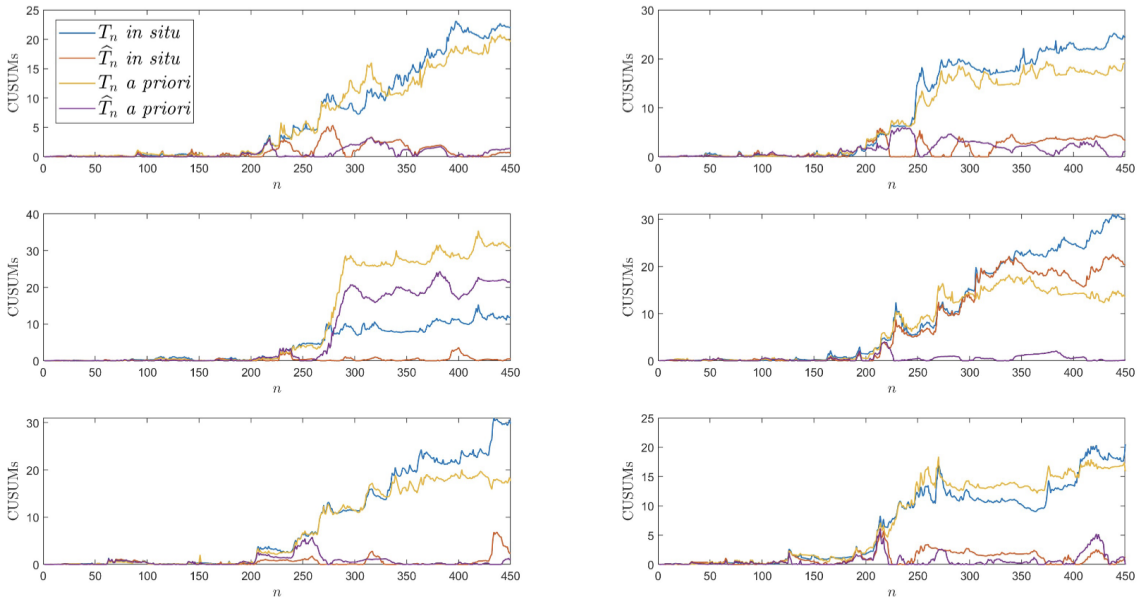


Figure 5.10: The generalized CUSUM statistics (i.e., T_n) and the CUSUM statistics that assume an instant change (i.e., $\widehat{T}_n$) with 6 ensembles of observations using a particle filtering approach with 100 particles, 6 *in situ* and *a priori* POD modes and $V_n \sim \mathcal{N}(0, 0.16)$.

Chapter 6

Conclusions and Future Work

This thesis examines the quickest change detection theory and algorithms in nonlinear HMMs to address surge and stall detections in the Moore-Greitzer PDE systems. In this chapter, a summary of the principal findings of this thesis is presented, along with a discussion on potential future directions for this research.

6.1 QCD Problems in Nonlinear HMMs

In this work, we studied the QCD problems in nonlinear HMMs and explained in detail why the standard model does not apply to our problems. As such, the generalized CUSUM procedure (i.e., T_n), where the post-change distribution depends on the unknown change point, was considered the most relevant change detection scheme. While T_n does not satisfy a simple recursion, we imposed the standard filtering theory to recursively approximate the associated log-likelihood ratios using particle methods. To reduce the computational cost of T_n due to its non-recursiveness, we reviewed a recursive CUSUM-like procedure that assumes the change occurs immediately, named $\widehat{T}_n$. Under certain conditions, T_n can be replaced by $\widehat{T}_n$, depending on the post-change dynamics of deterministic and stochastic systems.

More specifically, we researched the differences and similarities between T_n and $\widehat{T}_n$ in the context of the QCD problem within reduced planar Moore-Greitzer compressor models. Two general cases are discussed based on two post-change dynamics: one is a post-change fixed point, and the other one is a post-change limit cycle (caused by surge instability). For the former case, T_n and $\widehat{T}_n$ are similar, except for the case when the post-change transients

move towards the wrong direction of the post-change equilibrium. For the latter case, when there is no signal-noise, we found T_n and $\widehat{T}_n$ could look quite different. The extent of the difference depends on the phase error from the phase of the post-change cycle $\widehat{T}_n$ assumes and the real phase coming from the observations. It also depends on whether the pre-change steady state is inside or outside the post-change limit cycle. The introduction of a certain degree of signal noise can serve as an effective mitigation technique, as it randomizes the phase effect of the post-change limit cycle, thereby diminishing its impact.

It is worth noting that the performance of the generalized CUSUM statistic T_n and its related $\widehat{T}_n$ may depend on the number of particles in the implementation. This dependency could potentially limit the efficiency and robustness of the proposed method employed in the change detection problems. In extreme cases, an increased number of particles might make the generalized CUSUM statistics computationally impractical. As such, future work may consider the window-limited versions of statistical methods [49], which can provide some insight for enhancing the adaptability and computational efficiency of the generalized CUSUM statistic T_n. Additionally, it would be interesting to explore the least number of particles to effectively implement T_n and $\widehat{T}_n$ in the surge and stall detections in both deterministic and stochastic Moore-Greitzer models. To study the robustness of generalized CUSUM statistics, another potential research area is testing alternative nonlinear filtering techniques such as the ensemble Kalman filtering [28, 29].

In this thesis, we employed the particle filtering approach to numerically approximate the generalized CUSUM statistic to solve the associated QCD problem in nonlinear HMMs. An important assumption is that pre-change and post-change distributions are completely known. When the post-change distribution is not given as *a priori*, the QCD problem in nonlinear stochastic systems becomes more complicated. The approximation of the log-likelihood ratio using a particle filtering approach is not well-characterized since the post-change dynamical model can not be specified. Indeed, the QCD problem in the i.i.d. setting with unknown post-change distribution has been investigated by Page [65], Pollak, and Siegmund [68]. They assumed the post-change probability density function belongs to some exponential family, from which the generalized likelihood ratio (GLR) test and the mixture-based test were proposed. A more special case where the pre-change distribution is assumed to be known yet the post-change distribution of the observations is time-varying along with the detection algorithm was explored and proposed in [18]. To tackle these issues, one may incorporate the GLR [101] approach or robust hypothesis testing [45] along with the window-limited CUSUM [105, 52] to construct a more efficient generalized CUSUM test.

6.2 Detection of Stall Instability in the Deterministic and Stochastic Moore-Greitzer PDE Systems

In the second aspect of our research, we examined the scalability of our approach applied to higher-dimensional systems, in particular, the Moore-Greitzer PDE systems. To reduce the dimension of the Moore-Greitzer PDE systems, we first studied the proper orthogonal decomposition technique and expanded its conceptual framework [26] in Chapter 4. The relevant computational scheme for calculating the POD modes does not assume the ergodicity of the dynamical system. More importantly, we identified the relation between the POD modes and the Fourier modes, which accurately facilitates the numerical solution of the original Moore-Greitzer PDE system. We then derived a finite-dimensional reduced-order equation for the Moore-Greitzer PDE system through the POD Galerkin procedure utilizing the L^2 inner product. This was contrasted with the weak solution produced by the POD-Galerkin method within the H^1 Sobolev space. The error analysis indicates that the application of the H^1-POD-Galerkin method can enhance the POD reconstruction of the Moore-Greitzer snapshot data. However, the extent of this improvement depends on the degree of emphasis placed on the derivative information of the system during the construction of the POD modes.

With stochastic input, we focused on a more realistic model where deterministic forcing in the ODE component of the Moore-Greitzer model triggers a PDE (stall) bifurcation. To detect stall instability, we employ the generalized CUSUM statistics using a particle filtering approach with a POD Galerkin procedure. To obtain a more accurate reduced-order dynamic rule of the Moore-Greitzer model, the *in situ* and *a priori* POD modes were tested and compared in the stall detection problem. The simulation results demonstrate that both types of POD modes function similarly in terms of approximating the signals with limit cycle behaviors. This similarity had been shown in different positions of the values of θ and various numbers of POD modes. Some Monte Carlo simulations, with a few typical examples shown in this thesis, showed that the performance of T_n outperformed $\widehat{T}_n$ in terms of effectively detecting the change, while $\widehat{T}_n$ is a computationally efficient CUSUM-based statistic. Specifically, T_n consistently shows more robust behavior and less sensitivity to random noise and POD mode selection compared to $\widehat{T}_n$, as demonstrated in Figures 5.8, 5.9, and 5.10. Increasing the intensity of the observational noise makes stall detection more challenging, causing reductions in the Kullback–Leibler divergence of the CUSUM statistics. Although higher particle counts can improve detection accuracy, they also raise computational demands. Furthermore, both statistics exhibit delays due to transient dynamics immediately after the change occurs. Overall, T_n provides a more reliable and robust solution for stall detection in the stochastic Moore–Greitzer model.

A challenge faced in this research was the potential degradation of the POD reconstruction of the stochastic PDE solution, attributed to transient phases. To enhance the characterization of transient structures within the stochastic Moore-Greitzer model, a data-driven methodology to be considered in the future is the application of dynamic mode decomposition (DMD) [93]. Subsequent comparative analysis of POD and DMD techniques, as applied to stall detection in stochastic Moore-Greitzer PDE systems, can be conducted for further insights. In addition, the findings of stall detection in both deterministic and stochastic Moore-Greitzer models assume that both the pre-change and post-change distributions are fully specified. However, this will not generally be the case for some real-world QCD problems where partial or even no prior knowledge of the post-change distribution is known. Some window-limited versions of the generalized CUSUM statistics can be studied and tested in the future. In parallel, investigating the window-limited CUSUM method for high-dimensional systems is critical. This approach, as proposed by Xie et al. [105], can be particularly beneficial for detecting changes in scenarios with partially known or non-stationary post-change distributions. Exploring these strategies could further enhance the robustness and applicability of quickest change detection in complex, real-world settings, such as ecological monitoring, financial market anomaly detection, and engineering systems health monitoring.

A natural extension of this research is a deeper exploration of the phase structure of post-change limit cycles, specifically using the framework of isochrons introduced by Guckenheimer [40]. Isochrons characterize the timing of oscillatory dynamics in nonlinear systems, providing a powerful approach for understanding the intrinsic phase dynamics and synchronization properties of limit-cycle oscillations. Future research will involve a systematic analysis of how external forcing and initial conditions influence the phase dynamics. Such an analysis will provide deeper insights into the sensitivity and robustness of the compressor dynamics modeled by the Moore–Greitzer PDE system and potentially enable more effective and targeted strategies for instability detection and control. Another component of our study will be the case where the stochastic model for the observations is not completely specified. Graphical models [30], which describe statistical relationships in the form of a connected graph, could be another possible way to detect the change in high-dimensional data with an unknown post-change distribution. The lack of general criteria justifying the computational performance for T_n and $\widehat{T}_n$ in high-dimensional systems could limit the versatility of the proposed method in relevant QCD problems. Future research may include how to handle these problems.

Overall, these future research avenues represent crucial steps toward broadening the impact and scope of quickest change detection methods, ensuring their relevance and effectiveness in diverse applications beyond compressor dynamics

References

[1] C. Andrieu, A. Doucet, S. S. Singh, and V. B. Tadic. Particle methods for change detection, system identification, and control. *Proceedings of the IEEE.*, 92(3):423–438, 2004.

[2] AC. Antoulas. *Approximation of large-scale dynamical systems.* Vol. 6 of Advances in Design and Control, Society for Industrial and Applied Mathematics, 2005.

[3] M. S. Arulampalam, S. Maskell, N. Gordon, and T. Clapp. A tutorial on particle filters for online nonlinear/non-Gaussian Bayesian tracking. *IEEE Transactions on Signal Processing.*, 50(2), 2002.

[4] N. Aubry, P. Holmes, J. L. Lumley, and E. Stone. The dynamics of coherent structures in the wall region of a turbulent boundary layer. *Journal of fluid Mechanics*, 192, 1988.

[5] B. Azimi-Sadjadi and P. S. Krishnaprasad. A particle filtering approach to change detection for nonlinear systems. *EURASIP, Journal on Applied Signal Processing*, 15:2295–2305, 2004.

[6] A. Bain and D. Crisan. *Fundamentals of Stochastic Filtering.* Springer, Berlin, 2009.

[7] P. Baldi and M. Chaleyat-Maurel. An extension of Ventsel-Freidlin estimates. *In Stochastic analysis and related topics, Proc. Workshop, Silivri/Turk., Lect. Notes Math*, 1316:305–327, 1988.

[8] T. Banerjee and V. V. Veeravalli. Data-efficient minimax quickest change detection in a decentralized system. *Sequential Analysis*, 34:148–170, 2015.

[9] L. E. Baum and J. A. Eagon. An inequality with applications to statistical estimation for probabilistic functions of Markov processes and to a model for ecology. *Bulletin of the American Mathematical Society*, 73(3):360, 1967.

[10] L. E. Baum and T. Petrie. Statistical inference for probabilistic functions of finite state Markov chains. *The Annals of Mathematical Statistics*, 37(6):1554–1563, 1966.

[11] P. Baxendale. Unpublished notes on proper orthogonal decomposition. 2024.

[12] P. Baxendale, D. Li, and N. S. Namachchivaya. Quickest change detection in nonlinear hidden markov models using a generalized cusum procedure with particle filters. *Nonlinear Dynamics*, 113, 2024.

[13] T. Bengtsson, P. Bickle, and B. Li. Curse-of-dimensionality revisited: Collapse of the particle filter in very large scale systems. *IMS Collections: Probability and Statistics Essays in Honor of David A. Freedman*, 2:316– 334, 2008.

[14] D. Bertsekas. *Dynamic Programming and Optimal Control*, volume I and II. Belmont, Massachusetts: Athena Scientific, 1995.

[15] B. Birnir and H.A. Hauksson. A finite dimensional attractor of the Moore–Greitzer PDE model. *SIAM Journal on Applied Mathematics*, 59(2), 1998.

[16] B. Birnir, S. Hou, and N. Wellander. Derivation of the viscous Moore-Greitzer equation for aeroengine flow. *Journal of Mathematical Physics*, 48(6), 2007.

[17] J. Bjerknes. Atmospheric teleconnections from the equatorial pacific. *Monthly weather review*, 97(3), 1969.

[18] S.D. Blostein. Quickest detection of a time-varying change in distribution. *IEEE Trans. Information Theory*, 37(4):1116–1122, 1991.

[19] J. V. Braun and H. G. Müller. Statistical methods for DNA sequence segmentation. *Ann. Statist.*, 13(2):142–162, 1998.

[20] Y. Cao, J. Zhu, IM. Navon, and Z. Luo. A reduced-order approach to four dimensional variational data assimilation using proper orthogonal decomposition. *International Journal for Numerical Methods in Fluids*, 53(10):1571–1583, 2007.

[21] B. Chen and P. Willett. Quickest detection of hidden Markov models. *Proc. 36th Conf. Decision Contr.*, pages 3984– 3989, 1997.

[22] B. Chen and P. Willett. Detection of hidden Markov model transient signals. *IEEE Trans. Aerosp. Electron. Syst.*, 36(4):1253– 1268, 2000.

[23] M. Chen, L. Hu, and H. Tang. An approach for optimal measurements selection on gas turbine engine fault diagnosis. *Journal of Engine for Gas Turbines and Power-Transactions of the ASME*, 137(7):12031–12039, 2015.

[24] F. Chinesta, F. Huerta, G. Rozza, and K. Willcox. *Model Order Reduction: A Survey.* Wiley Encyclopedia of Computational Mechanics, 2016.

[25] J. David, N. F. Miller, and S. M. Ghalyan. HMM conditional likelihood based change detection with strict delay tolerance. *Mechanical systems and signal processing.*, 147, 2021.

[26] MS. Djouadi and S. Sahyoun. On a generalization of the proper orthogonal decomposition and optimal construction of reduced order models. *Proceedings of the American Control Conference*, IEEE: 85-92:1436–1441, 2012.

[27] A. Doucet, S. J. Godsill, and C. Andrieu. On sequential Monte Carlo sampling methods for Bayesian filtering. *Statistics and Computing*, 10(3):197– 208, 2000.

[28] G. Evensen. Sequential data assimilation with a nonlinear quasi- geostrophic model using monte carlo methods to forecast error statistics. *J. Geophys. Res.*, 99:10143 – 10162, 1994.

[29] G. Evensen. The ensemble Kalman filter: theoretical formulation and practical implementation. *Ocean Dyn.*, 53:343 – 367, 2003.

[30] E. Fox, E. Sudderth, M. Jordan, and A. Willsky. Bayesian nonparametric methods for learning Markov switching processes. *Signal Processing Magazine, IEEE*, 27(6):43–54, 2010.

[31] M. I. Freidlin and A. D. Wentzell. *Random Perturbations of Dynamical Systems.* Springer, New York, 1984.

[32] M. Frisen. Optimal sequential surveillance for finance, public health, and other areas. *Sequential Analysis*, 28(3):310–337, 2009.

[33] C. D. Fuh. SPRT and CUSUM in hidden Markov models. *Ann. Statist.*, 31(3):942–977, 2003.

[34] C. D. Fuh. Asymptotic operating characteristics of an optimal change point detection in hidden Markov models. *Ann. Statist.*, 32(5):2305–2339, 2004.

[35] C. D. Fuh and Y. Mei. Quickest change detection and Kullback-Leibler divergence for two-state hidden Markov models. *IEEE Transactions on Signal Processing.*, 63(18):4866–4878, 2015.

[36] C. D. Fuh and A. G. Tartakovsky. Asymptotic Bayesian theory of quickest change detection for hidden Markov models. *IEEE Transactions on Information Theory.*, 65(1):511–529, 2019.

[37] J. T. Gravdahl and O. Egeland. *Compressor surge and rotating stall: Modeling and control* . Springer-Verlag, 1999.

[38] E. M. Greitzer. Surge and rotating stall in axial flow compressors, part I/II. *ASME J. Engineering for Gas Turbines and Power.*, 98(2):190–217, 1976.

[39] C. Gu and J. Roychowdhury. Model reduction via projection onto nonlinear manifolds, with applications to analog circuits and biochemical systems. *IEEE/ACM International Conference on Computer-Aided Design*, pages 85–92, 2008.

[40] J. Guckenheimer. Isochrons and phaseless sets. *Journal of Mathematical Biology*, 1(3), 1975.

[41] J. Guckenheimer and P. Holmes. *Nonlinear oscillations, dynamical systems, and bifurcations of vector fields.* Springer-Verlag, 1983.

[42] D. J. Higham. An algorithmic introduction to numerical simulation of stochastic differential equations. *SIAM Review*, 43(3):525– 546, 2001.

[43] P. Holmes, J. L. Lumley, and G. Berkooz. *Turbulence, coherent structures, dynamical systems and symmetry.* Cambridge University Press, 1996.

[44] C. Hös, A. Champneys, and L. Kullmann. Bifurcation analysis of surge and rotating stall in the Moore–Greitzer compression system. *IMA Journal of Applied Mathematics*, 2003.

[45] P. J. Huber. A robust version of the probability ratio test. *Annals of Mathematical Statistics*, 36(6):1753–1758, 1965.

[46] T. Iliescu and Z. Wang. Are the snapshot difference quotients needed in the proper orthogonal decomposition? *SIAM J. Sci. Comput.*, 36(3), 2014.

[47] A. Iollo, S. Lanteri, and J.A. Désiéri. Stability properties of POD–Galerkin approximations for the compressible Navier–Stokes equations. *Theoret. Comput. Fluid Dyn.*, 13, 2000.

[48] R. A. Khan. Detecting changes in probabilities of a multicomponent process. *Sequential Analysis*, 14(4):375–388, 1995.

[49] T. L. Lai. Information bounds and quick detection of parameter changes in stochastic systems. *IEEE Trans. Inf. Theory*, 44(7):2917–2929, 1998.

[50] P. Li and V. Kadirkamanathan. Particle filtering based likelihood ratio approach to fault diagnosis in nonlinear stochastic systems. *IEEE Trans. Syst., Man, Cybern. C*, 31:337–343, 2001.

[51] Q. Li, H. Chen, and H. Wang. A proper orthogonal decomposition-compact difference algorithm for plate vibration models. *Numerical Algorithms*, 94, 2023.

[52] Y. Liang, A. G. Tartakovsky, and V. V. Veeravalli. Quickest change detection with non-stationary post-change observations. *IEEE Transactions on Information Theory*, 69(5), 2023.

[53] Y. Liang and V. V. Veeravalli. Quickest change detection with leave-one-out density estimation. *2023 IEEE International Conference on Acoustics, Speech and Signal Processing*, 2023.

[54] G. Lorden. Procedures for reacting to a change in distribution. *Ann. Math. Statist.*, 42(6):1897–1908, 1971.

[55] F. Lou and N. L. Key. Compressor stall warning using nonlinear feature extraction algorithms. *Journal of Engineering for Gas Turbines and Power*, 142(12), 2020.

[56] J. L. Lumley. The structure of inhomogeneous turbulent flows. *Atmospheric Turbulence and Radio Wave Propagation*, 1967.

[57] J. L. Lumley. Toward a turbulent constitutive relation. *Journal of Fluid Mechanics*, 41(2), 1970.

[58] Y. Mei. Efficient scalable schemes for monitoring a large number of data streams. *Biometrika*, (97(2):419–433, 2010.

[59] Y. Meng, N. S. Namachchivaya, and N. Perkowski. Hopf bifurcations of Moore-Greitzer PDE model with additive noise. *J Nonlinear Sci*, 33(5):(74), 2023.

[60] W. W. Mohammed, D. Blömker, and K. Klepel. Multi-scale analysis of SPDEs with degenerate additive noise. *Journal of Evolution Equations*, 14(2), 2014.

[61] F. K. Moore and E. M. Greitzer. A theory of post-stall transients in axial compression systems: Part I, II. *Trans. ASME, J. Engng for Gas Turbines and Power*, 108:68–76, 231–240, 1986.

[62] G. V. Moustakides. Optimal stopping times for detecting changes in distributions. *Ann. Statist.*, 14(4):1379–1387, 1986.

[63] E. Nitzan, T. Halme, H. V. Poor, and V. Koivunen. Deterministic multiple change-point detection with limited communication. *Proc. 54th Annu. Conf. Inf. Sci. Syst.*, pages 1–6, 2020.

[64] P. J. Olesen, L. Soucasse, B. Podvin, and C. M. Velte. Dissipation-based proper orthogonal decomposition of turbulent rayleigh-bénard convection flow. *Phys. Fluids*, 36(3), 2024.

[65] E. S. Page. Continuous inspection schemes. *Biometrika*, 41(1/2):100–115, 1954.

[66] M. Panesi. Lecture slides of AE 433: Introduction to aircraft gas turbine engines. *Department of Aerospace Engineering, University of Illinois at Urbana-Champaign.*

[67] M. Pollak. Optimal detection of a change in distribution. *The Annals of Statistics*, 13(1):206–227, 1985.

[68] M. Pollak and D. Siegmund. Approximations to the expected sample size of certain sequential tests. *Ann. Statist.*, 3:1267–1282, 1975.

[69] M. Pollak and A. G. Tartakovsky. Optimality properties of the Shiryaev-Roberts procedure. *Statistica Sinica*, 19:1729–1739, 2009.

[70] A. S. Polunchenko and A. G. Tartakovsky. On optimality of the Shiryaev–Roberts procedure for detecting a change in distribution. *Annals of Statistics*, 38(6):3445–3457, 2010.

[71] H. Vincent Poor and Olympia Hadjiliadis. *Quickest Detection.* Cambridge University Press, 2008.

[72] G. Da Prato and J. Zabczyk. *Stochastic Equations in Infinite Dimensions.* Cambridge University Press, 2014.

[73] J. Reeves, J. Chen, X. L. Wang, R. Lund, and Q. Q. Lu. A review and comparison of changepoint detection techniques for climate data. *J. Appl. Meteorol. Climatol.*, 46(6):900–915, 2007.

[74] M. Rewienski and J. White. Model order reduction for nonlinear dynamical systems based on trajectory piecewise-linear approximations. *Linear Algebra Appl.*, 415(2):426–454, 2006.

[75] Y. Ritov. Decision theoretic optimality of the CUSUM procedure. *Ann. Statist.*, 18(3):1464–1469, 1990.

[76] G. Rovatsos, J. Jiang, A. D. Domínguez-García, and V. V. Veeravalli. Statistical power system line outage detection under transient dynamics. *IEEE Transactions on Signal Processing*, 65(11):2787–2797, 2017.

[77] G. Rovatsos, S. Zou, and V. V. Veeravalli. Quickest change detection under transient dynamics. *Proceedings of the IEEE International Conference on Acoustics, Speech and Signal Processing (ICASSP)*, page 4785–4789, 2017.

[78] M. Scheffer, J. Bascompte, W. A. Brock, V. Brovkin, S. R. Carpenter, and et al. Early-warning signals for critical transitions. *Nature*, 461:53–59, 2009.

[79] W. A. Shewhart. Economic control of quality of manufactured product. *American Society for Quality Control*, 1931.

[80] A. N. Shiryaev. On optimum methods in quickest detection problems. *Theory of Prob and App*, 8:22–46, 1963.

[81] A. N. Shiryaev. Quickest detection problems: Fifty years later. *Sequential Analysis*, 29(4):345–385, 2010.

[82] A. N. Shiryaev. Optimal stopping rules. New York: Springer-Verlag, 1978.

[83] D. Siegmund. *Sequential Analysis - Tests and Confidence Intervals*. Springer-Verlag, 1995.

[84] L. Sirovich. Turbulence and the dynamics of coherent structures. *Q. Appl. Math.*, 45(3):561–571, 1987.

[85] L. Sirovich and J. D. Rodriguez. Coherent structures and chaos: A model problem. *Physics Letters A*, 120(5), 1987.

[86] C. Snyder, T. Bengtsson, P. Bickel, and J. Anderson. Obstacles to high-dimensional particle filtering. *Mon. Weather Rev.*, 136(12):4629 – 4640, 2008.

[87] A. Tartakovsky. *Sequential Change Detection and Hypothesis Testing: General Non-iid Stochastic Models and Asymptotically Optimal Rules*. CRC Press, 2019.

[88] A. G. Tartakovsky. Asymptotically minimax multialternative sequential rule for disorder detection. *Proceedings of the Steklov Institute of Mathematics*, 202(4):229–236, 1994.

[89] A. G. Tartakovsky. Multidecision quickest-change-point detection: Previous achievements and open problems. *Sequential Analysis*, 27(2):201–231, 2008.

[90] A. G. Tartakovsky, I. V. Nikiforov, and M. Basseville. *Sequential Analysis: Hypothesis Testing and Changepoint Detection*. Boca Raton, FL, USA: Chapman and Hall/CRC, 2014.

[91] A. G. Tartakovsky, M. Pollak, and A. Polunchenko. Third-order asymptotic optimality of the generalized Shiryaev-Roberts changepoint detection procedures. *ArXiv e-prints*, May 2010.

[92] A. G. Tartakovsky and V. V. Veeravalli. General asymptotic Bayesian theory of quickest change detection. *SIAM Theory of Prob. and App.*, 49(3):458–497, 2005.

[93] J. H. Tu, C. W. Rowley, D. M. Luchtenburg, S. L. Brunton, and J. N. Kutz. On dynamic mode decomposition: Theory and applications. *Journal of Computational Dynamics*, 1(2), 2014.

[94] V. V Veeravalli and T. Banerjee. Quickest change detection. *Academic press library in signal processing.*, 3:209–255, 2014.

[95] G. Verdier, N. Hilgert, and J. P. Vila. Adaptive threshold computation for CUSUM-type procedures in change detection and isolation problems. *Computational Statistics and Data Analysis*, 38(6), 2008.

[96] G. Verdier, N. Hilgert, and J. P. Vila. Optimality of CUSUM rule approximations in change-point detection problems: Application to nonlinear state-space systems. *IEEE Trans. Inf. Theory.*, 54(11):5102–5112, 2008.

[97] A. J. Volponi. Gas turbine engine health management past, present and future trends. *Journal of Engine for Gas Turbines and Power-Transactions of the ASME*, 136(5):051201, 2014.

[98] A. Wald. *Sequential Analysis*. Wiley, New York, 1947.

[99] A. Wald and J. Wolfowitz. Optimum character of the sequential probability ratio test. *Ann. Math. Statist.*, 19(3):326–339, 1948.

[100] D. Williams. *Probability with Martingales*. Cambridge, U.K.: Cambridge Univ. Press, 1991.

[101] A. S. Willsky and H. L. Jones. A generalized likelihood ratio approach to detection and estimation of jumps in linear systems. *IEEE Trans. Automat Contr.*, AC-21:108–112, 1976.

[102] K. N. Wilson, Q. Zhang, L. Chen, and Z. Liu. A review of stall detection in subsonic axial compressors. *Machines*, 13(1), 2024.

[103] M. Xiao. Quantitative characteristic of rotating stall and surge for Moore–Greitzer pde model of an axial flow compressor. *SIAM Journal on Applied Dynamical Systems*, 7(1), 2008.

[104] M. Xiao and T. Başar. Center manifold of the viscous Moore–Greitzer PDE model. *SIAM Journal on Applied Mathematics*, 61(3), 2000.

[105] L. Xie, G. V. Moustakides, and Y. Xie. Window-limited CUSUM for sequential change detection. *IEEE Transactions on Information Theory*, 69(9), 2023.

[106] Y. Xie and D. Siegmund. Sequential multi-sensor change-point detection. *The Annals of Statistics*, 41(2):670–692, 2013.

[107] Y. Xu, H. Gu, J. Sun, J. Zhang, and H. Imani. Surge and stall instabilities finite-time control of nonlinear uncertain-disturbed compression system by using a novel robust approach. *Automatika*, 65(3), 2024.

APPENDICES

Appendix A

Change Detection in Nonhomogeneous HMM

A.1 Proof of Lemma 3.1.1

Proof. For $n \geq k \geq 1$ we have

$$\begin{aligned} p_k(X_1^n) &= p_k(X_k^n|X_1^{k-1})p_k(X_1^{k-1}) \\ &= p_k(X_k^n|X_1^{k-1})p_0(X_1^{k-1}) \end{aligned}$$

and

$$p_0(X_1^n) = p_0(X_k^n|X_1^{k-1})p_0(X_1^{k-1}).$$

Therefore

$$LLR_n^k = \log \frac{p_k(X_1^n)}{p_0(X_1^n)} = \log \frac{p_k(X_k^n|X_1^{k-1})}{p_0(X_k^n|X_1^{k-1})}.$$

Moreover, we have

$$\begin{aligned} LLR_n^1 - LLR_{k-1}^1 &= \log \left(\frac{p_1(X_1^n)}{p_0(X_1^n)} \Big/ \frac{p_1(X_1^{k-1})}{p_0(X_1^{k-1})} \right) \\ &= \log \frac{p_1(X_k^n|X_1^{k-1})}{p_0(X_k^n|X_1^{k-1})}. \end{aligned}$$

Now, we see if $p_k(X_k^n|X_1^{k-1}) = p_1(X_k^n|X_1^{k-1})$ for all $1 \leq k \leq n$, then

$$LLR_n^k = LLR_n^1 - LLR_{k-1}^1$$

for all $1 \leq k \leq n$. Hence

$$\begin{aligned} T_n &= \max_{1\leq k\leq n+1} LLR_n^k = \max_{1\leq k\leq n+1} (LLR_n^1 - LLR_{k-1}^1) \\ &= \max_{1\leq k\leq n} (LLR_n^1 - LLR_k^1) = \widehat{T}_n. \end{aligned}$$

□

A.2 Proof of (3.27)

Proof. We start with

$$\begin{aligned} p(X_n, Y_0^n) &= \int p(X_{n-1}, X_n, Y_0^n) dX_{n-1} \\ &= \int p(X_{n-1}, Y_0^{n-1}) g_n(X_{n-1}, X_n) \\ &\qquad f_n(Y_n|X_n) dX_{n-1}, \end{aligned}$$

which yields

$$\begin{aligned} p(Y_0^n) &= \int p(X_n, Y_0^n) dX_n \\ &= \int\int p(X_{n-1}, Y_0^{n-1}) g_n(X_{n-1}, X_n) \\ &\qquad f_n(Y_n|X_n) dX_{n-1} dX_n. \end{aligned}$$

Therefore, we write

$$\begin{aligned} p(Y_n|Y_0^{n-1}) &= \frac{p(Y_0^n)}{p(Y_0^{n-1})} \\ &= \frac{1}{p(Y_0^{n-1})} \int\int g_n(X_{n-1}, X_n) f_n(Y_n|X_n) \\ &\qquad p(X_{n-1}, Y_0^{n-1}) dX_{n-1} dX_n \\ &= \int\int g_n(X_{n-1}, X_n) f_n(Y_n|X_n) \\ &\qquad p(X_{n-1}|Y_0^{n-1}) dX_{n-1} dX_n. \end{aligned}$$

□

Appendix B

The POD-Galerkin Procedure on the Deterministic Moore-Greitzer PDE System

It also follows from (2.15) and (4.24) that the PDE for $g(t,\theta)$ is given by

$$\begin{aligned}\sum_{\alpha=1}^{n}\dot{b}_\alpha(t)U_\alpha(\theta) = \sum_{\alpha=1}^{n}K^{-1}b_\alpha(t)\left(\frac{\nu}{2}U_\alpha''(\theta)-\frac{1}{2}U_\alpha'(\theta)\right)\\ + aK^{-1}\left[\psi_c\Big(\Phi+\sum_{\alpha=1}^{n}b_\alpha(t)U_\alpha(\theta)\Big)-\overline{\psi}_c\Big(\Phi,\sum_{\alpha=1}^{n}b_\alpha(t)U_\alpha(\theta)\Big)\right].\end{aligned} \tag{B.1}$$

Now, the question left is how we can appropriately evaluate the linear terms given at the top of (B.1) and nonlinearities at the bottom of (B.1) using the POD expansion given in (4.24), along with the orthogonality property of the POD modes. Indeed, we have

$$\begin{aligned}\frac{\partial g}{\partial t}(t,\theta) &= \sum_{\alpha=1}^{n}\dot{b}_\alpha(t)U_\alpha(\theta),\\ \frac{\partial g}{\partial \theta}(t,\theta) &= \sum_{\alpha=1}^{n}b_\alpha(t)U_\alpha'(\theta) = \sum_{j\in I_N} ij\Big(\sum_{\alpha=1}^{n}c_{\alpha,j}b_\alpha(t)\Big)e^{ij\theta},\\ \frac{\partial^2 g}{\partial \theta^2}(t,\theta) &= \sum_{\alpha=1}^{n}b_\alpha(t)U_\alpha''(\theta) = -\sum_{j\in I_N} j^2\Big(\sum_{\alpha=1}^{n}c_{\alpha,j}b_\alpha(t)\Big)e^{ij\theta}.\end{aligned} \tag{B.2}$$

Using the fact that $K^{-1}(\sum_{j\in I_N}\tilde{\phi}_j e^{ij\theta}) = \sum_{n\in I_N}\left(\frac{|j|}{|j|+ma}\right)\tilde{\phi}_n e^{ij\theta}$, we apply K^{-1} to $g(t,\theta)$:

$$K^{-1}g(t,\theta) = K^{-1}\Big(\sum_{j\in_{I_N}}\Big(\sum_{\alpha=1}^{n}c_{\alpha,j}b_\alpha(t)\Big)e^{ij\theta}\Big) = \sum_{j\in_{I_N}}\left(\frac{|j|}{|j|+ma}\right)\Big(\sum_{\alpha=1}^{n}c_{\alpha,j}b_\alpha(t)\Big)e^{ij\theta}. \tag{B.3}$$

Similarly, applying K^{-1} to the spatial derivatives gives to

$$\begin{aligned} K^{-1}\frac{\partial g}{\partial\theta}(t,\theta) &= K^{-1}\Big(\sum_{j\in_{I_N}} ij\Big(\sum_{\alpha=1}^{n}c_{\alpha,j}b_\alpha(t)\Big)e^{ij\theta}\Big) \\ &= \sum_{j\in_{I_N}}\left(\frac{|j|}{|j|+ma}\right) ij\Big(\sum_{\alpha=1}^{n}c_{\alpha,j}b_\alpha(t)\Big)e^{ij\theta}, \\ K^{-1}\frac{\partial^2 g}{\partial\theta^2}(t,\theta) &= -K^{-1}\Big(\sum_{j\in_{I_N}} j^2\Big(\sum_{\alpha=1}^{n}c_{\alpha,j}b_\alpha(t)\Big)e^{ij\theta}\Big) \\ &= -\sum_{j\in_{I_N}}\left(\frac{|j|}{|j|+ma}\right) j^2\Big(\sum_{\alpha=1}^{n}c_{\alpha,j}b_\alpha(t)\Big)e^{ij\theta} \end{aligned} \tag{B.4}$$

Hence, putting (B.3) and (B.4) in the linear part of the equation,

$$\frac{\partial g}{\partial t}(t,\theta) = K^{-1}\left(\frac{\nu}{2}\frac{\partial^2 g}{\partial\theta^2}(t,\theta) - \frac{1}{2}\frac{\partial g}{\partial\theta}(t,\theta)\right)$$

yields the linear β^{th} equation associated with the PDE for $g(t,\theta)$:

$$\begin{aligned} \Big\langle\sum_{\alpha=1}^{n}\dot{b}_\alpha(t)U_\alpha(\theta), U_\beta(\theta)\Big\rangle = \Big\langle\sum_{j\in_{I_N}}\left(\frac{|j|}{|j|+ma}\right)\Big(-\frac{\nu}{2}j^2 - ij\frac{1}{2}\Big) \\ \cdot\Big(\sum_{\alpha=1}^{n}c_{\alpha,j}b_\alpha(t)\Big)e^{i\,j\theta}, \sum_{k\in_{I_N}}c_{\beta,k}e^{ik\theta}\Big\rangle \end{aligned} \tag{B.5}$$

where $U_\beta(\theta) = \sum_{k\in_{I_N}}c_{\beta,k}e^{ik\theta}$, with $c_{\beta,k} := \frac{1}{\sqrt{M\lambda_\beta}}\sum_{l=1}^{M}\gamma_l^{(\beta)}\widetilde{g}_k(t_l)$, which are constants.

$$
\begin{aligned}
\dot{b}_\beta(t) &= \sum_{j\in I_N}\Big(\frac{|j|}{|j|+ma}\Big)\Big(-\frac{\nu}{2}j^2 - ij\frac{1}{2}\Big)\Big(\sum_{\alpha=1}^{n} c_{\alpha,j}b_\alpha(t)\Big)\frac{1}{2\pi}\int_0^{2\pi} e^{ij\theta}\sum_{k\in I_N}\overline{c_{\beta,k}e^{ik\theta}}d\theta \\
&= \sum_{j\in I_N}\Big(\frac{|j|}{|j|+ma}\Big)\Big(-\frac{\nu}{2}j^2 - ij\frac{1}{2}\Big)\Big(\sum_{\alpha=1}^{n} c_{\alpha,j}b_\alpha(t)\Big)\sum_{k\in I_N}\overline{c_{\beta,k}}\frac{1}{2\pi}\int_0^{2\pi} e^{i(j-k)\theta}d\theta \\
&= \sum_{j\in I_N}\Big(\frac{|j|}{|j|+ma}\Big)\Big(-\frac{\nu}{2}j^2 - ij\frac{1}{2}\Big)\Big(\sum_{\alpha=1}^{n} c_{\alpha,j}b_\alpha(t)\Big)\overline{c_{\beta,j}} \\
&= \sum_{\alpha=1}^{n}\Big(\sum_{j\in I_N}\Big(\frac{|j|}{|j|+ma}\Big)\Big(-\frac{\nu}{2}j^2 - ij\frac{1}{2}\Big)c_{\alpha,j}\overline{c_{\beta,j}}\Big)b_\alpha(t)
\end{aligned}
\tag{B.6}
$$

where (since λ_α and $\gamma^{(\alpha)}$ are real)

$$
\begin{aligned}
c_{\alpha,j}\overline{c_{\beta,j}} &= \frac{1}{\sqrt{M\lambda_\alpha}}\sum_{l=1}^{M}\gamma_l^{(\alpha)}\widetilde{g}_j(t_l)\ \frac{1}{\sqrt{M\lambda_\beta}}\sum_{l=1}^{M}\gamma_l^{(\beta)}\overline{\widetilde{g}_j(t_l)} \\
&= \frac{1}{M\sqrt{\lambda_\alpha\lambda_\beta}}\sum_{l=1}^{M}\gamma_l^{(\alpha)}\widetilde{g}_j(t_l)\ \gamma_l^{(\beta)}\overline{\widetilde{g}_j(t_l)}
\end{aligned}
\tag{B.7}
$$

Remark B.0.1. *While we may impose the orthonormality of the eigenvectors, i.e., $\gamma^{(\alpha)}$ and $\gamma^{(\beta)}$, such that*

$$
\sum_{l=1}^{M}\gamma_l^{(\alpha)}\gamma_l^{(\beta)} = \begin{cases} 1, & \alpha=\beta \\ 0, & \alpha\neq\beta, \end{cases}
$$

this would not necessarily make $\sum_{l=1}^{M}\gamma_l^{(\alpha)}\widetilde{g}_j(t_l)\ \gamma_l^{(\beta)}\overline{\widetilde{g}_j(t_l)} = 0$ when $\alpha=\beta$. So (B.7) is the simplest linear β^{th} for the time-dependent coefficients used in the POD expansions of $g(t,\theta)$. This property will be carried to the nonlinear terms in $b_\alpha(t)$ later in the following derivation.

Now, let us consider the projection of the terms associated with the nonlinearity that are linear in $b_\alpha(t)$ onto the space H using β^{th} POD mode, and this projection is denoted as $\mathcal{N}_\beta^{1,b_\alpha(t)}$.

$$\mathcal{N}_{\beta}^{1,b_\alpha(t)} = \Big(\frac{3Ha}{W^2}\Phi(t) - \frac{3Ha}{2W^3}\Phi^2(t)\Big)\Big\langle \sum_{j\in I_N}\Big(\frac{|j|}{|j|+ma}\Big)\Big(\sum_{\alpha=1}^{n} c_{\alpha,j}b_\alpha(t)\Big)e^{i\,j\theta}, \sum_{k\in I_N} c_{\beta,k}e^{ik\theta}\Big\rangle$$

$$= \Big(\frac{3Ha}{W^2}\Phi(t) - \frac{3Ha}{2W^3}\Phi^2(t)\Big)\sum_{j\in I_N}\Big(\frac{|j|}{|j|+ma}\Big)\Big(\sum_{\alpha=1}^{n} c_{\alpha,j}b_\alpha(t)\Big)\Big(\frac{1}{2\pi}\int_0^{2\pi} e^{i\,j\theta}\sum_{k\in I_N}\overline{c_{\beta,k}e^{ik\theta}}\,d\theta\Big)$$

$$= \Big(\frac{3Ha}{W^2}\Phi(t) - \frac{3Ha}{2W^3}\Phi^2(t)\Big)\sum_{j\in I_N}\Big(\frac{|j|}{|j|+ma}\Big)\Big(\sum_{\alpha=1}^{n} c_{\alpha,j}b_\alpha(t)\Big)\sum_{k\in I_N}\overline{c_{\beta,k}}\Big(\frac{1}{2\pi}\int_0^{2\pi} e^{i(j-k)\theta}d\theta\Big)$$

$$= \Big(\frac{3Ha}{W^2}\Phi(t) - \frac{3Ha}{2W^3}\Phi^2(t)\Big)\sum_{j\in I_N}\Big(\frac{|j|}{|j|+ma}\Big)\Big(\sum_{\alpha=1}^{n} c_{\alpha,j}b_\alpha(t)\Big)\overline{c_{\beta,j}}$$

$$= \frac{3Ha}{W^2}\Phi(t)\Big(1-\frac{\Phi(t)}{2W}\Big)\sum_{\alpha=1}^{n}\Big(\sum_{j\in I_N}\Big(\frac{|j|}{|j|+ma}\Big)c_{\alpha,j}\overline{c_{\beta,j}}\Big)b_\alpha(t).$$

Next, we find the equation of the terms associated with the nonlinearity that are quadratic in $b_\alpha(t)$, i.e.,

$$\frac{3H}{2W^2}\,a\sum_{\substack{j,k\in I_N\\(j+k\neq 0)}}\Big(\frac{|j+k|}{|j+k|+ma}\Big)\Big(\sum_{\alpha_1,\alpha_2=1}^{n} c_{\alpha_1,j}c_{\alpha_2,k}b_{\alpha_1}(t)b_{\alpha_2}(t)\Big)e^{i(j+k)\theta}$$

$$-\frac{3H}{2W^3}\Phi(t)\,a\sum_{\substack{j,k\in I_N\\(j+k\neq 0)}}\Big(\frac{|j+k|}{|j+k|+ma}\Big)\Big(\sum_{\alpha_1,\alpha_2=1}^{n} c_{\alpha_1,j}c_{\alpha_2,k}b_{\alpha_1}(t)b_{\alpha_2}(t)\Big)e^{i(j+k)\theta},$$

and project it using β^{th} POD mode. This is represented as $\mathcal{N}_{\beta}^{2,b_\alpha(t)}$. Let $\mathcal{F}(\Phi(t)) :=$

$\Big(\frac{3Ha}{2W^2} - \frac{3Ha}{2W^3}\Phi(t)\Big)$, then we have

$$N_\beta^{2,b_\alpha(t)} = \mathcal{F}(\Phi(t))\Big\langle \sum_{\substack{j,k\in I_N\\(j+k\neq 0)}} \left(\frac{|j+k|}{|j+k|+ma}\right)\Big(\sum_{\alpha_1,\alpha_2=1}^{n} c_{\alpha_1,j}c_{\alpha_2,k}b_{\alpha_1}(t)b_{\alpha_2}(t)\Big)e^{i(j+k)\theta}, \sum_{l\in_{I_N}} c_{\beta,l}e^{il\theta}\Big\rangle$$

$$= \frac{\mathcal{F}(\Phi(t))}{2\pi} \sum_{\substack{j,k\in I_N\\(j+k\neq 0)}} \left(\frac{|j+k|}{|j+k|+ma}\right)\Big(\sum_{\alpha_1,\alpha_2=1}^{n} c_{\alpha_1,j}c_{\alpha_2,k}b_{\alpha_1}(t)b_{\alpha_2}(t)\Big)\Big(\int_0^{2\pi} e^{i\,(j+k)\theta} \sum_{l\in_{I_N}} \overline{c_{\beta,l}e^{il\theta}}\, d\theta\Big)$$

$$= \frac{\mathcal{F}(\Phi(t))}{2\pi} \sum_{\substack{j,k\in I_N\\(j+k\neq 0)}} \left(\frac{|j+k|}{|j+k|+ma}\right)\Big(\sum_{\alpha_1,\alpha_2=1}^{n} c_{\alpha_1,j}c_{\alpha_2,k}b_{\alpha_1}(t)b_{\alpha_2}(t)\Big)\sum_{l\in_{I_N}} \overline{c_{\beta,l}}\Big(\int_0^{2\pi} e^{i(j+k-l)\theta}d\theta\Big)$$

$$= \frac{\mathcal{F}(\Phi(t))}{2\pi} \sum_{\substack{j,k\in I_N\\(j+k\neq 0)}} \left(\frac{|j+k|}{|j+k|+ma}\right)\Big(\sum_{\alpha_1,\alpha_2=1}^{n} c_{\alpha_1,j}c_{\alpha_2,k}b_{\alpha_1}(t)b_{\alpha_2}(t)\Big)\overline{c_{\beta,j+k}}$$

$$= \frac{\mathcal{F}(\Phi(t))}{2\pi} \sum_{\alpha_1,\alpha_2=1}^{n} \left(\sum_{\substack{j,k\in I_N\\(j+k\neq 0)}} \left(\frac{|j+k|}{|j+k|+ma}\right) c_{\alpha_1,j}c_{\alpha_2,k}\overline{c_{\beta,j+k}}\right) b_{\alpha_1}(t)b_{\alpha_2}(t)$$

Now consider the terms associated with the nonlinearity that are cubic in $b_\alpha(t)$ and define

$$\mathcal{M}(t,\theta) := -\frac{Ha}{2W^3} \sum_{\substack{j,k,l\in I_N\\(j+k+l\neq 0)}} \left(\frac{|j+k+l|}{|j+k+l|+ma}\right) e^{i(j+k+l)\theta} \times \Big(\sum_{\alpha_1,\alpha_2,\alpha_3=1}^{n} c_{\alpha_1,j}c_{\alpha_2,k}c_{\alpha_3,l}b_{\alpha_1}(t)b_{\alpha_2}(t)b_{\alpha_3}(t)\Big)$$

Similarly, taking the inner product with $U_\beta(\theta) = \sum_{q\in_{I_N}} c_{\beta,q}e^{iq\theta}$ yields

$$-\frac{Ha}{2W^3}\Big\langle \mathcal{M}(t,\theta), \sum_{q\in_{I_N}} c_{\beta,q}e^{iq\theta}\Big\rangle$$

$$= -\frac{Ha}{2W^3} \sum_{\substack{j,k,l\in I_N\\(j+k+l\neq 0)}} \left(\frac{|j+k+l|}{|j+k+l|+ma}\right)\Big(\sum_{\alpha_1,\alpha_2,\alpha_3=1}^{n} c_{\alpha_1,j}c_{\alpha_2,k}c_{\alpha_3,l}b_{\alpha_1}(t)b_{\alpha_2}(t)b_{\alpha_3}(t)\Big)\overline{c_{\beta,j+k+l}}$$

$$= -\frac{Ha}{2W^3} \sum_{\alpha_1,\alpha_2,\alpha_3=1}^{n} \left(\sum_{\substack{j,k,l\in I_N\\(j+k+l\neq 0)}} \left(\frac{|j+k+l|}{|j+k+l|+ma}\right) c_{\alpha_1,j}c_{\alpha_2,k}c_{\alpha_3,l}\overline{c_{\beta,j+k+l}}\right) b_{\alpha_1}(t)b_{\alpha_2}(t)b_{\alpha_3}(t)$$

Hence the complete β^{th} equation associated with the PDE for $g(t,\theta)$ approximated by the POD mode expansions is given by

$$\begin{aligned}
\dot{b}_\beta(t) &= \sum_{\alpha=1}^{n}\Big(\sum_{j\in I_N}\Big(\frac{|j|}{|j|+ma}\Big)\Big(-\frac{\nu}{2}j^2 - ij\frac{1}{2}\Big)c_{\alpha,j}\overline{c_{\beta,j}}\Big)b_\alpha(t) \\
&+ \frac{3Ha}{W^2}\Phi(t)\Big(1-\frac{\Phi(t)}{2W}\Big)\sum_{\alpha=1}^{n}\Big(\sum_{j\in I_N}\Big(\frac{|j|}{|j|+ma}\Big)c_{\alpha,j}\overline{c_{\beta,j}}\Big)b_\alpha(t) \\
&+ \Big(\frac{3Ha}{2W^2} - \frac{3Ha}{2W^3}\Phi(t)\Big)\sum_{\alpha_1,\alpha_2=1}^{n}\Bigg(\sum_{\substack{j,k\in I_N\\(j+k\neq 0)}}\Big(\frac{|j+k|}{|j+k|+ma}\Big)c_{\alpha_1,j}c_{\alpha_2,k}\overline{c_{\beta,j+k}}\Bigg)b_{\alpha_1}(t)b_{\alpha_2}(t) \\
&- \frac{Ha}{2W^3}\sum_{\alpha_1,\alpha_2,\alpha_3=1}^{n}\Bigg(\sum_{\substack{j,k,l\in I_N\\(j+k+l\neq 0)}}\Big(\frac{|j+k+l|}{|j+k+l|+ma}\Big)c_{\alpha_1,j}c_{\alpha_2,k}c_{\alpha_3,l}\overline{c_{\beta,j+k+l}}\Bigg)b_{\alpha_1}(t)b_{\alpha_2}(t)b_{\alpha_3}(t),
\end{aligned} \tag{B.8}$$

which are coupled to the ODE's given by

$$\begin{aligned}
\dot{\Phi}(t) &= \frac{1}{l_c}\Big(\bar{\psi}_c(\Phi(t),\hat{b}(t)) - \Psi(t)\Big) \\
\dot{\Psi}(t) &= \frac{1}{4B^2 l_c}\Big(\Phi(t) - \gamma\sqrt{\Psi(t)}\Big)
\end{aligned} \tag{B.9}$$

Notice that $\hat{b}(t) := ((b_1(t),\cdots,b_n(t))$, implying that $\bar{\psi}_c(\Phi(t),\hat{b}(t))$ depends on Φ as well as the decomposed time coefficients $b_1(t),\cdots,b_n(t)$ coming from $g(t,\theta)$ by averaging θ over $[0,2\pi]$. Using (4.19) yields

$$\bar{\psi}_c(t) = \psi_c(\Phi(t)) - \frac{3H}{2W^2}\left(\frac{\Phi(t)}{W}-1\right)\frac{1}{2\pi}\int_0^{2\pi} g^2(t,\theta)d\theta - \frac{H}{2W^3}\int_0^{2\pi} g^3(t,\theta)d\theta,$$

where we can express

$$
\begin{aligned}
g^2(t,\theta) &= \sum_{\alpha_1=1}^{n} b_{\alpha_1}(t)U_{\alpha_1}(\theta) \sum_{\alpha_2=1}^{n} b_{\alpha_2}(t)U_{\alpha_2}(\theta) \\
&= \sum_{\alpha_1=1}^{n} b_{\alpha_1}(t) \sum_{j\in_{I_N}} c_{\alpha_1,j}e^{ij\theta} \sum_{\alpha_2=1}^{n} b_{\alpha_2}(t) \sum_{k\in_{I_N}} c_{\alpha_2,k}e^{ik\theta} \\
&= \sum_{\alpha_1,\alpha_2=1}^{n} \sum_{j,k\in_{I_N}} c_{\alpha_1,j}c_{\alpha_2,k}e^{i(j+k)\theta}b_{\alpha_2}(t)b_{\alpha_1}(t), \\
g^3(t,\theta) &= \sum_{\alpha_1,\alpha_2,\alpha_3=1}^{n} \sum_{j,k,l\in_{I_N}} c_{\alpha_1,j}c_{\alpha_2,k}c_{\alpha_3,l}e^{i(j+k+l)\theta}b_{\alpha_2}(t)b_{\alpha_1}(t)b_{\alpha_3}(t).
\end{aligned}
$$

As such, we can write $\bar{\psi}_c$ as follows,

$$
\begin{aligned}
\bar{\psi}_c(\Phi(t),\hat{b}(t)) = \psi_c(\Phi(t)) &- \frac{3H}{2W^2}\left(\frac{\Phi(t)}{W}-1\right)\sum_{\alpha_1,\alpha_2=1}^{n} \sum_{\substack{j,k\in Z\setminus\{0\} \\ (j+k=0)}} c_{\alpha_1,j}c_{\alpha_2,k}b_{\alpha_2}(t)b_{\alpha_1}(t) \\
&- \frac{H}{2W^3}\sum_{\alpha_1,\alpha_2,\alpha_3=1}^{n} \sum_{\substack{j,k,l\in Z\setminus\{0\} \\ (j+k+l=0)}} c_{\alpha_1,j}c_{\alpha_2,k}c_{\alpha_3,l}b_{\alpha_2}(t)b_{\alpha_1}(t)b_{\alpha_3}(t).
\end{aligned}
\tag{B.10}
$$

Appendix C

The Fourier-Galerkin Procedure on the Stochastic Moore-Greitzer PDE System

As introduced in Section 2.1.1, the disturbance velocity $\varphi'(t,\theta,\eta)$, which is periodic in θ, vanishes as $\eta \to -\infty$, is given by

$$\varphi'(t,\theta,\eta) = \sum_{n\in I_N} \tilde{\varphi}_n(t) e^{|n|\eta + in\theta}, \tag{C.1}$$

which impies that

$$g(\theta,t) = \varphi'_\eta(t,\theta,\eta)\Big|_{\eta=0} = \sum_{n\in\mathbb{Z}\setminus\{0\}} \widetilde{g}_n(t) e^{in\theta}. \tag{C.2}$$

where

$$\widetilde{g}_n(t) := |n|\tilde{\varphi}_n(t). \tag{C.3}$$

Using the fact that

$$\psi_c(\phi) = \psi_{c_0} + H[1 + \frac{3}{2}(\frac{\phi}{W} - 1) - \frac{1}{2}(\frac{\phi}{W} - 1)^3]$$

yields

$$\psi_c\big(\Phi(t) + g(t,\theta)\big) = \psi_c(\Phi(t)) + \widetilde{\psi}(\Phi(t), g(t,\theta)), \tag{C.4}$$

where

$$\widetilde{\psi}(\Phi, g) = H\left[\frac{3}{2}\left[1-\left(\frac{\Phi}{W}-1\right)^2\right]\left(\frac{g}{W}\right)-\frac{3}{2}\left(\frac{\Phi}{W}-1\right)\left(\frac{g}{W}\right)^2-\frac{1}{2}\left(\frac{g}{W}\right)^3\right]. \tag{C.5}$$

Then it follows from the definition of $\bar{\psi}_c$ that

$$\bar{\psi}_c(t) = \psi_c(\Phi(t)) - \frac{3H}{2W^2}\left(\frac{\Phi(t)}{W}-1\right)\frac{1}{2\pi}\int_0^{2\pi} g^2(t,\theta)d\theta - \frac{H}{2W^3}\int_0^{2\pi} g^3(t,\theta)d\theta. \tag{C.6}$$

Notice that we can express

$$\begin{aligned} g^2(t,\theta) &= \sum_{j\in\mathbb{Z}\setminus\{0\}} \widetilde{g}_j(t)e^{ij\theta}\cdot\sum_{k\in\mathbb{Z}\setminus\{0\}}\widetilde{g}_k(t)e^{ik\theta} = \sum_{j,k\in\mathbb{Z}\setminus\{0\}}\widetilde{g}_j(t)\widetilde{g}_k(t)e^{i(j+k)\theta} \\ g^3(t,\theta) &= \sum_{j,k,l\in\mathbb{Z}\setminus\{0\}}\widetilde{g}_j(t)\widetilde{g}_k(t)\widetilde{g}_l(t)e^{i(j+k+l)\theta}, \end{aligned}$$

so we have

$$\bar{\psi}_c(\Phi(t),\widetilde{g}(t)) = \psi_c(\Phi(t)) - \frac{3H}{2W^2}\left(\frac{\Phi(t)}{W}-1\right)\sum_{\substack{j,k\in\mathbb{Z}\setminus\{0\}\\(j+k=0)}}\widetilde{g}_j(t)\widetilde{g}_k(t) - \frac{H}{2W^3}\sum_{\substack{j,k,l\in\mathbb{Z}\setminus\{0\}\\(j+k+l=0)}}\widetilde{g}_j(t)\widetilde{g}_k(t)\widetilde{g}_l(t). \tag{C.7}$$

Notice that the notation k throughout this Appendix has nothing to do with the change point but rather a wave number index given in a Fourier basis. Subtracting (C.7) from (C.4) gives to

$$\begin{aligned} \big(\psi_c(\Phi(t)+g(t,\theta)) - \bar{\psi}_c(t)\big) &= \frac{3H}{W^2}\Phi(t)\sum_{j\in\mathbb{Z}\setminus\{0\}}\widetilde{g}_j(t)e^{ij\theta} + \frac{3H}{2W^2}\sum_{\substack{j,k\in\mathbb{Z}\setminus\{0\}\\(j+k\neq 0)}}\widetilde{g}_j(t)\widetilde{g}_k(t)e^{i(j+k)\theta} \qquad \text{(C.8)} \\ &\quad - \frac{3H}{2W^3}\Phi^2(t)\sum_{j\in\mathbb{Z}\setminus\{0\}}\widetilde{g}_j(t)e^{ij\theta} - \frac{3H}{2W^3}\Phi(t)\sum_{\substack{j,k\in\mathbb{Z}\setminus\{0\}\\(j+k\neq 0)}}\widetilde{g}_j(t)\widetilde{g}_k(t)e^{i(j+k)\theta} \qquad \text{(C.9)} \\ &\quad - \frac{H}{2W^3}\sum_{\substack{j,k,l\in\mathbb{Z}\setminus\{0\}\\(j+k+l\neq 0)}}\widetilde{g}_j(t)\widetilde{g}_k(t)\widetilde{g}_l(t)e^{i(j+k+l)\theta}. \end{aligned}$$

It follows from (4.18) that

$$
\begin{aligned}
&aK^{-1}\Big(\psi_c(\Phi(t)+g(t,\theta))-\bar{\psi}_c(t)\Big)\\
&=\frac{3H}{W^2}\Phi(t)\ a\sum_{j\in\mathbb{Z}\setminus\{0\}}\left(\frac{|j|}{|j|+ma}\right)\widetilde{g}_j(t)e^{ij\theta}\\
&+\frac{3H}{2W^2}\ a\sum_{\substack{j,k\in\mathbb{Z}\setminus\{0\}\\(j+k\neq 0)}}\left(\frac{|j+k|}{|j+k|+ma}\right)\widetilde{g}_j(t)\widetilde{g}_k(t)e^{i(j+k)\theta}\\
&-\frac{3H}{2W^3}\Phi^2(t)\ a\sum_{j\in\mathbb{Z}\setminus\{0\}}\left(\frac{|j|}{|j|+ma}\right)\widetilde{g}_j(t)e^{ij\theta}\\
&-\frac{3H}{2W^3}\Phi(t)a\sum_{\substack{j,k\in\mathbb{Z}\setminus\{0\}\\(j+k\neq 0)}}\left(\frac{|j+k|}{|j+k|+ma}\right)\widetilde{g}_j(t)\widetilde{g}_k(t)e^{i(j+k)\theta}\\
&-\frac{H}{2W^3}\ a\sum_{\substack{j,k,l\in\mathbb{Z}\setminus\{0\}\\(j+k+l\neq 0)}}\left(\frac{|j+k+l|}{|j+k+l|+ma}\right)\widetilde{g}_j(t)\widetilde{g}_k(t)\widetilde{g}_l(t)e^{i(j+k+l)\theta}.
\end{aligned}
$$

Now making use of $g(t,\theta)=\sum_{n\in\mathbb{Z}\setminus\{0\}}\widetilde{g}_n(t)e^{in\theta}$, we have arranged the terms on the RHS of the PDE with linear in $\widetilde{g}$, quadratic in $\widetilde{g}$ and cubic in $\widetilde{g}$. Therefore, we have

$$
\begin{aligned}
&\sum_{j\in\mathbb{Z}\setminus\{0\}}\dot{\widetilde{g}}_j(t)e^{ij\theta}=\sum_{j\in\mathbb{Z}\setminus\{0\}}\left(\frac{|j|}{|j|+ma}\right)\Big(-\frac{\nu}{2}j^2-ij\frac{1}{2}\Big)\widetilde{g}_j(t)e^{i\,j\theta}\\
&+\frac{3H}{W^2}\Phi(t)\ a\sum_{j\in\mathbb{Z}\setminus\{0\}}\left(\frac{|j|}{|j|+ma}\right)\widetilde{g}_j(t)e^{ij\theta}+\frac{3H}{2W^2}\ a\sum_{\substack{j,k\in\mathbb{Z}\setminus\{0\}\\(j+k\neq 0)}}\left(\frac{|j+k|}{|j+k|+ma}\right)\widetilde{g}_j(t)\widetilde{g}_k(t)e^{i(j+k)\theta}\\
&-\frac{3H}{2W^3}\Phi^2(t)\ a\sum_{j\in\mathbb{Z}\setminus\{0\}}\left(\frac{|j|}{|j|+ma}\right)\widetilde{g}_j(t)e^{ij\theta}-\frac{3H}{2W^3}\Phi(t)a\sum_{\substack{j,k\in\mathbb{Z}\setminus\{0\}\\(j+k\neq 0)}}\left(\frac{|j+k|}{|j+k|+ma}\right)\widetilde{g}_j(t)\widetilde{g}_k(t)e^{i(j+k)\theta}\\
&-\frac{H}{2W^3}\ a\sum_{\substack{j,k,l\in\mathbb{Z}\setminus\{0\}\\(j+k+l\neq 0)}}\left(\frac{|j+k+l|}{|j+k+l|+ma}\right)\widetilde{g}_j(t)\widetilde{g}_k(t)\widetilde{g}_l(t)e^{i(j+k+l)\theta}=:F\Big(\sum_{j\in\mathbb{Z}\setminus\{0\}}\widetilde{g}_j(t)e^{ij\theta},\Phi(t)\Big)
\end{aligned}
$$

Taking the inner product of each side with the function with $e^{i\beta\theta}$, as in the Galerkin projection:

$$\dot{\widetilde{g}}_\beta(t) = \Big\langle F\Big(\sum_{j\in\mathbb{Z}\setminus\{0\}} \widetilde{g}_j(t)e^{ij\theta}, \Phi(t)\Big), e^{i\beta\theta}\Big\rangle, \quad \beta = \pm 1, \pm 2, \cdots \pm N.$$

To keep the notations simple for a fixed N by defining $I_N := j \in \mathbb{Z} \setminus \{0\}$

$$I_N := \big\{-N, -N+1, \cdots, -2, -1\big\} \cup \big\{1, 2, \cdots, N-1, N\big\}.$$

We shall consider each term on the RHS, separately. Starting with the terms associated with the linear PDE, i.e., $K^{-1}\left(\frac{\nu}{2}\frac{\partial^2 g}{\partial\theta^2}(t,\theta) - \frac{1}{2}\frac{\partial g}{\partial\theta}(t,\theta)\right)$. Then, β^{th} equation is given by

$$\begin{aligned} L_\beta &= \Big\langle \sum_{j\in I_N} \left(\frac{|j|}{|j|+ma}\right)\Big(-\frac{\nu}{2}j^2 - ij\frac{1}{2}\Big)\widetilde{g}_j(t)e^{i\,j\theta}, e^{i\beta\theta}\Big\rangle \\ &= \left(\frac{|\beta|}{|\beta|+ma}\right)\Big(-\frac{\nu}{2}\beta^2 - i\beta\frac{1}{2}\Big)\widetilde{g}_\beta(t). \end{aligned}$$

Now consider the terms associated with the nonlinearity that are linear in $\widetilde{g}_n(t)$:

$$\begin{aligned} \beta^{\text{th}} \text{ equation} \quad N_\beta^{1,\cdot} &= \Big(\frac{3Ha}{W^2}\Phi(t) - \frac{3Ha}{2W^3}\Phi^2(t)\Big)\Big\langle \sum_{j\in I_N}\left(\frac{|j|}{|j|+ma}\right)\widetilde{g}_j(t)e^{ij\theta}, e^{i\beta\theta}\Big\rangle \\ &= \frac{3Ha}{W}\Big(\frac{\Phi(t)}{W} - \frac{1}{2}\frac{\Phi^2(t)}{W^2}\Big)\left(\frac{|\beta|}{|\beta|+ma}\right)\widetilde{g}_\beta(t). \end{aligned}$$

Simiarly, we express the terms associated with the nonlinearity that are quadratic in $\widetilde{g}_n(t)$ as follows,

$$\begin{aligned} N_\beta^{2,\cdot} &= \Big(\frac{3Ha}{2W^2} - \frac{3Ha}{2W^3}\Phi(t)\Big)\Big\langle \sum_{\substack{j,k\in I_N \\ (j+k\neq 0)}}\left(\frac{|j+k|}{|j+k|+ma}\right)\widetilde{g}_j(t)\widetilde{g}_k(t)e^{i(j+k)\theta}, e^{i\beta\theta}\Big\rangle \\ &= \frac{3Ha}{2W^2}\Big(1-\frac{\Phi(t)}{W}\Big)\left(\frac{|\beta|}{|\beta|+ma}\right)\sum_{\substack{j\in I_N \\ (\beta\neq 0)}}\widetilde{g}_j(t)\widetilde{g}_{\beta-j}(t). \end{aligned}$$

Finally we consider the terms associated with the nonlinearity that are qubic in $\widetilde{g}_n(t)$.

$$\beta^{\text{th}} \text{ equation} \quad N_\beta^{3,\cdot} = -\frac{Ha}{2W^3}\Big\langle \sum_{j,k,l\in I_N}\left(\frac{|j+k+l|}{|j+k+l|+ma}\right)\widetilde{g}_j(t)\widetilde{g}_k(t)\widetilde{g}_l(t)e^{i(j+k+l)\theta}, e^{i\beta\theta}\Big\rangle$$
$$= -\frac{Ha}{2W^3}\left(\frac{|\beta|}{|\beta|+ma}\right)\sum_{\substack{j,k\in I_N\\(\beta\neq 0)}}\widetilde{g}_j(t)\widetilde{g}_k(t)\widetilde{g}_{\beta-j-k}(t).$$

Hence the complete β^{th} equation associated with the PDE for $g(t,\theta)$ is:

$$\begin{aligned}\dot{\widetilde{g}}_\beta(t) &= \left(\frac{|\beta|}{|\beta|+ma}\right)\Big(-\frac{\nu}{2}\beta^2 - i\beta\frac{1}{2}\Big)\widetilde{g}_\beta(t)\\ &+ \left(\frac{|\beta|}{|\beta|+ma}\right)\frac{3Ha}{W}\Big(\frac{\Phi(t)}{W} - \frac{1}{2}\frac{\Phi^2(t)}{W^2}\Big)\widetilde{g}_\beta(t)\\ &+ \left(\frac{|\beta|}{|\beta|+ma}\right)\frac{3Ha}{2W^2}\Big(1-\frac{\Phi(t)}{W}\Big)\sum_{\substack{j\in I_N\\(\beta\neq 0)}}\widetilde{g}_j(t)\,\widetilde{g}_{\beta-j}(t)\\ &- \frac{Ha}{2W^3}\left(\frac{|\beta|}{|\beta|+ma}\right)\sum_{\substack{j,k\in I_N\\(\beta\neq 0)}}\widetilde{g}_j(t)\,\widetilde{g}_k(t)\,\widetilde{g}_{\beta-j-k}(t),\end{aligned}$$

which is coupled to the ODEs given by

$$\begin{aligned}\dot{\Phi}(t) &= \frac{1}{l_c}\left(\psi_c\big(\Phi(t)\big) + \frac{3H}{2W^2}\left(1-\frac{\Phi(t)}{W}\right)\sum_{\substack{j,k\in Z\setminus\{0\}\\(j+k=0)}}\widetilde{g}_j(t)\,\widetilde{g}_k(t) - \frac{H}{2W^3}\sum_{\substack{j,k,l\in Z\setminus\{0\}\\(j+k+l=0)}}\widetilde{g}_j(t)\,\widetilde{g}_k(t)\,\widetilde{g}_l(t) - \Psi(t)\right),\\ \dot{\Psi}(t) &= \frac{1}{4B^2 l_c}\Big(\Phi(t) - \gamma\sqrt{\Psi(t)}\Big).\end{aligned} \tag{C.10}$$